Investigating the role of management and measurement technique on the temporal and spatial variability of carbon dynamics and nitrous oxide emissions from temperate grasslands

Thesis submitted for the degree of Doctor of Philosophy

April 2022

Rachael Murphy

The University of Dublin, Trinity College

Department of Botany

School of Natural Sciences

Artwork by T. Murphy (thomaseugenemurphy96@gmail.com)

Declaration

I declare that this thesis has not been submitted as an exercise for a degree at this or any other university and it is entirely my own work.

I agree to deposit this thesis in the University's open access institutional repository or allow the library to do so on my behalf, subject to Irish Copyright Legislation and Trinity College Library conditions of use and acknowledgement.

Signed,

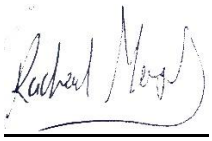

Abstract

The Earth's atmosphere consists primarily of nitrogen (N) in the form of dinitrogen (N_2), and oxygen as well as greenhouse gas (GHG) molecules including water vapour, carbon dioxide (CO_2), nitrous oxide (N_2O) and methane (CH_4). Anthropogenic activity through land use, land use change and intensive agricultural practices has contributed to the increase in ambient concentrations of these GHGs, reaching annual averages of 440 ppm for CO_2, 332 ppb for N_2O and 1866 ppb for CH_4 in 2021. Consequently, this has resulted in changing climatic variables such as increases in global surface temperatures of 0.99 ˚C between 2001 and 2020 relative to the period between 1850 and 1900. In Ireland, the occurrence of extreme climatic events has increased, particularly in last decade, including heatwaves, droughts, storms, heavy precipitation, flooding and extreme cold spells. Emissions of CH_4 and N_2O are important in forcing such climatic events due to their respective global warming (GWP) potentials of 28 and 265 respectively, relative to CO_2 over a lifespan of 100 years. In Ireland, agricultural landscapes are dominated by grasslands, accounting for approximately 58 % of the land surface area in Ireland, of which 40 to 279 kg N ha^{-1} yr^{-1} in the form of inorganic N is applied to grassland pastures depending on the stocking rate for dairy cows (1.0 to > 2.47 LSU/ha^{-1}). Furthermore in 2020, 37.1 % of Irelands total GHG emissions were derived from the agricultural sector, and of this, 57.5 % was derived from enteric fermentation, followed by agricultural soils at 26.8 %, and to a lesser extent manure management, fuel combustion, liming and urea application at 10.3, 3.0, 1.9 and 0.5 %, respectively. The intensification of agriculture to meet the demands of a growing global population has altered the natural production and emission of CH_4 and N_2O. The

formation of CH_4 is catalysed by methanogenic bacteria during anaerobic metabolism where soil organic materials are broken down. In agricultural systems, CH_4 is produced by enteric fermentation from ruminant livestock, accounting for 58 % of Ireland's agriculture derived GHG emissions in 2020. Sources of N_2O include the combustion of fossil fuels, waste management and industrial processes such as the formation of chemical N fertilizers. In Ireland, approximately 1 to 4 % of applied N to agricultural soils as chemical N fertilizers or animal excreta is emitted as N_2O depending on the N loading rate of the inputs as well as environmental conditions which will influence the rate of N_2O emissions produced, such as temperature and soil moisture. In Ireland, agriculture emits 90 % of the nation's N_2O emissions of which 38 % is derived from synthetic fertilizers, 23 % is derived from animal excreta during grazing and 14 % is derived manure management. Soil derived emissions of N_2O are formed as either a by-product of the microbial process of nitrification under aerobic conditions, or as a transitional product of denitrification under anaerobic conditions. The spatial heterogeneity of agricultural soils facilitates the presence of both aerobic and anaerobic microsites existing in close proximity, and gradients of soil conditions that will influence the magnitude of microbial produced N_2O, such as aeration, redox potential, temperature, moisture, substrate availability and N inputs. Following the application of N fertilizer to managed grasslands, N_2O fluxes typically display a peak and decay pattern over time which is characterized by a log-normal distribution, normally lasting between 5 and 20 days. Due to the inherent spatiotemporal variability associated with N_2O emissions from agricultural landscapes, it is still a difficult task to quantify field scale emissions of N_2O with low uncertainties. To date the most commonly used method to quantify field scale emissions of N_2O is the static chamber technique, which consists of taking manual gas samples, mainly once a day and over

small spatial domains, generally less than 1 m^2. Historically, these techniques has been used for investigating treatment effects on N_2O emissions, but due to its limited spatial and temporal resolution, flux measurements are often attributed with high uncertainties. Conversely, micrometeorological techniques, such as eddy covariance (EC) are capable of making continuous, high frequency ecosystem scale (1 km^2) flux measurements of N_2O through recent developments in fast, high precision absorption spectrometers such as quantum cascade lasers (QCL). On the other hand, both high and low flux measurements by EC are integrated over a given area (i.e. the footprint), and therefore it can be challenging to disaggregate between different emission sources over a given spatial domain.

The overarching aims of this thesis were:

1. To investigate the spatial and temporal variability and potential disparity between N_2O flux measurements made using static chambers and EC techniques from a uniformly emitting surface (i.e. a grassland under silage and fertilizer management) and additionally, to assess the methodologies used to analyse and integrate log-normal chamber N_2O flux data (arithmetic and Bayesian statistics) (Chapter 4).

2. To optimize the application and use of both static chambers and EC techniques to quantify N_2O emissions under a more complex, heterogeneous emitting surface (i.e. a grazed managed grassland), where the EC technique provides high resolution, low uncertainty field scale flux measurements, and the static chamber technique assess the source contribution of various N sources from the system in order to upscale localized N_2O flux measurements to the field scale (Chapter 5).

3. To assess the influence of cut and grazing management activities and their associated emissions (CO_2, N_2O and CH_4) on the net carbon (C), net N and net GHG balance (NGHGB) (i.e. the net GHG exchange minus C exports) of the grassland at the field scale (Chapter 6).

Key findings presented in Chapter 4 showed that EC and static chamber N_2O flux measurements were most comparable when N_2O flux values were high (> 115 N_2O-N μg m^{-2} hr^{-1}) and showed spatial and temporal alignment when the chamber sample size was large (n ≥ 15) and the log-normal distribution of the dataset was accounted for using Bayesian statics. Conversely, when the chamber sample size was small (n ≤ 5), the Bayesian model produced large uncertainties due to the inability of the model to constrain an arithmetic mean from a log-normally distributed data set, thus suggesting that greater replication is necessary for constraining the spatiotemporal variability of static chamber flux measurements. Field scale N_2O flux measurements using static chambers with Bayesian statistics (3.13 [± 0.24] kg N ha^{-1}) were closer in magnitude with N_2O flux measurements using EC techniques (3.35 [± 0.5] kg N ha^{-1}), compared to the arithmetic approach (2.98 [± 0.17] kg N ha^{-1}), highlighting the importance of accounting for the log-normal distribution of chamber N_2O flux measurements for quantifying more realistic estimates of field scale missions of N_2O.

In Chapter 5, the field site was under a grazing management regime, where different sources of N were applied in the form of fertilizer and animal excreta. As the EC technique is unable to disaggregate between emission sources, static chambers were used in tandem to quantify emissions from N sources that are characteristic of grazing systems including calcium ammonium nitrate (CAN), the combination of CAN and synthetic cow urine (SU+CAN), and the combination of CAN and dung (dung+CAN).

Mean emission factors (EF) for CAN, SU+CAN and dung+CAN were quantified from four grazing events at 2.78 ± 0.90, 0.59 ± 0.12 and 0.64 ± 0.15 %, respectively, and used to upscale localised N_2O flux measurements using static chambers to the field scale ($F_{CH\ FIELD}$) for comparability with field EC based flux measurements. Similar to the cumulative flux findings observed in Chapter 4, total N_2O-N emissions measured by EC were higher and with lower uncertainties relative to $F_{CH\ FIELD}$ at 6.62 ± 0.33 and of 5.16 ± 2.04 kg N ha^{-1}, respectively. The seven-fold higher uncertainty attributed to $F_{CH\ FIELD}$ measurements relative to EC, was due to the low spatial and temporal resolution of the static chamber technique coupled with a low sample size (n = 5 per treatment per grazing), which collectively makes constraining the uncertainty in static chamber N_2O flux measurements a difficult task. However using the static chamber technique in tandem with the EC technique provided valuable insights into the source contribution of field scale emissions of N_2O from a grazing system. For instance, approximately half of the total N_2O-N losses were derived from animal excreta, one third were derived from CAN and the remaining emissions represented background fluxes. Furthermore, approximately 20 % (1.01 kg N ha^{-1}) of the total N_2O-N flux calculated by $F_{CH\ FIELD}$ occurred during a spring grazing event, where this observation was further reinforced by statistical analysis showing a significant ($p < 0.001$) interaction between N_2O emission and time and treatment. These findings show that the timing of grazing events can have a significant impact on the total annual N_2O-N losses.

Chapter 6 synthesizes the impact that management activities described in chapters 4 and 5 have on the net N, C and overall NGHGB at the field scale by quantifying the N and C imports into and exports out of the grassland system. Findings from this study showed that N imports influenced the net N budget of the grassland, where under

silage management the system had a net neutral N balance of 0.1 ± 6.0 g N m^{-2} yr^{-1}. In contrast, under grazing management where N imports were higher (i.e. from both fertilizer application and animal excreta) and the system transitioned into a net N sink at -17.9 ± 5.5 g N m^{-2} yr^{-1}. The net C balance showed that the grassland was a greater sink of C under a grazing management relative to the cut management at -311.5 ± 81.8 and 61.6 ± 26.7 g C m^{-2} yr^{-1}, respectively. This was mainly due to both larger C exports from silage cuts reducing the C sink, while in comparison, biomass consumed by grazing livestock was recycled back into the system through excretion and additionally, due to a greater capacity for plants to assimilate C during grazing from ungrazed paddock strips while silage cuts removed all available biomass to approximately 4 cm. To assess the impact of emissions of non-CO_2 gases on the NGHGB, budget components and emissions of N_2O and CH_4 were converted to CO_2 equivalents (CO_2eq), by multiplying GHGs by their respective GWPs. Under the cut management, N_2O emissions reduced the net ecosystem exchange (NEE) sink (-2010.8 g CO_2 m^{-2} yr^{-1}) by 7 % (-1870.7 g CO_2eq m^{-2} yr^{-1}), however emissions of N_2O and CH_4 reduced the NEE sink under a grazing management (-1355.3 g CO_2 m^{-2} yr^{-1}) by 20 and 58 % (-296.5 g CO_2eq m^{-2} yr^{-1}), respectively. Overall, the grassland remained a sink of CO_2 with a NGHGB of -86.0 ± 90.1 and -84.4 ± 319.4 g CO_2eq m^{-2} yr^{-1}, under a cut and grazed management respectively. These findings show that at the field scale, both management practices greatly offset CO_2 sinks from temperate grasslands due large C exports from biomass removal from the system, thus limiting the capacity of the system to photosynthesize and also through emissions of non-CO_2 gases and their potent GWPs.

The key results from this thesis offer the following recommendations to the research community: (i) For quantifying field scale emissions of N_2O using the static chamber technique, a minimum of five chamber replicates should be used, but where practically feasible up to 15 chamber replicates should be considered to further reduce the uncertainty in flux measurements and to improve the statistical robustness of N_2O flux datasets; (ii) The frequency of static chamber flux measurements for quantifying baseline emissions should be at least once a week, but should increase to once a day for one to two weeks in order to capture the ecosystem response to additional N in puts from management over time i.e. the peak and decay pattern; (iii) Temporal upscaling of N_2O emissions for single management events can be achieved by using statistical methods which explicitly account for the log-normal distribution of N_2O emissions, for example, Bayesian statistics, however further development of the Bayesian approach is necessary for application to multiple management activities (i.e. fertilizer application and grazing) and interacting emission sources; (iv) To best quantify field scale emissions of N_2O over space and time from managed grasslands, using EC and static chamber techniques in a complimentary fashion is strongly recommended as it enables a more informed quantification of field scale emissions in response to management activities relative to utilizing both techniques in isolation; (v) At the field scale, agricultural practices greatly offset the C sink of the grassland system in this study, namely through C exports from biomass removal and GHG emissions from livestock production. In order to reduce the impact of these systems in forcing climate change, policy makers will be required to incentivise farmers to transition to more sustainable agricultural practices with the aim of preventing large C losses through grazing and harvest cuts, and to increase C inputs through enhanced organic fertilization or increase soil organic carbon (SOC) stocks for example, through biochar

additions below the 30 cm soil horizon where C decomposition rates are low and/or the establishment of multi-sward species with deep and extensive root systems to grassland systems.

Acknowledgements

I gratefully acknowledge the assistance of the following people in the preparation of this thesis:

Mr. Karl Bentley, your unconditional love, support and homemade chips have been the secret to my PhD success.

Bridie, Eugene and Dan Murphy, my biggest fans, thank ye for your love and continuous encouragement.

Dr. Matthew Saunders, to quote ABBA, it feels like you "took a chance on me" and I am forever grateful that you did. Your mentorship has been invaluable and has kept me motivated. Thank you for always believing in me, even when I didn't believe in myself.

Professor Gary Lanigan, your enthusiasm for research is contagious and inspires me in my work constantly. Thank you for your wisdom, guidance and encouragement over the duration of my PhD.

Dr. Nicholas Cowan, thank you for your patience, encouragement and *honest* opinions on my work. Your training and guidance gave me confidence to grow into the type of researcher I did not previously believe I could be.

Dr. Dominika Krol, thank you for your constant supervision, patience and support during my PhD.

Dr. Karl Richards, thank you for your support and trust which allowed me freedom while conducting research.

Dr. Luis Lopez-Sangil, thank you for constantly reminding me that there *is* light at the end of the PhD size tunnel.

Dr. Amanuel Gebremichael, thank you so much for all of your assistance in the field and with my horrific looking spreadsheets. Thank you for bringing joy into my time at Johnstown Castle.

Mr. James Rambaud, thank you for making fieldwork enjoyable and for reassuring me that the sky wouldn't fall in every time we were trouble-shooting the QCL (which was often).

Mrs. Maria Radford, Mr. Dennis Brennan, Mr Gareth Gillen and Mrs. Carmel O'Connor, thank ye all for your diligence and support in the laboratory. PhDs (research in general) are not possible without amazing technical staff.

Mr. Aidan Lawless and all the farm staff at the dairy farm at Johnstown Castle for their support and guidance in affiliating this research.

Ms. Sorcha Kelly, Ms. Rosie O'Neill and Ms. Courtney Doyle, my stunning Wexford roses, thank you all for the nights out, tea breaks and laughter which been a highlight of the last four years.

Ms. Joey Barron, thank you for letting me talk the head off of you regularly, and for making Wexford feel like a home, even when the world was on fire (literally).

Mr. Tom Murphy, thank you for listening to what were inaudible sounds down the phone in response to "*How is the PhD going*?".

To the women in STEM who have been an inspiration to me and whose work has paved the way for my own research, for this I am thankful - Dr. Alina Premrov, Dr. Juliette Maire, Dr. Orlaith Ní Choncubhair, Dr. Anne Wecking, Dr. Stephanie Jones, Ms. Orla O'Halloran, Ms. Marine Valmier and Ms. Ruchita Ingle.

Finally, a quote from my actual hero Taylor Swift. Her words resonate so strongly with me and I believe they do with many others in and outside of academia. I hope to take these words with me on my next adventure.

"*I need you to hear me when I say that there is no career path that comes free of negativity. If you're being met with resistance that probably means you're doing something new. If you're experiencing turbulence or pressure, that probably means you're rising. There might be times when you put your whole heart and soul into something, and it is met with cynicism or scepticism - you cannot let that crush you. You have to let that fuel you because we live in a world where anyone has the right to say anything that they want about you at any time. But just please remember, that you have the right to prove them wrong*."

Table of Contents

List of Figures

List of Tables

List of Abbreviations

ANOVA	Analysis of Variance	BD	Bulk Density
C	Carbon	CAN	Calcium Ammonium Nitrate
CAP	Common Agricultural Policy	C_{CH4}	Carbon lost methane emissions from dung depositions from grazing animals
C_{Dung}	Carbon imported from dung	$C_{Enteric}$	Carbon lost from methane emissions from enteric fermentation by livestock
CH	Static chamber	CH_4	Methane
CH_{All}	All chamber flux measurements averaged using the arithmetic mean	$C_{Harvest}$	Carbon exported through biomass
CH_{Bayes}	All chamber flux measurements averaged using the Bayesian mean	$CH_{Bayes-FP}$	Daily averaged chamber flux measurements within the footprint of the EC tower using the Bayesian mean
$CH_{Bayes-FP}$	Daily averaged chamber flux measurements within the footprint of the EC tower using the Bayesian mean	CH_{FP}	Daily averaged chamber flux measurements within the footprint of the EC tower using the arithmetic mean
C.I.	Confidence Interval	$C_{Leaching}$	Carbon exported through dissolved organic carbon
C_{Milk}	C exported through milk production	CO_2	Carbon dioxide
COVID	Coronavirus disease	C_{Urine}	C imported through urine depositions from grazing animals
CV	Coefficient of Variation	DAFM	Department Agriculture, Forestry and Marine
DOC	Dissolved Organic Carbon	EC	Eddy Covariance
EC_{All}	All eddy covariance measurements over the comparison period	EC_{CH}	Eddy covariance measurements during the time of chamber measurements
EF	Emission Factor	EF_1	IPCC default emission factor for synthetic fertilizers
$EF_{3\ cattle\ -\ dung}$	Irelands Tier 2 emission factor for cattle dung	$EF_{3\ cattle\ -\ urine}$	Irelands Tier 2 emission factor for cattle urine
EF_{3PRP}	IPCC default emission factor for pasture, range and paddocks	EPA	Environmental Protection Agency
$F_{CH\ FIELD}$	Upscaled static chamber N_2O flux measurements	F_{CH}	Chamber flux
F_{EC}	Eddy covariance flux	FP	Footprint
G1	Grazing 1	G2	Grazing 2
G3	Grazing 3	G4	Grazing 4
GC	Gas Chromatography	GCB	Global Carbon Budget
GHG	Greenhouse Gas	GLAS	Green, Low-carbon Agri-environmental Scheme
GPP	Gross Primary Productivity	GWP	Global Warming Potential

H_2O	Water	IPCC	Intergovernmental Panel on Climate Change
KCL	Potassium Chloride	LSU	Livestock Unit
N	Nitrogen	N_2	Dinitrogen
N_2O	Nitrous oxide	N_2O_{CAN}	Cumulative N_2O emissions from calcium ammonium nitrate
$N_2O_{Control}$	Cumulative N_2O emissions from a control	$N_2O_{Treatments}$	Cumulative N_2O emissions from grazing treatments
NBP	Net biome productivity	N_{CAN}	Nitrogen imports from calcium ammonium nitrate
N_{Dung}	Nitrogen imports from dung	NEE_{CO2}	Net ecosystem exchange of carbon dioxide
NEE_{N2O}	Net ecosystem exchange of nitrous oxide	N_{Feed}	Nitrogen imports from animal concentrate feed
NGHGB	Net greenhouse gas balance	NGHGE	Net greenhouse gas exchange
NH_3	Ammonia	NH_4^+	Ammonium
$N_{Harvest}$	Nitrogen exported through biomass removal	$N_{Leaching}$	Nitrogen exported from leaching
N_{milk}	Nitrogen exported from milk	N_{N2}	Nitrogen loss through dinitrogen emissions
N_{NH3}	Nitrogen exported through ammonia volatilization from dung and urine patches	NO_2^-	Nitrite
NO_3^-	Nitrate	NR	Reactive nitrogen
N_{Urine}	Nitrogen imports from urine	O_2	Oxygen
OM	Organic matter	P10	Paddock 10
P11	Paddock 11	PAR	Photosynthetic Active Radiation
QCL	Quantum cascade laser	R^2	Coefficient of determination
SD	Standard deviation	SOC	Soil Organic Carbon
SOM	Soil Organic Matter	SU	Synthetic Urine
TER	Total Ecosystem Respiration	UTC	Coordinated Universal Time
VWC	Volumetric Water Content	W	Vertical Wind Speed
WET	Water content, Electrical conductivity, Temperature	WFPS	Water Filled Pore Space
WPL	Webb-Pearman-Leuning		

Chapter 1: Introduction

1.1 Nitrous oxide emissions in Ireland

Irelands national greenhouse gas (GHG) inventory is dominated by the agricultural sector where approximately 37.1 % of Ireland's GHG emissions are derived from agriculture (EPA, 2019a). The primary GHG emissions from Irelands agricultural sector are methane (CH_4) (64 %) from enteric fermentation in cattle and nitrous oxide (N_2O) (31 %) from nitrogen (N) inputs from fertilizer or animal excreta to agricultural soils, with minor CO_2 emissions (5 %) associated with liming and urea application to pasture and fuel combustion (Lanigan et al., 2018). Emissions of N_2O are intimately linked with the increasing intensification of grassland systems to sustain livestock in order to meet the dietary demands (animal-based proteins) of a growing global population. As a result, there is potential for managed grasslands to act as a significant source of N_2O emissions. Temporal trends in Irelands' N_2O emissions by sector are shown in Fig. 1.1, but for the purpose of this thesis, focus will be attributed to the agricultural sector. Emissions of N_2O from agriculture increased in the late 1990's due to increased N inputs from synthetic fertilizers and animal excreta from larger herd sizes. In the early 2000's, N_2O emissions steadily decreased in response to a reduction of inorganic and organic N applications to soils as part of the Common Agricultural Policy (CAP) reform on animal numbers. However, between 2015 and 2019, increases in N_2O emissions were observed as a result of increased growth in the dairy sector and the use of N fertilizers (EPA, 2019b).

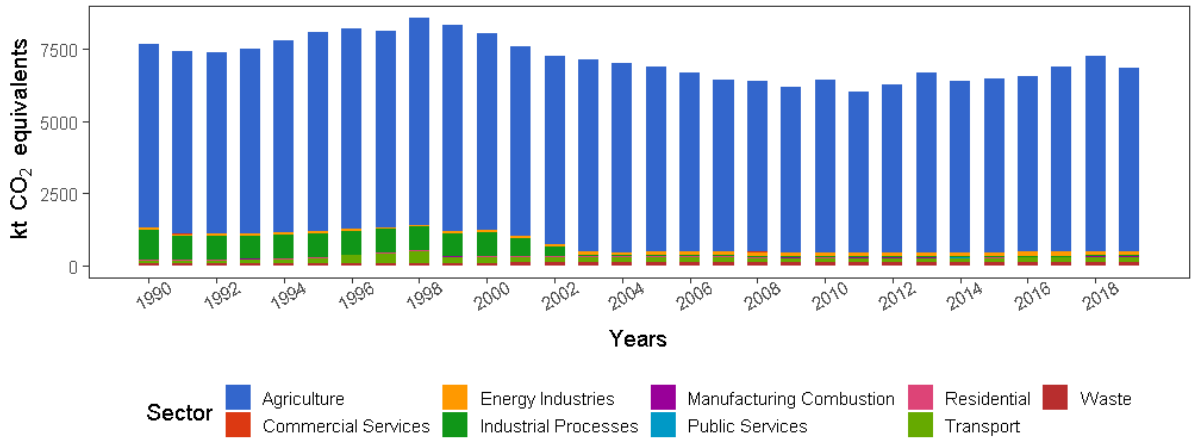

Figure 1.1: Nitrous oxide emissions by sector from 1990 to 2019. Data was sourced at https://www.epa.ie/our-services/monitoring--assessment/climate-change/ghg/summary-by-gas/#d.en.84384.

The production of N_2O in grasslands soils is mediated by the nitrification of nitrite (NO_2^-) to nitrate (NO_3^-) and subsequent denitrification of NO_3^- to N_2O. External N inputs to managed grasslands has essentially disrupted the natural soil N cycle, i.e. the balance between N_2O produced in the soil and its microbial transformation to inert N compounds to the atmosphere (Syakila and Kroeze, 2011, Wecking, 2021). The magnitude and duration of N_2O emissions depends on the complex interaction between climatic conditions and management practices that increase N inputs into the system, as well as altering the physical and chemical properties of the soil. The interaction between these variables forms a heterogeneous environment for N_2O production, thus making it challenging to accurately quantify, understand and mitigate emissions of N_2O (Voglmeier et al., 2019, Wecking, 2021). To date the most commonly used method to quantify N_2O emissions from agricultural soils is the static chamber technique (Rochette, 2011, Lammirato et al., 2018), as it is easy to deploy, inexpensive to operate, has many standardized protocols and is suitable for investigating treatment effects on N_2O emissions (de Klein and Harvey, 2015). However, individual static

chamber N_2O flux measurements are made over spatial areas less than 1 m^2 and under a low temporal resolution (e.g. once per week) and therefore, flux measurements are often associated with large uncertainties. It is only in more recent years that field scale flux measurements of N_2O at greater spatial scales and temporal frequencies have become available through the development of high frequency gas analysers such as quantum cascade laser (QCL) absorption spectrometers. When QCLs are incorporated into micrometeorological techniques such as eddy covariance (EC), near-continuous measurements of N_2O fluxes over large spatial domains (1 km^2) are made possible (Cowan et al., 2020, Liang et al., 2018, Wecking et al., 2020b). Prior to this study, there has only been one other EC station monitoring field scale fluxes of N_2O in Ireland that investigated the contribution of N_2O emissions to the GWP of a managed grassland, as well as the impact management has on N_2O emissions (Leahy et al., 2004, Scanlon and Kiely, 2003). Investigations comparing micrometeorological measurements of N_2O with the static chamber technique are necessary to determine the applicability of this new analytic approach in determining national N_2O emission inventories (Jones et al., 2011), as well as bridging the gaps in our understanding of the processes governing emissions at the field scale and thus leading to the development of enhanced agricultural mitigation strategies.

1.2 Project information

The funding for the Manipulation and Integration of Nitrogen Emissions project (grant number 15S655) was provided under the National Development Plan, through the Research Stimulus Fund, administered by the Department of Agriculture, Food and the Marine. This project was led by Teagasc in collaboration with Trinity College Dublin.

The field and laboratory analyses of this work were carried out in Teagasc, Johnstown Castle, Co. Wexford, Ireland.

1.3 Thesis objectives

The primary aim of the thesis was to investigate the spatial and temporal variability in N_2O emissions from an intensively managed temperate grassland using the static chamber and EC techniques, and to assess the impact that field scale management activities have on the climate mitigation potential of grasslands. Few studies have investigated flux dynamics from managed grasslands at different temporal and spatial sales and as a result, there is still significant uncertainty surrounding the impact agricultural practices have on soil N and C cycling and the exchange of N_2O between the atmosphere, soil and vegetation. The individual objectives of this thesis are therefore;

I. To assess the disparities and uncertainties in quantifying N_2O emissions at different spatiotemporal scales from a cut and fertilized managed grassland using the static chamber and EC technique, as investigated in Chapter 4.

II. To quantify N_2O emissions from a grazed grassland by utilizing the EC technique to measure high frequency, low uncertainty field scale fluxes and in tandem, use the static chamber technique to quantify the contribution of different N sources from grazed grasslands (i.e. fertilizer, and the addition of fertilizer to dung and urine) to both upscale localized N_2O flux measurements to the field scale, as investigated in Chapter 5.

III. To determine the impact agricultural practices have on the mitigation potential of managed grasslands to act as C, N and GHG sink at the field scale, as investigated in Chapter 6.

1.4 Thesis structure

This thesis consists of seven chapters. Chapter 1 provides a brief overview of Ireland's N_2O emissions, the microbial production of N_2O, the methods used to quantify N_2O emissions and the thesis objectives. Chapter 2 summarizes the background knowledge on the subject, identifies the gaps in the literature and highlights the necessity for the research conducted in this PhD thesis. Chapter 3 describes the methodological approaches used in the research chapters 4, 5 and 6, and explains their respective experimental set ups. Chapter 4 explores the application of the static chamber and EC technique in quantifying N_2O emissions over various spatiotemporal scales from a uniformly emitting surface (i.e. fertilizer application), and the application of log-normal statistics in constraining the uncertainty associated with chamber based N_2O flux measurements. The outcomes from this chapter provide recommendations that are applicable to similar future studies on how to optimize static chamber and EC techniques for robust field scale measurements of N_2O emissions. Chapter 5 investigates how best to quantify N_2O emissions from a heterogeneous emitting surface (i.e. from a grazing management) by using the static chamber and EC technique in tandem. Interactions between sources of N from grazed grasslands on N_2O emissions and their contribution to the total N_2O-N losses were assessed, and highlighted the necessity for quantifications of N_2O losses from interactive N sources (i.e. fertilizer applied in combination with dung and fertilizer applied with urine), as they best represent hotspots of N_2O from grazed pastures. Chapter 6 evaluates how the

management activities described in Chapters 4 and 5 influenced the capacity of the grassland to act as a sink of N, C and GHGs, and illustrates how changes in management regimes (i.e. a cut or grazing management) contribute differently to storing and removing C from grasslands, and emitting non-CO_2 GHGs. Chapter 7 synthesizes and discusses the key findings outlined in Chapters 4, 5 and 6 while also illustrating the limitations of these studies and the areas of research which require further exploration. This chapter outlines the applicability of the work presented in this thesis to further improve quantifying N_2O emissions in space and time from managed grasslands and the implications for improving the development of GHG mitigation strategies in the agricultural sector.

Chapter 2: Literature review

2.1 Climate change

Climate change is defined as the long-term changes in the Earth's temperature and weather patterns (Pachauri et al., 2014), and over the last century, changes in climate patterns have accelerated faster than ever before (Bereiter et al., 2015, Neukom et al., 2019). Between 2001 and 2020, mean global surface temperatures were 0.99 °C higher than the period between 1850 to 1900, with larger increases over land at 1.56 °C compared to oceans at 0.88 °C (IPCC, 2021a). In the Sixth Assessment Report (AR6) by the Intergovernmental Panel on Climate Change (IPCC), it was projected that for every 1 °C rise in global temperatures, extreme rainfall events will intensify by 7 % (IPCC, 2021a). Moreover, the AR6 also outlined the high likelihood of warmer climates intensifying very wet and dry weather and climatic events such as flooding or drought. Additionally, a 2 °C rise in global warming by the middle of the 21st century would exceed critical thresholds for the global agriculture sector (IPCC, 2021a). The driving force behind such adverse climate change is the input of anthropogenic greenhouse gases (GHGs) e.g. carbon dioxide (CO_2), nitrous oxide (N_2O) and methane (CH_4) associated with human activities such as fossil fuel burning, land-use change and intensive agriculture. These GHGs contribute to global warming by absorbing and trapping and then re-emitting longwave infrared radiation from the Earth's surface. There has been an overall consistent increase in the concentrations of these GHGs since the Industrial Revolution in 1750 as a result of human activity, and as of 2021 ambient concentrations of CO_2, N_2O and CH_4 were measured at 414 ppm, 334 ppb and 1888 ppb, respectively (NOAA, 2021). It is clearly outlined in the AR6 that human activity has been the primary cause for observed increases in ambient concentrations of GHGs

since the pre-Industrial Era. The consequences of high atmospheric concentrations of these GHGs is the occurrence of more frequent and extreme climatic events, such as heatwaves, droughts, heavy precipitation, storms and subsequent flooding. More over, extreme climatic events harbour significant global economic losses, accounting for USD 268 billion in infrastructure damages globally in 2020 (AON, 2020). The adverse effects of climate change can and have affected the agricultural sector, where drought conditions can cause nutrient immobilization and salt accumulation in soils, resulting in dry, saline and infertile soils and likewise, extreme flooding can erode the top soil and associated nutrients, resulting in reduced rates of crop productivity (Arora, 2019). During June and July 2018, Ireland experienced prolonged high temperatures, low rainfall and dry conditions which subsequently led to a severe drought which had various implications for Irish agriculture. For example, reduced crop yields from spring sown crops, as well as a decrease in the average farm income by 15 %, with greater reductions of 31 % from dairy farming systems due to inflation in animal feed costs (Dillon et al., 2019). Ultimately, climate change has the potential to threaten food security with a high likelihood of reduced production and subsequently inflated food prices if the current situation with GHGs emitted from agriculture and climate change persists. Ultimately the task of providing for an ever increasing global population is all the more challenging and as a result, there is an urgent need to better constrain the nitrogen (N), carbon (C) and GHG budgets of agricultural systems and to then develop and implement mitigation strategies which both maintain productivity within the agricultural sector without causing additional environmental harm in the form of increased GHG emissions.

2.2 Grasslands – a potential tool for climate change mitigation

Grasslands are ecosystems that are dominated by herbaceous vegetation, namely grasses, sedges and rushes and by this definition, grasslands account for 40.5 % or 52.5 million km^{-2} of global terrestrial area (Suttie et al., 2005). Managed grasslands are agricultural landscapes used to intentionally grow grasses or herbaceous forage for grazing and/or silage cuts for winter based feed (JKI, 2021). Such managed pastures represent 26 % of the global land surface area and 33 % of the land surface area within Europe, both of which are comparable with Ireland where 58 % of the land surface area is devoted to managed grasslands (CSO, 2020, Lemaire et al., 2011a, Van den Pol-van Dasselaar et al., 2019). Owing to the large spatial domain that managed grasslands occupy, these landscapes play a vital role in controlling rates of GHG emissions from the agricultural sector. The rate at which atmospheric CO_2 is sequestered, i.e. captured and stored in the vegetation or soil, will depend on two factors – the net C flow through the soil-plant-atmosphere continuum, which will equate to the difference in plant photosynthesis and plant respiration, and secondly, the mean residence time of C within vegetation and the soil (Lemaire et al., 2011b). The residence time of C within vegetation is relatively short, between 1 and 2.5 years due to the brief leaf lifespan of grassland species and the high decomposition rates associated with leaf litter (Klumpp et al., 2009). However, this will vary according to management where vegetation may be consumed by grazing animals prior to senescence, resulting in losses of C to the atmosphere in the form of CO_2 and CH_4 through animal respiration, enteric fermentation and excretal deposition. In contrast, the residence time in grassland soils is far greater, ranging between 1 to >1000 years, where C in the form of soil organic matter (SOM) is integrated into the soil through various pathways (Lemaire et al., 2011a), for example, from leaf litter incorporated by earthworms within soil micro-

aggregates, as well as organic matter inputs from excreta depositions by grazing animals (Lemaire et al., 2011a). It is important to note however, that the residence time of C in soils and subsequently plant productivity, will vary depending on the C:N ratio of the fresh organic matter inputs and as well as soil fertility, as N is linked to C by soil microbial processes (Lemaire et al., 2011a, Tateno and Chapin Iii, 1997). For example, on fertilized soils, plants that have low C:N ratios (i.e. high N concentrations in the foliage) and a high assimilation rate (i.e. the uptake of C from atmospheric CO_2 to form organic compounds), will return leaf litter with a low C:N ratio to the soil (Tateno and Chapin Iii, 1997). This in turn, stimulates N mineralization due to the low C:N content of the leaf litter, and promotes further plant growth and the potential to assimilate C through photosynthesis. In contrast, the opposite can be true for infertile soils, where the C:N ratio of leaf litter will be high, thus reducing the rate of N mineralization and in turn plant growth and C assimilation (Tateno and Chapin Iii, 1997). The management of grassland soils is therefore an important factor in determining the capacity of these systems to store C, however, it is projected that the intensification of managed grasslands will increase in order to meet the dietary demands of an increasingly growing global population (Shukla et al., 2019). If the enhanced intensification of agricultural practices is not undertaken sustainably, it is estimated that global GHG emissions from agriculture (mainly from crop and livestock activities at the farm scale) are likely to increase by approximately 30-40 % by 2050 (Shukla et al., 2019). Therefore understanding the impact management practices have on grasslands and the associated biogeochemical cycles is crucial in both dictating and optimizing the mitigation potential of managed grasslands against climate change.

2.3 Biogeochemical cycles

2.3.1 The terrestrial global carbon cycle

The C cycle describes the movement of C as it is recycled and reused through the Earth system as well as the long-term (>1000 years) processes of C sequestration to remove C from the atmosphere and store it within soils and vegetation. An overview of the terrestrial global carbon cycle is shown in Fig 2.1. Atmospheric CO_2 corresponds to a mass of 828 Pg C yr^{-1} (Joos et al., 2013, Prather et al., 2012), where the removal of CO_2 from the atmosphere is mediated by plant photosynthesis, where light energy is used to split molecules of CO_2 and water into carbohydrates and oxygen for plant cellular function. The amount of CO_2 converted to carbohydrates is known as the gross primary productivity (GPP) and globally accounts for the assimilation of 123 Pg C yr^{-1}. Part of the C which is fixed in plants by photosynthesis can be returned back into the atmosphere by autotrophic (plant) and heterotrophic (animals and soil microbes) respiration, where the sum of both make up the total ecosystem respiration (TER). Approximately 119 Pg C yr^{-1} is returned to the atmosphere through TER. The difference between the GPP and the TER gives the total net ecosystem exchange (NEE), which subsequently accounts for a net sink of 4 Pg C yr^{-1} stored globally in terrestrial systems. However this value is only representative of the net CO_2 balance and not the total C balance, as C can also be imported and exported from terrestrial ecosystems through dissolved C and agricultural management such as organic inputs through slurry fertilizer applications and biomass removals from harvest cuts and/or grazing (Jones et al., 2017, Merbold et al., 2014, Myrgiotis et al., 2021). By quantifying these C imports and exports we can then develop a more robust assessment of the net biome productivity (NBP) which describes the net rate of C uptake or loss by subtracting additional C inputs and outputs from the NEE.

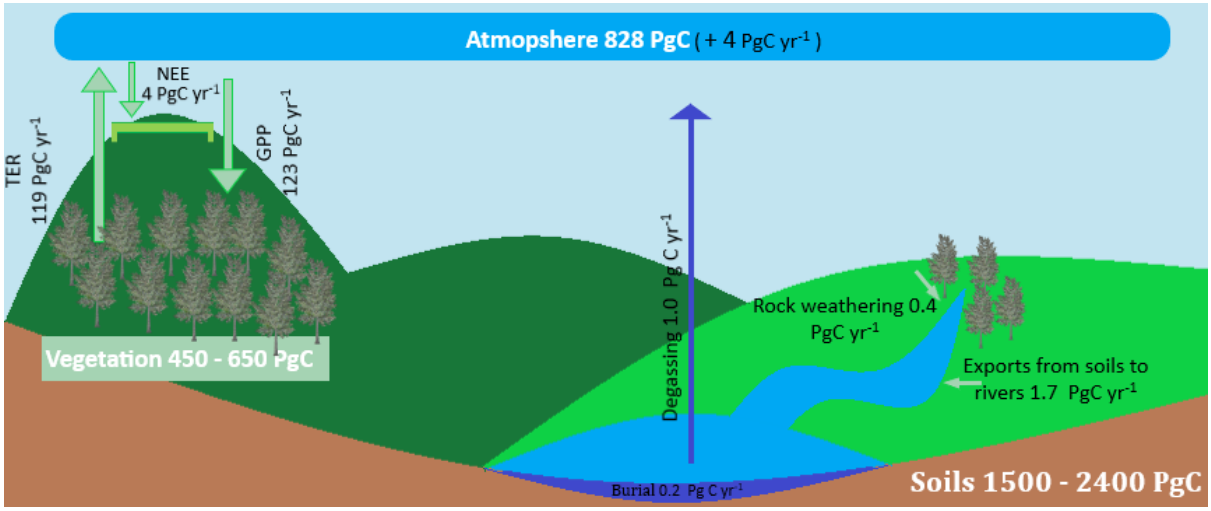

Figure 2. 1: The global terrestrial carbon cycle adapted from Ni Choncubhair (2014). Values are derived from Ciais et al. (2014) where white numbers represent carbon stocks in PgC and black numbers represent annual C exchange fluxes in Pg C yr^{-1} over the period between 2000 and 2009. TER is the total ecosystem respiration, GPP is the gross primary productivity and NEE is the net ecosystem exchange i.e. the difference between GPP and TER.

To date, there is a lot of uncertainty surrounding the potential of managed grasslands to serve as a sink of C, where previously published studies have shown rates of C sequestrations ranging between 15 to 587 g C m^{-2} yr^{-1} (Chang et al., 2015, Jones et al., 2017), others have highlighted that the intensification of managed grasslands has transitioned these systems to net sources of C at a rate of between 29.1 to 266 g C m^{-2} yr^{-1} (Jones et al., 2017, Soussana et al., 2007). Variability in previously reported C budgets are likely due to differences in weather and soil conditions between studies as well as management activities such as the timing and frequency of cut and grazing events as well as differences in the type and amount of N inputs. Moreover, as the residence of soil C in grasslands spans over many hundreds of years, therefore the legacy effects of land use and land management will also influence the amount of C quantified over a given period of time (Smith, 2014). Often comparing the net C balance

or NBP between studies is complicated due to inconsistency of variables within respective budgets. As a result, there is an urgent need for robust data on the implications that management practices have on the net C source or sink strength of grasslands, and subsequently their climate change mitigation potential.

2.3.2 The nitrogen cycle

The C and N cycle are intrinsically linked through plant productivity where CO_2 is assimilated through photosynthesis using N containing organelles (i.e. chorophyll) and compounds (for e.g. ATP and NADH) and therefore, the net C assimilation rate in plants (and consequently net primary productivity) is a function of leaf N content (Tateno and Chapin Iii, 1997). Prior to the Industrial Era, the creation of reactive N ([N_r]; all N nitrogen species except dinitrogen [N_2]) occurred primarily through biological nitrogen fixation (NBF) (Galloway et al., 2003), by a specialized group of prokaryotes, for example, *Rhizobium* and *Bradyrhizobium* that form a symbiotic relationship with legumes and other plants (Postgate, 1982). The prokaryotes utilize the enzyme nitrogenase to catalyse the conversion of atmospheric N_2 to ammonia (NH_3) (Fig. 2.2). In addition to this, atmospheric deposition provides inorganic forms of ammonium (NH_4^+) and nitrate (NO_3^-) as additional N sources into terrestrial ecosystems (Boring et al., 1988, Ghaly and Ramakrishnan, 2015). Gaseous species of N_r are readily available to undergo a series of plant-soil biochemical transformations that are mediated through plant litter production, the decomposition of soil organic matter (SOM) and the redox potential of the soil (Buffam and Mitchell, 2015, Tipping et al., 2016). Such transformations include the mineralization of organic forms of N (NH_3) into ammonium (NH_4^+) from the decomposition of SOM by microbial communities. The rate of soil mineralization of N will vary depending on the C:N content of the soil organic

matter deposited into the soil, where low C:N ratios of organic matter will enhance N mineralization and conversely a high C:N with reduce the rate of N mineralization (Tateno and Chapin Iii, 1997). Under anoxic/anaerobic conditions, the process of denitrification occurs whereby denitrifying microbes use NO_3^- as a terminal electron acceptor, producing N_2O and N_2. The balance between partial denitrification to N_2O and total denitrification to N_2 is primarily driven by soil redox potential, with a higher N_2/N_2O ratio at lower redox potentials (Stevens and Laughlin, 1998). Additional Nr losses of inorganic NO_3^- through leaching can occur during periods of intense and heavy rainfall as NO_3^- is negatively charged and so cannot bind to silt/clay particles (Chapin III et al., 2011).

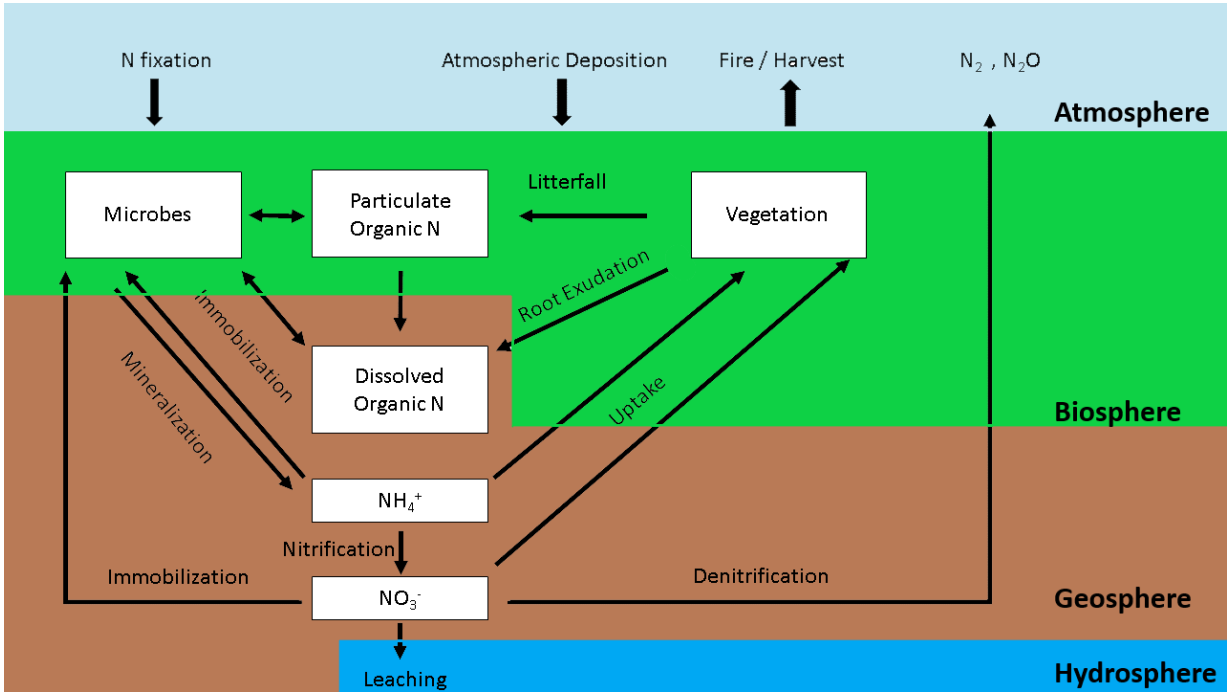

Figure 2. 2: Simplified illustration of the terrestrial nitrogen cycle adapted from Buffam and Mitchell (2015). White boxes represent major nitrogen pools and arrows represent fluxes.

2.3.3 Anthropogenic impacts on the nitrogen cycle

The global N cycle has been disrupted by human activity with N_r increasing by 150 Tg N yr^{-1} between 1860 and 2000, primarily through food production activities such as the production and application of synthetic fertilizer and leaching of N_r that is not assimilated by crops (Galloway and Cowling, 2002, Galloway et al., 2003). The anthropogenic pressures on agricultural land to produce food are likely to increase as it is estimated that the global population increases by 0.9 % or 80 million per year, with a projected population of 9.74 billion by 2050 (United Nations, 2019). However the natural supply of N_r is not sufficient to sustain current or future population growth (Galloway et al., 2008). It was only through the invention of the Haber-Bosch process, where N_r is combined with hydrogen to produce NH_3 under high pressures and temperatures, that the nutrient limitations of agricultural land was overcome using synthetic fertilizers. In managed grasslands, synthetic N fertilizer and animal excreta account for the majority of additional N_r (Davidson, 2009, Tian et al., 2016). In 2019, global estimates of N_r emissions from managed soils in the form of N_2O from synthetic fertilizers and animal manure accounted for 2.88 and 0.71 Tg N, respectively (FAOSTAT, 2021). The N loading rate of a cow dung or urine patch can be as high as 1020 kg N ha^{-1} (Chadwick et al., 2018) and 2000 kg N ha^{-1} (Selbie et al., 2015), respectively, making animal excreta prone to high losses of N_r. Where N_r from N fertilizer, dung and urine are in excess of plant demands, the negative consequences can be far reaching within the Earth's systems known as the N cascade (Galloway et al., 2008). These impacts include, eutrophication of aquatic and terrestrial systems as well as biodiversity loss in N sensitive ecosystems (Pitcairn et al., 2002), the production of tropospheric ozone and aerosols that have negative impacts on human health including respiratory illnesses, cardiac disease and cancer (Follett and Follett, 2001,

Wolfe and Patz, 2002), acidification of terrestrial and aquatic ecosystems (Gao et al., 2014) and increases in N_2O emissions (Skiba et al., 2005). In addition to this, grazing and cut managements decouple the natural soil N and C cycles by (1) biomass removal either by cutting or grazing animals which reduces the photosynthetic capacity for grasslands to assimilate C (Gitelson et al., 2014); (2) biomass consumed by grazing animals is returned to the atmosphere by releasing digestible C as CO_2 and CH_4 from enteric fermentation (Soussana and Lemaire, 2014); (3) N is excreted to the soil surface as dung and urine, and prone to leaching where the stocking density is high and consequently the density of urine patches is large (Ledgard et al., 2009) and finally; (4) emissions of CH_4 from grazing animals and N_2O from animal excreta and synthetic fertilizers can offset the soil C sequestration and deteriorate the net GHG balance (Jones et al., 2017, Soussana et al., 2010). To date there have been few investigations into the implications N_r has on C balances (Jones et al., 2017, Merbold et al., 2014, Wecking et al., 2020b) despite the necessity of such data for understanding GHG dynamics in managed grassland systems, and developing appropriate sustainable agriculture practices.

2.4 Nitrous oxide

It is estimated that global N_2O emissions reach 17.7 Tg N per year of which 6.7 Tg are derived from human activity and of this, agricultural soils account for 2.8 Tg N yr^{-1} (Menon et al., 2007). Ambient concentrations in N_2O have steadily increased since 1750 (Industrial Revolution), where pre 1750 atmospheric concentrations of N_2O were 280 ppb and today are at an unprecedented 332 ppb (IPCC, 2021a). According to Ehhalt et al. (2001), atmospheric concentrations of N_2O over the next century are projected to rise to between 350 to 460 ppb under all IPCC emission scenarios outlined

in Nakicenovic et al. (2000). The global warming potential (GWP) (i.e. the radiative efficiency in W m^{-2} pbb^{-1}) of a GHG is defined as how much energy the emissions of 1 tonne of a gas will absorb over a given period of time, compared to the emissions of 1 tonne of CO_2 (EPA, 2020). The GWP of N_2O is approximately 265 over a lifespan of 100 years, making N_2O an extremely potent GHG in terms of driving climate change.

2.4.1 Soil microbial production of nitrous oxide emissions

The majority of N_2O produced is through the microbial pathways of nitrification by autotrophic aerobic nitrification by ammonia-oxidizing bacteria and nitrite-oxidizing bacteria and denitrification by anaerobic denitrification by denitrifying bacteria (Signor and Cerri, 2013). Additional microorganisms involved in denitrification and nitrification include anammox bacteria which can convert NH_4^+ and NO_2^- into N_2 under anaerobic conditions, some fungi are involved in both denitrification and codenitrification which can produce N_2 and N_2O (Rex et al., 2018), and archeae have previously been reported to stimulate denitrification in soils (Hayatsu et al., 2008). Non-biological processes can also produce a small fraction N_2O including chemidenitrification, which is the chemical decomposition of nitrite [NO_2^-], and hydroxylamine (NH_2OH) oxidation, although the N_2O produced in these processes are considered negligible (Bremner, 1997, Bremner et al., 1980). In the oxidation of NH_4^+ to NO_3^-, the intermediate compound NH_2OH is cable of producing more N_2O relative to the chemidentrification process (Bremner, 1997).

The form of N_r emitted from soils is heavily determined by nitrification and denitrification, and as both microbial pathways are intimately linked, they essentially dictate the rate of N_2O exchanged across the soil – plant – atmosphere continuum. (Butterbach-Bahl et al., 2013, Harris et al., 2021, Norton and Ouyang, 2019).

Nitrification is the aerobic oxidation of NH_4^+ to NO_3^- and occurs in a two-step process (Signor and Cerri, 2013); (1) nitritation; the oxidation of NH_4+ to NO_2^- by *Nitrosomonas* sp., *Nitrosococcus* sp, and *Nitrosospira* sp. (Eq. 2.1) and (2) nitration; where NO_2^- from nitritation is further oxidized to NO_3^- (Eq. 2.2)

$$2NH_4^+ + 3O_2 \rightarrow 2NO_2^- + H_2O + 4H^+ + energy \quad \text{Equation 2.1}$$

$$2NO_2^- + O_2 \rightarrow 2NO_3^- + energy \quad \text{Equation 2.2}$$

Complete denitrification is the anaerobic reduction of NO_3^- formed from nitrification, to N_2 (Eq. 2.3), however where denitrification is incomplete, a greater proportion of NO_3^- is converted to N_2O instead of N_2 (Smith, 2010)

$$5(CH_2O) + 4NO_3^- + 4H^+ \rightarrow 5CO_2^- + 7H_2O + 2N_2 + energy \quad \text{Equation 2.3}$$

Both nitrification and denitrification can occur simultaneously where soil conditions are favourable for both processes in adjacent microsites. In coupled nitrification – denitrification, NO_2^- or NO_3^- produced during nitrification can be used by denitrifers (Wrage et al., 2001). Early work by Khdyer and Cho (1983) measured both nitrification and denitrification activity within a soil column treated with urea and under steady-state O_2 gradients. Nitrification occurred in the aerobic surface layer, while denitrification activity was observed within the anaerobic sites. The authors showed that N_2O was predominately produce along the boundary of anaerobic – aerobic conditions where the GHG diffused towards the soil surface, suggesting that N_2O emissions were greatest under conditions that were partially optimal for both nitrifiers and denitrifers. It is important to note that coupled nitrification – denitrification and nitrifier denitrification are different microbial pathways that produce N_2O. Nitrifier denitrification is a pathway of nitrification where autotrophic

NH_3-oxidizers facilitate the oxidation of NH_3 to NO_2^- followed by the reduction of NO_2^- to N_2O and N_2 (Wrage et al., 2001). A summary of the key soil microbial pathways for the production of N_2O can be seen in Fig. 2.3

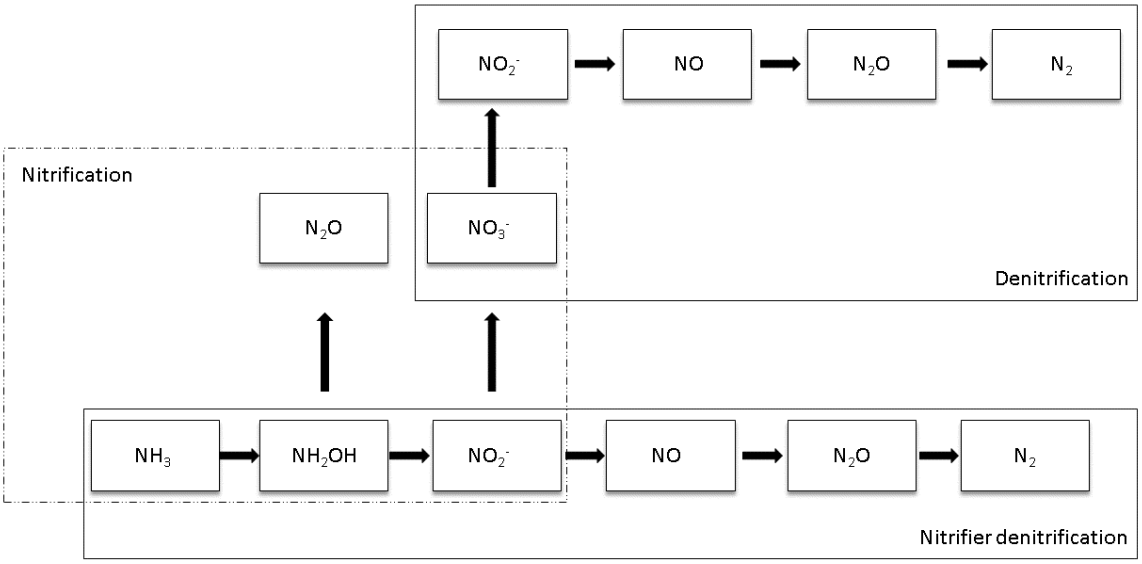

Figure 2. 3: Simplified diagram of the soil microbial processes that produce N_2O. Adapted from Wrage et al. (2001).

2.4.2 Drivers of soil nitrous oxide emissions

As previously discussed, the production of N_2O in soils is mediated by microbial processes of nitrification and denitrification which are dependent on a combination of factors including, soil oxygen concentrations, soil temperature, soil moisture, the soil C:N and N_2O:N_2 ratio, nutrient availability and soil texture (Bremner, 1997, Butterbach-Bahl et al., 2013, Cameron et al., 2013, Zhu et al., 2020). For example, in dry, well aerated and drained, coarse textured soils, nitrification will dominate N_2O production. In contrast, wet, poorly aerated soils with a high C content and a fine texture, N_2O production will mainly be driven by denitrification (Signor and Cerri,

2013). The microbial and ecological elements that control the production of N_2O in soil can be described by the conceptual model of Firestone and Davidson (1989) , known as the "hole-in-the-pipe" (Fig. 2.4). The analogy of a leaky pipe represents the production and consumption of N_2O. The flow of N through the pipe characterizes the total rate of nitrification and denitrification which is regulated at the cellular level by oxygen availability, substrate availability (NH_3, NH_4^+ and NO_3^-) and electron donor availability. The size of the holes along the pipe are a function of the presence of favourable environmental conditions for the microbial production of N_2O, and relate to the amount of gas released (Signor and Cerri, 2013, Wecking, 2021).

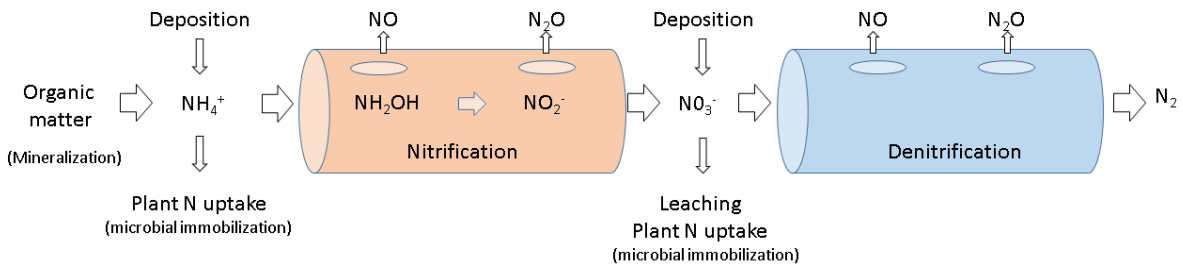

Figure 2. 4: "Hole-in-the-pipe" model by Firestone and Davidson (1989) adapted from Inatomi et al. (2019)

As the redox potential of soils is a key regulator of whether N_2O production will be stimulated by nitrification or denitrification, soil moisture (i.e. the water-filled pore space[WFPS]) is considered a significant driver of N_2O (Davidson, 1991). Linn and Doran (1984) illustrated that variation in the WFPS could dictate whether nitrification or denitrification was occurring, for instance up to a maximum WFPS of 60 %, nitrification increases linearly and thereafter decreases while anaerobic denitrification is considered negligible at a WFPS of 60 % but increases towards saturation with increased soil moisture. At a WFPS of between 60 to 80 % maximum

rates of N_2O production have been observed (Rafique et al., 2011) however where the WFPS exceeds 80 % (i.e. approaching water logged soil conditions), complete denitrification occurs and the ratio of N_2O:N_2 decreases. Furthermore, Congreves et al. (2019) showed the simultaneous occurrence of nitrification and denitrification at a soil WFPS of between 53 and 78 %. The redox potential of soils is also mediated by soil temperature where a positive feedback between denitrification and temperature exist as increasing soil temperature enhances soil microbial activity and consequently soil respiration, which in turn depletes the soil of oxygen creating an increase in anaerobic sites for denitrification (Signor and Cerri, 2013, Wang et al., 2021). Soil temperature also influences the ratio of N_2:N_2O, for example, Maag and Vinther (1996) found that the N_2:N_2O increased exponentially with increasing temperature. Lai and Denton (2018) reported a temperature threshold of 35 °C for maximum N_2O emissions, past which N_2O emissions production reduced and N_2 production increased.

The amount of N_2O emissions produced is also governed by management practices, i.e. fertilizer application and/or grazing, as this activity determines the soil N input which is predominately in the form of NH_4^+ and NO_3-, while also adding organic C. Previously reported N_2O emission factors (EFs) (i.e. the percentage of N applied lost as N_2O) from synthetic N fertilizers have ranged from 0.58 to 8.3 % (Cardenas et al., 2019, Harty et al., 2016, Velthof and Losada, 2011), which is considerably larger than the refined Intergovernmental Panel on Climate Change (IPCC) default value for synthetic fertilizers (EF_1) in wet temperate climate zones at 1.6 % (1.3-1.9 %). Variability in reported N_2O emissions from agricultural landscapes is likely due to differences in management activity (e.g. N inputs), soil and environmental conditions which are site specific and additionally, interactions between these variables which will vary over

space and time. Earlier N_2O emissions reported from grazing systems (urine and/or dung) have ranged from 0.0027 to 0.95 %, which is within range to the IPCC revised EF for pasture range and paddocks (EF_{3PRP}) for cow urine and dung of 0.6 % (0 – 2.6 %) for wet temperate climates (Chadwick et al., 2018, Hyde et al., 2016, Krol et al., 2016, Simon et al., 2018). Additionally, the N loading rate from such management activities affects the total amount of N_2O emissions lost from agricultural landscapes. For example, annual N_2O emissions from a winter wheat sown pasture treated with 400 kg N ha^{-1}in the form of CAN produced emissions that were nearly twice as high as pastures treated with 220 kg N ha^{-1} at 0.56 % and 0.34 %, respectively, emitted as a proportion of the N applied (Lebender et al., 2014).

2.4.3 The spatial and temporal variability of nitrous oxide emissions in managed grasslands

As previously discussed, soil properties, environmental conditions and agricultural management influence the rate of N_2O emissions but these variables change over space and time, thus making N_2O emissions extremely variable both spatially and temporally. Studying N_2O emissions from intensively managed grasslands is challenging due to the heterogeneity of fertilizer and grazing related N inputs applied to these systems. This can result in high N inputs to small areas across the pasture, which are liable to create brief but high rates of N_2O emissions known as hotspots. Hotspots of N_2O occur where multiple factors which favour the microbial production of N_2O occur simultaneously. For example, near water troughs or gateways, grazing animals are prone to congregate and the soil compaction created by grazing animals' results in localized changes to the soil bulk density, reducing the macro-pore space and subsequently increase the WFPS, thus altering the redox potential of the soil. When combined with additional N inputs from urine and dung depositions, this favours the microbial production of N_2O (Abbasi

and Adams, 2000). Abdalla et al. (2009b) showed that modelled N_2O emissions from an intensively managed Irish grassland increased by 62 % when the bulk density of the soil increased from 1.4 to 1.8 g cm^{-1} (29 % increase). Hotspots of N_2O have also been observed within managed grasslands, for example, Cowan et al. (2015) reported N_2O fluxes ranging from 2 to 79,000 µg N_2O-N m^{-2} hr^{-1} from a livestock farm in Scotland and showed that 55 % of N_2O fluxes were derived from 1.1 % of the field area which represented shaded areas where sheep congregated in warm weather and manure heaps.

Furthermore, the temporal variability of N_2O emissions adds to the complexity of accurately quantifying N_2O fluxes from managed grasslands. Due to the episodic nature of N_2O emission events, it remains a difficult task to measure patterns of short-lived N_2O pulses over time from managed pastures (Barton et al., 2015, Song et al., 2021). Hot moments of N_2O exhibit disproportionally high rates of emissions over a short time frame, relative to longer periods of time (McClain et al., 2003). Such emission events can occur either as a result of agricultural practices where external N inputs are added to the system, enhancing substrate availability for the microbial production of N_2O or as a result of the heterogeneity of soil properties where favourable conditions for nitrification and denitrification can co-occur resulting in elevated baseline emissions (Congreves et al., 2019, Song et al., 2021). Such events are a common phenomenon within managed grassland systems, for example, Li et al. (2015) reported hot moment events from a managed grassland in Japan of 114.46 µg N m^{-2} hr^{-1} 9 days following harvest, and 109.90 µg N m^{-2} hr^{-1} and 206.83µg N m^{-2} hr^{-1} 13 days after fertilizer application. The authors also observed that fertilizer application coincided with 60.4 % of the total N_2O hot moments measured, and that such emission events accounted

for 68.6 % of the total annual cumulative flux measured from the grassland. Similar observations have been reported from an intensively grazed grassland in Ireland where hot moment N_2O emission events accounted for 51.1 % of the total cumulative flux (Scanlon and Kiely, 2003). Diurnal trends in peak N_2O emissions are still debated within the flux community, with many published N_2O studies not observing consistent or regular peak emissions at a given time of day (Cowan et al., 2020, Jones et al., 2011). On the contrary, a recent meta-analysis study by Wu et al. (2021) investigating the diurnal variability in soil N_2O emissions reported that out of the 286 datasets analysed, approximately 80 % of studies showed diurnal N_2O patterns, with roughly 60 % of N_2O emission peaks occurring during the day and 20 % occurring during night. It is important to note that while the authors found similar diurnal patterns of N_2O across seasons, the sample size for autumn (n = 24), was considerably less relative to spring (n = 138), and summer (n= 96), and winter N_2O fluxes were not accounted for, thus the results for the overall diurnal patterns observed in N_2O fluxes may be biased. Moreover, in managed grassland systems peak N_2O emissions observed during the daytime could be due to the timing or legacy effects of agriculture practices and may not be representative of a true diurnal pattern. While trends and correlations with temperature are frequently used as a determinant for whether a diurnal relationship exists within N_2O emissions observed (Liang et al., 2018), additional parameters relating to plant photosynthesis and the C cycle, such as solar radiation and photosynthetic active radiation (PAR) have recently been applied, where labile organic C through root exudation stimulated by PAR are suggested to control diurnal variants in N_2O emissions (Keane et al., 2018, Shurpali et al., 2016). For example, Keane et al. (2018) showed that diurnal patterns in observed N_2O emissions from an arable site in the United Kingdom were more strongly related to PAR than temperature, implying

that the availability of C from photosynthate influenced the diurnal trends in N_2O emissions. The transfer of C from assimilating leaves to roots that will discharge C to soil microbes provides an energy source for dentrifiers, and subsequently the production N_2O by denitrification under anaerobic soil conditions. At the seasonal scale, N_2O emissions from intensively managed pastures can vary with changes in temperature, rainfall and soil moisture. Krol et al. (2016) showed that N_2O EFs from synthetic cow urine were lowest in summer (0.51 %), higher in spring (0.91 %) and greatest in autumn (1.09 %) while EFs from dung were higher in autumn (0.52 %) compared to spring (0.09 %) or summer (0.21 %). On the same experimental grounds, Maire et al. (2020) showed that N_2O EFs from cow urine were low and similar in both spring (0.33 %) and summer (0.28 %) but were significantly different and highest in autumn (0.82 %), while N_2O EFs for CAN were negligible in summer (0.07 %), higher in spring (0.31 %) and greatest in autumn (0.72 %). Despite a century worth of investigations into understanding the processes driving N_2O emissions, the multiple scales of spatial and temporal variability of N_2O emissions from managed grasslands makes quantifying this powerful GHG with high certainty a persistently difficult task. (Butterbach-Bahl et al., 2013).

2.4.4 Mitigating nitrous oxide emissions from intensively managed grasslands

Current mitigation practices often don't account for the heterogeneous nature of N_2O emissions from agricultural soils, and instead enforce uniform management practices across farmlands (Rees et al., 2020). In order to accurately mitigate N_2O emissions from managed grassland systems, the spatial and temporal variability in emissions needs to be incorporated into future mitigation strategies. Such strategies can broadly be categorised as (1) reducing organic and inorganic (animal excreta) N inputs; (2)

manipulation of soil conditions and the processes of nitrification and denitrification and (3) precision agriculture where agricultural practices are optimized in accordance with plant nutritional needs as well as weather conditions to avoid direct and indirect losses of N_2O from managed pastures to the atmosphere and aquatic systems (de Klein et al., 2020b, Rees et al., 2020). Previous studies have unequivocally shown a strong positive correlation between N intake and animal N excreta (Huhtanen et al., 2008, Kebreab et al., 2001, Mulligan et al., 2004). Therefore it is evident that reducing animal N intake could reduce organic N inputs into managed pastures, provided the modified diet was still able to meet the animals' metabolic requirements for e.g. sufficient crude protein levels, sugars and starch (Dalley et al., 2017). In New Zealand, studies have shown a reduction in the N concentration of urine from animals grazing plantain (*Plantago lanceolata* L.) or mixed pastures where it is incorporated, with a strong likelihood of reducing the total amount of urinary N excreted (Box et al., 2017, Cheng et al., 2017, Totty et al., 2013). Furthermore, O'Connell et al. (2016) showed that a plantain diet could cause diuresis in sheep, which could explain the lower urinary N concentration results in the studies cited above. Another strategy to reduce N_2O emissions could be to allocate more of the excreted N into dung compared to urine as the EF for dung is generally lower than for urine. For example, Irelands Tier 2 EF for cattle dung and urine is 0.3 and 1.2 % (Duffy et al., 2021), respectively, and similarly so is New Zealand's Tier 2 EFs at 0.25 and 1 % for dung and urine, respectively (Ministry for the Environment, 2018). Previous studies have shown that incorporating condensed tannins (CT) into livestock diets reduced urinary-N-excretion and increased the amount of N excreted in dung, while improving the overall N retention in animals (Carulla et al., 2005, Misselbrook et al., 2005). Recent developments in remotely piloted aircraft systems (RPAS) have enabled the quantification of the spatial

heterogeneity of animal excreta (Maire et al., 2018), and this coupled with site specific EFs further enables estimates of field scale N_2O emissions (Rees et al., 2020). Such data provides baseline information that can used to improve the application of other mitigation tools such as the use of urease and nitrification inhibitors on animal excreta. These synthetic compounds inhibit soil enzymes that are responsible for the production of NH_3 by urea hydrolysis and N_2O by nitrification and denitrification. On the other hand, urine patches only become visible approximately a week after defaecation by visible variations in vegetation growth and colour (Auerswald et al., 2010), during which significant N_2O losses can occur. An alternative approach could be fitting grazing animals with GPS, thermal or urine sensors to enable quick deployment of inhibitors to dung and urine patches (Betteridge et al., 2010, da Silva et al., 2020, Misselbrook et al., 2016). Furthermore, recent developments in mapping urine patches by measuring changes in the soil electrical conductivity have been conducted in New Zealand and Ireland (Bates et al., 2015, Jolly et al., 2021) which would allow for fast mediation and application of inhibitors to reduce N_2O emissions.

Targeting the soil microbial processes that produce N_2O in order to reduce emissions is necessary for the development of N_2O mitigation strategies. Studies have shown that plant secondary metabolites are capable of supressing or inhibiting soil N transformation processes, such as nitrification through the release of nitrifying inhibitors from certain plant species roots, known as biological nitrification inhibition (BNI) (Subbarao et al., 2013, Villegas et al., 2020). For example, Villegas et al. (2020) found a 30 to 70 % reduction in nitrification rates across 119 germplasm accessions of Guineagrass (*Megathyrsus maximus* L.), an important tropical crop for livestock production. Byrnes et al. (2017) reported that N_2O emissions from urine patches were

three times lower where urine patches were deposited on tropical forage grasses with a high BNI capacity (*Brachiaria humidicoola cv. Tully*) relative to tropical forage grass species with low BNI capacity (*Brachiaria hybrid cv. Mulato*). Luo et al. (2018) showed that urine patches deposited in monoculture pots of plantain (*Plantago lanceolat*a L.) emitted N_2O emissions that were on average 28 % lower relative to urine patches in monoculture pots of perennial ryegrass and attributed this reduction in emissions to BNI mechanisms in plantain. Moreover, Carlton et al. (2018) showed lower rates of nitrification and NO_3^- leaching from plantain soil compared to perennial ryegrass/white clover soil due to a lower abundance of soil ammonia oxidiser bacteria (AOB) in the plantain plots.

2.5 Quantifying nitrous oxide emissions

To date there are a variety of methodologies used to quantify N_2O emissions over different spatial and temporal scales. Over small spatial scales, the most commonly used method is the closed chamber technique consisting of manually operated (i.e. static chambers), where the chamber is closed and open by the person sampling (Clough et al., 2020) or automated closed chambers whereby the chambers are opened or closed through a pneumatic system (Rapson and Dacres, 2014). When measuring N_2O fluxes using the static chamber approach, gas samples are manually taken from the chamber headspace through a rubber septa using a syringe equipped with a needle and stored in evacuated glass vials until processed using the analytical method known as gas chromatography (GC). The attractiveness of the static chamber technique for quantifying field fluxes of N_2O is primarily due to its low cost to operate, enabling flux measurements from multiple locations but the main disadvantage of this technique is its low temporal resolution as flux measurements are frequently made once a day and

generally within a constrained time window (Rapson and Dacres, 2014). In contrast, automated chambers equipped with fast response gas analysers enable higher frequency measurements of N_2O fluxes, such as Fourier transform infrared spectrometer, tunable diode laser absorption spectrometers and quantum cascade lasers (QCLs) (Cowan et al., 2014, Wecking et al., 2020a). More recently, gas analysers specifically designed for measuring soil derived GHG fluxes have become commercially available, such as the LI-7820 N_2O/H_2O trace gas analyser, which when coupled with the portable 8200-01S Smart Chamber by LICOR, enables the quantification of high frequency N_2O fluxes from multiple locations. In addition to automated chamber systems, high frequency gas analysers, in particular QCLs, have recently been equipped to eddy covariance (EC) apparatuses to allow for near continuous measurements of the exchange of N_2O between the atmosphere, soil and vegetation (Cowan et al., 2016, Wecking et al., 2020b). The application of EC systems to measure field scale emissions of N_2O is a relatively new area of research, providing exciting opportunities for determining the long term effects of management and climate on N_2O emissions as well as providing avenues for modelling and predicting N_2O emissions under different agricultural practices and climate scenarios. However at present, there are few long-term datasets of continuous N_2O flux measurements from managed pastures (Cowan et al., 2020, Merbold et al., 2021), and subsequently there is a strong need for such robust data sets in order to understand the long-term implications climate and management have on N_2O emissions. Investigations into the application of static chamber and EC flux measurements of N_2O from intensively managed pastures are central to the findings of this thesis, with aims of investigating the spatial and temporal discrepancies between the EC and static chamber techniques from a fertilized management (Chapter 4), as well as optimizing their application under a grazing

management in the presence of mixed N sources (i.e. fertilizer and animal excreta) (Chapter 5).

2.5.1 Static chambers

To date the static chamber technique is the most commonly used method to quantify N_2O fluxes, accounting for 95 % of all soil derived N_2O flux measurements (Lammirato et al., 2018). Measurements of N_2O are determined by measuring the change in gas concentration within the chamber headspace over time. Fluxes are typically calculated in accordance with the Ideal Gas law (Eq. 2.4)

$$F_{CH} = \left(\frac{dC}{dT}\right) * \left(\frac{M\ x\ P}{R\ x\ T}\right) * \left(\frac{V}{A}\right) \quad \text{Equation 2.4}$$

Where F_{CH} is the soil derived gas flux measured by the static chamber technique using linear regression, dC is the change in headspace concentration of N_2O during the enclosure period in ppbv, dT is the enclosure period in hrs^{-1}, M is the molecular weight of N_2O at 44.01 g mol^{-1}, P and T are the atmospheric pressure in Pa and temperature in K at the time of gas sampling, respectively, R is the ideal gas law constant at 8.314 J K^{-1} mol^{-1}, V is the volume in the chamber headspace in m^3 and A is the ground area enclosed by the chamber in m^2.

Measurements of N_2O from static chambers are made over small spatial scales (typically between 0.1 and 0.5 m^2) and generally once a day (typically between 10am and 2pm), from the chamber headspace where the gas concentration accumulates over time (Hoffmann et al., 2018, Pihlatie et al., 2005a, Rochette and Eriksen-Hamel, 2008). Historically, this technique has been used to investigate treatment effects on N_2O (Hyde et al., 2016, Harty et al., 2016, Maire et al., 2020), and quantify EFs which have been incorporated into national (Duffy et al., 2021) and international (Buendia et al.,

2019) N_2O emission inventories. A summary of the advantages and disadvantages of this technique are shown in Table 2.

Table 2. 1: An overview of the advantages and disadvantages of the static closed chamber technique.

Advantages	Reference	Disadvantages	Reference
Inexpensive to operate	Jones et al. (2011)	Low spatial and temporal resolution	Jones et al. (2011)
Easy to deploy	Jones et al. (2011)	Requires a dedicated measuring campaign	Maire et al. (2020)
Ideal for treatment or source specific investigations	Hyde et al. (2016)	High uncertainties in flux measurements	Lammirato et al. (2018)
Standardised guidelines	Clough et al. (2020), Pavelka et al. (2018)	Prone to artefacts during sampling, such as pressure differentials (Venturi effect)	Davidson et al. (2002)
Low power source (unless a fan is used)	Jones et al. (2011)	Increases in temperature in the chamber headspace can impact microbial processes and increase N_2O dilution via increased humidity	Rochette and Hutchinson (2005)

Upscaling chamber N_2O flux measurements to the field scale is often associated with a high degree of uncertainty due to the heterogeneity of N_2O emissions across agricultural landscapes (Cowan et al., 2015, McDaniel et al., 2017, Wecking et al., 2020b). As a result it is still a very challenging task but a necessary one to overcome in order to understand how localized changes in N_2O are represented at the larger, ecosystem scale. Alternatively, the automated chamber approach can overcome the temporal limitations of the static chamber technique by operating at far higher frequencies, and is therefore able to capture the variability in N_2O emissions over time.

2.5.2 Eddy covariance

The EC technique continuously measures the exchange of GHGs between the atmosphere, vegetation and the soil at high frequencies (10 - 20 Hz depending on the experimental set up) and over areas as large as 1 km^2. In essence, the EC GHG flux (F_{EC}) can be described as the covariance between the gas concentration (C) and the vertical wind speed (w) where fluxes calculated from a given area are determined by the wind speed and direction (Eq. 2.5)

$$F_{EC} = \overline{w'C'} \qquad \text{Equation 2.5}$$

The EC technique has frequently been used to measure CO_2 fluxes and quantify C balances in grasslands (Byrne et al., 2007, Lalrammawia and Paliwal, 2010), cropland (Ní Choncubhair et al., 2017, Morrison et al., 2020), peatlands (Mikhaylov et al., 2019, Sottocornola and Kiely, 2010) and forests (Campioli et al., 2016, Saunders et al., 2014). Less research has been conducted using the EC technique for measuring ecosystem scale fluxes of N_2O due to the low concentration changes that are required to be detected and as a result, there are few of datasets available with the high spatial and temporal resolution required to better understand N_2O flux dynamics (Cowan et al., 2020, Jones et al., 2011, Merbold et al., 2014, Wecking et al., 2020b). A summary of the advantages and disadvantages of the EC technique can be found in Table 2.2. One of the main disadvantages of using the EC technique for quantifying field scale emissions of N_2O is the inability of this method to distinguish between different sources of N within the footprint (i.e. the area over which fluxes are measured) and as a result it is difficult to determine the contribution of different N sources to the total N_2O losses from a heterogeneously emitting surface. Moreover, sources of N from managed pastures such as urine or dung patches, represent hotspots of N_2O (Hyde et al., 2016)

which can greatly contribute to the total N_2O losses quantified from grazed grasslands (Chadwick et al., 2018, Cowan et al., 2015). As the presence of hotspots within managed grasslands varies spatially and temporally (Cowan et al., 2015, Liang et al., 2018), in combination with changes in the EC footprint according to the EC mast height, wind direction and speed, atmospheric turbulence and canopy height (Burba and Anderson, 2010), this means that the EC technique may not always capture hotspot emissions of N_2O.

Table 2.2: An overview of the advantages and disadvantages of the eddy covariance technique

Advantages	Reference	Disadvantages	Reference
Non-disruptive to the surrounding environment	Kumar et al. (2017)	Can't disaggregate between emission sources	Wecking et al. (2020b)
Does not require a dedicated sampling campaign	Jones et al. (2011)	Expensive to operate and requires long term maintenance	IPCC (2021b)
Provides high resolution data in time and space	Burba and Anderson (2010)	Requires a high level of expertise	Jones et al. (2011)
Useful for investigating inter annual variability in GHG in response to changes in climate and land use	Kumar et al. (2017)	Requires a continuous energy supply	Kumar et al. (2017)
Standardised guidelines	FLUXNET (2021)	Dependence on atmospheric and environmental conditions	Kumar et al. (2017)

2.5.2.1 Quantum Cascade Laser Spectroscopy

The recent development and deployment of high frequency, absorption spectrometers such as QCLs integrated with EC systems has enabled the quantification of ecosystem scale emissions of N_2O (Gelfand et al., 2018, Wang et al., 2020, Wojtas et al., 2011). QCLs consist of alternating layers of semiconductors from which light is created by electron transitions between two excited conduction-band states in quantum wells. As a result

the emission wave-length of QCLs are independent of the materials used within its structure and therefore, can be tuned by design to measure over specific spectral ranges for different trace gases (for example, N_2O, CO, CH_4 or NO_x) (Chen et al., 2016, Maamary et al., 2016, Paiella, 2011, Sobanski et al., 2021). A single electron is able to cause the emission of multiple photons as it cascades through the layers of semi-conductors (Rapson and Dacres, 2014). One of the main advantages of QCLs relative to other optical techniques is that it does not require cryogenic cooling and can operate at room temperatures with minimal sensor drift. This feature enables QCL systems to be coupled with EC for field scale measurements (Cowan et al., 2016, Merbold et al., 2021, Wecking et al., 2020b). In addition to this, QCLs operate at high sensitivities, with standard units in ppb, which is essential when trying to capture spatial and temporal changes in low atmospheric concentrations of N_2O (Curl et al., 2010).

2.6 Reporting greenhouse gas emissions

2.6.1 Intergovernmental Panel on Climate Change (IPCC) Tier Methodologies

Inventories of N_2O are determined using EFs that are derived by quantifying the amount of N_2O emitted relative to the amount of N applied. The application of EFs in national inventories is advised by the IPCC, through a Tier system consisting of three distinct methodological approaches; Tier 1, which represents the use of default EFs provided by the IPCC, Tier 2, which are country specific EFs that includes activity data or distinguishes between different N forms, e.g. livestock number, type of N applied and varying application rates of N fertilizer; and Tier 3, which utilizes process based (for example, DNDC and DAYCENT), and empirical models (such as the Cool Farm Tool or CCAFS-MOT), and high resolution land use and land-use change data (Pachauri et al., 2014).

To date, most countries have adopted either the Tier 1 or Tier 2 approach in reporting national N_2O inventories including Switzerland (Bretscher, 2013), New Zealand (Ministry for the Environment, 2018), the United Kingdom (Thorman et al., 2020) and Ireland, where Ireland's Tier 2 EFs are shown in Table 2.3 (Duffy et al., 2021), and with the exception of America (McGlynn et al., 2019), Tier 3 inventories are significantly under- developed. This can partially be attributed to a lack of available long term, high resolution N_2O flux datasets to enable low uncertainty modelling (Reay et al., 2012). Default EFs for N_2O from agricultural landscapes are available for synthetic N fertilizers and grazing (i.e. pasture, range and paddocks, EF_{3PRP}) as outlined in the IPCC's 2006 and 2019 Good Practice Guidelines (Buendia et al., 2019, Eggleston et al., 2006). However such EFs have large uncertainties attributed with them, with numerous studies reporting higher or lower N_2O losses suggesting that Tier 1 EFs are insufficient for capturing emissions which are driven by changes in site specific management activities and weather conditions (Chadwick et al., 2018, O'Neill et al., 2020, O'Neill et al., 2021, Simon et al., 2018, Thorman et al., 2020, Zhou et al., 2017). As a result, the Tier 1 2006 guidelines have since been revised and further disaggregated into N sources derived from agricultural landscapes such as urine and dung depositions from grazing animals, as well as wet and dry temperate climates (Table 2.3) (Buendia et al., 2019).

Table 2. 3: Nitrous oxide (N_2O) emission factors (EFs) from the IPCC (2006) guidelines on greenhouse gas inventories, the revised EFs in the 2019 revisions of the 2006 EFs , and the Tier 2 EFs used in Ireland as part of the national emission inventory report.

N_2O EFs	IPCC (2006)	IPCC (Revised 2019)*	Ireland
	%		
EF_{1CAN}	1 (0.3 - 3)	1 (1.3 – 1.9)	1.4
EF_{1Urea}	-	-	0.25
$EF_{1Urea+NBPT}$	-	-	0.4
EF_{3PRP}	2 (0.7-6)	0.6 (0 - 2.6)	-
$EF3_{cattle\ urine}$	-	0.77 (0.03-3.82)	1.2
$EF3_{cattle\ dung}$	-	0.13 (0 – 0.53)	0.31

*EFs listed are for wet temperate climates

Presently, there is a lack of available data on EFs from individual N inputs and even less for integrated N sources which characterize grazing systems. For example, in a standard grazing management, synthetic fertilizer will be applied to stimulate grass growth and following sufficient increases in plant productivity, animals will enter the pasture to graze, depositing urine and dung. In some cases, organic fertilizer in the form of slurry will also be applied between grazing events. Therefore, grazing systems are not only dominated by N_2O emissions from fertilizer, urine and dung but rather from the additive N inputs where synthetic fertilizer is combined with urine and/or dung and potentially overlapping urine and dung patches. However, there is limited data available which quantifies emissions from these mixed sources (Table 2.4), which makes upscaling emissions from managed grasslands with low uncertainties a difficult task. Hyde et al. (2016) showed that the application of CAN fertilizer with dung had an additive effect on N_2O-N emissions, while CAN added to urine showed a multiplicative effect. Furthermore, emissions from urine and dung patches can have considerable legacy effects, lasting between 10 and 70 days after deposition (Buckthought et al., 2015, Flessa et al., 1996, Bell et al., 2015, Hyde et al., 2016, Krol et al., 2017).

Considering that agricultural soils account for 90 % of N_2O emissions in Ireland, of which 38 % is derived from synthetic fertilizers and 23 % is from animal excreta during grazing (Teagasc, 2021b), there is an urgent necessity for robust data sets which capture emission events from interactive sources. This in turn would provide more accurate inventories of N_2O emissions from managed grasslands, and would also offer realistic and reliable data which will further support the modelling of N_2O emissions.

Table 2.4: Nitrous oxide (N_2O) emission factors (EFs) and cumulative N_2O-N emissions from interactive treatments of cattle urine, dung and calcium ammonium nitrate (CAN)

Author	Treatment	N loading	EF	Cumulative
		kg N ha^{-1}	%	kg N_2O-N ha^{-1}
Hyde et al. (2016)	urine and dung	1629	-	0.56
	dung and CAN	525	-	2.12
	urine and CAN	1284	-	5.52
Krol et al. (2017)	urine and CAN	901	0.55	5.07
Maire et al. (2020)	urine and CAN[1]	635	0.74	4.87
	urine and CAN[2]	788	0.52	4.18
	urine and CAN[3]	701	0.76	5.39
Buckthought et al. (2015)	urea and urine[1]	1000	0.3	3.19
	urea and urine[1]	1200	0.3	4.33
	urea and urine[3]	1000	0.53	6.1
	urea and urine[3]	1200	0.47	6.44

1 = spring, 2=summer, 3= autumn

2.6.2 Greenhouse Gas Budgets

Determining the net C balance of managed grasslands by quantifying changes in CO_2 uptake and loss over time, as well as the lateral movement of C imports to and C exports from agricultural landscapes is important for assessing the baseline warming or cooling effect exerted from managed grasslands. This initial net warming or cooling response to management is further exacerbated through emissions of non-CO_2 GHGs such as N_2O and CH_4, which are driven by temporal changes in soil and weather

conditions as well as the intensity and timing agricultural practices (Cowan et al., 2021, Luo et al., 2013). The net GHG budget (NGHGB) of a managed pasture quantifies the sum of C imported into the system (for example, through plant assimilation of C or external C inputs from management, for example organic fertilizer), and C exported from the system (for example, by processes of autotrophic and heterotrophic respiration as well as the removal of biomass from the pasture in silage cuts), as well as the net GHG exchange (NGHGE) in terms of CO_2 equivalents. The NGHGB is an important tool at both the global and farm scale for determining if managed grasslands are a net C source or sink and subsequently the role these system play in mitigating or forcing climate change.

At the global scale, C budgets are a useful tool for reporting country scale emissions and aligning them with climate change policy. The global C budget (GCB) quantifies the amount of CO_2 that can be emitted to stay within a defined global temperature (Mc Guire et al., 2020). The GCB provides the foundation upon which goals within international legislation are determined and developed. For example, Article 2 of the Paris Agreement describes keeping global mean temperatures "well below 2 °C" relative to pre-industrial levels, with a strong emphasis on capping global temperatures to 1.5 °C and additionally, Article 4 is focused on achieving net-zero GHG emissions (Paris Agreement, 2015). The European Green Deal is the roadmap towards the goal of net zero emissions outlined in the Paris Agreement, with an intermediate target of reducing emissions by 55 % by 2030. European member states of the Paris Agreement have utilized C budgets to monitor progress towards country specific objectives to attain C neutrality by 2050. For example, France utilizes legally binding, short-term (4-5 year) C budgets which are disaggregated by sector to govern progress

made towards emission reduction targets (Ministry of ecology sustainable development and energy, 2015). In the French 2015-2018 C budget efforts to reduce emissions were deemed insufficient as emissions were in excess of 14 % (or 62 Mt CO_2-eq) (Fontan et al., 2019). Reporting and reviewing C budgets in the short term is useful as it enables the revision of current mitigation practices and the implementation of improved mitigation strategies.

At the field or farm scale, C budgets can provide meaningful insights into the contributions of managed grasslands in driving or mitigating against climate change and the implications management and environmental conditions have on this. For example, Jones et al. (2017) showed that the C balance from a managed grassland in Scotland over a nine year period illustrated system transitions between a net C source at 57.6 g C m^{-2} yr^{-1} to a net C sink at -587.7 g C m^{-2} yr^{-1}. In years where the grassland was net C sink, this was driven by high C uptake from the NEE of CO_2, while in years where the system was a net C source the authors attributed this to the grazing regime where the stocking densities were relatively high (~0.90 LSU ha^{-1}) resulting in higher contributions of CO_2-C losses through animal respiration. Jones et al. also showed that N_2O emissions (in terms of CO_2 equivalents) measured from the grassland offset the sink strength of the NEE of CO_2 by 29 % over the nine year period, illustrating the potency of the global warming potential (GWP) of N_2O. Myrgiotis et al. (2021) employed model-data fusion (MDF) algorithms to illustrate both the impact of management and extreme weather conditions on the C budget of managed grasslands across Britain in 2017 and 2018. Their findings showed that sward composition and timing, intensity and type of defoliation were key factors in determining the C balance. Additionally, the authors observed a nine-fold increase in the number of paddocks

acting as C sources in 2018 during extreme drought conditions relative to 2017, no extreme weather events were observed. Ammann et al. (2007) calculated the C budget of a newly established temperate grassland in Switzerland that was segregated into two plots, one plot under an intensive management (200 kg N ha^{-1} yr^{-1} and frequent cutting) and the other plot under an extensive management (no N application and lower cutting frequencies). The authors showed that the intensive management sequestered C at a rate of 147 ± 130 g C m^{-2} yr^{-1}, and conversely the extensive management was a source of C at a rate of 57 (+ 130/-110) g C m^{-2} yr^{-1}, although this was considered non-significant and thus could be considered neutral.

Chapter 3: Materials and Methods

3.1 Experimental Site

The work presented in this thesis was conducted on an intensively managed temperate grassland in the south-east of Ireland in Co. Wexford at Teagasc Johnstown Castle, Environmental Research Centre (52.30°N, 6.40°W, 67 m above sea level) (Fig. 3.1[a]). The field site is approximately 2.65 ha^{-1} in size and compromises of two paddocks – paddock 10 (P10) and paddock 11 (P11) (Fig. 3.1[a]). A summary of the site characteristics and management interventions applied during the course of this study can be seen in Table 3.1 and Table 3.2, respectively. This field site was chosen as it is a long term experimental research site, operating since 2002, where various studies on greenhouse gas (GHG) dynamics had previously been conducted and long-term data on agricultural management and soil characteristics are available (Krol et al., 2016, Maire et al., 2020, Ní Choncubhair et al., 2017) . An eddy covariance (EC) tower equipped with a 3-D sonic anemometer (CSAT-3, Campbell Scientific Ancillary, Logan, UT, USA) is located in the north-west of the field site which is facilitated to measure the ecosystem to atmosphere exchange of greenhouse gases (GHG), including carbon dioxide (CO_2) (LI-7500, LI-COR Biosciences, Lincoln, NE, USA) and nitrous oxide (N_2O) (LGR 23R N_2O/CO analyser Los Gatos Research, California, USA). The EC mast was set up at 2.2m and was equipped with a range of ancillary sensors, measuring air temperature and relative humidity (HMP155C, Campbell Scientific, Logan, UT, USA) soil temperature at 2-6 cm depth (TCAV-L, Campbell Scientific, Logan, UT, USA), rainfall (Young, Michigan, USA), volumetric water content at 15 cm depth (CS616, Campbell Scientific, Logan, UT, USA), photosynthetic active radiation (PAR) (PQS1,

Kipp and Zonen, Delft, The Netherlands) and net radiation (NR-Lite, Kipp and Zonen, Delft, The Netherlands).

Additionally there is weather station < 1 km from the field site which was used to gap-fill missing meteorological data and extracting long-term averages (LTA). In the south-west of the field site, a grazing exclusion area was erected in 2020 for dedicated experimental trials (Fig. 3.1[b]). The mean air temperature and precipitation for the field site in 2019 and 2020 was 11 and 10 ^{o}C, respectively, and 81 and 56 mm, respectively, which were similar to the long term average (LTA) (1991 – 2010) for the field site at 11 ^{o}C, and 76 mm. (Fig. 3.2).

Figure 3. 1: (a) Map of the island of Ireland where the red square marks the location of the experimental field site at Teagasc Johnstown Castle, Environmental Research Centre, Co. Wexford. (b) Map of the experimental field site where the light grey shaded areas represent

the field site, P10 and P11 represent paddock 10 and 11, respectively, the dark grey area represents the trial plot for the experimental campaign that was conducted in 2020 and the black square in P10 represents the location of the eddy covariance tower.

Table 3. 1: Site characteristics where values in brackets represent the standard deviation.

Area ha^{-1}	C %	K mg/kg	Mg mg/kg	N %	OM %	P mg/kg	pH -	Sand/Silt/Clay %	Soil type -	Main grass species -
2.65	3.51 (0.12)	72.98 (5.29)	129.83 (3.81)	0.38 (0.01)	8.56 (0.18)	4.95 (0.20)	6.06 (0.04)	53/33/14	Moderately drained sandy loam	Perennial ryegrass (*Lollium perenne L.*)

Table 3. 2: A summary of the field management activity in 2019 and 2020

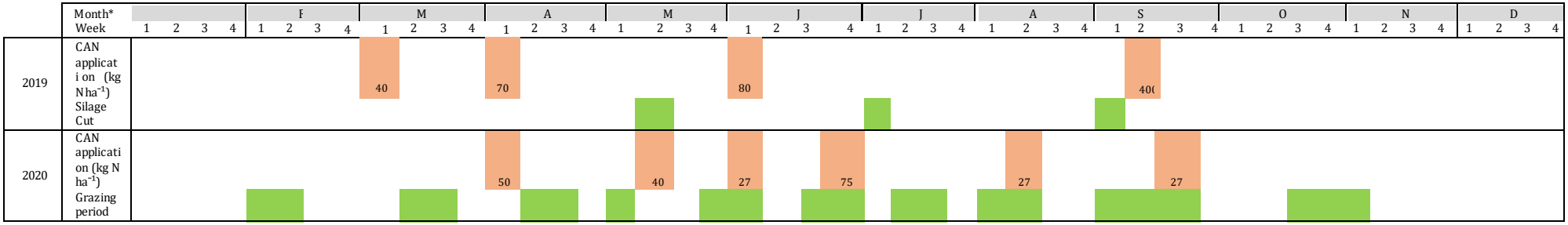

*From left to right: J = January, F =February, M = March, A = April, M = May, J = June, J = July, Aug = August, S = September, O = October, N = November, D= December

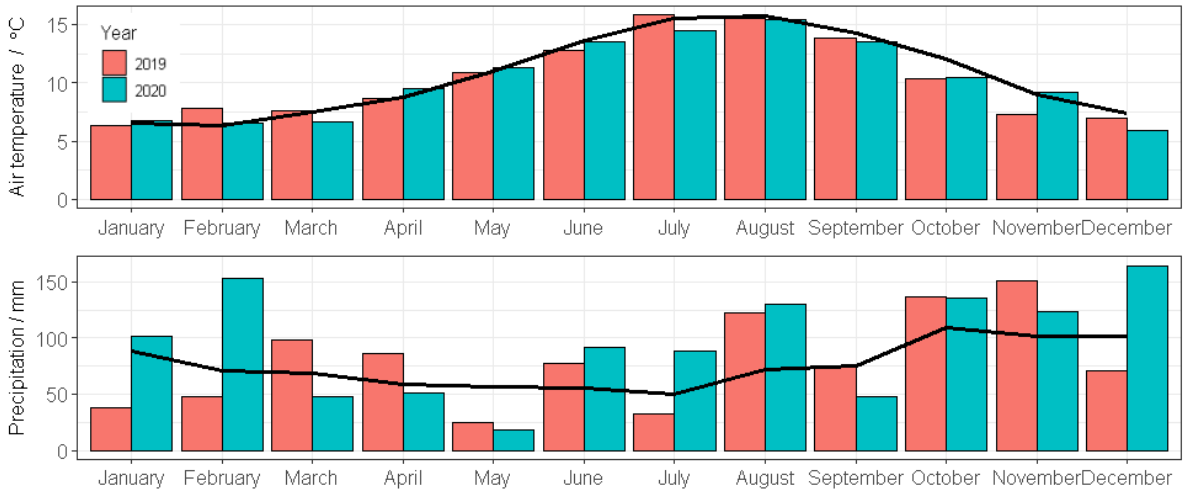

Figure 3. 2: Mean monthly (a) air temperature and (b) precipitation for 2019 and 2020, where the straight black line represents the long term average (LTA) between 1978 – 2007 (Met Eireann, 2021) for the field site.

3.2 N_2O flux measurements

Measuring the spatial and temporal dynamics in N_2O emissions is the focus of the objectives of the work presented in this thesis. To date measurements of N_2O emissions have been undertaken using a range of techniques including chamber methods, both manual (Maire et al., 2020) and automatic (Courtois et al., 2019), micrometeorological methods for example, eddy covariance (Cowan et al., 2020), and analytical techniques for instance, gas chromatography (GC) (Wecking et al., 2020a) and quantum cascade lasers (QCL) (Wecking et al., 2020b). Improvements in N_2O flux measurements have greatly enhanced our understanding of the processes involved in controlling the production and emissions of N_2O from agricultural landscapes at both the molecular and ecosystem scale (Groffman et al., 2000, Kumar et al., 2020). However, due to the multitude of abiotic and biotic factors which govern N_2O emissions in space and time (Butterbach-Bahl et al., 2013), it is still a difficult task to quantify N_2O fluxes with low uncertainties.

3.2.1 Static chamber

The static chamber method is based on the accumulation of GHGs emitted from the soil surface within a chamber and collecting gas samples from the chamber headspace over a short period at regular intervals for analysis by gas chromatography (Collier et al., 2014). Mean daily N_2O fluxes are typically estimated from chamber measurements taken once a day, generally in the morning to midday hours, while spatially and temporally integrated cumulative N_2O emissions are based on the sum of frequent mean daily N_2O fluxes from a given number of chamber replicates, and are typically calculated at the seasonal or annual scale (de Klein et al., 2020a).

The static chamber design was consistent between individual experiments in this study, and identical to those from previous experimental work conducted on this field site (Cummins et al., 2021, Krol et al., 2017, Maire et al., 2020). The chamber design consisted of a 40 cm x 40 cm stainless steel collar and lids that were 10 cm high creating an approximate headspace volume of 21 L (Fig 3.3). Chamber collars were inserted into the ground at approximately 5 – 10 cm depth at least, and at a minimum of 48 - 72 hrs^{-1} prior to chamber N_2O flux measurements in order minimize uncertainties associated with disturbing the surrounding soil and vegetation following installation. The chamber headspace was measured after installation using a ruler and the volume of vegetation inside the chamber was considered negligible (Rafique et al., 2012). The inner rim of the chamber collar was lined with a rubber (neoprene) or water seal, and a 10 kg weight was placed on top of the chamber, both practices were to ensure an air tight seal to prevent gas leaking between the collar and chamber (Fig 3.3). The chamber lids were fitted with two double-wadded rubber septa (Becton Dickinson, Oxford, UK) to facilitate gas measurements.

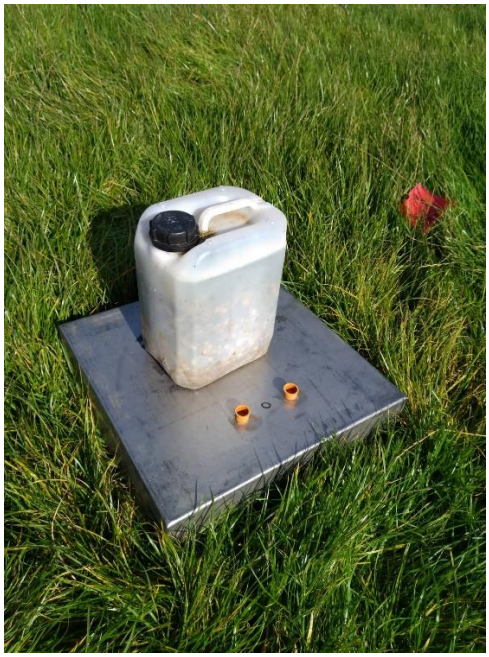

Figure 3. 3: An image of the static chamber design used in to measure N_2O flux measurements in this study.

In 2019, chambers were positioned randomly across P10 and P11 (Fig. 3.4) using both sector randomization (Chadwick et al., 2014) and pre-existing data on the soil properties of the field site, thus ensuring that chamber locations were not biased towards a certain collection of soil conditions.

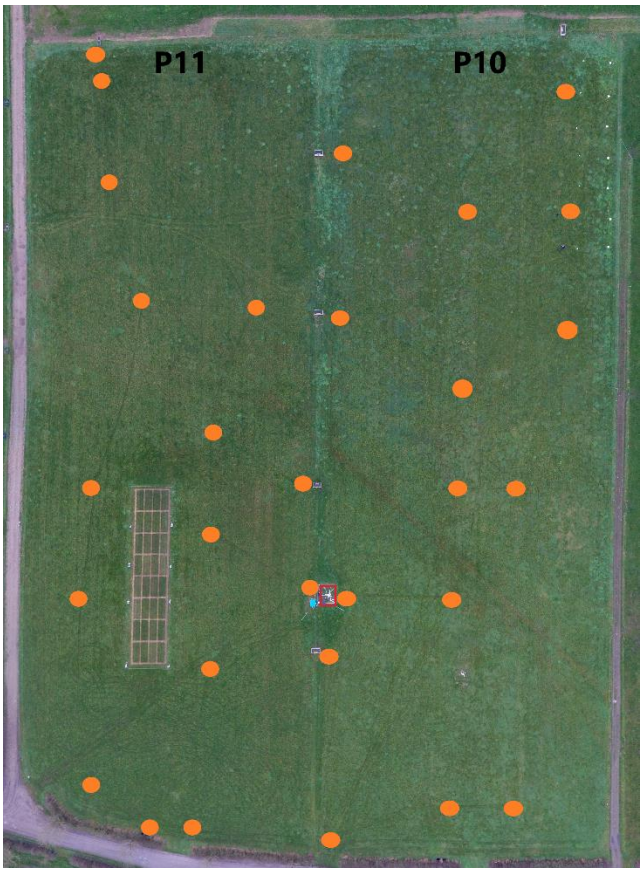

Figure 3.4: Chamber locations in paddocks 10 (P10) and 11 (P11) for the experimental period January 1st to December 31st 2019, as indicated by orange circles. The red square marks the location of the eddy covariance tower in P10.

In 2020 static chambers were placed in the south-west of P10 within a fenced off trial plot to avoid interference from grazing animals. The chamber trial plot consisted of a gas sampling zone of five plots/replicates for measuring N_2O emissions, and three plots/replicates for measuring changes in soil mineral N. Soil and flux measurements were made from four treatments – (1) control: without N application, (2) fertilizer in the form of CAN, (3) SU+CAN and (4) dung+CAN. Both soil and gaseous measurements were made from four grazing (G) events - 03/03/2020 - 02/04/2020 (G1), 03/05/2020-10/05/2020 (G2), 25/05/2020-03/06/2020 (G3) and 31/08/2020 - 21/09/2020 (G4). This enabled a quantification of the temporal variability in N_2O

fluxes over the measurement period. A schematic description of the trial plot is shown in Fig. 3.5.

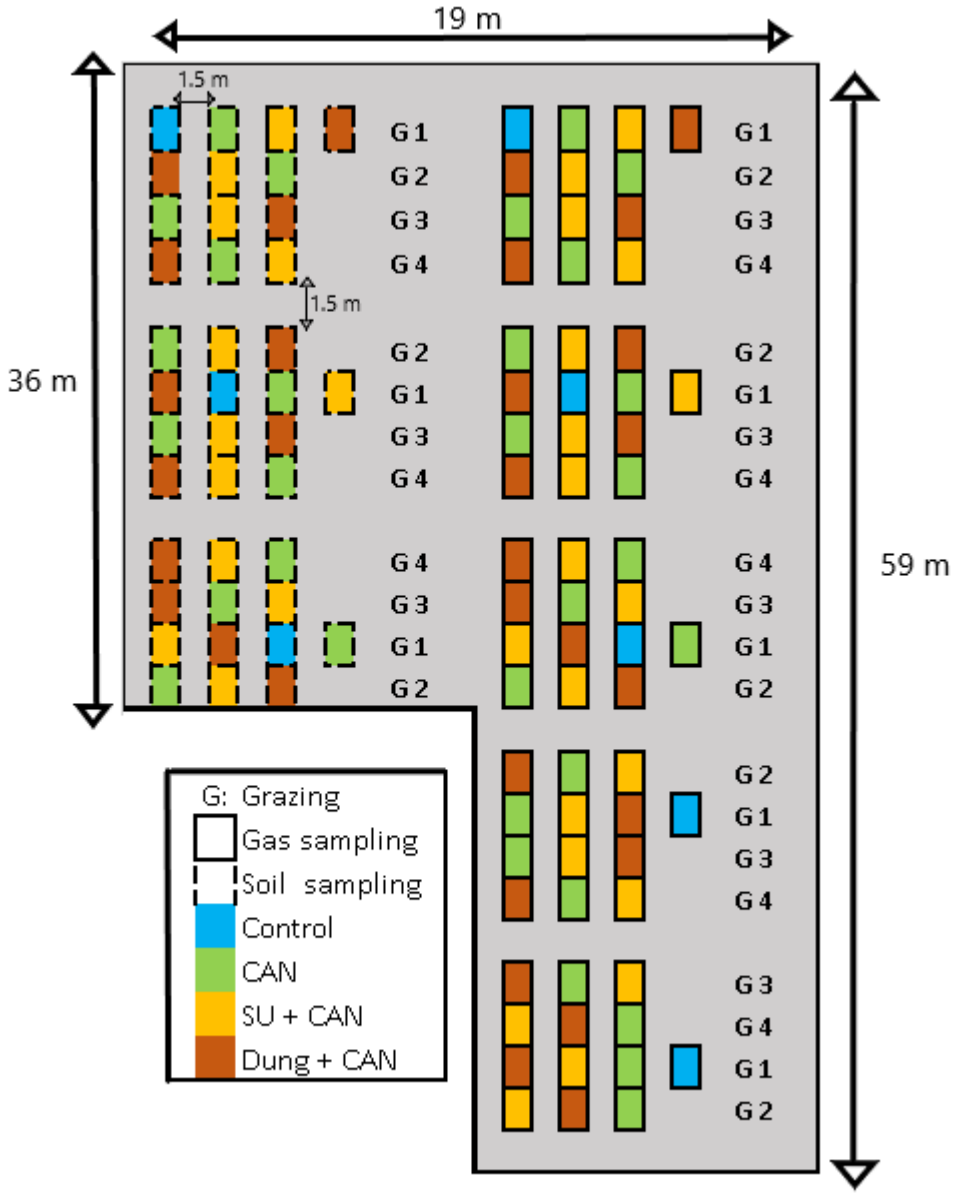

Figure 3. 5: Schematic of the randomized block design trial plot for soil sampling (left plots) and N_2O flux measurements by static chambers (right plots). Each plot represents a different replicate (i.e. 5 replicates for chamber measurements and 3 replicates for soil measurements) and each row in each plot represents a different grazing event.

.

3.2.1.1 Sampling N_2O fluxes

Gas samples were taken between 10 am and 2 pm using a 10ml polypropylene syringe (BD Plastiplak, Becton Dickinson) fitted with a hypodermic needle (BD, Microlance 3; Becton Dickinson) to extract the gas sample from the chamber headspace through a rubber septum. Gas samples were taken at three time intervals – 0 , 20 and 40 minutes and 0, 15 and 30 minutes in 2019 and 2020 respectively. The longer time period between consecutive sampling per chamber in 2019 relative to 2020 was to accommodate a greater distance between chambers. Background gas samples, i.e. gas samples which are representative of baseline emissions at the time, were taken on at least two occasions prior to treatment application. Following treatment application in both experimental years, gas samples were taken four times a week for the first two weeks, twice a week for the following two weeks, and then once a week for the duration of the experiment. In the experimental trial in 2020, the frequency of measurements was extended post treatment application to account for prolonged legacy effects on emissions. The same measurement frequency described was implemented but on the fifth week post treatment application, gas samples were taken once a week for the following five weeks, reducing to twice a month up until week 17 post application and afterwards once a month until the end of the experiment.

3.2.1.2 Processing N_2O gas samples

Gas samples taken from the chamber headspace were injected into a pre-evacuated 7 ml screw-cap septum glass vial and analysed in the laboratory using gas chromatography (GC) immediately after sampling (Scion 456-GC, Kirkton Campus Livingston, UK). All vials were over pressurised with a 10 ml gas sample to prevent leaking over time if immediate analysis was not possible. The GC used in this research

was equipped with an electron capture detector (ECD) using dinitrogen (N_2) as the carrier gas. Concentrations of N_2O were calculated by using the software MS Workstation by Bruker, to integrate the area under the N_2O peak. Concentrations of (CO_2) were measured in tandem to N_2O using a thermal conductivity detector. The calibration of the GC used a set of five certified standards with ranges of 0.2 – 10 ppm for N_2O and 500 – 10,000 ppm for CO_2. For each sequence of gas samples from a chamber, the flux was calculated in accordance with the Ideal Gas Law (Eq. 3.1)

$$F_{CH} = \left(\frac{dC}{dT}\right) * \left(\frac{M\ x\ P}{R\ x\ T}\right) * \left(\frac{V}{A}\right) \qquad \text{Equation 3.1}$$

Where F_{CH} (μg m^{-2} hr^{-1}) is the soil derived gas flux measured by the static chamber technique using linear regression (LR), dC is the change in headspace concentration of N_2O during the enclosure period in ppbv, dT is the enclosure period in hrs^{-1}, M is the molecular weight of N_2O at 44.01 g mol^{-1}, P and T are the atmospheric pressure in Pa and temperature in K at the time of gas sampling, respectively, R is the ideal gas law constant at 8.314 J K^{-1} mol^{-1}, V is the volume in the chamber headspace in m^3 and A is the ground area enclosed by the chamber in m^{-2}.

3.2.1.3 Post processing N_2O fluxes

Establishing a quality control procedure for flagging bad quality chamber N_2O flux values is difficult due to the large spatial (Cowan et al., 2015, Turner et al., 2008) and temporal (McDaniel et al., 2017, Wu et al., 2021) variability attributed with N_2O measurements. As CO_2 fluxes were measured in parallel with N_2O fluxes, ecosystem respiration rates were used as a quality control check for leaks or non-linear responses (de Klein and Harvey, 2015). In addition to this, if the correlation coefficient (r^2)

between N_2O concentrations and time was < 0.70, N_2O fluxes were further assumed to be non-linear and removed from the data set.

Analysing static chamber N_2O flux data is challenging due to the inherent spatial and temporal limitations of this method (Jones et al., 2011), often resulting in high uncertainties in N_2O flux measurements, which are further exacerbated by frequently small samples sizes ($n \leq 5$) (Chadwick et al., 2014, Maire et al., 2020). Moreover, emissions of N_2O typical display a peak and decay pattern over time, which is characterised by a few high flux measurements following N inputs from fertilizer or animal excreta in combination with favourable environmental and soil conditions, followed by a return to baseline emissions in the days following the emission event (Cowan et al., 2016, Hyde et al., 2016, Krol et al., 2016). This temporal pattern in N_2O emissions follows a log-normal distribution which further adds to the complexity of handling static chamber N_2O flux measurements with low uncertainties. Traditionally, 'normal statistics' are used to calculate daily mean fluxes from static chamber N_2O flux datasets but this is problematic as conventional approaches such as the arithmetic mean, will give equal weight to all flux values in the dataset, even if the probability of high flux measurements is far lower than low flux measurements. Consequently, where the sample size is small and high flux values are present in chamber N_2O flux dataset set, arithmetic approaches will typically overestimate the sample mean and likewise, where high flux values are absent from the dataset the sample mean will be underestimated (Levy et al., 2017). Therefore, statistical methods which account for the log-normal distribution of chamber N_2O flux measurements can reduce some of the temporal uncertainty attributed with the static chamber method. In this study, Bayesian statistics were applied to static chamber N_2O flux data measured in 2019

under a fertilizer treatment, as it explicitly accounts for the log-normal distribution of the data and in doing so, reduces some of the intrinsic uncertainty associated with the temporal upscaling of N_2O flux measurements, and subsequently provides more robust means and ranges of uncertainty relative to arithmetic approaches. Despite the advancements of Bayesian statics in handling chamber N_2O flux datasets from single management events (Cowan et al., 2019, Levy et al., 2017), its application on multiple management events (i.e. grazing and fertilizer applications) has not yet been successful, and therefore Bayesian statistics were not applied to chamber N_2O fluxes presented in Chapter 5. Indeed, upscaling chamber N_2O emissions from a grazing and fertilizer management regime is still a massively complicated and difficult task for a variety of reasons. Firstly, there are multiple hotspots of N_2O from grazed pastures from dung and urine patches from grazing animals and the application of fertilizer to these patches in combination with the spatial heterogeneity of soil characteristics such as the present of anaerobic and aerobic microsites which help mediate the microbial production of N_2O. The duration of emission events from animal excreta varies considerably, with previous studies reporting between 10 and 70 days to reach background rates post application (Buckthought et al., 2015, Flessa et al., 1996, Bell et al., 2015, Hyde et al., 2016, Krol et al., 2017). Additionally, the magnitude of N_2O fluxes measured will depend on both the N loading rate from urine and dung deposits as well as the probability of overlapping urine and dung patches. These factors will in turn vary according to the length of the grazing event, water intake and diet. In this thesis, chamber N_2O fluxes measured under a grazing regime in 2020 were upscaled to the field scale using site specific emission factors (EF) calculated from calcium ammonium nitrate (CAN), the addition of CAN to cow synthetic urine (SU+CAN) and the addition of CAN to cow dung (dung+CAN) for four out of nine grazing events, and scaled

according to the length of the specific grazing event, the number of grazing animals and estimated urine and dung depositions.

Missing mean daily N_2O flux values from days not sampled and after filtering were gap-filled using linear interpolation methods which draw a straight line between measured flux values to create a gap-filled dataset over time. The simplicity of this technique is in large the reason why it is the most commonly used method to gap-fill N_2O fluxes (Dorich et al., 2020). On the other hand, linear interpolation does not account for current soil and environmental conditions, and management activity and is therefore subject to over or under-estimating emissions for where the data gap is large, i.e. more than seven days (Barton et al., 2015). In order to minimize the uncertainty in interpolating between data points, flux measurements were made frequently as previously described in section 3.2.1.1.

3.2.2 Eddy Covariance

The EC tower was installed to the north-west of paddock 10 in order to maximize the footprint from the prevailing south-westerly wind direction (Fig. 3.1). An image of the EC set up is shown in Fig. 3.6. Data from the EC system was stored and collected on a CR3000 micrologger (Campbell Scientific, Logan, UT, USA). Fluxes of CO_2 and N_2O were measured using an open-path infrared gas analyser (IGRA) installed at 2.2 m (LI-7500, LI-COR Biosciences, Lincoln, NE, USA) and a closed-path quantum cascade laser (QCL) absorption spectrometer (LGR 23R N_2O/CO analyser Los Gatos Research, California, USA) which was stored in a temperature regulated trailer (161 cm x 98 cm x 127 cm) adjacent to the EC tower, respectively. Flux measurements were made at 10 Hz and blocked averaged over 30 minutes to account for the transport of larger eddies across the field site. A 3-D sonic anemometer (CSAT-3, Campbell Scientific Ancillary, Logan,

UT, USA) also mounted at 2.2m to the EC mast was used in tandem with the gas analysers to measure fluctuations in the 3-D wind components also at a frequency of 10Hz. Due to the closed path nature of the QCL, a perfluoroalkoxy (PFA) tube (10m long, 10mm inner diameter) was attached from the QCL inlet and placed 30 cm apart from the sonic anemometer in the same horizontal axis. A 2 mm fabric mesh was attached 2cm from the entrance of the PFA tube in order to prevent debris from entering the inlet line. In addition to this, two 2µm filters (SS-4FW4-2, Swagelok™) sealed with polytetrafluoroethylene (PFTE) tape along the threads were fitted along the inlet tube on the outside of the QCL and a 2µm and 10µm (Los Gatos Research, California, USA) filters were fitted at the entrance of the inlet tubing inside the QCL and upstream of the internal pump, respectively. In order to draw air into the inlet and the QCL cell, the QCL was connected to an external dry scroll vacuum pump (XDS35i, Edwards, West Sussex, UK) using a 2.4m long and 2.5cm wide PDTE clear suction hose with steel spiral wired rings (Tec Industry, Dublin, Ireland). The cell pressure and temperature was set to 85 torrs and 34 ^{o}C, respectively.

The EC set-up was equipped with a range of ancillary sensors for measuring variability in environmental conditions every 30 minutes. These included an air temperature and relative humidity probe (HMP155C, Campbell Scientific, Logan, UT, USA), two self-calibrating soil heat flux plates installed at 5 cm soil depth (HFP01SC, Hukseflux, Delft, The Netherlands), averaging soil temperature probes (TCAV-L, Campbell Scientific, Logan, UT, USA) installed at 2 cm and 6 cm depth above the soil heat flux plates, two net radiation sensors (NR-Lite, Kipp and Zonen, Delft, The Netherlands), photosynthetic active radiation (PAR) sensors (PQS1, Kipp and Zonen, Delft, The Netherlands), a tipping bucket rain gauge (Young, Michigan, USA) and time domain

reflectometers (CS616, Campbell Scientific, Logan, UT, USA) which measured soil VWC in the upper 15 cm of soil.

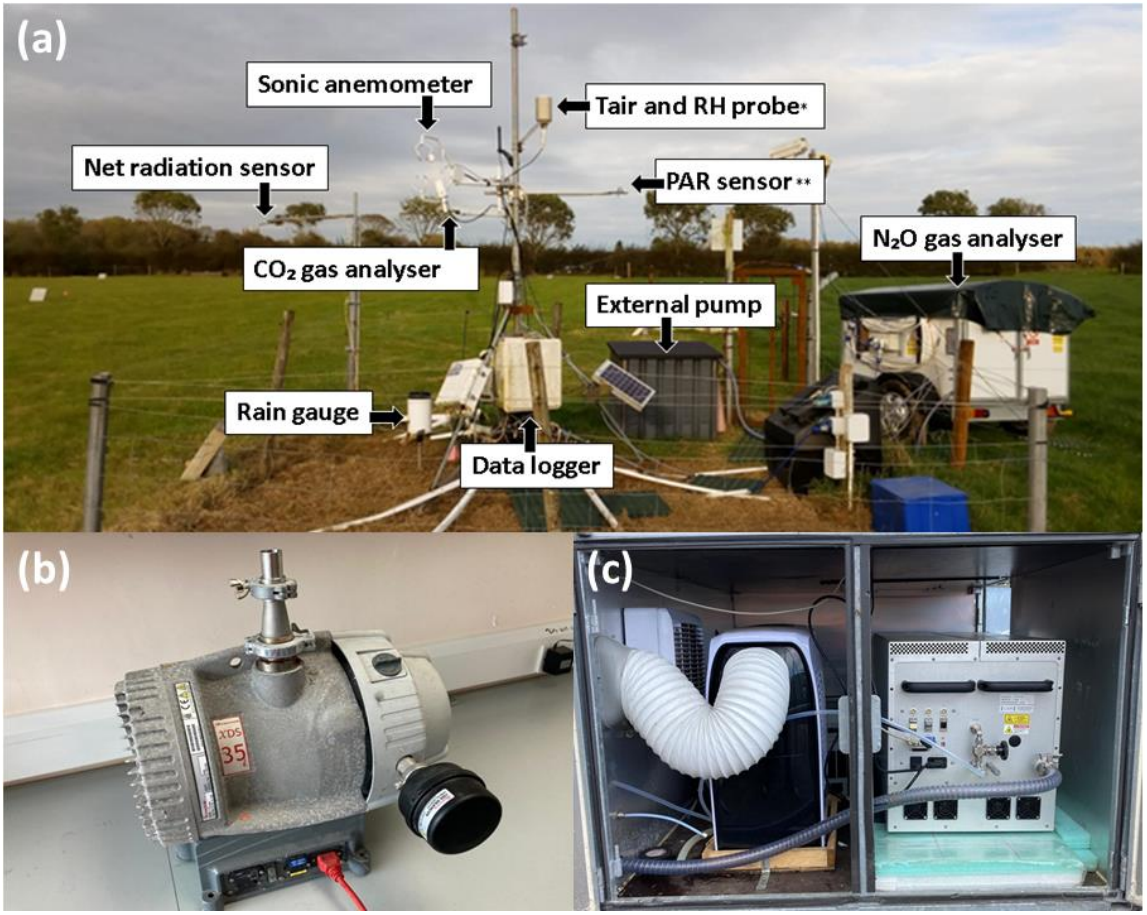

Figure 3.6: (a) The eddy covariance tower used in this research for measuring carbon dioxide (CO_2), nitrous oxide (N_2O), and environmental conditions (soil sensors are not shown). (b) Inside the grey slated plastic box was the external pump for running the QCL in a high flow mode in order to draw air from the opening the inlet tube to within the cell of thee QCL. (c) Inside the trailer there is the central processing unit (left) for operating the quantum cascade laser (right). *Tair = air temperature, RH = relative humidity; **PAR = Photosynthetic active radiation

3.2.2.1 Post processing greenhouse gas fluxes

Raw flux data was screened and post processed using the Eddypro software version 7.0.4. (www.licor.com/eddypro). Fluxes were quality controlled checked according to

various peer viewed tests including statistical tests by Vickers and Mahrt (1997) for drop-outs, amplitude resolution, absolute limits, skewness and kurtosis. Kaimal and Finnigan (1994) double rotation test was performed to compensate for the anemometer tilt. Low and high pass spectral corrections were determined using the analytic methods outlined by Fratini et al. (2012) and Moncrieff et al. (2004), respectively. For CO_2, air density fluctuations were corrected using the WPL term (Webb et al., 1980). For N_2O, a time lag between measurements of the gas concentration and the vertical wind component was assessed using the covariance maximization method in a two-step procedure. Firstly, the maximization of covariance was determined for a small subset of data (six consecutive hours) over a wide window of 10 seconds. Once a constant time lag was identified over the six hour block of data, the covariance maximization procedure was repeated over a constricted time window of 0.3 seconds using the median running time lag over a 7 day period as the mid-point. Secondly, the mixing ratio of the data was re-paired with the wind data at a constant time lag of -0.5 seconds based on the output from the previous maximization of covariance and N_2O fluxes were calculated with this time lag over a 30 minute period. Flux data was further screened for bad quality and removed from the dataset under the following quality control criteria:

- Less than 70 % of the flux contribution came from beyond the boundaries of the field site as calculated by the analytical footprint model described by Kormann and Meixner (2001).
- If the flux quality control flags outlined by Foken (2003) were category 6 or above

- Where turbulence was low, defined as a friction velocity < 0.1 $m^{-1} s^{-1}$ (Lognoul et al., 2019).
- Where the flux random uncertainty integrated over a 10 second correlation period was > 0.001 µmol N_2O m^{-2} s^{-1} or > 0.01 µmol CO_2 m^{-2} s^{-1} (Finkelstein and Sims, 2001).
- Where flux values were unrealistic for the field site such that N_2O fluxes that were < -0.1 µmol m^{-2} s^{-1}, and CO_2 fluxes were < -40 µmol m^{-2} s^{-1} and/or > 20 umol m^{-2} s^{-1}.
- Where the optical path of the IRGA was dirty or blocked defined as an automatic gain control (AGC) value > 50.
- Where the standard deviation between 30 minute CO_2 concentration values were > 5 ppm.

After removing bad quality fluxes, gaps in the CO_2 and N_2O flux datasets required gap-filling. The diurnal dynamics of CO_2 are well understood, where CO_2 uptake through plant photosynthesis occurs during the day time (gross primary productivity [GPP]) and is mediated by temperature, vapour pressure deficit but predominately PAR (Falge et al., 2001), and CO_2 release by ecosystem respiration (R_{eco}) occurs both during the daytime but mainly during the night time and is driven by temperature (Atkin et al., 2005, Reichstein et al., 2005). Therefore, robust and validated empirical models for gap-filling CO_2 are well established. In this thesis, CO_2 fluxes were gap-filled by firstly, partitioning the dataset into day-time and night-time by using a PAR threshold of 10 µmol m^{-2} s^{-1}, respectively. Fluxes of R_{eco} (µmol m^{-2} s^{-1}) were then modelled using the temperature response function of Lloyd and Taylor (1994) (Eq. 3.3).

$$R_{eco} = R_{10}(e\left(E_0\left(\left(\frac{1}{283.2-230}\right)\right)-\left(\left(\frac{1}{((T+273.2)-230)}\right)\right)\right) \quad \text{Equation 3.3}$$

Where R_{10} is the ecosystem respiration rate at a reference temperature of 10°C, E_0 is the coefficient for ecosystem respiration (309) and T is air temperature (°C). Modelled R_{eco} was then subtracted from measured daytime 30 minute values of net ecosystem exchange (NEE) to derive GPP (µmol m^{-2} s^{-1}). Gaps in the GPP dataset were then modelled using the light response curve described by Rabinowitch (1951) (Eq. 3.4):

$$GPP = \frac{(\propto * PPFD + A_{max}) - \left(\sqrt{(\propto * PPFD + A_{max}}\right)^2) - (4 * \gamma) * (\propto * PPFD * A_{max})}{2 * \gamma} \quad \text{Equation 3.4}$$

Where α is the quantum yield based on incident irradiance (mol CO_2 [mol photon]$^{-1}$), Amax is the maximum CO_2 assimilation rate (µmol CO_2 m^{-2} s^{-1}) and y is the convexity coefficient. The gap-filling methods employed within the N_2O flux community, include generalized additive models (GAM) (Cowan et al., 2016), autoregressive integrated moving averages (ARIMA) (Mumford et al., 2019), random forest (RF) (Philibert et al., 2013), artificial neural networks (Goodrich et al., 2021) and biogeochemical models (Giltrap et al., 2020). However, these methods lack significant validation due to a lack available long term N_2O datasets and limited N_2O modelling research and are therefore subject to high uncertainty when predicting N_2O emissions over time. Therefore, in this thesis gaps in the N_2O flux dataset measured by EC were filled using a custom multi-variate linear model. Firstly, N_2O fluxes were segregated into two datasets prior to gap-filling in order to isolate the influence of N inputs and environmental conditions on fluxes. Firstly, "treatment" fluxes which was defined as the first 30 days post treatment application and second "background" fluxes were defined as the first 30 days after the treatment application. By segregating N_2O fluxes into a treatment and background

dataset, peak N_2O fluxes observed outside of the treatment period were assumed to be driven by environmental drivers and not directly due to N inputs from management activity. Each dataset was gap-filled separately using a multivariate linear model that included (1) air and soil temperature, water filled pore-space (WFPS), and rainfall over 6 hr^{-1}, 12 hr^{-1}, 24 hr^{-1}, 48 hr^{-1}, 100 hr^{-1} periods that were significantly correlated with the log(N_2O-N flux) as determined from a subsets regression model using the leaps package in Rstudio; (2) days since treatment application and (3) the previous and next measured flux in the dataset. The gapfilled datasets were then combined, creating a fully gap-filled EC N_2O flux dataset.

3.3 Field sampling

3.3.1 Soil sampling

Soil sampling was conducted in order to understand both the drivers of N_2O emissions and the influence of substrate availability on N_2O emissions by soil microorganisms. Soil sampling protocols have been optimized and developed over the last century by Teagasc in Johnstown Castle (Teagasc, 2017). Soil was sampled approximately 1m away from the chamber location in the paddock during the experimental campaign in 2019 or within a dedicated soil sampling plot in the grazing exclusion zone in the south west of paddock 10, approximately 10 m away from chamber locations in 2020. A summary of the soil sampling design in 2019 and 2020 can be seen in Table 3.4. Soil samples were taken at approximately 10 cm depth using either a soil corer or probe. A slightly narrower soil probe was used in 2020 to minimize soil destruction and enhance longevity of the soil sampling plots. Soil samples were stored in plastic zip lock bags at 4 °C if same day analysis was not possible. In preparation for analysis, soil samples were thoroughly mixed and wet sieved (<4 mm). Three replicate

measurements of soil temperature, moisture and electrical conductivity were taken 1 m from the chamber locations using a handheld WET sensor (Delta-T Devices Ltd, Burwell, UK) and averaged. The bulk density (mass of dry soil/volume of soil) of the field site was measured prior to commencing experiments by taking 30 samples of the surface topsoil using cylindrical rings that were 10 cm in depth and 3.7 cm in diameter, drying the soil samples at 105 °C for 48 hrs^{-1} and weighing samples for their dry weight.

Table 3. 3: Details on the soil sampling design for 2019 and 2020 including the treatment, depth at which samples were taken, the tool used to take samples, the number of samples per sampling campaign, the frequency of sampling campaigns and the tests used on fresh soil samples including nitrate (NO_3^-) and ammonium (NH_4^+) concentrations, soil organic carbon (SOC) and pH.

	2019	2020
Treatment	CAN	Control, CAN, synthetic urine + CAN, dung + CAN
Depth (cm)	5 – 10	5 - 10
Tool	Soil corer (10 cm depth, 1.7cm diameter)	Soil probe (10 cm depth, 1.5cm diameter)
No. samples / campaign	30	12 (3 samples per treatment)
Frequency	Once prior to and post CAN application	Once a week for the first eight weeks post treatment application
Analysis	NO_3^-, NH_4^+, SOC, pH	NO_3-, NH_4^+

3.3.2 Soil analysis

3.3.2.1 KCL extraction for ammonium and nitrate analysis

Analysis for soil concentrations of NH_4^+ and NO_3- followed the guidelines of the American Soil Society for soil analysis. Soil mineral N components were extracted by creating a solution of 100 ml of 1 mol L^{-1} potassium chloride (KCL) solution added to 20 g of freshly sieved soil and placed onto an orbital shaker (Orbital Shaker SSL1,

Stuart, Staffordshire, UK) for 1 hr^{-1}. Samples were then filtered using grade two Whatman filter paper and stored at -18 °C prior to analysis, with additional blank samples of deionised water. Concentrations of NH_4^+ and NO_3 - were determined within 48 hrs^{-1} of producing the filtrate sample using an Aquakem 600 Discrete Photometric Analyzer (Thermo Electron OY, Vantaa, Finland). The concentrations of NH_4^+ and NO_3- from the blank samples were deducted from mineral N concentrations from the treatment samples. The mass of N in the form of NH_4^+ or NO_3 - ($Mass_N$) in g per kg soil was determined using (Eq. 3.5):

$$Mass_N = \frac{C*V}{M} \qquad \text{Equation 3.5}$$

Where C is the concentration of NH_4^+ and NO_3 - in the KCL extract in mg L^{-1}, V is the volume of the of the solution in which the soil sample was mixed with KCL in L, m is the mass of the dry soil mixed with the KCL solution calculated as the gravimetric water content.

3.3.2.2 Soil organic carbon and pH

Of the remaining soil sample not used in the mineral N analysis, analyses to determine the soil organic carbon (SOC) content and soil pH were performed. For SOC the previously dried and sieved soil sample, was ball milled into a fine powder and a micro - sample was weighed onto the autoloader of the LECO TruSpec Micro (St Joseph, Michican, USA). The micro-sample (0.2 g) was then dropped into the high-temperature combustion furnace where carbon is converted to CO_2. Scrubbing agents were then used to transport CO_2 from the furnace to an infrared detector where the carbon components of the sample are assessed. Soil samples analysed for pH were processed using the Gilson 215 Liquid Handler, Middleton, USA and the processing software Aqualyser 2.

3.3.3. Biomass sampling

Biomass sampling was conducted in both experimental years. In 2019, biomass samples (n = 4 per paddock) were taken randomly in a zig-zag pattern prior to silage cuts over an approximate area of 10 m^2 using a biomass harvester by Haldrup GmbH and in 2020, biomass samples (n =8 per paddock) were taken in the same random procedure using a 1 x 1 m quadrat. Biomass samples were stored in thin plastic porous bags and the fresh weight of the samples was measured prior to placing the sample in an oven at 70 °C for four days. Following drying, samples were re-weighed to determine the dry biomass weight and grounded for total C and N content analysis using the TrueSpec Micro elemental analyser as described above. Additionally, grass height was also monitored over the course of this study in order to determine both dry matter yields and changes in canopy height which may influence the size of the EC footprint. Grass height measurements were taken once a week using a manual rising plate meter (Charleville, Co. Cork, Ireland).

3.4 Animal excreta

3.4.1 Synthetic urine

The N loading rate of a urine patch can vary between 400 and 1200 kg N ha^{-1} (Haynes and Williams, 1993, Jarvis et al., 1995b), and this in turn can vary with the N content and C:N ratio of animal feed (Van Vuuren et al., 1993, Yan et al., 2007), the fertilization intensity of grazed pastures (Petersen et al., 1998) and water intake by livestock (Paquay et al., 1970). As it was not feasible to monitor and measure these variables over the duration of the grazing season, synthetic urine was used according to the protocol outlined in de Klein et al. (2003). This approach was chosen as it provided an N loading rate that was comparable to that of typical cow urination (Haynes and

Williams, 1993). The total N loading rate of the synthetic urine solution was determined by taking three replicate1:500 dilutions of homogenized sub-samples and performing a Ganimede analysis (Hach Ganimede N analyser, Co. Cork, Ireland). Alkaline potassium persulphate was used to partition the N compounds in the synthetic urine solution under a temperature and pressure of 150 °C and 8 atmospheres of pressure, respectively. The mean N loading rates from both batches is shown in Table 3.5. Synthetic urine was created on two occasions during 2020 in 60 L batches and stored at 4 °C prior to application, which occurred when cattle were grazing in strips in the south-west of paddock 10. The synthetic urine solution was applied at a rate of 1.8 L (Misselbrook et al., 2014) as opposed to the more common application of 2.0 L (Selbie et al., 2014) to minimize impacting the soil moisture content and to avoid saturation within the chamber (Maire, 2020). A watering can was used to apply synthetic urine within the chamber collar (0.16 m^{-2}) to facilitate infiltration (Forrestal et al., 2017).

Table 3. 4: The mean total nitrogen content of the 1:500 diluted synthetic urine solution used (g N/ L), and the equivalent application rate considering the volume of application (1.8 L) and the area (0. 16 m^{-2}) of application (kg N ha^{-1}). Values in brackets represent the range surrounding the mean.

Date		g N/L	kg N ha^{-1}
26/03/2020	Batch #1	8.2 (7.3 - 9.4)	517.3 (458.7 - 587.2)
06/06/2020	Batch #2	9.7 (8.9 - 10.5)	606.6 (554.2 - 659.0)

3.4.2 Dung

Dung was collected immediately after deposition from dairy cows in pastures grazed within a week prior to grazing commencing in paddocks 10 and 11. Dung depositions

were carefully scrapped from the top of the soil using a hand-held spear in order to avoid incorporating topsoil and biomass into the sample, and stored at 4 °C in a 25 kg bucket, where the lid was pierced with holes to prevent the build-up of manure gas (hydrogen sulphide, methane, ammonia and CO_2). Composite sub-samples of dung were taken from the bucket for total C and N analysis. Sample preparation involved freeze drying samples at – 20 °C for 48 hrs^{-1} (ScanVac Freeze Dryer, Vassingerød, Denmark) and ball milling frozen samples in a mixer mill (Retsch MM200, Darmstadt, Germany) at a vibration frequency of 25 Hz for one minute (Ashekuzzaman et al., 2019). Ball milled samples were then analysed for total C and N as previously described in section 3.3.3. The mean N and C loading rates from dung sub-samples for grazing events monitored by chamber flux measurements is shown in Table 3.6. The dry matter content of dung was determined by drying 20 g of fresh dung for 24 hrs^{-1} at 105^{o}C. Dung applications inside the chamber collar and the allocated soil sampling area within the trial plot were made in tandem with synthetic urine applications. Dung was applied within a 30 cm diameter area within the chamber collar at 2 kg (Krol et al., 2016).

Table 3. 5: The mean total nitrogen and carbon of dung (g m^{-2}) used and the equivalent application rate (kg ha^{-1}). Values in brackets represent the range surrounding the mean.

Date	Grazing	g N m^{-2}	kg N ha^{-1}	g C m^{-2}	kg C ha^{-1}
28/02/2020	1	55.1 (52.9 - 56.3)	550.8 (528.8 – 563.0)	669.8 (646.9 - 691.3)	6697.5 (6468.7 - 6912.5)
27/04/2020	2	55.9 (53.8 - 59.4)	559.2 (538.2 - 593.9)	680.4 (648.6 - 726.5)	6803.6 (6485.9 - 7265.2)
21/05/2020*	3	40.5	405.0	473.4	473.4
28/08/2020	4	35.1 (31.2 - 39.3)	351.2 (311.9 - 392.7)	465.7 (424.2 - 517.3)	465.6 (4242.4 - 5172.7)

*Only 1 replicate was available for grazing 3

Chapter 4: Assessing nitrous oxide emissions in time and space with minimal uncertainty using static chambers and eddy covariance from a temperate grassland

Abstract

Where nitrogen input from fertilizer application exceeds plant demands, hotspots of microbially produced nitrous oxide (N_2O) can exhibit disproportionately high rates of emissions relative to longer periods of time, known as hot moments. Hotspots and hot moments of N_2O are sensitive to changes in agricultural management and weather, making it difficult to accurately quantify N_2O emissions. This study investigates the spatial and temporal variability of N_2O emissions using both static chambers (CH) and eddy covariance (EC) techniques, measured at a grassland site subject to four fertilizer applications of calcium ammonium nitrate (CAN) in 2019. Daily mean CH emissions were calculated using the arithmetic method and Bayesian statistics to explicitly account for the log-normal distribution of the dataset. N_2O fluxes measured by CH and EC were most comparable when flux measurements were > 115 N_2O-N μg m^{-2} hr^{-1}, and EC and CH measurements showed spatial and temporal alignment when CH $n \geq 15$. Where $n \leq 5$, the Bayesian method produced large uncertainties due to the difficulty of fitting an arithmetic mean from a log-normally distributed data set with few flux measurements. Annual EC fluxes, gap-filled using a multi-variate linear model, showed a strong correlation with measured flux values ($R^2 = 0.92$). Annual cumulative fluxes by EC were higher (3.35 [± 0.5] kg N ha^{-1}) than CH using the arithmetic (2.98 [± 0.17] kg N ha^{-1}) and Bayesian method (3.13 [± 0.24] kg N ha^{-1}), which quantified emission factors of 1.46, 1.30 and 1.36 %, respectively. This study implies that a large sample size and frequent CH flux measurements are necessary for comparison with EC fluxes

and that Bayesian statistics are an appropriate method for estimating realistic means and ranges of uncertainty for CH flux data sets.

Work presented in this chapter is published in Agricultural and Forest Meteorology (https://doi.org/10.1016/j.agrformet.2021.108743) with author list as: Murphy, R.M. Richards, K.G. Krol, D. Gebremichael, A, Lopez-Sangil, L. Rambaud, J. Cowan, N. Lanigan G.J. and Saunders, M.

Author Contributions: RM, MS, and GL designed the experiment. RM conducted the experiment and analysed the samples that were collected alongside JR, LL-S and AG. Samples were analysed in the Teagasc Johnstown Castle with the support of laboratory technicians. RM with the help of NC conducted the flux data analysis. RM wrote the article with the contributions from all co-authors

The overarching objective of this thesis chapter was to compare the application of static chambers and the eddy covariance technique to quantify the spatiotemporal variability in N_2O emissions from a managed pasture and in doing, highlight the disparities and uncertainties associated with measuring N_2O emissions over different spatial and temporal domains.

4.1 Introduction

Nitrous oxide (N_2O) is a powerful greenhouse gas (GHG), with a global warming potential (GWP) 265 times that of carbon dioxide (CO_2), and a lifespan of over 100 years (Stocker, 2013). The global average concentration of atmospheric N_2O reached 331.1 ± 0.1 ppb in 2018, 23 % greater than pre-industrial levels (270 ppb) and is primarily associated with the application of mineral or organic nitrogen (N) to soils (WMO, 2019). Nitrogen fertilizers provide mineral N in the form of ammonium (NH_4^+)

and nitrate (NO_3^-) for the purpose of growing crops; however, soil microbes also consume this N to produce N_2O through the processes of nitrification and denitrification (Luo et al., 2017). Where N is applied to soil when conditions favour these microbial processes (water filled pore space (WFPS) 70 – 80 %, (Linn and Doran, 1984), substrate availability ($NO_3^-$and NH_4^+) (Zanatta et al., 2010), temperature induced increases in soil respiration (Butterbach-Bahl *et al.* 2013), hotspots of N_2O can occur, releasing short-lived, but excessively high rates of emissions (Hargreaves et al., 2015). Hotspots coincide with changes in substrate availability, resources or the physical environment (Pickett and White, 1985) for example, dry-wetting cycles of soils or increases in soil moisture following fertilizer application where soil conditions become favourable for microbial N_2O production (Fuchs et al., 2018). Pulses of N_2O from hotspots can exhibit rates of emissions that are 15-30 % higher relative to longer periods of time. These emission events are known as hot moments (McClain et al., 2003), and typically last between 5-20 days (Groffman et al., 2009). The occurrence of N_2O hotspots and hot moments result in extremely heterogeneous emissions across agricultural landscapes (Cowan et al., 2017) and it is extremely difficult to accurately quantify N_2O emissions without large uncertainties.

Micrometeorological techniques such as eddy covariance (EC) have been extensively used to quantify fluxes of CO_2 and methane (CH_4) between the soil and the atmosphere within grassland ecosystems (Felber et al., 2015, Soussana et al., 2010). One main advantage of EC techniques is that it continuously measures the ecosystem to atmosphere exchange of key gas scalars that are integrated at the ecosystem scale without disturbing the soil or altering the microclimate (Wang et al., 2013). However, due to the lower atmospheric concentrations of N_2O and the higher sensitivities

needed to capture baseline emissions (relative to CO_2), it is only in more recent years that the EC technique has been capable of reliably measuring field-scale N_2O fluxes through the development and deployment of fast, high precision absorption spectrometers such as quantum cascade lasers (QCL) (Voglmeier et al., 2019). In contrast, static chambers (CH) measurements are the most commonly used method for quantifying field fluxes of N_2O (Bell et al., 2015, Maire et al., 2020, Rochette, 2011). Manually-operated CH are relatively inexpensive to run, easy to deploy, have well-established standardised guidelines for GHG measurements and are a highly cited method for investigating N fertilization effects on soil N_2O fluxes (de Klein and Harvey, 2015, Krol et al., 2017, Maire et al., 2020). However, CH flux measurements provide lower spatial and temporal resolution when compared to EC techniques, as single measurements are typically made at a daily time-step over an area less than 1 m^2. Therefore, peak emissions, diurnal variation and decay patterns of N_2O over time following rainfall or re-wetting of dry soils and/or management interventions such as fertilizer application, are not always fully captured using CH methods (Jones et al., 2011). The peak and decay pattern which is commonly observed in CH N_2O fluxes over time, typically display a log-normal distribution in space which is characterized by a small number of high flux values (Levy et al., 2017). The probability density of a log-normally distributed N_2O flux ($Flux_{N_2O}$) at a given time is (Eq. 4.1):

$$f\left(Flux_{N_2O}\right) = \frac{1}{\sqrt{2\pi}\,\sigma_{log}\,Flux_{N_2O}} e^{-\left(\log\left(Flux_{N_2O}\right)-\mu_{log}\right)^2/2\sigma_{log}^2} \qquad \text{Equation 4.1}$$

where μ_{log} and σ_{log} are the mean and standard deviation of the log-transformed flux. The mean distribution without log transformation is given by (Eq. 4.2):

$$\mu = \exp(\mu_{log} + 0.5\,\sigma_{log}^2) \qquad \text{Equation 4.2}$$

Quantifications of the variables which make up the log-normal distribution, μ_{log} and σ_{log} (and therefore the true μ) are often insufficient because of the large variability, measurement error and small sample size (Levy et al., 2017). In order to improve estimates of CH flux measurements and make localized field measurements more comparable with ecosystem scale EC flux measurements over space and time, a method is required, that accounts for the uncertainty in μ which arises from estimating field-scale fluxes from a small, log-normally distributed sample. More recently, Bayesian statistics have been utilized to analyse N_2O fluxes as a lognormal distribution and in doing so, reduce the spatiotemporal uncertainty associated with CH flux measurements (Cowan et al., 2020, Nishina et al., 2009).

The objective of this paper was to investigate both technical disparities (spatially and temporally) between EC and CH in measuring N_2O fluxes, as well as the methods used to handling CH N_2O flux data (arithmetic and Bayesian) for a complete comparison between methodologies. In this study we aim to (i) address the uncertainty in upscaling CH N_2O flux measurements to the field scale by using a Bayesian approach to account for the log-normal distribution of flux measurements and to provide realistic means (ii) compare N_2O emissions quantified by both CH and EC methods in a temperate grassland under a fertilized treatment and (iii) identify the influence of fertilizer application and the environment in driving variability in N_2O emissions in space and time.

4.2 Materials and Methods

4.2.1 Site and experimental description

The study was carried out between January and December 2019 at the Long Term Carbon Observatory experimental field site at Teagasc Environmental Research

Centre, (Johnstown Castle, Co. Wexford) in the south-east of Ireland (52.30 °N, 6.40 °W, 67 m above sea level). This area has a temperate oceanic climate with a mean annual temperature and rainfall of 10.1 °C and 1011 mm respectively. The EC system was set up in the northern part of the experimental field site (Fig. 4.1). The field site has clay loam alfisols and consists of two paddocks (known as paddocks 10 and 11) with a collective area of 2.65 ha^{-1}. The sward composition of the grassland is dominated by perennial ryegrass (*Lolium perenne*) with white clover (*Trifolium repens*), herb-Robert (*Geranium robertianum*) and broad-leaved dock (*Rumex obtusifolius*) (Maire et al., 2020).

In the year prior to measurements (2018), paddock 10 was managed for silage production and paddock 11 was grazed by Holstein-Friesian dairy cows. During the measurement year (2019), there were four fertilizer applications of CAN and three silage cuts. N_2O flux measurements were performed using both CH and EC techniques and both were compared over seven comparison periods during this time (see Table 4.1). Six different methods were used to calculate summary N_2O flux statistics to investigate spatial (CH inside or outside the half-hourly EC footprint (FP)) and temporal differences (half-hourly EC measurements for the day or made at the same time as CH measurements) in measurements (Table 4.2). Mean fluxes measured from CHs were calculated using the arithmetic method and the Bayesian method (see section 4.2.6) to account for uncertainties in the log-normal distribution of N_2O fluxes in time.

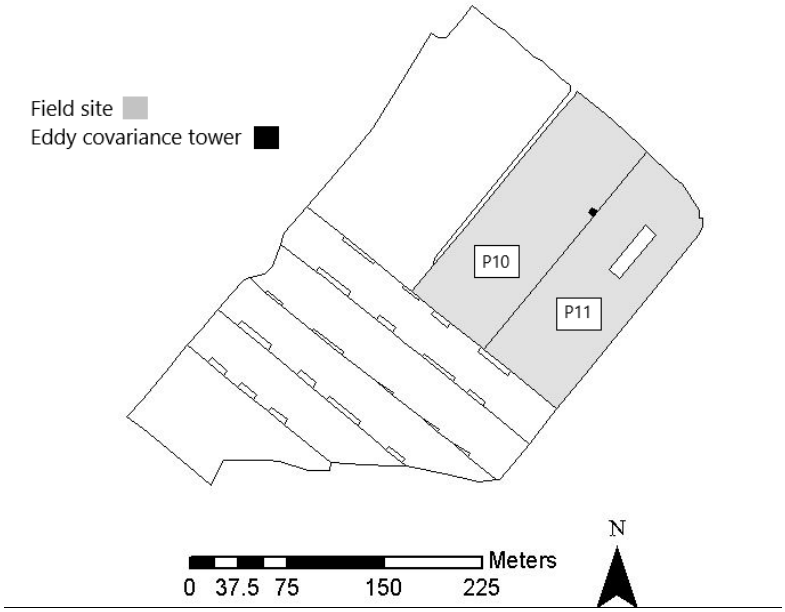

Figure 4. 1: Map of the field site where boundaries represent paddocks (P), grey paddocks 10 and 11 represent the experimental field site (2.65 ha^{-1}) and the black square represents the eddy covariance tower.

Table 4. 1: A summary of comparison periods where N_2O fluxes were measured by eddy covariance and static chambers. The table provides information on the length of each comparison period (*N*), management interventions including silage cuts and fertilizer application (calcium ammonium nitrate [CAN]) dates and the N loading rates in addition to key meteorological variables including cumulative rainfall (mm), average air temperature (Tair) and at 6.5cm depth soil temperature (Tsoil), water-filled pore space (WFPS), electrical conductivity (EC), and at 10 cm depth organic C, pH, ammonium (NH_4^+) and nitrate (NO_3^-).

Comparison period	*N*	Management			Rain	Tair	Tsoil	WFPS	EC	Organic C	pH	NH_4	NO_3
		Silage cut date	Fertilizer date	Application rate									
				[kg N ha^{-1}]	[mm]	[°C]	[°C]	[%]	[mS m^{-1}]	[%]		[kg ha^{-1}]	[kg ha^{-1}]
8/1/2019 - 7/2/2019	30				54.1	5.8	9	61.4	56.9			7.9	5.4
4/3/2019 - 26/3/2019	22		05/03/2019	40	67.9	7.5	10.4	70.7	60.2			8.8	4.4
1/4/2019 - 24/4/2019	23		01/04/2019	70	70.2	8.5	11.6	66	78.4	3	5.9	16.2	28.7
4/6/2019 - 27/6/2019	23	14/05/2019	05/06/2019	80	73.7	8.8	16.9	48.6	90	3.1	5.9	43.7	57.9
7/8/2019 - 27/8/2019	20	04/07/2019			100.9	15.4	20.7	44	70.3	3.2	6	2.5	19.3
2/9/2019 - 2/10/2019	30	05/09/2019	11/09/2019	40	79.3	13.7	17.8	42.9	85.1	3.2	5.9	20.4	47.5
10/10/2019 - 3/12/2019	54				247.3	8.1	12	49.7	54.1				
Total / Average	202			230	693.4	9.7	14.1	54.8	70.7	3.1	5.9	16.6	27.2

Table 4.2: Eddy covariance (EC) and static chamber (CH) N_2O fluxes were partitioned into six different methods to calculate summary N_2O flux statics to investigate spatial and temporal differences in measurements from both techniques.

Abbreviation	Method
EC_{All}	All EC measurements over the comparison period
EC_{CH}	EC measurements during the time of chamber measurements
CH_{All}	All CH flux measurements averaged using the arithmetic mean
CH_{Bayes}	All CH flux measurements averaged using the Bayesian mean
CH_{FP}	Daily averaged CH flux measurements within the footprint of the EC tower using the arithmetic mean
$CH_{Bayes-FP}$	Daily averaged CH flux measurements within the footprint of the EC tower using the Bayesian mean

4.2.2 Static chamber measurements

N_2O fluxes were measured using the closed CH method, as outlined in de Klein *et al*. Thirty square stainless-steel collars (40 cm wide, 15 cm height) were installed in September 2018 across the field site to a depth of 5-10 cm depth following a sector randomization design (Chadwick et al., 2014). The CH lids were 10 cm high which created a headspace of approximately 20-22 L. CHs were closed during tractor spreading of CAN fertilizer, opened immediately afterwards and subsamples of CAN fertilizer were applied at the same rate homogeneously by hand within the chamber area. N_2O fluxes were measured between 10:00 h and 14:00 h (GMT) to best reflect daily average N_2O emissions (de Klein and Harvey, 2015). Background N_2O fluxes were measured once a week. Following CAN fertilizer applications, the measurement frequency increased to 4 measurements per week (for the first 2 weeks) and 2 times per week (for the following 2 weeks) before returning to the background (weekly) measurement frequency.

Gas samples were taken from the CH headspace over a 40-minute period at 20 minute intervals (T_0, T_{20} and T_{40}). Headspace gas measurements were extracted through a rubber septum (Becton Dickinson, Oxford, UK) using a 10ml polypropylene syringe (BD Plastiplak, Becton Dickinson) fitted with a hypodermic needle (BD, Microlance 3; Becton Dickinson). Gas samples were injected into a pre-evacuated (to -1,000 mbar) 7ml screw-cap septum glass vials (Labco, High Wycombe, UK). N_2O concentrations were analysed using gas chromatography (GC) with a detection limit of 0.05 ppm (Scion 456-GC, Kirkton Campus Livingston, UK), equipped with an electron capture detector with high purity helium as a carrier gas. Hourly fluxes in μg N_2O m^{-2} hr^{-1} were calculated by linear regression of changes in N_2O concentration within the chamber headspace between T_0 to T_{40} (Krol et al., 2017) (Eq. 4.3)

$$F_{chamber} = \left(\frac{\Delta C}{\Delta T}\right) x \left(\frac{M \; x \; P}{R \; x \; T}\right) x \left(\frac{V}{A}\right) \qquad \text{Equation 4.3}$$

Where ΔC is the change in headspace concentration of N_2O during the enclosure period in ppbv, ΔT is the enclosure period in hours, M is the molecular weight of N_2O (44.01 g mol^{-1}), P and T are the atmospheric pressure and temperature at the time of gas sampling, respectively, R is the ideal gas law constant (8.314 J K^{-1} mol^{-1}), V is the headspace volume in a closed chamber (m^3) and A is the area covered by the collar of the gas chamber (m^2). Linearity of N_2O accumulation within the chamber headspace was determined by assessing the coefficient of determination (R^2); where the $R^2 < 0.7$ flux measurements were removed from the dataset. In addition to this, CO_2 concentrations were measured adjacent to N_2O by GC, and where CO_2 concentrations showed deviations from a linear accumulation within the chamber headspace (i.e. a transition from plant respiration to photosynthesis), it was assumed there was a leak within the chamber and N_2O flux measurements were removed from the dataset.

4.2.3 Soil measurements

Soil temperature (°C), electrical conductivity (mS m^{-1}) and volumetric water content (VWC %) measurements (WET sensor, Delta-T Devices Ltd, Burwell, UK) were taken at the same time as the CH flux measurements at 6.5 cm depth and 50 cm from the CH location. Topsoil cores were taken a meter away from CH locations 48 hours before and 24 hours after each fertilization event, using a 10 cm depth and 1.7 cm diameter soil corer. Data derived from soil core analysis were used to characterize the key soil characteristics across the field site over the annual sampling campaign (Table 4.1). Soil cores were kept undisturbed and refrigerated at 4 °C until thoroughly mixed and wet sieved (4 mm). Composite subsamples were immediately taken to determine mineral N contents (NH_4^+ and NO_3^-), using 2M KCL as extractant (1:5 ratio), 1-h agitation and filtration (Whatman No. 2) following recommendations from Jones and Willett (2006). Extracts were analysed using an Aquakem 600 discrete analyser (Thermo Electron OY, Vantaa, Finland) for NH_4^+-N (Standing Commitee of Analysts, 1981) and NO_3-N (Askew, 2012). The remainder of the mineral N soil subsample was oven dried at 105 °C over 24 hours to determine soil moisture content. The rest of the composited sample was air-dried and analysed for pH (Gilson 215 Liquid Handler, Middleton, USA) and soil organic carbon (SOC) contents (infrared CN analyser after ball-milling; LECO TruSpec, USA). Sharpened cylindrical rings (n =30; 10 cm depth; 3.7 cm diameter) were used to sample the soil bulk density (BD, debris > 2 mm not considered) of surface topsoil across the field site prior to commencing the experiment and subsequently, the water-filled pore space (WFPS) by dividing the VWC by the total porosity of the BD sample (Linn and Doran, 1984).

4.2.4 Micrometeorological measurements

An EC mast was installed with a 3-D sonic anemometer (CSAT-3, Campbell Scientific Ancillary, Logan, UT, USA) mounted at 2.2m to measure fluctuations in the 3-D wind components at a frequency of 10 Hz. A 10 m long, 10 mm inner diameter perfluoroalkoxy (PFA) tube was attached and placed 30 cm apart from the sonic anemometer in the same horizontal axis. To minimize debris and pollution obstructing the PFA tubing, a 2 mm fabric mesh was fitted approximately 2cm out from the tip of the inlet tubing. The air inlet extended to a temperature controlled trailer (161 cm x 98 cm x 127 cm) where it was connected to a quantum cascade laser (QCL) absorption spectrometer (LGR 23R N_2O/CO analyser, Los Gatos Research, California, USA) for measuring N_2O fluxes at 10 Hz with a detection limit of 0.03 ppb over a 30 minute period. The inlet tube was fitted with two in-line 2 µm filters (SS-4FW4-2, Swagelok™) and the filter threads were wrapped in polytetrafluoroethylene (PFTE) tape to minimize air leaks. Additional 2 µm and 10 µm (Los Gatos Research, California, USA) filters were fitted within the QCL at the entrance of the inlet tubing and upstream of the internal pump, respectively. A 2.4 m long and 2.5 cm wide PDTE clear suction hose with steel spiral wired rings (Tec Industry, Dublin, Ireland) connected the QCL to a dry scroll vacuum pump (XDS35i, Edwards, West Sussex, UK) which was used to draw air into the inlet and cell of the QCL with an approximate flow rate of 30 -35 standard L min^{-1}. The cell pressure was set at 85 torr and the replacement rate of air within the cell was 0.097 s^{-1}.

Ancillary sensors at the EC site included an air temperature and relative humidity probe (HMP155C, Campbell Scientific, Logan, UT, USA), two net radiation sensors (NR-

Lite, Kipp and Zonen, Delft, The Netherlands), two self-calibrating soil heat flux plates installed at 5 cm soil depth (HFP01SC, Hukseflux, Delft, The Netherlands), photosynthetic active radiation (PAR) (PQS1, Kipp and Zonen, Delft, The Netherlands) and averaging soil temperature probes (TCAV-L, Campbell Scientific, Logan, UT, USA) installed at 2 cm and 6 cm depth above the soil heat flux plates. Time domain reflectometers (CS616, Campbell Scientific, Logan, UT, USA) measured soil VWC in the upper 15 cm of soil. Data from the EC system was stored and collected from the CR3000 micrologger (Campbell Scientific, Logan, UT, USA).

4.2.5 Post-processing eddy covariance flux data

Ecosystem scale N_2O fluxes were continuously measured over a 365-day period in 2019 with the exception of short equipment maintenance intervals that accounted for 45 days. Raw EC data at 10 Hz was processed using the Eddypro software, version 7.0.4 (www.licor.com/eddypro). EC N_2O fluxes (µmol m^{-2} s^{-1}) were calculated as the covariance between the vertical wind speed (w) and the N_2O concentration (ρc) (Eq. 4.4) (Burba, 2013). To compare EC N_2O fluxes to CH N_2O fluxes, units were converted from µmol N_2O m^{-2} s^{-1} to µg N_2O-N m^{-2} hr^{-1}.

$$F_{EC} = \overline{w'\rho c'} \qquad \text{Equation 4.4}$$

Raw data was screened and statistically evaluated according to Vickers and Mahrt (1997) for drop-outs, amplitude resolution, absolute limits, skewness and kurtosis tests for de-spiking tests. Double rotation was performed to compensate for the anemometer tilt by nullifying the average cross-stream and vertical wind components (Kaimal and Finnigan, 1994). Block averaging was used to calculate turbulent fluctuations. The time lag for N_2O was estimated using the covariance maximization procedure in two steps. First, the maximization of covariance of data over six hour

chunks of sequential data was determined over a large window of 10 seconds. Second, once a steady time lag was identified throughout the measurement period, a second covariance of maximization of the same six hour data chunk was re-run over a narrower window of 0.3 seconds, using the median running time-lag over a 7 day period as the mid-point. Finally, the mixing ratio data was re-paired with the wind data at a fixed time-lag of 0.5 seconds based on the previous maximisation of covariance, and eddy pro was run with a fixed time-lag, with fluxes calculated over a 30 minute period. Spectral attenuation effects following analytic methods described in Fratini et al. (2012) and Moncrieff et al. (2004) determined low and high-pass spectral correction factors for the data, respectively. A 5-step quality control protocol was applied for filtering bad quality N_2O fluxes. Flux data was removed from the data set if (1) less than 70 % of the flux contribution came from inside of the boundaries of the field site, as determined by the analytical footprint model described by Kormann and Meixner (2001), (2) if flux quality control flags by Foken (2003) were category 6 or above; (3) where low turbulent conditions were present, defined as the friction velocity (u^*) < 0.1 $m^{-1} s^{-1}$ (Lognoul et al., 2019); (4) where the flux random uncertainty integrated over a fixed 10s correlation period was > 0.001 μmol N_2O m^{-2} s^{-1} as estimated by the method of Finkelstein and Sims (2001); and (5) where flux values were < -0.1 μmol N_2O m^{-2} s^{-1} as such values were deemed unrealistic for this field site and similarly managed grasslands (Wecking et al., 2020b). After filtering, 46 % of measured fluxes passed the quality control procedure. N_2O flux measurements were partitioned into two dataset (1) fertilizer events, defined as the first 30 days following fertilizer application, and (2) background, defined as 30 days outside of a fertilizer event. Each dataset was gap-filled separately using a simple multivariate process based model that included: (1) rolling averages of Tair, Tsoil, WFPS and rolling sums of

rainfall over 6 hr^{-1}, 12 hr^{-1}, 24 hr^{-1}, 48 hr^{-1}, 100 hr^{-1} periods (Mishurov and Kiely, 2011) where data correlated significantly with log(N_2O-N flux) as determined from a subsets regression model performed in R studio (Rstudio Team, 2020); (2) days since fertilizer application; and (3) the previous and next measured flux in the dataset. The gap-filled fertilizer events and background datasets were merged, creating a gap-filled EC N_2O flux data set for the experimental year.

4.2.6 Data analysis

The coefficient of variation (CV) was used to describe the variability of N_2O fluxes over each comparison period for each subset of EC and CH data Eq (4.5):

$$CV = \left(\frac{\partial}{\mu}\right) * 100 \qquad \text{Equation 4.5}$$

Where ∂ is the standard deviation and μ is the arithmetic mean, expressed in percentage. An overlay analysis was performed on ArcMap (Plummer, 2015) to identify which CH measurements were within the footprint of the EC. Using a hand-held GPS device (GPSMAP 64, Garmin, Shaffhausen, Switzerland), GPS coordinates of CH locations within the field site were measured and overlaid on images of the EC footprint (Kljun et al., 2015) during the time of CH measurements (Fig. 4.2). Comparisons between EC and CH flux measurements were made using orthogonal regression in order to avoid biases between methodologies (Jones et al., 2011). CH hourly fluxes were assumed to be representative of daily emissions and were used to calculate the daily mean N_2O flux. In order to approximate the total N_2O produced from CAN, cumulative fluxes by CH and EC were calculated by linear interpolation between daily mean fluxes. Cumulative fluxes were used to derive emission factors (EFs) from CAN (Eq. 4.6). EFs represent the % of N_2O-N emitted from CAN applied.

$$EF = \left(\frac{[N_2O_{CAN} - N_2O_{Control}]}{\text{N applied}}\right) * 100 \qquad \text{Equation 4.6}$$

Where N_2O_{CAN} is the cumulative N_2O emissions (kg N_2O-N ha^{-1} yr^{-1}) from CAN, $N_2O_{Control}$ is the cumulative N_2O emission (kg N_2O-N ha^{-1} yr^{-1})from a control (in this study, defined as 0), N applied is the rate of CAN applied (kg N ha^{-1} yr^{-1}). In order to compare field scale CH flux measurements with ecosystem scale EC flux measurements, daily mean CH measurements were upscaled using a Bayesian approach (Wild et al., 1996). Markov Chain Monte-Carlo (MCMC) simulations were performed using Gibbs sampling to estimate the posterior distribution of μ by combining the prior data with this study's data. MCMC simulations were run on the freely-available JAGS software (Plummer, 2015). The prior dataset selected for this study was from Cowan et al. (2017) as log-normal distributions from both datasets overlapped well. The posterior distribution is primarily influenced by the data, except where the data does not possess a log-normal distribution and therefore cannot constrict the fit of μ_{log} and σ_{log} variables. The prior prevents the range of μ from expanding into unrealistic ranges by reducing the influence high, outlier values have on μ. The Bayesian method was used to estimate μ and the 95 % confidence intervals of the posterior distribution from CH measurements (see Table 4.3).

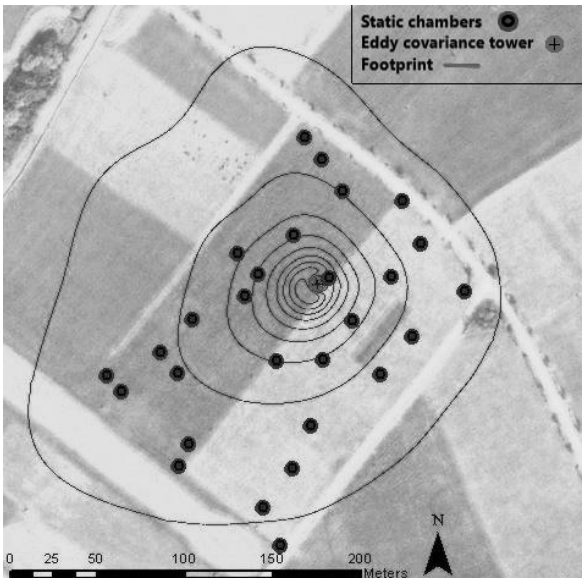

Figure 4. 2: Static chamber (CH) locations within the eddy covariance (EC) footprint for 2019 (Kljun *et al.* 2015) where black circles with rings represent CH, the grey circle with a cross is the EC tower and grey contour lines represent the footprint of the EC where the outer to inner contour line represents 90 % – 10 % of the footprint, respectively.

4.3 Results

4.3.1 Meteorological data

Meteorological data measured at the EC station can be seen in Fig. 4.3. Mean daily air temperature ranged from 0.9 °C in January to 18.2 °C in July, with an annual mean temperature of 10.3 °C (Fig. 4.3a). Soil temperature at 6cm depth was greatest in July and lowest in December with values of 20.0 °C and 1.7 °C, respectively. WFPS measured in the upper 15 cm of the soil, peaked in November at 74.9 % and was lowest in September at 39.6 % (Fig. 4.3b). Prolonged dry periods (greater than 14 consecutive days at <50 % WFPS) were observed in July and September. The total annual rainfall for the experimental period was 958.4 mm (Fig. 4.3c), with heavy rainfall events of 40.1 mm and 30.7 mm occurring in August and April, respectively.

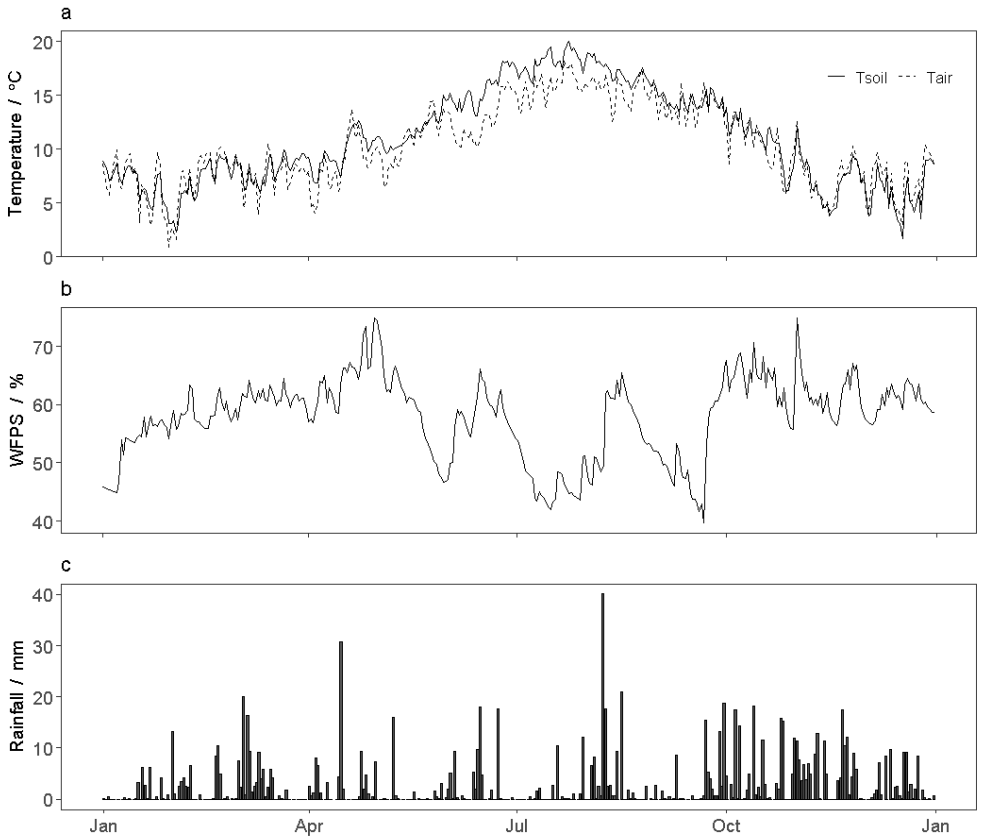

Figure 4. 3: Meteorological data measured at the field site from January 2019 to December 2019 where panels (a), (b) and (c) show mean daily, soil temperature (°C) (Tsoil) (solid line) , and air temperature (°C) (Tair) (dashed line), water-filled pore space (WFPS %), and rainfall (mm) respectively.

4.3.2 Observed fluxes of N_2O using chamber and eddy covariance methods

All N_2O-N fluxes measured by both CH and EC exhibited a log-normal distribution throughout the year (Fig. 4.4). Measured N_2O-N emissions from both techniques increased exponentially in the days immediately following fertilizer application (Fig. 4.5). Fluxes returned to background magnitude (defined as 48 N_2O-N μg m^{-2} hr^{-1} which represents the 85 % quantile for flux measurements made 30 days post fertilizer application) between 4 and 29 days. The maximum mean daily N_2O-N fluxes observed were 814.76 μg N_2O-N m^{-2} hr^{-1} using EC technique and occurred 18 days post- summer

fertilizer application and was preceded by a heavy rainfall event (17.6 mm). Maximum mean daily N_2O-N fluxes measured by CH were observed in spring at 538.89 µg N_2O-N m^{-2} hr^{-1}, also coinciding with a heavy rainfall event (20.9 mm). Delayed peaks in N_2O-N emissions were also measured during autumn, with peak emissions of 417.14 µg N_2O-N m^{-2} hr^{-1} (CH) and 313.22 µg N_2O-N m^{-2} hr^{-1} (EC) occurring 31 days post application, during which the WFPS increased from 48.77 % to 63.85 % (Fig. 4.3b). Minimum daily averaged N_2O flux measurements represented a zero flux from the system and were observed in winter at -0.14 µg N_2O-N m^{-2} hr^{-1} and -0.40 µg N_2O-N m^{-2} hr^{-1} for EC and CH techniques, respectively.

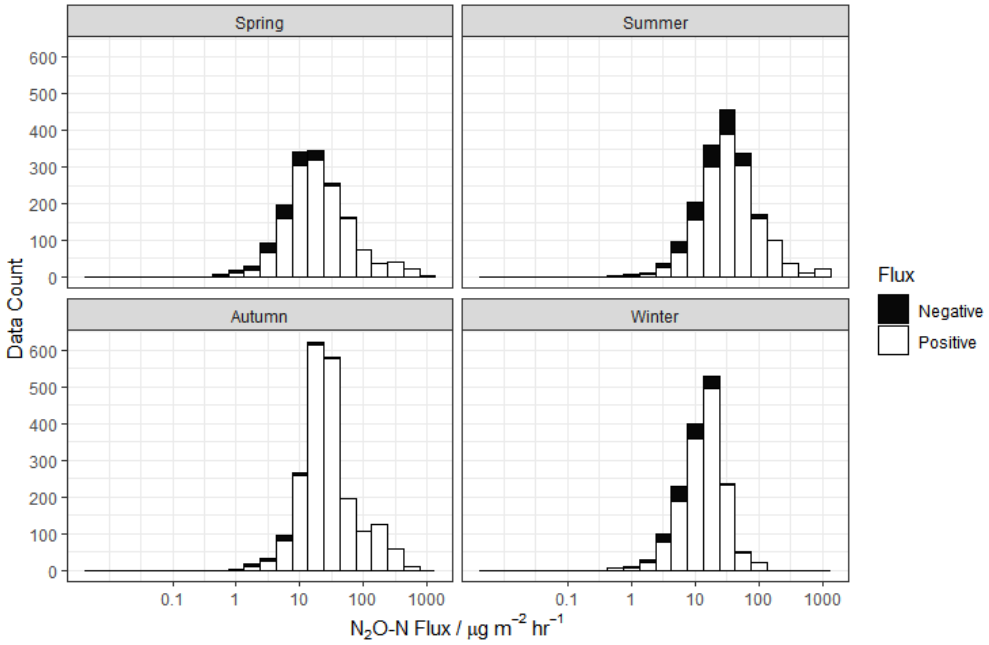

Figure 4. 4: Frequency distribution of collective N_2O fluxes measured from both chambers and eddy covariance in 2019 for each season where spring fluxes were measured in February, March and April, summer fluxes were measured in May, June and July, autumn fluxes were measured in August, September and October and winter fluxes were measured in November, December and January. N_2O fluxes are shown on a log-transformed axis but real values on the axis. Negative fluxes are shown on a positive scale but coloured black.

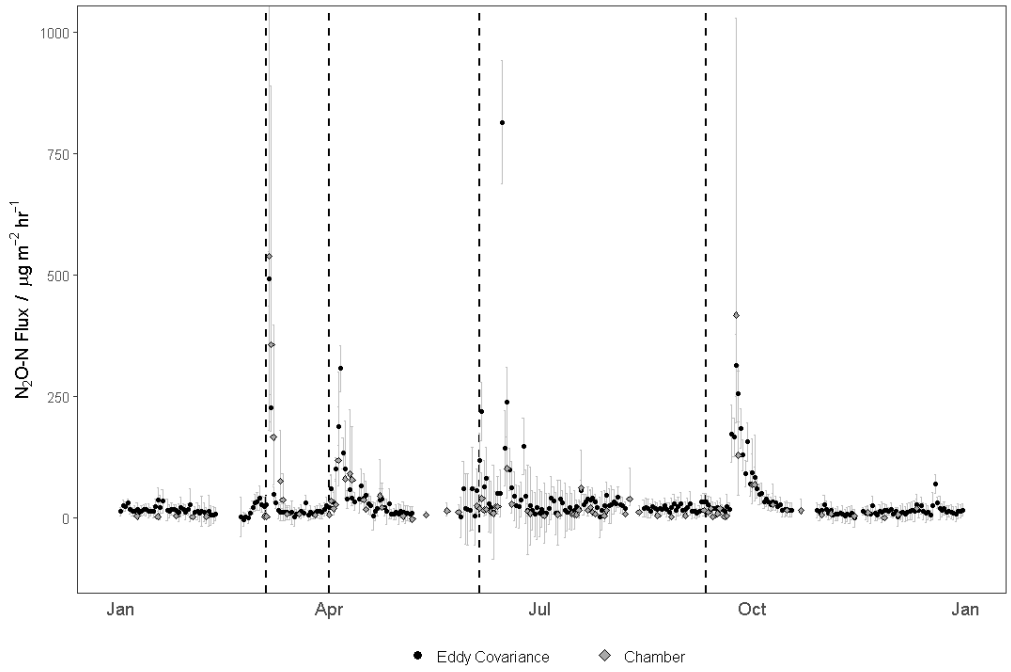

Figure 4. 5: 2019 N_2O-N fluxes where black circles represent mean daily eddy covariance flux measurements, grey diamonds represent mean daily chamber flux measurements, grey lines represent the 95 % confidence interval of flux measurements, and broken lines mark the date of fertilizer application.

4.3.3 Comparison of chamber and eddy covariance fluxes

Linear comparisons between subsets of daily averaged EC and CH (see Table 4.2) N_2O flux measurements from the comparison periods (see Table 4.1 for dates) are shown in Fig. 4.6. Summary statistics on flux measurements for each subset for each comparison period are shown in Table 4.3. Over the individual comparison periods, CH measurements were within the range of EC measurements. The most robust relationship between CH and EC measurements was for EC_{CH} and CH_{FP} (R^2 = 0.81) (Fig. 4.6d), where both methods were measuring N_2O fluxes over the same space and time, EC_{CH} and CH_{All} (R^2 = 0.79) (Fig. 4.6b) and EC_{CH} and CH_{Bayes} (R^2 = 0.80) (Fig. 4.6f) where EC measurements made during the time of CH measurements are in close agreement with CH measurements where the sample size was large (n ≈ 30) and the log-normal

distribution of the sample size was accounted for. This suggests that temporal alignment between techniques was more import than spatial alignment for comparable flux measurements. The weakest relationships involved smaller subsets of CH data calculated by the Bayesian method (EC_{All} vs $CH_{Bayes\text{-}FP}$ R^2= 0.45 [Fig. 4.6g]; EC_{CH} vs $CH_{Bayes\text{-}FP}$ R^2 = 0.36 [Fig. 4.6h]). Agreement between subsets of CH and EC fluxes, was primarily driven by a few high flux measurements following fertilizer applications, which made up only a small portion of the dataset (15 %). For smaller subsets for daily averaged CH measurements inside the footprint of the EC tower, the Bayesian method produced asymmetrical error bars. Where flux values were greater than 115 µg N_2O-N m^{-2} hr^{-1}, error bars were often several orders of magnitude larger than the estimated flux, due to the inability to constrain an arithmetic mean from a log-normally distributed data set with a low number of measurement points. In general, variability in N_2O-N flux measurements (CV %) was greater for N_2O-N fluxes measured by CH compared to EC over the comparison periods (Table 4.3).

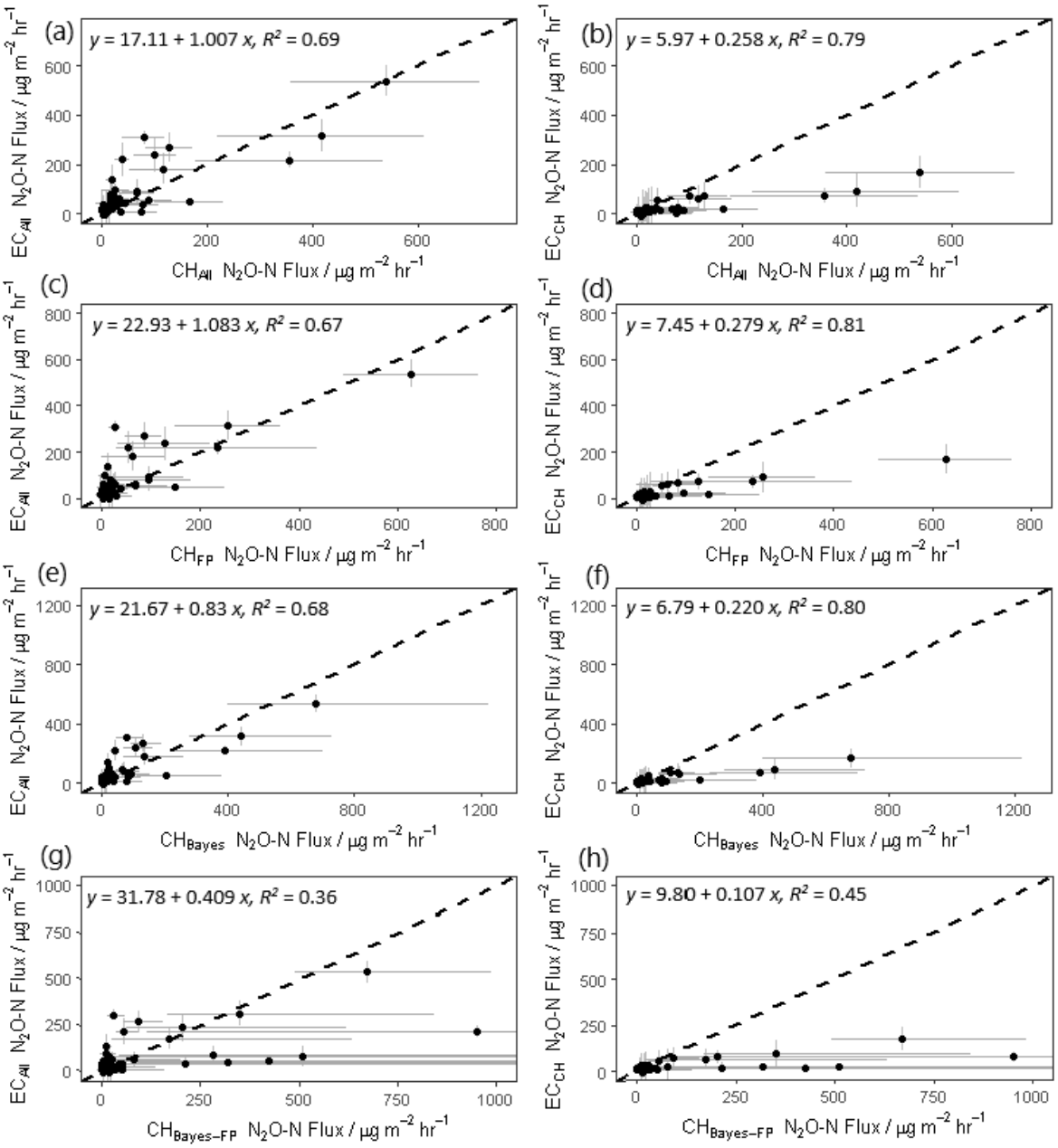

Figure 4. 6: Comparison plots for (a) all half-hourly eddy covariance (EC) N_2O-N fluxes (EC_{All}) and all daily averaged chamber (CH_{All}) N_2O-N fluxes and (b) EC measurements during the time of chamber measurements (EC_{CH}) and CH_{All}, (c) EC_{All} and daily averaged chamber flux measurements within the footprint of the EC tower (CH_{FP}), (d) EC_{CH} and CH_{FP}, (e) EC_{All} and all chamber flux measurements daily averaged using the Bayesian mean (CH_{Bayes}), (f) EC_{CH} and CH_{Bayes}, (g) EC_{All} and daily averaged chamber flux measurements within the footprint of the EC tower using the Bayesian mean ($CH_{Bayes\text{-}FP}$) and (h) EC_{CH} $EC_{T.ch}$ and $CH_{Bayes\text{-}FP}$. Black bars

represent the 95 % confidence interval error of half-hourly EC N_2O-N flux measurements, grey bars represent the 95 % confidence interval error of daily averaged chamber N_2O-N flux, and the broken grey line represents the 1:1 ratio. Ranges on the error bars have been curtailed for showing clearer comparisons between both techniques. See Table A.1 and Table A.2 in the Appendix for full values.

Table 4. 3: Summary statistics of N_2O flux measurements from chambers (CH) and eddy covariance (EC) for seven comparison periods. No. of samples represents the number flux measurements made during the measurement period. Methods used for calculating N_2O fluxes for each comparison period included all daily averaged chambers flux measurement (CH_{All}) and daily averaged chamber flux measurements from chambers that were located within the EC footprint (CH_{FP}), calculated using both arithmetic and Bayesian methods, all half-hourly EC flux measurements (EC_{All}) and half-hourly EC flux measurements that were made during the time of chamber measurements (EC_{CH}). The Coefficient of Variation (CV %) is averaged over all flux measurements (either daily arithmetic averages or half-hourly flux measurements).

				N_2O-N flux μg m^{-2} hr^{-1}						
Comparison period	#	Method	*N*	Arithmetic			Bayesian			
				95 % C.I.			95 % C.I.			
			no. of samples	min	max	mean	min	max	mean	CV %
8/1/2019-7/2/2019	1	CH_{All}	105	1.77	2.58	2.18	1.77	2.60	2.18	97.57
		CH_{FP}	43	1.62	2.69	2.15	1.61	2.72	2.16	82.54
		EC_{All}	94	59.89	62.01	13.89				118.25
		EC_{CH}	12	1.72	46.48	15.74				74.29
4/3/2019-26/3/2019	2	CH_{All}	295	79.04	139.71	109.38	67.67	100.60	82.77	243.02
		CH_{FP}	87	56.94	147.98	102.46	54.82	120.56	82.03	211.41
		EC_{All}	367	20.07	1088.96	96.29				202.40
		EC_{CH}	31	1.08	640.27	97.25				191.77
1/4/2019-24/4/2019	3	CH_{All}	353	35.05	43.91	52.77	33.19	44.32	38.46	160.96
		CH_{FP}	59	12.49	23.37	34.24	15.21	30.14	22.04	125.63
		EC_{All}	341	34.48	345.85	86.17				99.25
		EC_{CH}	39	15.53	304.51	70.82				76.86
4/6/2019-27/6/2019	4	CH_{All}	390	20.83	29.39	25.11	21.03	25.81	23.34	171.60
		CH_{FP}	94	22.56	48.47	35.51	26.30	39.49	32.36	180.28
		EC_{All}	321	81.07	418.44	104.15				92.43
		EC_{CH}	43	58.38	329.71	80.72				109.07
7/8/2019-27/8/2019	5	CH_{All}	150	6.71	11.56	16.41	8.14	13.04	10.50	184.70
		CH_{FP}	39	6.12	9.63	13.14	6.43	13.48	9.73	90.06
		EC_{All}	99	12.10	51.02	18.11				53.36
		EC_{CH}	14	12.10	35.69	18.09				79.29
2/9/2019-2/10/2019	6	CH_{All}	388	38.24	55.89	73.54	35.65	48.07	41.48	241.23
		CH_{FP}	123	29.90	46.13	62.35	31.18	51.53	40.46	147.25
		EC_{All}	339	29.85	539.44	102.59				126.31
		EC_{CH}	58	2.68	403.32	79.56				139.07
10/10/2019-3/12/2019	7	CH_{All}	299	8.36	10.79	13.22	8.63	12.02	10.29	162.31
		CH_{FP}	69	9.42	14.57	19.72	10.25	19.46	14.53	110.61
		EC_{All}	283	46.48	61.30	17.17				90.33
		EC_{CH}	34	46.48	41.44	15.29				129.07

4.3.4 N_2O fluxes and environmental variables

Diurnal patterns in N_2O emissions were not observed suggesting that changes in temperature between day and night and potential root exudation of carbon during photosynthesis (and therefore changes in soil carbon availability), did not have a significant control on N_2O production. Mean daily log(N_2O-N) emissions showed the greatest variability within a temperature range of 7 °C and 15 °C, across WFPS values of 55 % to 65 % and with increasing cumulative rainfall. Rolling averaged data presented in Table 4.4 best explained the variability in log(N_2O-N) fluxes from the respective environmental factor, as determined by a subset regression model. The full output of this model can be seen in Table A.3. Correlations with background log(N_2O-N) fluxes (30 days outside of fertilizer events) and WFPS, rainfall, air and soil temperature were weak but improved in the 30 days following fertilizer application. Environmental variables in Table 4.4 were significantly correlated ($p < 0.05$) with log(N_2O-N) flux measurements.

Table 4. 4: Variance in log(N_2O-N) fluxes explained by a subset regression model on water-filled pore space (WFPS %), rainfall (mm) air temperature (Tair ^oC) and soil temperature (Tsoil ^oC) over rolling averages of 48hrs^{-1} and 100 hrs^{-1} periods in the 30 days following fertilizer application (Fertilizer) and in the 30 days outside of fertilizer applications (Background).

Variable	Treatment	R^2
WFPS 48 hr^{-1}	Fertilizer	0.50
Rainfall 100 hr^{-1}	Fertilizer	0.50
T_{soil} 100 hr^{-1}	Fertilizer	0.48
T_{air} 100 hr^{-1}	Fertilizer	0.43
WFPS 100 hr^{-1}	Background	0.31
Rainfall 48 hr^{-1}	Background	0.31
T_{soil} 48 hr^{-1}	Background	0.31
T_{air} 100 hr^{-1}	Background	0.27

4.3.5 Modelled eddy covariance N_2O emissions

A linear multivariate regression model consisting of (1) WFPS, rainfall, air and soil temperature over 6 hr^{-1}, 12 hr^{-1}, 24 hr^{-1}, 48 hr^{-1} and 100 hr^{-1} periods (Table. A.4); (2) time since fertilizer application; and (3) the previous and next available measured flux value between the gap in the dataset, was used to gap-fill EC flux measurements, and calculate the associated uncertainty. Where correlation between environmental variables and fluxes were found to be significant ($p<0.05$), these were included in the gap-filling model (see Table A.4 for a summary of the model output). Modelled and measured flux values showed a strong correlation ($R^2 = 0.92$) (Fig. A.1). The upper and lower uncertainty surrounding modelled N_2O-N flux values was expressed as the 2.5 % and 97.5 % confidence intervals (Fig. 4.7). Uncertainty was greatest for high N_2O flux values (particularly around fertilizer events) compared to flux measurements outside of fertilizer events.

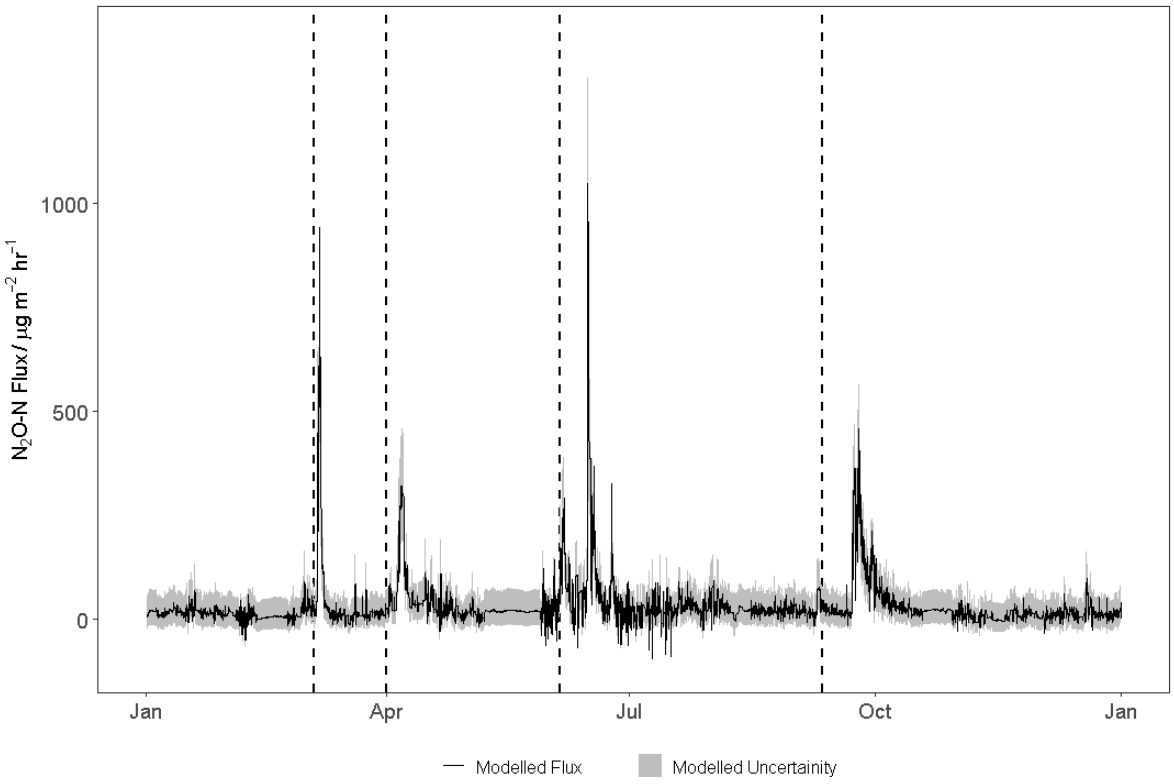

Figure 4. 7: Linearly modelled half-hourly N_2O-N flux values (black line) and uncertainty (shaded areas), which represents the upper (97.5 %) and lower (2.5 %) limits of the modelled flux value. The dashed lines represent fertilizer applications (see Table 2 for dates).

4.3.6 Measured Cumulative fluxes

Cumulative N_2O fluxes were calculated for each subset of EC and CH data over each comparison period (see Table A.5 for a summary). Cumulative N_2O emissions measured by EC were greater than cumulative emissions measured by CH. Cumulative N_2O emissions for EC_{All}, CH_{All} and CH_{Bayes} were lowest in the winter (comparison #1) and greatest in the autumn (comparison #6). Cumulative emissions from $CH_{Bayes\text{-}FP}$ were consistently higher than other CH methods due to the small sample size and high variance in the data. Modelled flux values were used to gap-fill measured EC flux values in order to calculate cumulative emissions for the field site for 2019. Cumulative annual N_2O-N fluxes from January to December were 3.35 (± 0.5) kg N ha^{-1}, 2.98 (± 0.17)

kg N $ha^{-1}$and 3.13 (± 0.24) kg N ha^{-1}, which translated to EFs of 1.46, 1.30 and 1.36 % for EC, and CH fluxes by the arithmetic and Bayesian method, respectively (Fig. 4.8). Cumulative fluxes between CH (both arithmetic and Bayesian) and EC were quite similar overall, with both methods showing four distinct emission events following fertilizer applications. EC cumulative emissions were consistently lower than CH emissions from March to mid-June but following the June fertilizer application, higher cumulative flux values were observed by EC compared to CH for the duration of the year.

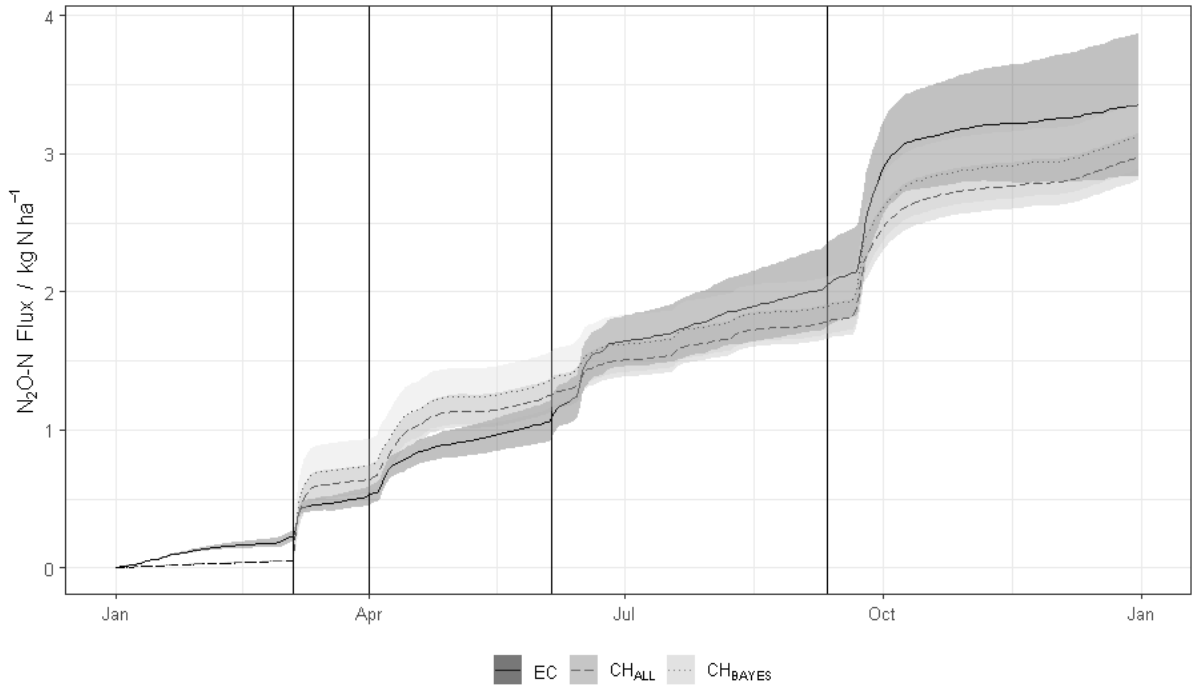

Figure 4. 8: Cumulative daily averaged N_2O-N fluxes (black line) and uncertainty (shade) (expressed as the least squares) from January to December 2019 by eddy covariance (solid line) and chambers by the arithmetic (dashed line) and Bayesian method (dot-dashed line) and the solid vertical lines represent fertilizer applications.

4.4. Discussion

4.4.1 Drivers of N_2O fluxes observed

The range of N_2O fluxes observed in this study from CH and EC methods are comparable with those at other fertilized temperate grassland sites (e.g., Cowan et al. 2020 for EC, Rafique et al. 2011 for CH). N_2O emissions were greatest in the summer and autumn following fertilizer application where extended dry periods (< 50 % WFPS) were followed by heavy rainfall events (≥ 17 mm) and which led to higher WFPS values (> 60 %). Similar temporal trends in N_2O emissions following fertilizer application have been documented in cropland sites (Waldo et al., 2019), restored grasslands (Merbold et al., 2021) and at various soil systems (Shcherbak and Robertson, 2019). While N_2O emission events often coincided with the climatic conditions described above, peak emission events were driven by management. The variability in N_2O emissions was better explained by WFPS, air and soil temperature and rainfall following fertilizer application ($R^2 \leq 0.50$) compared to outside of management ($R^2 \leq 0.31$). Similar drivers of variability in N_2O emissions were identified in Krol et al. (2016) and Maire et al. (2020). N inputs from fertilizer in excess of plant demands can result in N losses of up to 50 % (Fageria and Baligar, 2005), where residual N accumulates in soils. N-fertilizers create peak N_2O emission events by creating hotspots of N_2O through the introduction of substrates for denitrification (NH_4^+ and NO_3^-) into the soil, where by emissions of N_2O increase with greater soil NO_3^- (Zanatta et al., 2010). Increases in soil NH_4^+ and NO_3^- were observed following fertilizer application (Table 4.1), with the highest mineral N content following the June fertilizer application (43.7 kg ha^{-1} NH_4^+ and 57.9 kg ha^{-1} NO_3^-), which coincided with the greatest emission event of the entire experimental period at 814.76 µg N_2O-N m^{-2} hr^{-1} .

4.4.2 Comparison of chamber and eddy covariance flux measurements

CH and EC flux measurements were most comparable when flux measurements were high (>115 μg m^{-2} hr^{-1}), the CH sample size was large for a given day (n ≥ 15) (for both the arithmetic and Bayesian approach) and when EC and CH measurements were taken over the same area and time (i.e CH flux measurements made in the EC footprint and EC flux measurements made during the time of CH measurements). This agreement between EC and CH fluxes has been observed in previous studies (Christensen et al., 1996, Jones et al., 2011, Laville et al., 1997). Using the arithmetic mean when all CH measurements were considered (n ≈ 30) was sufficient in estimating the sample mean and comparable with daily mean EC flux values (EC_{CH} and CH_{All} (R^2 = 0.79) (Fig. 4.6b)). This is because the arithmetic sample mean will not deviate systemically from the population mean where the sample size is large and variance is low. However, as a large sample size is required (which is not always the case in CH flux studies - (Hyde et al., 2016, Krol et al., 2017, Maire et al., 2020, Wecking et al., 2020b)), the arithmetic mean is considered an unreliable estimator of the true flux mean within a sample (Levy et al., 2017). Where the sample size is small and the variance is large (as is typical of N_2O flux data), the arithmetic method will typically underestimate the sample mean as infrequent, high flux values will often be absent from the sample. Where high flux values are included in the sample, the arithmetic mean will typically overestimate the sample mean. The Bayesian approach on the other hand, reduces some of the bias in N_2O flux measurements by accounting explicitly for the log-normal distribution and as a result providing realistic ranges of uncertainty within flux measurements. Where the CH sample size was small on a given day (n ≤ 5) (i.e. when selecting CH flux measurements that are only in the EC footprint), the Bayesian approach produced larger, more asymmetrical uncertainties compared to the arithmetic method. In this

instance, N_2O flux measurements did not meet the expectations based on the Bayesian model (i.e flux measurements showing a peak and decay pattern or multiple peaks or a large sample size with low variance) (Levy et al., 2017) and therefore, the N_2O flux data collected was not sufficient for accurately capturing the existing variability of N_2O fluxes.

Over the 86 days where both EC and CH measurements were compared, mean daily EC flux measurements were greater than CH flux measurements for a total of 63 days. Similar to the findings in this study, Wang et al. (2013) showed that CH N_2O flux measurements were lower than EC flux measurements by 17-20 % from a cotton field. However, numerous studies have reported contrasting results. For example, Pihlatie et al. (2005b) found CH N_2O flux measurements were consistently greater than EC measurements and Jones et al. (2011) found that 70 % of N_2O fluxes measured by EC were within the range of CH N_2O measurements in a grassland system, although this varied seasonally. Likewise, disagreement between EC and CH flux measurements have also been observed for CO_2 respiration rates, both in agri-ecosystems (Schrier-Uijl et al., 2010) and peatland sites (Cai et al., 2010). Disparities in flux measurements from both CH and EC can be the product of the limitations of the methods themselves. The CV was frequently greater in CH measurements compared to EC measurements due to the small scale variability detected in CH measurements. CH flux measurements represent single point measurements in space and time and, as a result, sudden dynamic variations in emissions due to either management or weather events for example, are not always quantified (Kroon et al., 2008). However, EC provides continuous, high frequency measurements and is therefore capable of capturing high emission events derived from hotspots and hot moments of N_2O. For example, two

days post fertilizer application in March and in conjunction with a cumulative rainfall event of 27.3 mm over this period, daily average EC emissions were 219.02 μg N_2O-N m^{-2} hr^{-1}, while CH fluxes measured at midday and integrated as a daily average were 36.63 μg N_2O-N m^{-2} hr^{-1}. Moreover, the footprint of the EC tower may not always overlap with the location of where CH measurements are made and therefore take measurements over different sources of N_2O emissions, for example in Fig. 2, 70 % of the EC flux footprint contribution does not encompass CH locations in the far South-West region of the field site.

In addition, EC measurements are completely *in situ* and thus, avoid artefacts caused by enclosure within a CH which are prone to under or over estimating the soil derived flux (Davidson et al., 2002). Such artefacts are caused by a) pressure differentials (Venturi effect) when lids are closed or in windy conditions, b) alterations in the boundary layer conditions and disturbance of diffusion gradients which can affect canopy coupling to the atmosphere within the CH, c) increases in temperature which can impact on both microbial processes and increase N_2O dilution via increased humidity (Davidson et al., 2002, Rochette and Hutchinson, 2005, Bain et al., 2005, Bertora et al., 2018, Clough et al., 2020).

4.4.3 Gap-filling N_2O flux data

Unlike CO_2 fluxes, there are no robust, validated process-based models available for gap-filling N_2O fluxes (Moffat et al., 2007). Emissions of N_2O are primarily controlled by N inputs (in the form of NH_4^+ and NO_3^-) into the system (Harty et al., 2016), as well as soil physical and microclimatic properties such as WFPS (Davidson et al., 2000), temperature (Butterbach-Bahl and Dannenmann, 2011), texture (Tan et al., 2009) and porosity (Choudhary et al., 2002). While repeated measurements of these variables are

feasible, in many cases continuous high frequency measurements (both spatially and temporally) are too costly or logistically not viable. Commonly used methods for gap-filling N_2O fluxes include linear interpolation (Mishurov and Kiely, 2011), 30-day running medians (Merbold et al., 2021) and general additive models (Cowan et al., 2020). While these methods have been accepted within the flux community, they should be used with due consideration for any potential limitations. Such gap-filling approaches for N_2O measurements are either too simplistic in approach, prone to large uncertainties or where a model is applied, are subject to overfitting and multicollinearity, which can reduce the sensitivity of model predictions by underestimating the variance of the fitted modelled parameters (Dorich et al., 2020). Here we proposed a multi-variate linear model that incorporates environmental data where the temporal pattern in the data is retained in order to account for 'emission events' over time and in doing so, provides an empirical method for interpolating between data points. The relatively high data coverage, with limited gaps exceeding a few hours and not during fertilization events (or the 30 days after), helped to reduce the uncertainties in this study. Though it is important to note that while this model was successful in gap-filling N_2O flux measurements in this study, it incorporates environmental and management data which are site-specific, and therefore may not be as successful where the experimental site is under a different management, climate and where the gaps in the data are more common. In order to further reduce uncertainties in gap-filling N_2O fluxes, we need to enhance our understanding of microbial communities and their role in N_2O production (Thompson et al., 2016) and implement methods that can facilitate this at high resolutions, both spatially and temporally. As flux datasets become larger, the use of neural networks (NN) for data-driven predictive modelling of N_2O will become more viable (Dorich et al., 2020).

4.4.4 Cumulative N_2O fluxes and emission factors

Cumulative CH N_2O fluxes are derived from non-continuous measurements commonly made during the daytime, expressed as a daily average and linearly interpolated between days (Dorich et al., 2020). Where the frequency of measurements are low, the uncertainty in the integration of measurements for cumulative flux estimates increases. As N_2O is highly variable in space and time, reducing the uncertainty in interpolating between measurement points requires many and frequent flux measurements (Lammirato et al., 2018).

In this study, cumulative N_2O emissions by CH were greater than EC cumulative fluxes prior to the June fertilization event, but following this event, cumulative emissions measured by EC were consistently greater than CH. Daily emissions of N_2O measured by EC peak following the June fertilizer event at 814.76 µg N_2O-N m^{-2} hr^{-1} following a rainfall event of 17.6 mm. Daily emissions captured by CH during this period were considerably lower at 7.74 µg N_2O-N m^{-2} hr^{-1}, suggesting that both frequency and the time of CH measurements (midday) were not sufficient to capture the N_2O emission event observed in the EC measurements. Similarly, cumulative EC emissions from the time of CH emissions (EC_{CH}) (typically between 10:00am and 2:00pm) were 19 % - 38 % (depending on the comparison period [Table A.5]) lower than cumulative EC emissions from the entire day (EC_{All}). While studies have shown higher N_2O emissions in the midday (Liang et al., 2018, Shurpali et al., 2016) our results suggest that only considering midday flux measurements could under-estimate the cumulative flux, and the magnitude of this under-estimation could be greater following fertilizer application. We recommend that daily CH flux measurements should be made at least twice a day (mid-day and night), with increasing frequency following N-inputs into the

system and rainfall events. Ideally, an automated chamber system should be used for comparison with EC flux measurements, where continuous flux measurements are available over high temporal resolutions. Annual cumulative N_2O fluxes measured by EC (3.35kg N ha^{-1}) were more similar to CH cumulative fluxes determined using the Bayesian method (3.13 kg N ha^{-1}) compared to the arithmetic method (2.98 kg N ha^{-1}). The Bayesian method captures the post-fertilization temporal pattern of peak and decay that is commonly observed in N_2O flux measurements (Cowan et al., 2019, Levy et al., 2017) by accounting for the log-normal distribution of the data. In doing so, the Bayesian mean will not attribute equal weight to all data points, as the arithmetic method does, and is therefore less likely to over or under-estimate the sample mean and will provide a more robust mean for a log-normally distributed dataset. EFs from this study for EC and CH derived using arithmetic and Bayesian methods were 1.46, 1.30 and 1.36 %, respectively, which is higher than the Intergovernmental Panel on Climate Change (IPCC) Tier 1 default value of 1 % (0.03 –3 %) EF for all fertilizers (Pachauri et al., 2014). EFs reported are within a similar range for EFs calculated by Harty et al. (2016) in a permanent pasture in Ireland (0.58 - 3.1 %), Cowan et al. (2020) in managed grasslands across the British Isles (0.7 – 1.3 %) and Smith et al. (2012) in grassland and arable sites across the United Kingdom (0.9 - 3.93 %). While a control treatment was not used in this study, we estimate that EFs with the inclusion of a cumulative control N_2O-N flux (Krol et al., 2016) would be 1.25, 1.09 and 1.16 % for EC and CH by the arithmetic and Bayesian methods respectively. Our study suggests that a default EF value for mineral fertilizer is too simplistic to account for the variability of N_2O at different spatial and temporal scales. The Tier 1 approach does not incorporate changes in emissions due to agricultural management or environmental variability (Dobbie and Smith, 2003). When considering the development of national and regional

level EFs for N_2O (Tier 2), it is essential that management data (e.g. fertilizer rates) is available over different spatial and temporal scales in order to produce robust estimates of N_2O emissions (Skiba et al., 2012).

4.5. Conclusions

Fluxes of N_2O measured by CH and EC were most comparable when (1) N_2O fluxes were high (>115 μg N_2O-N m^{-2} hr^{-1}); (2) both methodologies were measuring fluxes over the same space and time; and (3) when the number of CH replicates were ≥ 15 on a given sampling day. Measurements of N_2O emissions using the EC technique were greater than CH flux measurements (arithmetic or Bayesian) 76 % of the time over the outlined comparison periods. The Bayesian method was useful in upscaling CH N_2O flux measurements and providing reliable means and confidence intervals by accounting for the log-normally distributed nature of the data. Where the CH sample size was ≥ 15, the arithmetic and the Bayesian method showed similar daily averaged fluxes over the comparison periods. Where n ≤ 5, uncertainties in CH flux measurements calculated by the Bayesian method were large and asymmetrical due to the inability to fit an arithmetic mean from a log-normally distributed data set where the sample size is low. A multi-variate linear model that incorporates environmental data was used to gap-fill annual N_2O fluxes measured by EC and showed a strong correlation with measured flux values (R^2 = 0.92). Annual cumulative N_2O fluxes from January to December 2019 from gap-filled EC fluxes and CH fluxes derived from the arithmetic and Bayesian method, were 3.35 (± 0.5) kg N ha^{-1}, 2.98 (± 0.17) kg N $ha^{-1}$and 3.13 (± 0.24) kg N ha^{-1} respectively. EFs from EC and CH by the arithmetic and Bayesian method were 1.46, 1.30 and 1.36 %, respectively. N_2O emissions were greatest following CAN fertilizer application when conditions for denitrification were

favourable (WFPS > 60 %). In order to reduce EFs from mineral N fertilizer application, applications should be made where conditions for denitrification are limited, such as low soil moisture content and rainfall. Where potential hotspots of N_2O are present on agricultural landscapes (Cowan et al., 2017), N fertilizer application should be avoided on theses hotspot areas or nitrification and urease inhibitors should be used to reduce the availability of N for N_2O production (Luo *et al.* 2016).

Chapter 5: Nitrous oxide emission factors from an intensively grazed temperate grassland: a comparison of cumulative emissions determined by eddy covariance and static chamber methods.

Abstract

Quantifying nitrous oxide (N_2O) emissions from grazed pastures can be problematic due to the presence of hotspots and hot moments of N_2O from animal excreta and synthetic fertilizers. In this study, we quantified field scale N_2O emissions from a temperate grassland under a rotational grazing management using eddy covariance (EC) and static chamber techniques. Measurements of N_2O by static chambers were made for four out of nine grazing events for a control, calcium ammonium nitrate (CAN), synthetic urine (SU)+CAN and dung+CAN treatments. Static chamber N_2O flux measurements were upscaled to the field scale ($F_{CH\ FIELD}$) using site specific emission factors (EF) for CAN, SU+CAN and dung+CAN. Mean N_2O EFs were greatest from the CAN treatment while dung+CAN and SU+CAN emitted similar N_2O-N emissions. Cumulative N_2O-N emissions over the study period measured by $F_{CH\ FIELD}$ measurements were lower than gap-filled EC measurements. Emission factors of N_2O from grazing calculated by $F_{CH\ FIELD}$ and gap-filled were 0.72 and 0.96 %, respectively. N_2O-N emissions were derived mainly from animal excreta (dung and urine) contributing 50 % while N_2O-N losses from CAN and background accounted for 36 and 14 %, respectively. The study highlights the advantage of using both the EC and static chamber techniques in tandem to better quantify both total N_2O-N losses from grazed pastures while also constraining the contribution of individual N sources. The EC technique was most accurate in quantifying N_2O emissions, showing a range of uncertainty that was seven times lower relative to that attributed to static chamber

measurements, due to the small chamber sample size per treatment and highly variable N_2O flux measurements over space and time.

Work presented in this chapter is published in Agriculture, Ecosystems and Environment (https://doi.org/10.1016/j.agee.2021.107725) with author list as: Murphy, R.M. Saunders, M. Richards, K. G. Krol, D. J. Gebremichael, A. W. Rambaud, J. Cowan, N. and Lanigan, G. J.

Author Contributions: RM, MS, DK and GL designed the experiment. RM conducted the experiment and analysed the samples that were collected alongside JR and AG. Samples were analysed in the Teagasc Johnstown Castle with the support of laboratory technicians. RM with the help of NC conducted the flux data analysis. RM wrote the article with the contributions from all co-authors.

The overarching objective of this thesis chapter was to quantify field scale N_2O emissions from a grazed pasture using both static chambers and EC in tandem, where site specific N_2O emission factors from N sources (fertilizer, urine and dung) were used to upscale chamber N_2O measurements to the field scale, and the contribution of fertilizer, urine and dung to the total N_2O-N losses was determined for identifying source specific mitigation strategies.

5.1 Introduction

Nitrous oxide (N_2O) is a potent greenhouse gas (GHG), with a global warming potential (GWP) 265 times higher than carbon dioxide (CO_2), over a 100 year lifespan (Pachauri et al., 2014). The largest contribution to global anthropogenic emissions of N_2O comes from the agricultural sector, and livestock production systems account for 30-50 % of the total N_2O emissions from agriculture (Grossi et al., 2018). Sources of N_2O from

agriculture include the use of chemical and organic nitrogen (N) fertilizers and animal excreta (Flechard et al., 2007), with nitrogen in these materials converted to N_2O either as a by-product of the microbial process of nitrification or as an intermediate product of denitrification (Davidson et al., 2000). Intensively managed grassland pastures require frequent N fertiliser applications to stimulate grass growth between rotational grazing events. As a result, a portion of the mineral N applied as fertilizer is added to pre-existing N pools deposited by animal excreta, which can substantially increase N_2O losses (Hyde et al., 2016). The spatial heterogeneity of urine and dung deposits (Carpinelli et al., 2020, Maire et al., 2018) can lead to 'hotspots' of N_2O, with N loading rates of 400-2000 kg N ha^{-1} in the affected areas (Jarvis et al., 1995b). Such concentrations of N outweigh the uptake capacity of grass in the affected area, and this in conjunction with temporal variation in plant N demand and soil microclimatic conditions can further increase N_2O emissions from pastures (O'Connell et al., 2004). As a result, it can be difficult to accurately quantify N_2O-N losses at the field scale from grazing systems.

The Intergovernmental Panel on Climate Change (IPCC) developed a standardised method for reporting N_2O emissions using a tiered approach based on emission factors (EFs) to quantify the amount of N_2O-N lost as a proportion of N applied to pastures (De Klein et al., 2010). The IPCCs default (Tier 1) EFs for mineral fertilizers (EF_1) is 1 % with an uncertainty range of 0.3 – 3 %, and for urine and dung N deposition on pasture, range and paddocks by grazing animals (EF_{3PRP}) is 2 % with an uncertainty range of 0.7 – 6 % (Eggleston et al., 2006). However, numerous studies have reported lower EFs for N_2O-N from urine and dung patches, ranging from 0.12 to 0.69 % and 0.0027 to 0.19 %, respectively (Chadwick et al., 2018, Hyde et al., 2016, Krol et al., 2016, Simon

et al., 2018). As a result, the IPCC has revised the default EF_{3PRP} from 2 % down to 0.6 % (0 - 2.6 %) and has disaggregated grazing EFs for dung at 0.13 % (0 – 0.53 %) and urine 0.77 % (0.03-3.82 %), as well as revising the EF_1 at 1.6 % (1.3 – 1.9 %) in wet temperate climates (Buendia et al., 2019). However, (van der Weerden et al., 2021)reported higher mean emissions from dung and urine in wet temperate climates relative to the revised IPCC default values at 0.20 % (0.17 – 0.27 %) and 0.95 % (0.88 – 1.03 %). Default EFs reported by the IPCC use a Tier 1 methodology for reporting national N_2O emissions, however, there are large uncertainties surrounding these values. As a result, the IPCC encourages the use of country-specific (Tier 2) values which incorporate data on soil and climatic conditions, and farm management (Skiba et al., 2012). Ireland has developed Tier 2 disaggregated EFs for calcium ammonium nitrate (CAN) $EF_{1\,CAN}$ (1.4 %), cattle urine, $EF_{3cattle-urine}$ (1.2 %), and cattle dung, $EF_{3cattle-dung}$ (0.31 %) (Harty et al., 2016, Krol et al., 2016, Roche et al., 2016).

The most commonly used method to quantify N_2O EFs is the chamber technique, accounting for 95 % of the total field data on N_2O flux measurements (Rochette et al., 2008, Rochette, 2011, Wecking et al., 2020b). Manually-operated chambers are the most commonly used method for investigating treatment effects on soil N_2O fluxes at small spatial scales (Clough et al., 2020, Krol et al., 2017, Maire et al., 2020). However, due to the highly heterogeneous nature of N_2O emissions from intensively managed pastures (Cowan et al., 2017), and the limited spatial and temporal resolution of single point static chamber measurements (Jones et al., 2011), the chamber technique is not always sufficient to characterise field-scale emissions of N_2O from grazing systems. In addition, static chamber flux measurements are often associated with large uncertainties due to artefacts that de-couple the chamber microclimate from external

conditions. These include pressure differentials in the chamber headspace, as well as fluctuations in temperature and humidity (Hutchinson and Livingston, 2002, Rochette et al., 2008). Conversely, the eddy covariance (EC) technique provides real time, continuous measurements of the ecosystem to atmosphere exchange of N_2O that are integrated from multiple sources at the ecosystem scale. This technique is widely used to measure field scale N_2O emissions within agricultural landscapes (Cowan et al., 2016, Cowan et al., 2020, Haszpra et al., 2018, Liang et al., 2018), however, as EC flux measurements represent a single non-replicated flux value that is integrated over a large spatial area, it does not provide disaggregated emissions from various emission sources. Therefore, in order to more accurately quantify emissions from grazed pastures, the use of static chamber and EC techniques in a complimentary fashion is advised (Cowan et al., 2017, Wecking et al., 2020b). Flux estimates by EC can be used to quantify field scale emissions, while individual contributions from various sources can be determined by static chambers.

The objectives of this study were to 1) quantify the total field scale N_2O fluxes associated with a temperate grassland under a rotational grazing management system using the EC technique; 2) assess the contributions of background, fertilizer and animal excreta as determined by static chamber N_2O flux measurements and 3) evaluate how field scale emissions of background (i.e. no N applied), calcium ammonium nitrate (CAN), synthetic urine (SU)+CAN and dung+CAN compare with previously reported values in the literature.

5.2 Materials and Methods

5.2.1 Site description and experimental design

The study was carried out from January 1st to October 14th 2020 on a sandy loam soil site at the Teagasc Environmental Research Centre, Johnstown Castle, Co. Wexford in the south-east of Ireland (52.30 °N, 6.40 °W, 67 m above sea level. The mean annual air temperature and rainfall for this region over the last 10 years, is 10.1 °C and 1101 mm, respectively. The field site has a soil pH of 6.06, carbon (C), nitrogen (N) and phosphorus content of 3.52 % (± 0.12 %), 0.38 % (± 0.01 %) and 4.95 % (±0.20 %), respectively. The field site is a perennial ryegrass (*Lolium perenne*) grassland, consisting of two paddocks (10 and 11) with a total area of 2.65 ha^{-1} (Fig. 5.1). Historically, paddock 10 was managed for silage production receiving 230 kg of CAN ha^{-1} in 2019 and 255 kg CAN ha^{-1} in 2018. Paddock 11 has been under both a silage production system (the same as paddock 10 in 2019) and managed for livestock production, grazed by Holstein Friesian dairy cows in 2018, receiving 277 kg ha^{-1} of urea coated with the urease inhibitor (n-Butyl) thiophosphoric triamide, (NBPT). In this study, there was a total of nine rotational grazing events occurring approximately every 21 days, with an average stocking density of 3.2 livestock units (LU) ha^{-1}, and six fertilizer applications of CAN (see Table. 5.1). The prevailing wind direction is south-westerly, and the EC tower was set up in the North-East part of the field site to maximize the footprint (Fig. 5.1). During the measurement campaign, N_2O flux measurements were not available between 23rd March – 27th March, and 13th June – 15th June, for instrument maintenance. Additionally, field measurements of N_2O fluxes by EC were also not possible after the 14th of October due to delays in acquiring parts necessary for maintenance of the quantum cascade laser (QCL) as a result of the

coronavirus (COVID-19) pandemic. The chamber trial plot was located in the south-west of paddock 10 (Fig. 5.1) and was 93 x 20 m in size and fenced off from surrounding grazing animals. The chamber trial plot consisted of two zones; a gas sampling zone (59 m X 10 m) and an adjacent soil sampling zone (36 m X 9 m). The grass within the trial plot (excluding inside chambers) was mechanically cut with an Etesia mower (Hydro 124 DL) while grass within the chamber was cut with a strimmer and removed following grazing outside the trial plot, within the paddocks. The gas sampling zone consisted of five different sub-trial zones for measuring N_2O emissions, and the soil sampling zone consisted of three different sub-trial zones for measuring soil mineral N (NH_4^+ and NO_3^-), both from four grazing events (see Table 5.1 for dates) - one in spring, two in summer and one in autumn in order to account for the temporal variability in N_2O fluxes. Each grazing sub-trial was designed in a randomized block of five replicate blocks for gas sampling or three replicate blocks for soil sampling, from four treatments – (1) control: without N application, (2) fertilizer in the form of CAN, (3) SU+CAN and (4) dung+CAN. Stainless steel collars and associated chambers were identical to those described by Harty et al. (2016), and collars were inserted into the soil 1.5 m apart both in length and width, in order to minimize cofounding effects between treatments. SU was prepared in the laboratory as outlined in de Klein et al. (2003), in 60 L batches that were stored at 4 °C prior to application. The N loading rate was equivalent to that of a standard cow urination (at approximately 500 – 700 kg N ha^{-1}) (Haynes and Williams, 1993). Dung was collected a week prior to application in the field immediately after defecation and stored as described above for SU. Composite sub-samples of SU and dung were analysed for total N using the LECO TruSpec high temperature Dumas Combustion system (St Joseph, Michican) and Ganimede analysis, respectively, and subsequent N loading rates were calculated for each application

(Table. 5.1). Dung and SU treatments were applied to the gas and soil measurement areas within the chamber trial plot when cows were grazing in strips within the South-West region of paddock 10, in front of the chamber trial plot. SU was applied using a water can to facilitate infiltration (Forrestal et al., 2017) at a volume of 1.8 L (Misselbrook et al., 2014) in an area of 0.16 m^2 within a chamber frame to reduce runoff through soil pores outside of the chamber. Dung was applied at 2kg to a 30 cm diameter area within the chamber collar (Krol et al., 2016).

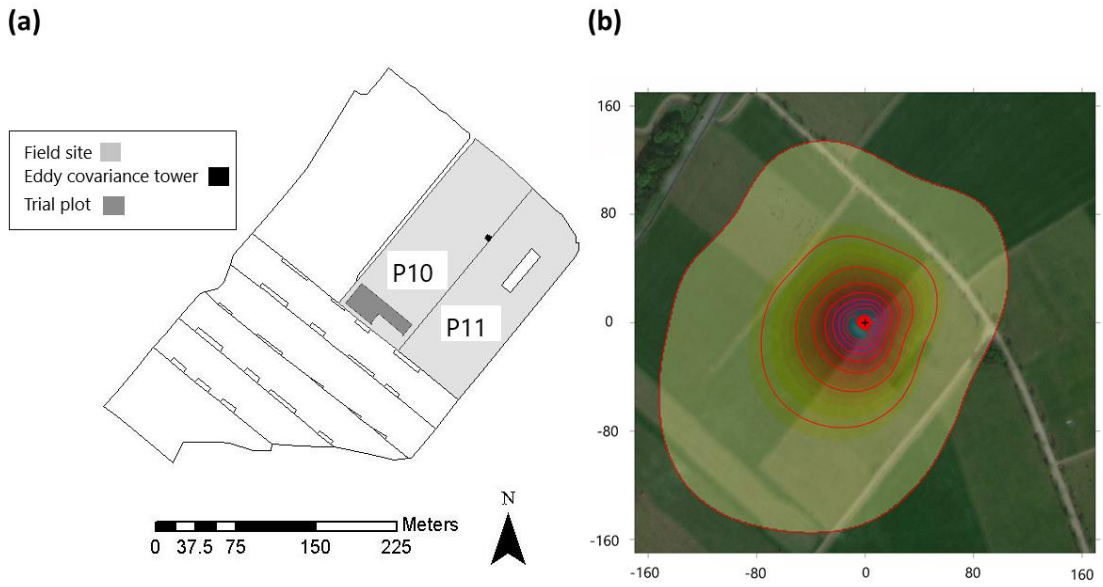

Figure 5. 1: (a) Map of the experimental field site at Johnstown Castle. Boundaries represent paddocks. P10 and P11 denote paddock 10 and paddock 11, respectively. The light grey paddocks represent the experimental field site (2.65 ha^{-1}) and the dark grey patch represents the chamber trial plot (0.09 ha^{-1}). The black square in P10 represents the eddy covariance (EC) tower and panel (b) shows the EC footprint for 2020 as calculated by the footprint model outlined in Kljun et al. (2015). The footprint contour lines represent 10 % to 90 % of the flux

source in 10 % increments. The axis represents distance (meters) from the EC tower (black cross).

Table 5.1: Management for the experimental site in 2020 and rates of application (kg nitrogen (N) ha^{-1}) for calcium ammonium nitrate (CAN), synthetic urine (SU) and dung that were applied to static chambers for four out of nine grazing events.

Date	Management	Application date	Application rate		
			kg N ha^{-1}		
			CAN	SU	Dung
04/02/2020 - 10/02/2020	Grazing[1*+]	-	-	-	-
03/03/2020 - 22/03/2020	Grazing[1×]	03/03/2020	-	517	551
02/04/2020	Fertilizer[1×]	02/04/2020	50	-	-
10/04/2020 - 18/04/2020	Grazing	-	-	-	-
03/05/2020-10/05/2020	Grazing[2×]	04/05/2020	-	517	559
11/05/2020	Fertilizer[2×]	11/05/2020	40	-	-
25/05/2020-03/06/2020	Grazing[3×]	25/05/2020	-	517	405
03/06/2020	Fertilizer[3×]	03/06/2020	27	-	-
17/06/2020 - 24/06/2020	Grazing	-	-	-	-
29/06/2020	Fertilizer	-	20	-	-
09/07/2020 - 18/07/2020	Grazing	-	-	-	-
01/08/2020 -12/08/2020	Grazing	-	-	-	-
14/08/2020	Fertilizer	-	27	-	-
31/08/2020 - 21/09/2020	Grazing[4×]	01/09/2020	-	542	355
14/09/2020	Fertilizer[4×]	14/09/2020	27	-	-

x Grazing events and CAN applications where N_2O emissions and mineral N were monitored for the duration of the experiment within the chamber trial plot . 1,2,3,4 is the number assigned to each grazing period, and is herein used in tables and figures.

+ Due to wet soil conditions, spring grazing events were extremely sporadic and inconsistent, and as a result grazing 1 was extended from February to March.

5.2.2 Chamber N_2O sampling and analysis

N_2O measurements were made using the closed static chamber technique as outlined in de Klein and Harvey (2015). Stainless steel 40 cm x 40 cm chambers were inserted into the ground at 5 – 10 cm depth at least three days prior to flux measurements. Chamber lids were 10cm high creating an approximate headspace volume of 20-22 L. During sampling, chambers were closed for 30 minutes and flux measurements were taken at 0, 15 and 30 minutes from chamber closure through a rubber septum (Becton Dickinson, Oxford, UK) using a 10ml polypropylene syringe (BD Plastiplak, Becton Dickinson) fitted with a hypodermic needle (BD, Microlance 3; Becton Dickinson). Gas

samples were injected into a pre-evacuated 7ml screw-cap septum glass exetainers (Labco, High Wycombe, UK). N_2O fluxes measurements occurred between 10:00h and 14:00h (UTC) to best reflect daily average N_2O emissions (Charteris et al., 2020b). Measurements were made more frequently following the application of CAN, dung and SU inside chambers, with five sampling measurements for the first week, four sampling measurements in the second week post treatment application, two sampling measurements per week for following two weeks, then one sampling measurement a week for the following five weeks before reducing the measurement frequency to twice a month until week 17 post application, and thereafter once a month until the end of the experiment. N_2O concentrations were analysed using gas chromatography (GC) with a detection limit of 0.05 ppm (Scion 456-GC, Bruker Inc., Kirkton Campus Livingston, UK) equipped with an electron capture detector. For each series of gas samples from a chamber, the hourly flux (F_{CH}) (μg N_2O m^{-2} hr^{-1}) was calculated using the following equation (Eq. 5.1)

$$F_{CH} = \left(\frac{\Delta C}{\Delta T}\right) x \left(\frac{M \; x \; P}{R \; x \; T}\right) x \left(\frac{V}{A}\right) \qquad \text{Equation 5.1}$$

Where ΔC/ ΔT is the change in headspace concentration of N_2O (ppbv) during the enclosure period in hours calculated by linear regression, M is the molecular weight of N_2O (44.01 g mol^{-1}), P and T are the atmospheric pressure (Pa) and temperature (K) at the time of gas sampling, respectively, R is the ideal gas law constant (8.314 J K^{-1} mol^{-1}), V is the headspace volume in a closed chamber (m^3) and A is the ground area enclosed by the chamber (m^2). Linearity of N_2O accumulation within the chamber headspace was checked from three headspace samples per chamber (de Klein and Harvey, 2015).

5. 2.3 Eddy covariance flux measurements

The EC system was equipped with a 3-D sonic anemometer (CSAT-3, Campbell Scientific Ancillary, Logan, UT, USA) mounted at 2.2 m to measure fluctuations in the 3-D wind components at a frequency of 10 Hz. Concentrations of N_2O and H_2O were measured at 10 Hz by a quantum cascade laser (QCL) (Los Gatos Research, California, USA), with a detection limit of 0.03 ppb over a 30 minute period. The QCL was housed in a temperature controlled trailer adjacent to the EC mast. The inlet line into the QCL was a 10 m long, 10 mm inner diameter perfluoroalkoxy (PFA) tube with an airflow rate of approximately 30 - 35 standard L min^{-1}, controlled by an external dry scroll vacuum pump (XDS35i, Edwards, West Sussex, UK). Two in line 2 µm filters (SS-4FW4-2, Swagelok™) were fitted on the PFA tube and an additional 2 µm and 10 µm (Los Gatos Research, California, USA) filters were fitted within the QCL at the entrance of the inlet tubing and upstream of the internal pump, respectively. The air inlet into the QCL sensor was placed in the same horizontal axis, 30 cm apart from the sonic anemometer reference. The QCL contained an internal temperature regulator that maintained the cell temperature to 34 °C ± 0.5 °C and the cell pressure was set at 85 torr. Environmental variables at the EC site were measured using a range of sensors including an air temperature and relative humidity probe (HMP155C, Campbell Scientific, Logan, UT, USA), tipping bucket rain gauge (Young, Michigan, USA), two net radiation sensors (NR-Lite, Kipp and Zonen, Delft, The Netherlands), two self-calibrating soil heat flux plates that were installed at 5 cm soil depth (HFP01SC, Hukseflux, Delft, The Netherlands), photosynthetic active radiation (PAR) (PQS1, Kipp and Zonen, Delft, The Netherlands) and averaging soil temperature probes (TCAV -L, Campbell Scientific, Logan, UT, USA) that were installed at 2 cm and 6 cm depth above

the soil heat flux plates. Time domain reflectometers (CS616, Campbell Scientific, Logan, UT, USA) measured soil volumetric water content (VWC) in the upper 15 cm of soil. Soil bulk density (0-10 cm) was measured prior to the experiment by a core method (USDA, 1999) in order to calculate the water filled pore space (WFPS %) as outlined in Linn and Doran (1984). Data from the EC system was recorded and collected weekly from the CR3000 micrologger (Campbell Scientific, Logan, UT, USA). EC fluxes of N_2O (F_{EC}) were calculated over 30 minute intervals using the Eddypro software version 7.0.4 (www.licor.com/eddypro), based on the covariance between the N_2O concentration (N) and wind speed (w) Eq (5.2):

$$F_{EC} = \overline{w'N'} \qquad \text{Equation 5.2}$$

Raw half-hourly EC N_2O flux measurements were initially processed for amplitude resolution, drop-outs, absolute limits, skewness and kurtosis, as outlined in Vickers and Mahrt (1997). To compensate for the tilt of the sonic anemometer, double rotation was performed to nullify the average cross-stream and vertical wind component (Kaimal and Finnigan, 1994). Low and high pass spectral corrections were accounted for using the analytical methods described by Fratini et al. (2012) and Moncrieff et al. (2004), respectively. The covariance maximization procedure was used to calculate the time lag for N_2O as described in Cowan et al. (2020). Flux data were removed if less than 70 % of the flux contribution came from outside of the field site (Kormann and Meixner, 2001) and if flux values were < -0.1 μmol N_2O m^{-2} s^{-1}. Additional filtering for bad quality fluxes were derived from Cowan et al. (2020). Missing N_2O fluxes were gap-filled using a multi-variate linear model including the previous and next measured value in the dataset, and air and soil temperature, WFPS and rainfall over 2, 12, 24, 48

and 100 hour periods. Gap-filled EC N_2O flux measurements presented in this study are expressed as a daily average.

5.2.4 Soil sampling and analysis

Soil was sampled on 45 occasions during the experimental period, once before treatment application and once a week for the next eight weeks following treatment application, in a randomized block design sampling area adjacent to the gas sampling area within the trial plot. The soil cores were taken using a hand core at 10 cm depth and 15 mm diameter and then mixed, homogenised and processed in the laboratory for ammonium (NH_4^+), nitrate (NO_3^-) and gravimetric moisture content within 24 hrs. Soil mineral N concentrations were analysed from a 20g sample of freshly sieved soil (<4 mm), extracted with 100ml KCL (1 M) and analysed colorimetrically using an Aquakem 600 discrete analyser (Thermo Electron OY, Vantaa, Finland) for NH_4^+-N (Standing Committee of Analysts, 1981) and NO_3-N (Askew, 2012) concentrations. The gravimetric moisture content was determined by oven-drying samples at 105 °C for 24 hrs.

5.2.5 Data analysis

Data analysis was carried out on the statistical software R (Rstudio Team, 2020). Hourly chamber fluxes were assumed to be representative of daily emissions and were used to calculate the daily mean N_2O flux. In order to approximate the total N_2O produced from CAN, dung+CAN and SU+CAN, cumulative fluxes were calculated using loess regressions. Cumulative chamber N_2O fluxes were used to derive EFs for each treatment and each grazing (Eq. 5.3). EFs represent the % of N_2O-N emitted from dung+CAN, SU+CAN or CAN applied

$$EF = \left(\frac{[N_2O\ _{Treatments} - N_2O\ _{Control}]}{N\ applied}\right) * 100 \quad \text{Equation 5.3}$$

Where N applied is the N applied from the treatment (CAN, SU or dung) (kg N ha^{-1} yr^{-1}), $N_2O_{Treatments}$ is the cumulative N_2O emissions (kg N_2O-N ha^{-1} yr^{-1}) from dung+CAN, SU+CAN or CAN per grazing and $N_2O_{Control}$ is the average N_2O emission (kg N_2O-N ha^{-1} yr^{-1}) from the control treatment per grazing cumulated over the duration of the grazing event (Cowan et al., 2019). The IPCC Tier 1 methodology assumes a standard, annual EF (Pachauri et al., 2014), however, in this study treatment EFs were calculated over 29, 34, 27 and 28 days for grazing 1, 2,3 and 4 respectively. Therefore the EFs reported in this study are considered partial EFs, but are unlikely to vary from those measured at annual scales as N_2O emissions from control plots were deducted from N_2O emissions measured from treatment plots and over a range of temporal conditions (Maire et al., 2020).

A direct comparison between chamber and EC cumulative flux measurements for a 288 day period was possible by upscaling chamber measurements to the paddock scale. Chamber fluxes were upscaled ($F_{CH\ FIELD}$) by using EF from grazing 1-4 for each treatment (Table 5.3) (Eq. 5.4).

$$F_{CH\ FIELD} = \frac{Napp * EF}{100} \quad \text{Equation 5.4}$$

Where Napp is the N applied to the field (kg N ha^{-1}) and EF is the mean emission factor (%) calculated over the 4 grazing events for a given treatment. For livestock emissions of dung and urine, the Napp at the field scale ($Napp_{Livestock}$) (Eq.5.5) was determined by the N rate per patch (N_{patch}) and total number of daily patches ($Patch_{daily}$)

$$Napp_{Livestock} = Patch_{daily} * N_{patch} \quad \text{Equation 5.5}$$

Where $Patch_{daily}$ (Eq. 5.6) was calculated as,

$$Patch_{daily} = grazing\ duration * herd\ size * Patch_{no.} \quad \text{Equation 5.6}$$

where the grazing duration is the time cows spent grazing (hr^{-1}), herd size quantified the number of cows grazing, $Patch_{no.}$ was the number of urine or dung patches specified for Holstein Friesian at 7.5 (Dennis et al., 2011) and 10.9 (White et al., 2001) per grazing day ($21hrs^{-1}$), and N_{patch} (Eq. 5.7) was quantified as

$$N_{patch} = Area_{patch} * \mu(Napp) \quad \text{Equation 5.7}$$

Where $Area_{patch}$ was the wetted surface for each deposition event, with 0.33 m^{-2} for urine (Dennis et al., 2011) and 0.12 m^2 for dung (Wilkinson and Lowrey, 1973) and μ(Napp) was the average N application rate for dung or SU from grazing 1-4 (Table. 5.1) quantified as 443 kg N ha^{-1} and 554 kg N ha^{-1}, respectively.

Literature values for EFs of CAN (Harty et al., 2016), dung (Krol et al., 2016)and urine (Maire et al., 2020) were used to calculate cumulative emissions for comparison with this study as these studies were carried out at the same experimental site or sites within the same research farm (Table. 5.4) (Fig. 5.4). These literature background cumulative emissions were also derived from a previous study on the same experimental site (Krol et al., 2017).

The 95 % confidence interval (2σ) was used to determine if differences between N_2O emissions measured by chambers from individual treatments were significantly different from zero. The Shapiro-Wilk Test was used to assess normality in the N_2O flux datasets (both chambers and EC) using the stats package in R. Where the p value from the Shapiro-Wilk Test was greater than 0.05, the dataset was deemed normally distributed. Where the p value was less than 0.05, i.e. the dataset was log normally

distributed, measured N_2O fluxes were transformed to a normal distribution using the bestNormalize package in R (Peterson and Cavanaugh, 2019) for statistical analysis. Linear correlations between daily field scale N_2O fluxes by EC and rainfall and WFPS were performed to determine significance and the coefficient of determination (R^2). A repeated measures ANOVA was used to investigate interaction effects between chamber N_2O fluxes, treatment and time using the car package in R.

5.3 Results

5.3.1 Weather and eddy covariance N_2O flux data

Daily weather and field-scale N_2O flux data measured at the EC station between January 1st and October 14th 2020 is shown in Fig 5.2. Daily mean air temperature ranged from 2.2°C in February to 19.8°C in August (Fig 5.2a), which represented a cooler February and warmer August, relative to the 10 year mean (2009-2019) for those respective months (Table B.1). Soil temperature at 6 cm depth was greatest in June and lowest in January with values of 20.3 °C and 2.1 °C (Fig 5.2a), respectively, which represented a warmer June and colder January compared to the 10 year mean for these months (Table B.1). Cumulative rainfall for the experimental period was 502 mm (Fig 5.2b). Rainfall was most frequent in the winter and spring resulting in high WFPS (≥ 60 %) but the heaviest events (>15 mm daily) were observed in the summer and autumn. Extended dry periods (<50 % WFPS) were observed between May 25th and 18th June (Fig 5.2c).

Peaks in daily N_2O emissions principally occurred post-fertiliser application or during grazing, but both emission intensity and timing were strongly mediated by both temperature and rainfall (Fig 5.2a, b, d). A bell-curve relationship was observed with N_2O fluxes and WFPS, and N_2O emissions were greatest within a WFPS range of 60 % -

70 % (Fig B.1). Daily mean N_2O emissions were greatest within a soil temperature range of 15 °C – 20 °C (Fig 5.1A) but were only significantly correlated ($p < 0.05$) with soil temperature during the February ($r^2 = 0.63$) and March ($r^2 = 0.29$) grazing (Table B.2). Daily emissions of N_2O were significantly correlated with rainfall ($p < 0.05$) for grazing events' in February ($r^2 = 0.84$), March ($r^2 = 0.14$), May ($r^2 = 0.67$), and June ($r^2 = 0.47$) (Table. B.2) .Emissions of N_2O were also significantly correlated with WFPS ($p < 0.05$) during grazing events' in February ($r^2 = 0.66$), March ($r^2 = 0.20$), April ($r^2 = 0.58$), June ($r^2 = 0.76$) and July ($r^2 = 0.34$) (Table. B.2). Rainfall prior and during the June grazing co-occurred with fluctuations in N_2O emissions ranging from 0.05 nmol N_2O-N m^{-2} s^{-1} to 2.9 nmol N_2O-N m^{-2} s^{-1}. The highest emission event observed was 9.9 nmol N_2O-N m^{-2} s^{-1}, following a series of small rainfall events (< 0.6 mm) and increasing WFPS from 48 % to 61 %. No peaks were observed during grazing periods in early spring (February-March) where rainfall was consistent (WFPS >50 %) and soil temperatures were < 10 ^oC.

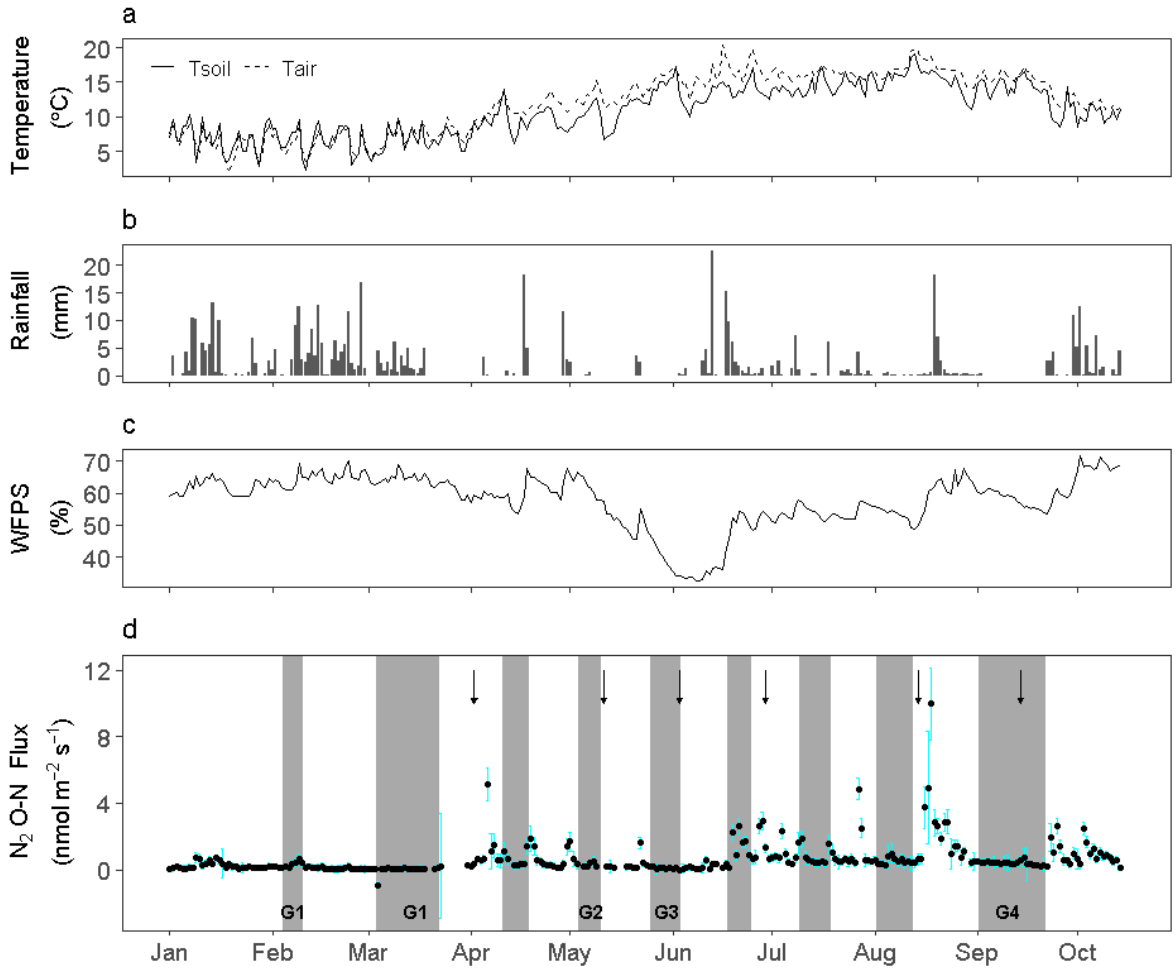

Figure 5. 2: Panels (a) - (c) represent the daily mean soil temperature (Tsoil) (solid line) and air temperature (Tair), (dashed line), daily sums of rainfall and daily mean water-filled pore space (WFPS), respectively. Panel (d) represents daily average N_2O-N fluxes measured by eddy covariance where blue lines represent the 95 % confidence interval. The grey back drop represents grazing periods where G1-G4 represents grazing events 1-4 that were measured for N_2O flux measurements by static chambers. Black arrows mark the date of fertilizer applications.

5.3.2 Cumulative N_2O emissions from grazing treatments

Cumulative N_2O-N emissions and partial N_2O-N EFs measured by chambers from control, CAN, SU+CAN and dung+CAN for grazing events' 1-4 are shown in Table. 5.2. There was a significant interaction between N_2O emissions and time and treatment (p<

0.001). The control treatment (no N applied) showed low cumulative emissions with a mean value of 0.12 ± 0.07 kg N ha^{-1}. Mean cumulative N_2O-N emissions were significantly lower ($p < 0.05$) for CAN (1.24 ± 0.44 kg N ha^{-1}) compared to SU+CAN (3.42 ± 0.69 kg N ha^{-1}) and dung+CAN (3.35 ± 0.83 kg N ha^{-1}). The N loading applied to the treatments varied with grazing due to differences in CAN rates and the N contents of dung and SU (Table. 5.1). EFs were calculated for comparability between treatments (Table. 5.2). Over the four grazing events, mean EFs from CAN were greatest (2.78 ± 0.90 %), followed by dung+CAN (0.64 ± 0.15 %) and SU+CAN (0.59 ± 0.12 %). The CAN treatment had consistently higher EFs in each grazing event compared to SU+CAN and dung+CAN treatments. The EF for SU+CAN was greater than the EF for dung+CAN in grazing 1 (spring) at 1.28 ± 0.31 % and 0.38 ± 0.14 %, respectively. The dung+CAN treatment showed higher EFs compared to SU+CAN in grazing 2 during summer (dung+CAN 1.01 ± 0.24 %; SU+CAN 0.28 ± 0.06 %) and in grazing 4 during autumn (dung+CAN 0.87 ± 0.16 %; SU+CAN 0.49 ± 0.06 %). In grazing 3 during summer EFs for the SU+CAN and dung+CAN treatments were the same at 0.30 ± 0.04/0.06 %.

Table 5. 2: Cumulative N_2O-N emissions and partial emission factors (EF) measured by static chambers for each treatment per grazing (n = 5 per treatment per grazing). Treatments included no N applied (Control), fertilizer in the form of calcium ammonium nitrate (CAN), synthetic urine (SU) and CAN applied together and dung and CAN applied together

Grazing	Cumulative N_2O-N emissions								Partial N_2O-N EF					
	Control		CAN		SU+CAN		Dung+CAN		CAN		SU+CAN		Dung+CAN	
	kg N ha^{-1}	95 % C.I.	kg N ha^{-1}	95 % C.I.	kg N ha^{-1}	95 % C.I.	kg N ha^{-1}	95 % C.I.	%	95 % C.I.	%	95 % C.I.	%	95 % C.I.
1	0.27	0.21	3.06	1.48	7.51	1.83	2.53	0.95	5.58	2.70	1.28	0.31	0.38	0.14
2	0.07	0.02	0.71	0.06	1.64	0.36	6.12	1.47	1.60	0.14	0.28	0.06	1.01	0.24
3	0.08	0.03	0.68	0.17	1.69	0.23	1.36	0.25	2.22	0.57	0.30	0.04	0.30	0.06
4	0.06	0.01	0.53	0.06	2.84	0.33	3.37	0.64	1.73	0.18	0.49	0.06	0.87	0.16
Mean	0.12	0.07	1.24	0.44	3.42	0.69	3.35	0.83	2.78	0.90	0.59	0.12	0.64	0.15

5.3.3 Field scale cumulative N_2O emissions by eddy covariance and upscaled chambers

Upscaling chamber fluxes (section 5.2.5) to the paddock scale allowed for a direct comparison with EC fluxes on a daily basis. Cumulative N_2O emissions over 288 days of the grazing period were calculated for gap-filled EC fluxes and $F_{CH\ FIELD}$. Emissions of 5.16 ± 2.04 kg N ha^{-1} measured from $F_{CH\ FIELD}$ compared well with EC emissions of 6.62 ± 0.33 kg N ha^{-1} showing a similar cumulative pattern over time (Fig 5.3). $F_{CH\ FIELD}$ emissions were consistently higher than EC emissions following the April grazing, up until the August fertilizer application where an increase in EC emissions was observed. The largest proportion of the total $F_{CH\ FIELD}$ emissions (5.51 kg N ha^{-1}), at 19.67 % were observed from management in April, followed by management activities in September at 14.20 % and March at 12.56 % (Table 5.3). The February grazing accounted for the lowest proportion of the total cumulative flux at 1.34 %, while emissions from early and late May, June, July and August accounted for 8.18, 10.14, 9.34, 9.61 and 11.92 % of the total $F_{CH\ FIELD}$ emissions, respectively (Table 5.3).

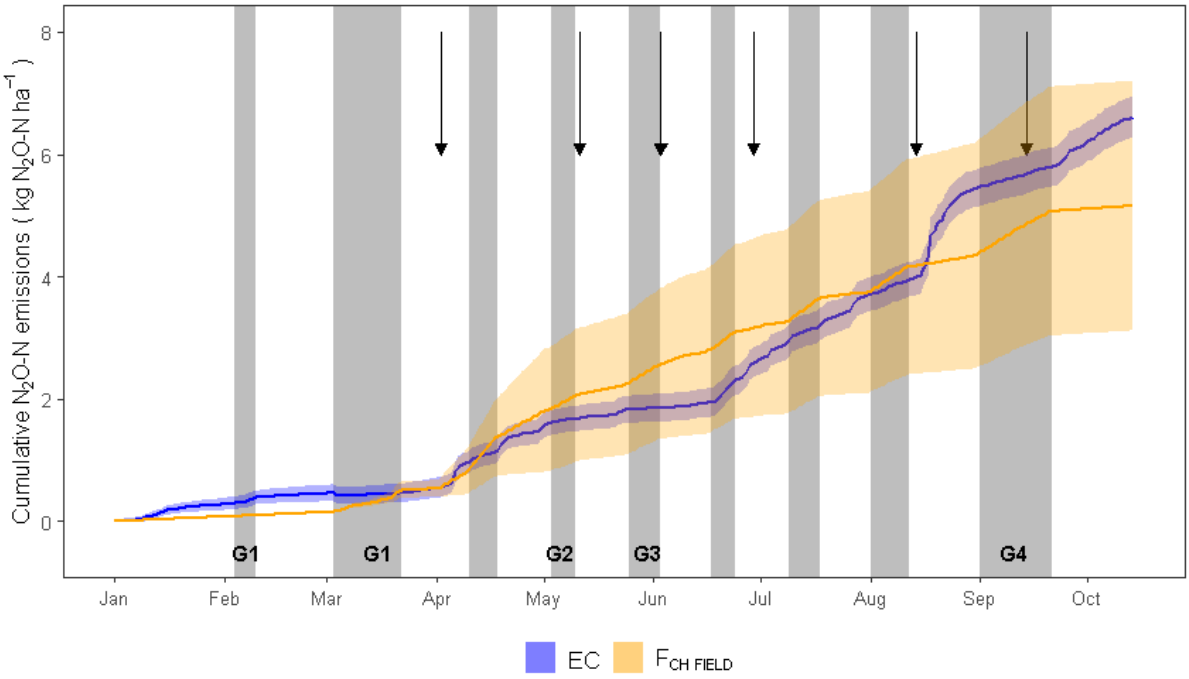

Figure 5. 3: Field scale cumulative N_2O-N emissions over 288 days by gap-filled eddy covariance (EC) (blue line) and up scaled static chamber ($F_{CH\ FIELD}$) (orange line) and where the blue and orange shades represent the 95 % C.I. for EC and chamber measurements, respectively. The grey back drop represents grazing periods where G1-G4 represents grazing events 1-4 that were measured for N_2O flux measurements by static chambers. See Table 5.1 for dates on management activities. Black arrows mark the date of fertilizer applications.

Table 5.3: The proportions of cumulative emissions from each grazing period to the total field scale chamber cumulative ($F_{CH\ FIELD}$). N is the number of days incorporated into the cumulative, which is the period between the start of a grazing event and the beginning of the next grazing event.

Event #	Grazing	N	Cumulative N_2O-N flux	Proportion of total flux
			kg N ha^{-1}	%
Pre-grazing	01/01/2020 - 03/02/2020	34	0.08	1.63
1	04/02/2020 - 10/02/2020	28	0.07	1.34
2	03/03/2020 - 02/04/2020	38	0.65	12.56
3	10/04/2020 - 18/04/2020	23	1.01	19.67
4	03/05/2020 - 10/05/2020	22	0.42	8.18
5	25/05/2020 - 03/06/2020	22	0.52	10.14
6	17/06/2020 - 24/06/2020	23	0.50	9.61
7	09/07/2020 - 18/07/2020	23	0.48	9.34
8	01/08/2020 - 12/08/2020	30	0.60	11.62
9	31/08/2020 - 21/09/2020	22	0.73	14.20
Post-grazing	22/09/2020 - 14/10/2020	23	0.09	1.71
Total		288	5.16	100.00

5.4 Discussion

5.4.1 Temporal trends in N_2O emissions

Mean daily N_2O emissions observed were within the range of similar studies where livestock grazing and mineral fertiliser events occurred in tandem (Hyde et al., 2016, Liang et al., 2018, McAuliffe et al., 2020, Wecking et al., 2020b). The significant interaction ($p < 0.05$) between N_2O measurements by chambers and treatment and time indicates that the timing of management activities affects the rate of N_2O emissions. Similar findings have also been reported by Krol et al. (2017) and Hyde et al. (2016) from the same experimental grounds. Emissions in April accounted for the highest proportion of the total $F_{CH\ FIELD}$ N_2O-N flux and similarly, high instantaneous emission events were recorded by EC in April. Such high emission events are likely due to denitrification for a number of reasons. Firstly, observations of heavy (> 3 mm) and/or consistent rainfall and subsequently an increasing the WFPS (> 60 %), prior to

the April emission event as well as moderate soil temperatures (mean 11 ± 1 °C standard deviation) were recorded. It is important to note that all of the above listed environmental variables are key regulators for the production of N_2O by dentrifiers (Butterbach-Bahl et al., 2013). Secondly, WFPS, rainfall and soil temperature were positively and significantly correlated with N_2O-N emissions during this period (Table B.2), further validating the significance of the observations mentioned. An additional stepwise regression analysis merging N_2O-N EF and soil property data measured in this study with data from the same experimental site by Krol et al. (2016) and Maire et al. (2020) also showed that soil moisture drives N_2O emissions from this site (Table B.3). It is worth mentioning, that similar environmental conditions were also recorded during the August N_2O emission peak measured by EC. Finally, N inputs from both urine and dung from grazing animals, and fertilizer N showed high mean concentrations of NH_4^+ and NO_3^- prior to April at 13.7 and 21.4 mg N kg^{-1} soil, respectively, suggesting an availability of N substrates for denitrification during April (Table B.4). The co-occurrence of favourable environmental conditions promoting anoxic conditions in combination with sufficient substrate availability from management, thus creates optimum conditions for the denitrification of NO_3^- to N_2O (Butterbach-Bahl et al., 2013). Overall, these findings suggest that reducing or delaying management activity during wet seasons or periods could potentially reduce annual N_2O emissions i.e. implementing precision management (Rees et al., 2020).

Low N_2O emissions were observed for grazing events in February and March by EC despite coinciding with consistent rainfall and an elevated WFPS (> 60 %). In this case, it is likely that the potential for nitrification was reduced as determined by low mean NO_3^- concentrations measured in February and March at 9.5 and 11.0 NO_3^--N mg kg

soil, respectively (Table B.4). Additionally, lower soil temperatures (mean 6.7 ± 1.5 °C SD) relative to the rest of the year, could have resulted in changes in the composition of denitrifying communities, potentially limiting the soil microbial production of N_2O emissions (Braker et al., 2010) . Furthermore, it is possible that low N_2O emissions were due to available NO_3^- being utilized for N_2 production via codenitrification. Selbie et al. (2015) reported high N losses following urine deposition of 55.8 g N m^{-2} as N_2 by the process of codenitrification. Despite unfavourable conditions for the production of N_2O during this period (G1), high emissions were reported by static chamber measurements. Flux measurements of N_2O by static chambers typically display a log-normal distribution over time which is characterized by a few high flux measurements (Cowan et al., 2015, Hyde et al., 2016, Maire et al., 2020). Due to the limited spatial and temporal resolution of this technique, where high flux values are recorded, static chambers will typically over-estimate the sample mean, and where such values are absent from the dataset, chamber fluxes will underestimate the sample mean (Levy et al., 2017). In this study chamber flux values ranged over five orders of magnitude (Fig B.2), where the sample mean is weighted towards a few high flux measurements. Due to the small sample size (n = 5 per treatment), it is difficult to constrain the variability and therefore the high uncertainty associated with chamber flux measurements. Previous studies have also reported large spatial differences in chamber N_2O flux measurements. For example, Cowan et al. (2015) measured N_2O fluxes ranging from 2 to 79,000 µg N_2O-N m^{-2} hr^1 over 100 sampling points, from a 7 hectare grazed grassland in Scotland. Similarly, Turner et al. (2008) recorded N_2O fluxes from an Australian irrigated dairy pasture that ranged from 45 to 765 ng N_2O-N m^{-2} s^{-1} in summer and 20 to 953 ng N_2O-N m^{-2} s^{-1} in autumn. Conversely, the EC technique is cable of integrating both high and low fluxes over large areas (approximately 1 km^2)

with constant 24 h measurement coverage, thus providing more certain estimates of field scale emissions of N_2O relative to the static chamber technique. Therefore higher emissions reported by static chambers compared to EC are likely due to its limited spatial and temporal resolution and potential for large interpolation uncertainties, a major disadvantage of static chambers which previous studies have reported on (Cowan et al., 2019, Jones et al., 2011).

5.4.2 Emission factors of CAN, SU+CAN and dung+CAN

In this study EFs for CAN, SU+CAN and dung+CAN were highly variable over the four grazing events. CAN showed the highest EF relative to the other treatments, with a mean EF of 2.78 % (1.60 – 5.58 %). The lower-end CAN emissions observed in this study have also been reported by Cardenas et al. (2019) from four grassland sites in the UK (0.58 – 1.36 %) and Harty et al. (2016) from two different grassland sites in Ireland (1.44 ± 0.90 % and 1.67 ± 0.49 %). Harty et al. (2016) also reported similar high-end EFs from CAN from an additional grassland site in Ireland at 3.81 ± 0.20 % and Velthof and Losada (2011) reported a maximum EF of 8.3 % from a grassland site in the Netherlands. The variability in CAN EFs could be explained by soil conditions at the chamber location, with the greatest emissions occurring in grazing 1 in spring where the soil moisture content was predominately high (WFPS > 60 %), favouring denitrification (Linn and Doran, 1984), whereas EFs were lower during summer grazing events where soil conditions were relatively drier (WFPS < 60 %).

To date, only a few studies have quantified N losses from the interactive effects of CAN applied to urine and dung patches from grazed pastures (Hyde et al., 2016, Krol et al., 2016, Maire et al., 2020). Interactions between fertilizer N and animal excreta create hotspots of N_2O which are a common feature of rotational grazing management (Luo

et al., 2017). Currently there are no recommended default EFs by the IPCC or at the national level, for mineral N fertilizer applied to urine or dung patches. In this study, EFs from SU+CAN and dung+CAN were measured in order to quantify emission events which are representative of rotational grazing systems. The SU+CAN treatment EF was 0.59 % (0.28 – 1.28 %) which was approximately four times lower than the combined EF_1 and EF_{3PRP} for cattle urine by the IPCC of 2.37 % and Irelands combined Tier 2 $EF_{1\ CAN}$ and $EF_{3cattle\text{-}urine}$ of 2.6 %. However, mean EFs for SU+CAN were comparable with previously reported SU+CAN EFs in Ireland, by Maire et al. (2020) at 0.26-0.74 % and Krol et al. (2017) at 0.55 %. Hyde et al. (2016) showed a multiplicative effect on cumulative N_2O emissions from CAN and urine applied together, relative to N_2O emissions from these treatments individually. In this study, emissions from SU+CAN showed more of an additive effect where frequently, cumulative N_2O-N losses from SU+CAN were approximately twice that of N_2O-N losses observed from the CAN treatment.

In this study, mean EFs quantified from dung+CAN were 0.64 % (0.30 -1.01 %), which was roughly half of the combined EF_1 and EF_{3PRP} for cattle dung by the IPCC, and Irelands combined Tier 2 inventory value for $EF_{1\ CAN}$ and $EF_{3cattle\text{-}dung}$, both at 1.7 % . Few studies have investigated the interactive effects of dung and CAN on N_2O emissions, however Hyde et al. (2016) showed that applying dung and CAN together had additive effects on N_2O emissions, reporting N losses of 2.15 %. Cumulative emissions from the dung+CAN treatment were greater than cumulative emissions from the CAN treatment alone for grazing 2 and 3, which could be explained by possible additive effects between treatments. An independent dung treatment however, would be necessary to validate these assumptions. The readily available carbon (C) in dung

can increase rates of microbial oxygen consumption, thus creating anaerobic conditions (van Groenigen et al., 2005). Increased C availability can also accelerate microbial activity as nitrifiers and denitrifiers require readily available C for the oxidation of NH_4^+ and the reduction of NO_3^- (Wang et al., 2021). Additionally, the soil nitrate N pool available from CAN alone was frequently lower than the dung+CAN treatment (Table B.3). This in combination with pre-existing amino-sugars from the dung patch, and high soil moisture, would create optimum conditions for the production of N_2O by either denitrification or co-denitrification, thus increasing emissions (Rex et al., 2018, Rex et al., 2019).

5.4.3 Field scale grazing N_2O emissions

Total cumulative N_2O-N emissions measured by gap-filled EC and $F_{CH\ FIELD}$ were 6.62 ± 0.33 kg N ha^{-1} and 5.16 ± 2.04kg N ha^{-1}, which represent a global EF of 0.96 and 0.72 %, respectively, and both are similar to mean of the IPCCs default value for EF_1 and EF_{3PRP} at 0.95 %. It is important to note that larger disparities between gap-filled EC and $F_{CH\ FIELD}$ cumulative N_2O-N emissions would have been observed if the temporal frequency of static chamber flux measurements were lower. For example, if N_2O flux measurements were not measured during March and April (which accounted for 32.23 % of the total $F_{CH\ FIELD}$ emissions [Table. 5.3]), the cumulative N_2O losses calculated from $F_{CH\ FIELD}$ would have been 3.45 kg N ha^{-1}, which is approximately 50 % lower than total N_2O emissions measured by EC. Our study highlights the importance of high chamber replication and measurements both spatially and temporally in order to make field scale estimates of N_2O comparable with high frequency N_2O flux measurements by EC. Similar conclusions were also outlined by Murphy et al. (2022a), who showed that N_2O flux measurements by static chambers and EC were most comparable when

chamber replication was high and when measurements from both techniques displayed temporal and spatial alignment.

Both F_{CH_Field} and EC cumulative emissions were within range for previously reported N_2O-N emissions from intensively grazed dairy pastures. Flechard et al. (2007) reported total emissions of 6.48 kg N_2O-N ha^{-1} using the static chamber technique from a grassland site in the Netherlands which received 300 kg N ha^{-1}. Hörtnagl et al. (2018) quantified cumulative emissions by EC of 2.55 – 7.89 kg N_2O-N ha^{-1} from a grassland site in Switzerland with an N application rate of 232 – 219 kg N ha^{-1} , while Wecking et al. (2020b) reported cumulative N_2O emissions of 3.82 and 7.30 kg N_2O-N ha^{-1} measured by static chambers and EC respectively, from a grazing system in New Zealand which received 40 kg N ha^{-1} from fertilizer and 424 kg N ha^{-1} from animal excreta during grazing.

The uncertainty associated with $F_{CH\ FIELD}$ was approximately seven times greater than the uncertainty attributed to emissions measured by gap-filled EC. The high uncertainty associated with $F_{CH\ FIELD}$ estimates can partly be explained by small sample sizes per treatment (n = 5 * treatments per grazing). Studies have shown that where chamber sample sizes are large (n > 40), the uncertainty in chamber flux measurements is reduced (Cowan et al. 2020). However, it is not always practical or feasible to manage high static chamber replications for multiple treatments. Where the sample size is small and the data is both highly variable and exhibits a log-normal distribution, as is frequently the case for N_2O flux datasets (Cowan et al., 2016), conventional arithmetic methods for handling flux data are not sufficient for providing robust estimates of uncertainty. More recently, Bayesian methods have been used to report N_2O EFs and uncertainty from static chamber measurements (Cowan et al.,

2020). Bayesian statistics provide more robust estimates of uncertainty relative to arithmetic methods, by explicitly accounting for the log-normal distribution of the dataset and is therefore, less likely to over or underestimate the sample mean and associated uncertainty (Levy et al., 2017). Previous studies have demonstrated the success of the Bayesian method in quantifying the uncertainty of chamber N_2O emissions from single management events (Cowan et al., 2019). However, at present the Bayesian method still requires further development in order to quantify chamber measurements of N_2O from emission events arising from consecutive, multiple management practices. Flechard et al. (2007) reported high uncertainty values of up to 50 % in annual flux measurements by static chambers due to the spatial and temporal limitations of the technique. Due to the low temporal and spatial resolution of static chamber measurements relative to the EC technique, static chambers are not suitable for capturing hot moments and hotspots of N_2O due to management, rainfall events and re-wetting of dry soils (Jones et al. 2011).

In this study, gap-filled EC cumulative emissions exceeded $F_{CH\ FIELD}$ estimates following the August fertilizer application and the September grazing, which coincided with heavy rainfall events (sum 35 mm) and high soil temperatures (mean 16 ^{o}C). Maximum differences between EC and $F_{CH\ FIELD}$ cumulative emissions were 1.09 kg N ha^{-1} during these periods. Our results imply that quantifying N_2O emissions using only the static chamber approach could lead to underestimations of annual N_2O-N flux estimates from grazing systems where climatic conditions favour hotspots and hot moments of N_2O, as the total variability in N_2O emissions may not be captured due to the low spatial and temporal resolution of the static chamber technique.

Cumulative estimates of $F_{CH\ FIELD}$ N_2O-N emissions showed the same total cumulative N_2O-N losses as reported in literature values (Table. 5.4). This study had consistently higher $F_{CH\ FIELD}$ cumulative estimates across all treatments compared with literature value with the exception of CAN, where emissions were 65.61 % lower (difference of 0.98 kg N ha^{-1}) compared to literature values. Emissions from background accounted for 14 % (0.71 kg N ha^{-1}) and CAN accounted for 36 % (1.87 kg N ha^{-1}) of the total N_2O-N losses reported in this study, while animal excreta accounted for 50 % (34 % or 1.77 kg N ha^{-1} – urine; 16 % or 0.81 kg N ha^{-1} - dung). Voglmeier et al. (2019) also reported high contributions of N_2O-N losses from urine (57 %) but reported lower contributions from dung (5 %) from an intensively managed grassland in Switzerland. Variability in reported EFs from grazing systems in this study and the literature, may be due to the interactive affects between treatments, which can increase N_2O-N emissions due to enhanced substrate availability and soil moisture (Hyde et al., 2016).

Table 5. 4: Cumulative N_2O-N emissions for background (i.e. no N application), calcium ammonium nitrate (CAN), urine and dung using literature emission factor (EF) values by Krol et al. (2017), Harty et al. (2016), Krol et al. (2016) and Maire et al. (2020), respectively.

Author	Treatment	EF		N applied to field	Cumulative N_2O-N flux	
		%	95 %.CI	kg N ha^{-1}	kg N ha^{-1}	95 % C.I.
Krol et al. 2017	Background	-	-	-	0.11	-
Harty et al. 2016	CAN	1.49	0.71	191	2.85	1.36
Krol et al. 2016	Dung	0.38	0.31	125	0.39	0.31
Marie et al. 2020	Urine	0.47	0.10	299	1.41	0.50

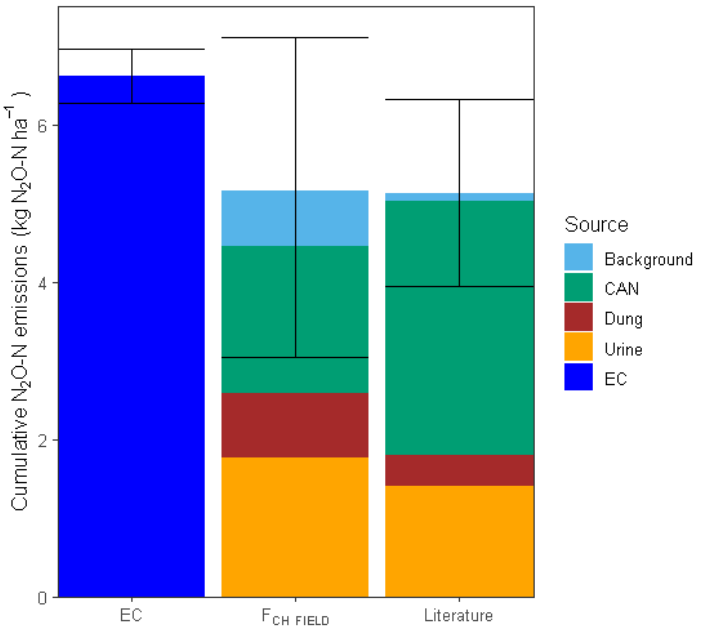

Figure 5. 4: Cumulative N_2O-N emissions by gap-filled eddy covariance (EC) measurements (dark blue) and upscaled static chamber measurements ($F_{CH\ FIELD}$) for background emissions (light blue), calcium ammonium nitrate (CAN) (green), dung (brown) and urine (orange). Literature values for background, CAN, dung and urine can be seen in Table 5.4. Error bars represent the 95 % confidence interval.

5.4.4 Recommendations for future N_2O flux studies

In this study, constant values from the literature were used to quantify the number and area of dung and urine patches per day (Dennis et al., 2011, White et al., 2001, Wilkinson and Lowrey, 1973). The N content of dung and urine is often unknown or is simulated using a constant N content to evaluate the effect of deposition timing on emissions. The N content of urine varies greatly over the season reflecting factors such as the feed N content, feed dry matter, feed and water intake and inter animal differences. To date, there is still a lot of variability surrounding the use of constant values in characterizing dung and urine depositions (Aland et al., 2002, Moir et al., 2011, Oudshoorn et al., 2008, Weeda, 1967). Ideally, site specific quantifications of

dung and urine deposition events should be made for more accurate estimates of upscaled N_2O emissions from static chamber measurements. For instance, using survey-grade global positioning system (GPS) technology to precisely measure field scale variability in distribution, coverage and diversity of excreta patches (Carpinelli et al., 2020, Dennis et al., 2011, Maire et al., 2018). Furthermore, there is still at large a degree of ambiguity surrounding the probability of overlapping urine or dung patches occurring during grazing, that could potentially lead to greater N losses than individual patches (Cichota et al., 2013, Snow et al., 2017). As a result, there is still a necessity to further our understanding in the variability of N_2O emissions from combined treatments of fertilizer, urine and dung and quantifying dung and urine patches at high precision at the field scale. There is also a need to trial management practices to reduce N_2O emissions such as precision fertilisation and grazing to avoid hot moments (Rees et al., 2020). Additionally, we need more datasets quantifying N_2O emissions and investigating the associated drivers from grazing systems to improve and reduce the uncertainty in modelling EFs from grazed pastures (Tier 3). Improvements in modelling N_2O EFs would in turn avoid the burden of conducting dedicated measurement campaigns for estimating local EFs (López-Aizpún et al., 2020).

5.5 Conclusions

Quantifying field scale emissions of N_2O in grazed pastures is complicated due to the spatial heterogeneity of dung and urine patches by grazing animals. The EC technique provided spatially and temporally robust annual estimates of N_2O emissions (6.62 ± 0.34 kg N ha^{-1}) from the grazing management, while high uncertainties in emission factor derived chamber cumulative flux ($F_{CH\ FIELD}$) estimates were observed (5.09 ± 2.01 kg N ha^{-1}). Using chamber N_2O flux measurements in a complimentary fashion

with N_2O flux measurements made by EC provided insights in the differential contributions of grazing and fertilization on the field N_2O budget over the grazing season. Management related emissions accounted for 86 % of the total cumulative N_2O-N emission, with 50 % of N_2O-N losses derived from animal excreta.

Chapter 6: The net nitrogen, carbon and greenhouse gas budget of an intensively managed temperate grassland system at the field scale.

Abstract

Globally managed grasslands represent approximately a quarter of the land surface area and can therefore contribute to greenhouse gas (GHG) mitigation, but also in forcing climate change. We assessed the net nitrogen (N), carbon (C) and GHG balance (NGHGB) of a temperate grassland under a cut and grazed management in 2019 and 2020, respectively, at the field scale. Imports and exports were quantified through eddy covariance measurements of ecosystem scale carbon dioxide (CO_2) and nitrous oxide (N_2O) fluxes, farm management data and/or literature values for where both field and methane (CH_4) flux measurements were not possible. The N budget was dominated by imports from fertilizer in both years and additionally, animal excreta in 2020. Accounting for all measured and estimated N exports and imports, the grassland had a net neutral N balance under a cut management (0.1 ± 6.0 g N m^{-2} yr^{-1}), but transitioned into a higher net N sink under the grazing management (-17.9 ± 5.5 g N m^{-2} yr^{-1}), due to greater N imports. The net ecosystem exchange (NEE) results showed a higher C assimilation rates under the cut management (-547.9 g C m^{-2} yr^{-1}) relative to the grazing management (-369.3 g C m^{-2} yr^{-1}) but was weakened by C exports, mainly biomass removal in 2019 (482.3 g C m^{-2} yr^{-1}) and enteric fermentation (23.8 g C m^{-2} yr^{-1}) in 2020, yielding an estimated net biome productivity of -61.6 ± 24.6 g C m^{-2} yr^{-1} and -311.5 ± 81.8 g C m^{-2} yr^{-1} under a cut and grazing management, respectively. In terms of CO_2eq, the NGHGB of the site under cut and grazed management was -86.0 ± 91.8 and -84.4 ± 319.4 g CO_2eq m^{-2} yr^{-1}, respectively, where emissions of CH_4 and N_2O reduced the GHG sink by 58 and 27 % respectively, over the two year period. This study

shows the impact that both management activities, (namely biomass removal) and non-CO_2 gas emissions have on offsetting the net C sink of managed grasslands, and highlights the need for sustainable agricultural practices in order to reduce the potential of these systems in forcing climate change.

Work presented in this chapter is based on the manuscript to be submitted to Science of the Total Environment with the authors list as: Murphy, R.M. Lanigan G.J. Richards, K.G. Krol, D. K. Gebremichael, A. W. Rambaud, J. Maire, J. Cowan, N. and Saunders, M.

Author Contributions: RM, DK, MS, and GL designed the experiment. RM conducted the experiment and analysed the samples that were collected alongside JR and AG. Samples were analysed in the Teagasc Johnstown Castle with the support of laboratory technicians. RM with the help of NC and DK conducted the flux data analysis. RM wrote the article with the contributions from all co-authors

The overarching objective of this thesis chapter was to investigate the impact that silage cut and grazing management have on the N and C sinks of managed grasslands by quantifying the flow of N and C imports and exports into and out of the system, in addition to greenhouse gas emissions of CO_2, N_2O and CH_4 associated with the management regimes at the field scale. In doing so, this study highlights areas where large losses of CO_2 are emerging at the field scale from management activities, and offers potential mitigation strategies.

6.1 Introduction

Managed grasslands account for approximately 26 % of the global land surface area (Lemaire et al., 2011a) and 58 % of land surface area in Ireland (CSO, 2020). Therefore, the influence of this land cover on greenhouse gas (GHG) emissions, (carbon dioxide

[CO_2], nitrous oxide [N_2O], methane [CH_4]) and carbon (C) sequestration across managed grasslands is of both global and national importance. Quantifying emissions of N_2O and CH_4 from managed grasslands is particularly important due to their global warming potentials (GWP) of 265 and 28, respectively, relative to CO_2 over a lifespan of 100 years. In natural grasslands, nitrogen (N) and C cycles are coupled closely through plant productivity via the assimilation of CO_2 and N leading to plant growth (Rumpel et al., 2015). Following plant senescence, leaf litter is returned to the soil, microbial decomposition is initiated, and decoupling of the N and C cycles is mediated through N mineralisation. The C and N balance in managed grassland systems is further influenced via nutrient inputs through fertilization or animal excreta, grazing and cutting exports and soil disturbance due to reseeding and/or compaction (Wall and Lanigan, 2020). In the long term however, the tight coupling between the N and C cycles is reduced as the N/C ratio of soil increases. For instance, the addition of N from synthetic fertilizers or animal excreta to grassland systems produces low C:N leaf litter which is returned to the soil and stimulates the mineralization of organic N to inorganic nitrogen (i.e. ammonium [NH_4^+]) which is then oxidized to nitrate (NO_3^-) in the microbial process of nitrification and finally, the resulting NO_3^- is then reduced by denitrifiers to produce N_2O as an intermediate product of denitrification (Tateno and Chapin Iii, 1997). Over time, the microbial production of N_2O emissions can outweigh the benefits of increased soil organic carbon (SOC) from decomposing plant litter (Davidson et al., 2000, Jones et al., 2017).

In addition to N_2O, grasslands can be a sink (Mosier et al., 1997) or source of ecosystem CH_4 emissions (Flessa et al., 2002) depending on the microbial processes that control the production or consumption of this GHG. In soils, methanogenic bacteria produce

CH_4 during the breakdown of organic material under anaerobic conditions and high soil organic carbon contents and simultaneously, CH_4 consuming bacteria known as methantrophs are also present in soils, thus reducing the potential for soil derived CH_4 emissions (Cowan et al., 2021, Stams, 1994). Furthermore, grassland systems managed for livestock production will also produce CH_4 through enteric fermentation of ruminant livestock. In enteric fermentation, CH_4 is produced during the microbial degradation of carbohydrates, mainly in the form of cellulose, in the digestive tract of ruminants (Crutzen et al., 1986). In managed pastures, fluxes of CH_4 from grazing animals by enteric fermentation far exceed those reported from soils alone (Dangal et al., 2020), and vary with livestock density and feed digestibility (Allard et al., 2007).

As a result, there is still a large degree of ambiguity concerning the role of managed grasslands as a potential sink or source of C. In terms of actual net C balances, Soussana et al. (2007) showed that nine European grasslands acted as a sink of C with a mean measured flux of -240 ± 70 g C m^{-2} yr^{-1}, subsequently translating to a net C sink of -104 ± 73 g C m^{-2} yr^{-1}, after C exports and imports were accounted for. Conversely, Smith (2014) argued that such C sequestration rates are likely due to improved grassland management and/or legacy effects of land use prior to commencing flux measurements, and it should not be assumed that grasslands sequester C continuously. Likewise, Jones et al. (2017) showed from a multi-year C balance from a grassland site under a rotationally grazed management in Scotland, that the system transitioned from a source of C in 2004 (57.4 g C m^{-2} yr^{-1}) to a sink of C in 2009 (-587.7 g C m^{-2} yr^{-1}), due to greater C imports from the NEE and lower C exports from animal utilization (i.e. meat and wool) and leaching in 2009 relative to 2004. In terms of GHG equivalents of CO_2 (CO_2eq), recent studies have reported that, although still a net C sink, intensively

managed grasslands have acted as a net GHG source over the last decade at a rate of 2.0 ± 0.4 Gt CO_2e yr^{-1} (Chang et al., 2021), which is comparable to cropland systems at 2.0 ± 2.2 Gt CO_2eq yr^{-1} (Carlson et al., 2017). The inconsistency in previously reported values highlights the strong need for robust data to investigate the net source or sink strength of grassland systems, and subsequently the contribution to GWPs under different management regimes over time.

As part of the European Green Deal, the EU aims to achieve climate neutrality by 2050, with an intermediate target of at least a 55 % net reduction in GHG emissions by 2030. In order to achieve such ambitious targets, several mitigation strategies have been developed within the Agriculture, Forestry and Other Land Use sector in Ireland. For example, the Common Agricultural Policy (CAP) provides financial incentives to farmers for implementing sustainable land use practices (e.g. preserving permanent grasslands) which maintain or increase SOC under the Green, Low-carbon Agri-environmental Scheme (GLAS) (DAFM, 2015). Furthermore, the Nitrates Directive (91/676/EEC) prohibits the application of organic and inorganic fertilizers past the 14th of September and 14th of October, respectively (Department of Housing Local Government and Heritage, 2021). In doing so, N inputs into grassland systems is limited during wet weather conditions which would favour N leaching and the microbial production of N_2O (Velthof et al., 2014).

One way in which we can assess the effectiveness of such GHG reduction strategies is through an understanding and quantification of the C and net GHG balance (NGHGB) of managed grasslands. In a grassland ecosystem, the C balance is determined by the net biome productivity (NBP) which accounts for the difference between the net ecosystem exchange (NEE) of CO_2 and C imports to and exports from the system. In

managed grasslands, C imports are mainly from the application of organic fertilizers and animal excreta, while C exports are primarily through biomass removal. In addition to this, emissions from N_2O and CH_4 can make considerable contributions to the overall NGHGB. For example, Merbold et al. (2014) found that N_2O emissions accounted for 48 % of a GHG flux budget from an intensively managed grassland in Switzerland and Soussana et al. (2007) showed that CH_4 emissions from four grazed pastures in Europe offset the CO_2 assimilated through NEE by between 13 and 95 %.

The objective of this study was to assess the impact of management practices and their associated emissions (CO_2, N_2O and CH_4) on the net C and N balance of an intensively managed grassland at the field scale. We also assess the impact that GHG emissions from differing management practices have on the net GWP of the grassland site as inferred by the net CO_2eq flux of the system.

6.2 Materials and Methods

6.2.1 Site description and management

The experimental site, Johnstown Caste, is located in the South-East of Ireland, in Co. Wexford. (52.30°N, 6.40°W, 67 m above sea level). The mean annual air temperature and rainfall (2009 – 2018) for this region is 10 ± 4 °C and 952 ± 352 mm, respectively. The soil type is sandy loam with a pH of 6.1 and C, N and phosphorus contents of 3.5 ± 0.1 %, 0.4 ± 0.01 % and 5.0 ± 0.2 %, respectively. The field site consisted of two perennial ryegrass (*Lolium perenne*) paddocks (paddock 10 and 11 Fig. 6.1), where the eddy covariance (EC) tower was positioned in the North-East part of the field site to maximize the footprint contribution from the prevailing south-westerly wind direction (Fig. 6.1). EC measurements were made from the 1st January 2019 to the 31st December 2020, during which flux measurements were not available for a total of 53 days due to

instrument maintenance. The field site has been under a permanent grassland management for >20 years, and in 2019 the site was managed for silage production receiving 230 kg of N ha^{-1} in the form of calcium ammonium nitrate (CAN). In 2020 the field site was under an intensive rotation-based grazing management (21-day rotation) consisting of nine grazing events with an average stocking density of 3.2 LSU ha^{-1}. During 2020 the field site also received 191 kg N ha^{-1} in the form of CAN (see Table 6.1 for further details). The N loading rate (kg ha^{-1}) from excreta by grazing animals was calculated by multiplying the number of dung [10.9 patches over 21 hrs^{-1} (White et al., 2001)]or urine deposits [7.5 patches over 21 hrs^{-1} (Dennis et al., 2011)] from each cow per day, with the N application of a single dung (5 g N ha^{-1}) or urine (10 g N ha^{-1}) patch. Total N contents of dung and urine were determined by analysing composite sub-samples of dung and synthetic urine according to the protocol outlined in de Klein et al., using the LECO TruSpec high temperature Dumas Combustion system (St Joseph, Michican, USA) and Ganimede analysis (Hach Ganimede N analyser, Co. Cork, Ireland), respectively.

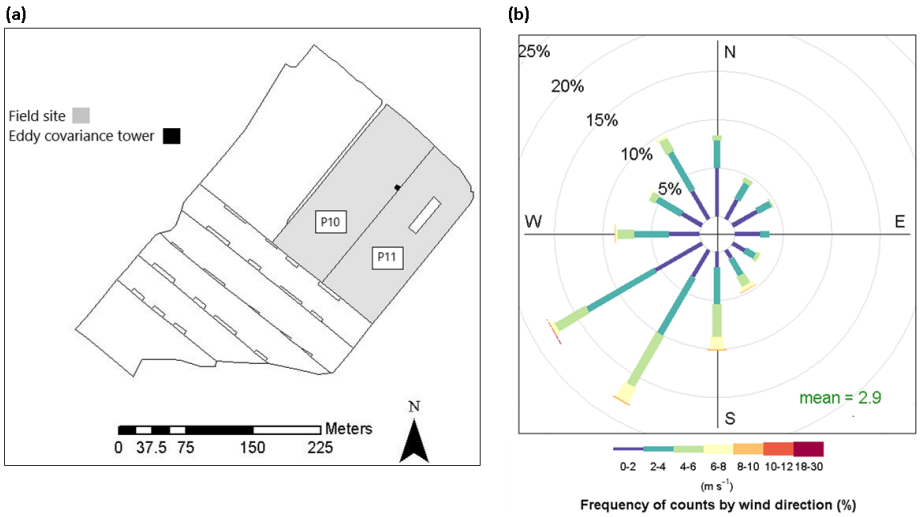

Figure 6. 1: (a) Boundaries represent paddocks where the light grey paddocks represent the experimental field site (2.65 ha^{-1}) at Johnstown Castle. Paddocks, P10 and P11 are paddock 10

and paddock 11, respectively. The black square in P10 represents the eddy covariance (EC) tower. (b) Wind rose plot for the experimental site from the 1st January 2019 to 31st December 2020, illustrating the predominant wind direction, south-westerly and the contribution of varying wind speed classes in m/s^{-1}.

Table 6. 1: Management for the experimental site in 2019 and 2020, and rates of application in kg nitrogen (N) for calcium ammonium nitrate (CAN) and grazing (dung and urine), respectively.

Year	Date	Management	Application rate kg N ha^{-1}
2019	05-Mar	CAN	40
	01-Apr	CAN	70
	14-May	Silage cut	-
	05-Jun	CAN	80
	04-Jul	Silage cut	-
	05-Sep	Silage cut	-
	11-Sep	CAN	40
2020	04-Feb - 10-Feb*	Grazing	-
	03-Mar - 02-Apr	Grazing	29
	02-Apr	CAN	50
	10-Apr - 18-Apr	Grazing	46
	03-May - 10-May	Grazing	45
	11-May	CAN	40
	25-May - 03-Jun	Grazing	51
	03-Jun	CAN	27
	17-Jun - 24-Jun	Grazing	46
	29-Jun	CAN	20
	09-Jul - 18-Jul	Grazing	53
	01-Aug- 12-Aug	Grazing	64
	14-Aug	CAN	27
	31-Aug - 21-Sep	Grazing	91
	14-Sep	CAN	27
	22-Oct – 07-Nov	Grazing	99

*Due to wet soil conditions this grazing event was incomplete, consisting of a few hours (< 21 hrs) in total and therefore emissions were considered negligible

6.2.2 Carbon and nitrogen imports and exports

6.2.2.1. Net ecosystem exchange of CO_2 and N_2O

Flux measurements of CO_2 and N_2O were made using the EC technique. The EC mast was set-up at 2.2 m and consisted of a 3-D sonic anemometer (CSAT-3, Campbell Scientific Ancillary, Logan, UT, USA) coupled with an open-path infrared gas analyser (IGRA) (LI-7500, LI-COR Biosciences, Lincoln, NE, USA) to measure concentrations of CO_2 and H_2O, and a quantum cascade laser (QCL) (Los Gatos Research, California, USA) to measure concentrations of N_2O. The QCL was stored in a temperature controlled trailer where an inlet line of perfluoroalkoxy (PFA) tube (10 m long and 10 mm inner diameter) was positioned 30 cm apart from the sonic anemometer in the same horizontal axis. Two 2 μm filters (SS-4FW4-2, Swagelok™) were fitted along the inlet line and a 2 and 10 μm filter (Los Gatos Research, California, USA) were fitted on the inside of the QCL at the entrance of the inlet tubing and upstream of the internal pump, respectively. Airflow along the inlet tubing was controlled by an external dry scroll vacuum pump (XDS35i, Edwards, West Sussex, UK), which maintained the airflow rate at 30-35 standard L min^{-1} and the QCL cell pressure at 85 torr. The QCL cell temperature was maintained at 34 °C ± 0.5 °C by an internal temperature regulator.

Fluxes were calculated over 30 minute intervals at 10 Hz based on the covariance between the gas concentration and the vertical wind speed using Eddypro 7.0.6. (Eq. 6.1) (LICOR, 2017)

$$Flux_{GHG} = \overline{W'GHG'} \qquad \text{Equation 6.1}$$

The overbar signifies time averages, *GHG'* is the 30 minute concentrate of the respective GHG (ppm for CO_2; ppb for N_2O) and *W'* is the vertical wind speed. Data from the EC system was logged and collected weekly from the CR3000 micrologger

(Campbell Scientific, Logan, UT, USA). Raw half-hourly GHG fluxes were statistically evaluated and screened as outlined in Vickers and Mahrt (1997). Double rotation was performed to compensate for the anemometer tilt by nullifying the average cross-stream and vertical wind components (Kaimal and Finnigan, 1994). Spectral attenuation effects following analytic methods described in Fratini et al. (2012) and Moncrieff et al. (2004) determined low and high-pass spectral correction factors for the data, respectively. Air density fluctuations were accounted for according to Webb et al. (1980) for CO_2. As the QCL is a closed path gas analyser, the time lag between measurements of N_2O concentrations and the vertical wind speed was accounted for by using the covariance maximization procedure as outlined in Cowan et al. (2020).

Flux measurements of N_2O and CO_2 were removed from the dataset according to the following criteria: (1) where values were deemed unrealistic for the field site (-40 μmol m^{-2} s^{-1} < CO_2 > 20 μmol m^{-2} s^{-1}; < -0.1 μmol N_2O m^{-2} s^{-1}); (2) if less than 70 % of the flux contribution was derived from the experimental site as calculated by the analytical footprint model of Kormann and Meixner (2001); (3) where flux quality control flags by Foken (2003) were ≥ category 6; (4) where turbulence was low, defined as a friction velocity (u*) < 0.1 m^{-1} s^{-1} (Lognoul et al., 2019); (5) where the flux random uncertainty, estimated by the method of Finkelstein and Sims (2001) integrated over a fixed 10 s correlation period, was > 0.01 μmol m^{-2} s^{-1} ; (6) where the optical path of the IGRA was dirty (automatic gain control, AGC > 50); and finally (7) where the standard deviation between half-hourly concentrations of CO_2 were > 5 ppm.

Missing flux values of N_2O and CO_2 were gap-filled by correlating flux data with common driver variables. A multivariate linear model was used to gap-filling missing half-hourly N_2O fluxes as described by Murphy et al. (2022b). Missing half-hourly CO_2

fluxes (i.e. the NEE) was partitioned into ecosystem respiration (R_{eco}) and gross primary productivity (GPP) by segregating the dataset into night and day time, respectively. It was assumed that the plant canopy was photosynthetically inactive at night, defined by a photosynthetic photon flux density (PPFD) < 10 µmol m^{-2} s^{-1}, if PPFD values were > 10 µmol m^{-2} s^{-1}, it was considered day time data (Merbold et al., 2014). R_{eco} was modelled by using the exponential Lloyd and Taylor (1994) equation (Eq. 6.2)

$$R_{eco} = R_{10}(e\left(E_0\left(\left(\frac{1}{283.2-230}\right)\right)-\left(\left(\frac{1}{((T+273.2)-230)}\right)\right)\right) \quad \text{Equation 6.2}$$

Where R_{10} is the ecosystem respiration rate at a reference temperature of 10 °C, E_0 is the coefficient for ecosystem respiration which is defined as 309 and T air temperature (°C). GPP was initially estimated by subtracting modelled R_{eco} from measured daytime half-hourly NEE. Missing values in GPP following this were modelled using a light response function (Rabinowitch, 1951) (Eq. 6.3)

$$GPP = \frac{(\propto * PPFD + A_{max}) - \left(\sqrt{(\propto * PPFD + A_{max}}\right)^2) - (4 * \gamma) * (\propto * PPFD * A_{max})}{2 * \gamma} \quad \text{Equation 6.3}$$

Where α is the quantum yield based on incident irradiance (mol CO_2 [mol photon]$^{-1}$), A_{max} is the maximum CO_2 assimilation rate (µmol CO_2 m^{-2} s^{-1}) and y is the convexity coefficient.

6.2.2.2 Dinitrogen emissions

Dinitrogen (N_2) emissions were not measured from our field site during the experiment, but are recognised as an important element which is frequently overlooked in N balances within grassland systems (Zistl-Schlingmann et al., 2019). Therefore we estimated N_2 emissions from the ratio of N_2O:N_2 in the first top 10 cm of soil as outlined in Jahangir et al. (2010) at 1.42:1 (N_{N2}). This ratio was chosen as work

by Jahangir et al. (2010) was conducted on the same experimental grounds as this study.

6.2.2.3. Nitrogen imports by management

The N applications from CAN (N_{CAN}) in 2019 and 2020 are presented in Table 6.1. Cows were given a feed concentrate of 3.98 (18 % protein), 2.44 (14 % protein) and 2.15 (16 % protein) kg day^{-1} during the grazing season in spring, summer and autumn/winter, respectively. This resulted in an average extra N import of 0.07 kg N day^{-1} per cow (N_{Feed}). Imports of N from animal excreta ($N_{Excreta}$) during grazing were calculated as described in section 6.1 and are shown in Table 6.1.

6.2.2.4 Carbon and nitrogen export from harvest

In 2019, biomass samples were taken randomly (n = 4 per paddock) prior to silage cuts at 4 cm over an approximate area of 10 m^{-2} using a biomass harvester by Haldrup GmbH. Biomass were processed to determine the dry matter (DM) content (%) by weighing freshly harvested biomass from the paddocks followed by oven drying at 70 °C for 4 days, and then re-weighing biomass samples. The C and N content of the biomass harvested in 2019 was not measured and therefore, C and N values outlined in Maire et al. (2020) from the same experimental site during the summer harvest for the CAN treatment were used in this study. In 2020 biomass samples were taken from P10 and P11 prior to grazing events, by randomly placing a 0.25 m^2 quadrat across the field site (n = 16 per sampling campaign) and harvesting material to 4 cm using shears and also processed for DM content. Dry biomass samples were ground to measure the total N ($N_{Harvest}$) content using a TruSpec Micro elemental analyzer (LECO Corp., St. Joesph, MI, USA).

6.2.2.5 Carbon and nitrogen export from leaching

Dissolved organic carbon (DOC) ($C_{Leaching}$) was not measured in this study, therefore values were derived from Maire et al. (2020) from the same experimental site. N leaching ($N_{Leaching}$) in the form of nitrate (NO_3^-) was measured and analysed as outlined in Clagnan et al. (2018), also on the same experimental site. It was estimated that of the total amount of N leached, 0.75 % was indirectly emitted as emissions of N_2O (Buendia et al., 2019).

6.2.2.6 Carbon and nitrogen export from milk

The average fat and protein content from milk in this study was 4.26 and 3.56 %, respectively. The N content in milk (N_{Milk}) was calculated as the amount of milk protein produced per cow per year divided by 6.38, which is the conversion factor of milk protein to N (Poulsen and Kristensen, 1998). The C content of milk fat and protein (C_{Milk}) was assumed to be 70 and 46 %, respectively (Wells, 2001).

6.2.2.7 Methane emissions in the field

It was assumed that dung depositions per cow accounted for 2.5 g CH_4 day^{-1} (C_{CH4}) according to experimental work by Jarvis et al. (1995a), where authors investigated the magnitude of CH_4 emissions from dung deposited by grazing cows under different managements. It was estimated that each cow emitted 121.56 kg CH_4 $head^{-1}$ yr^{-1} through enteric fermentation according to Ireland's national GHG inventory report (Duffy et al., 2021) ($C_{Enteric}$).

6.2.2.8 Ammonia volatilization from animal excreta and CAN

The volatilization of ammonia (NH_3) from urine and dung was determined according to the findings outlined in Fischer et al. (2016) from the same experimental grounds, where NH_3-N losses from dung were 5.3, 2.8 and 3.5 % in spring, summer and autumn,

respectively, and NH_3-N losses from urine were 14.9, 9.8 and 8.7 % in spring, summer and autumn, respectively. Volatilization of NH_3 from CAN was assumed to be 0.8 % in accordance with national inventory on NH_3 emissions (Carbo, 2016).

6.2.2.9 Atmospheric nitrogen deposition

Data on N deposition was derived from the European Monitoring and Evaluation Programme (EMEP) database (https://emep.int/) over the most readily available and most recent periods between 2017 and 2019. Of the total N deposited, it was assumed that 0.25 % was emitted as indirect N_2O emissions (Krol et al., 2017).

6.2.2.10 Soil carbon and nitrogen measurements

The total C content of the soil was measured in 2019 in April, June and July and in 2021 in March. The total N content was also measured in March 2021. Soil cores were taken at 0-10 cm using a using a soil corer and samples were thoroughly mixed and wet sieved at 4mm prior to being oven dried at 40 °C over 36 hrs. Total C and N concentrations were determined using the LECO TruSpec high temperature Dumas Combustion system (St Joseph, Michican, USA) elemental analyser. The bulk density of the field site was measured in both 2019 and 2020 across using sharpened cylindrical rings (10 cm depth and 3.7 cm diameter) that were inserted vertically into the soil surface.

6.2.3 Carbon and nitrogen balance

The C and N budget was constructed by either measuring or estimating the import and export of relevant fluxes to and from the grassland on a yearly basis. With the exception of CH_4 emissions from dung and the C content of milk fat and protein, all literature values were derived from the same experimental site as used in this study. Throughout this paper, positive fluxes represent the loss of either C or N from the grassland to the

wider environment (i.e. exported from the field), and negative fluxes represent the uptake or assimilation of either C or N (i.e. imported to the field). We assumed that the NEE of CO_2 measured by the EC system, quantified the difference between C uptake through photosynthesis and C lost through both heterotrophic and autotrophic respiration. The change in the C balance (ΔCB) within the grassland over time (ΔT) is equivalent to *NBP* which can be considered as follows (Eq. 6.4)

$$\frac{\Delta CB}{\Delta T} = NBP = NEE_{co_2} + C_{Harvest} + C_{Leaching} + C_{CH_4} + C_{Enteric} + C_{Milk} \qquad \text{Equation 6.4}$$

where NEE_{CO2} is the NEE of CO_2; $C_{Harvest}$ is the C offtake through biomass; $C_{Leaching}$ is C lost through dissolved organic carbon (DOC); C_{CH4} is CH_4-C emissions from dung depositions made within the field; $C_{Enteric}$ is CH_4-C emissions from enteric fermentation by livestock and C_{Milk} is the C offtake through milk production. Weight gain increases were considered negligible as the average dairy cow weight at the start of the grazing season was approximately 590 kg, with minor weight gain increases of 40 kg during lactation, returning to 590 – 600 kg at the end of the grazing season. The input of C from dung and urine deposits from grazing animals was not included in the budget as it was assumed to be recycled within the system. Emissions of C from on farm operations, such as tractor emissions, and off-farm activities, such as fertilizer production, are not included in the C budget.

The change in the N balance (ΔNB) within the grassland over time (ΔT) can be considered as follows (Eq. 6.5)

$$\frac{\Delta NB}{\Delta T} = NEE_{N_2o} + N_{Excreta} + N_{CAN} + N_{Dep} + N_{N_2} + N_{Feed} + N_{Harvest} + N_{Leaching} + N_{Milk} + N_{NH_3} \qquad \text{Equation 6.5}$$

where NEE_{N2O} is the NEE of N_2O and includes indirect emissions of N_2O from NH_3 leaching and total N deposition; $N_{Excreta}$ is N inputs from dung and urine deposits from grazing animals; N_{CAN} is N inputs from CAN fertilizer; N_{N2} is N loss through N_2, N_{Feed} is N inputs through concentrate feed; $N_{Harvest}$ is the N removal through biomass; $N_{Leaching}$ *is* N losses through NO_3^- leaching, N_{Milk} is the N incorporated in milk production and N_{NH3} is N loss through NH_3 volatilization from dung and urine patches and CAN.

The NGHGE for the grassland site was calculated from annual NEE_{CO_2}, NEE_{N_2O} and estimated CH_4 emissions from dung and enteric fermentation using a global warming potential of 265 and 28 relative to CO_2 over a time horizon of 100 years for N_2O and CH_4, respectively (Pachauri et al., 2014). Finally, the net GHG balance (NGHGB) was determined by including $C_{Harvest}$, $C_{Leaching}$, C_{Milk}, C_{CH4} and $C_{Enteric}$ (Eq. 6.6)

$$NGHGB = NGHGE + C_{Harvest} + C_{Leaching} + C_{Milk} + C_{CH_4} + C_{Enteric} \quad \text{Equation 6.6}$$

6.2.4 Ancillary measurements

The EC station was equipped with a range of ancillary sensors to measure air temperature and relative humidity (HMP155C, Campbell Scientific, Logan, UT, USA), soil temperature at 2 and 6 cm depth (TCAV-L, Campbell Scientific, Logan, UT, USA), precipitation (tipping bucket rain gauge, Young, Michigan, USA) net radiation (NR-Lite, Kipp and Zonen, Delft, The Netherlands), PPFD (PQS1, Kipp and Zonen, Delft, The Netherlands), soil heat flux at 5 cm depth (2 x HFP01SC, Hukseflux, Delft, The Netherlands) and volumetric water content (VWC) at 15 cm depth (CS616, Campbell Scientific, Logan, UT, USA).

6.2.5 Uncertainty analysis

As the modelled output from equations 6.2 and 6.3 did not produce estimates of uncertainty for each gap-filled half hourly flux, a conservative approach was applied for estimating the uncertainty in gap-filled CO_2 fluxes. This involved calculating the difference between the 95 % and 2.5 % quantile of binned fluxes according to air temperature and the PPFD to give an estimate of flux uncertainty for each half-hour. The uncertainty on the cumulative CO_2 flux was calculated using the least squares method, i.e. the square root of the sum of the model uncertainty for each half-hourly flux squared. The uncertainty in the cumulative gap-filled N_2O flux was also calculated using the least squares method on the 95 % confidence interval for each half-hourly flux. The uncertainty in N and C budget components was calculated as the 95 % confidence interval and the total estimated uncertainty on the final value for the total C exports from management (M_{ex}), the net N balance, the net C balance or NBP, and NGHGB was calculated using the least squares method on the uncertainty of the individual components of the respective balances. Where budget components were derived from the literature, the estimated uncertainty was considered conservative as literature values were predominately derived from studies conducted on the same experimental grounds.

6.3 Results

6.3.1 Weather data

Monthly weather data for 2019 and 2020 can be seen in Fig. 2 where spring represents February, March and April, summer represents May, June and July, autumn represents August, September and October and winter represents November, December and January. Air temperature followed similar trends in both 2019 and 2020, with a mean

annual temperature of 15 °C. Soil temperature was frequently lower in 2019 compared to 2020, showing lower monthly values in summer, autumn and winter. Precipitation was greater in 2020 (1150 mm) compared to 2019 (959 mm) but was highly variable, with higher rainfall observed in autumn/early winter (74 –150 mm) in 2019 and late-winter/early spring (101 – 164 mm) in 2020. Periods of low precipitation were observed in summer in both years ranging from 24 to 77 mm in 2019, and 17 to 61 mm in 2020. The same temporal pattern was observed in the annual variation in VWC measurements with high soil moisture observations in spring, autumn and winter ranging from 33 to 41 % in 2019 and 38 to 45 % in 2020, and low soil moisture observations in summer ranging from 30 to 39 % in 2019 and 28 to 35 % in 2020.

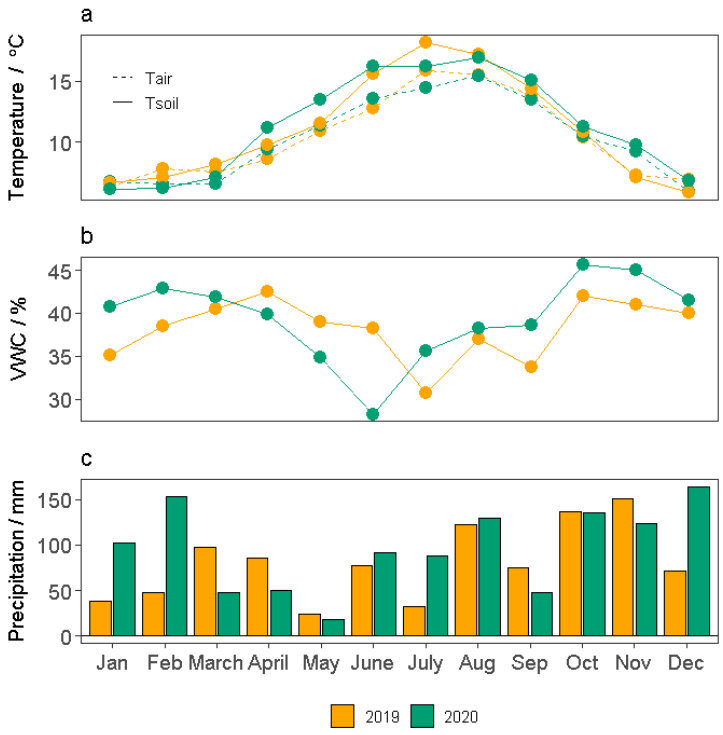

Figure 6. 2: Mean monthly values for (a) soil temperature (dashed line) and air temperature (solid line), (b) volumetric water content (VWC) and (c) total precipitation for 2019 (orange) and 2020 (green).

6.3.2 Nitrogen budget

The N budget and net balance for the grassland site in 2019 and 2020 is shown in Table 6.2. The total N imports in 2020 were greater compared to 2019 at -51.4 and -23.7 g N m^{-2} yr^{-1}, respectively. Of the -51.4 g N m^{-2} yr^{-1} imported in 2020, animal excreta accounted for -19.8 g N m^{-2} yr^{-1}. Total N exports in 2020 were also larger compared to 2019 at 33.5 and 23.7 g N m^{-2} yr^{-1}, respectively. The largest N export was from biomass removal, either through harvest cuts in 2019 (21.7 g N m^{-2} yr^{-1}) or through biomass grazed by livestock in 2020 (22.2 g N m^{-2} yr^{-1}). The remaining N exports in 2019 of N_2O, N_2, NO_3^- leaching and NH_3 volatilization from CAN were small relative to the harvest at 0.3, 0.2, 1.3 and 0.2 g N m^{-2} yr^{-1}, respectively. The second largest N export in 2020 was NH_3 volatilization from animal excreta at 5.3 g N m^{-2} yr^{-1}, followed by NO_3^- leaching at 3.0 g N m^{-2} yr^{-1}, which was approximately twice that of N losses from milk at 1.6 g N m^{-2} yr^{-1}. NH_3 volatilization from CAN was the same in 2020 to 2019 values at 0.2 g N m^{-2} yr^{-1}. Losses of N from N_2O and N_2 were greater in 2020 compared to 2019 at 0.7 and 0.5 g N m^{-2} yr^{-1}, respectively. Under a cut management, the site had an overall net neutral N balance of 0.1 ± 6.0 g N m^{-2} yr^{-1}, while under a grazing management the site was a greater net sink of N at a rate of -17.9 ± 5.5 g N m^{-2} yr^{-1}. Soil N stocks derived from soil cores taken at 0-10 cm in 2021 were 507 g N m^{-2} (Table 6.4).

Table 6. 2: Nitrogen budget and balance for the grassland site under a cut (2019) and grazed (2020) management (g N m^{-2} yr^{-1}) where values in brackets represent the uncertainty, calculated using the least squares method. Negative values represent nitrogen imports, while positive values represent nitrogen exports.

Component	2019		2020	
	g N m^{-2} yr^{-1}			
CAN	-23.0	[2.0]	-24.6	[1.3]
Animal excreta	-	-	-19.8	[1.5]
Concentrate feed	-	-	-6.3	[0.4]
Total deposition	-0.66	[0.09]	-0.66	[0.09]
N_2O	0.3	[0.004]	0.7	[0.002]
N_2	0.2	[0.1]	0.5	[0.1]
Harvest	21.7	[5.6]	-	
Biomass consumed by livestock	-	-	22.2	[5.0]
Milk	-	-	1.6	[0.03]
NO_3- leaching	1.3	[0.4]	3.0	[1.0]
NH_3 volatilization (excretion)	-	-	5.3	[0.6]
NH_3 volatilization (CAN)	0.2	[0.02]	0.2	[0.01]
Net nitrogen balance	0.1	[6.0]	-17.9	[5.5]

6.3.3 Carbon dioxide fluxes

Half hourly fluxes of NEE measured under a cut (2019) and grazed (2020) management are shown in Fig 6.3. Maximum rates of instantaneous net CO_2 assimilation were recorded in June 2019 at -30.9 µmol CO_2 m^{-2} s^{-1} and July 2020 at -36.2 µmol CO_2 m^{-2} s^{-1} (Fig. 6.3). The grassland showed lower rates of R_{eco} in 2019 relative to 2020, with maximum C losses of 14.8 and 35.6 µmol CO_2 m^{-2} s^{-1}, respectively (Fig. 6.3). The temporal trends in CO_2 uptake and release showed a typical seasonal pattern (Fig. 6.3 and 6.4). The NEE remained positive (emission source of CO_2) for January and February in both years, after which NEE became increasingly negative (CO_2 sink) during the growing season (March – September). Increases in the NEE C sink reduced from September in 2019 and November in 2020, when the assimilation

capacity of the system was lower. The grassland showed a greater capacity to assimilate C under a cut management at a cumulative rate of -547.9 g C m^{-2} yr^{-1}, compared to the grazing management at a cumulative rate of -369.3 g C m^{-2} yr^{-1}. Following silage cuts, recovery in the photosynthetic activity was rapid with maximum daily rates of GPP of -9.0, -7.3, and -3.1 g C m^{-2} in the first 30 days following harvest and subsequent fertilizer application in May, July and September, respectively. Overall maximum daily rates of GPP in 2019 of -10.6 and -10.5 g C m^{-2} were recorded in June and August, respectively. Increases in R_{eco} were observed with plant growth following silage cuts and fertilizer application, where maximum daily R_{eco} of 5.0 g C m^{-2} was observed in September, seven days following fertilizer application. The grazing management in 2020 showed maximum rates of daily GPP in May, August and July, with values of -10.1, -9.1 and -8.9 g C m^{-2}, respectively. In 2020 higher rates of R_{eco} were observed relative to 2019, where maximum daily values of 6.4, 5.8 and 5.4 g C m^{-2} were measured during the July grazing event, following the August fertilizer application and during the October grazing event, respectively.

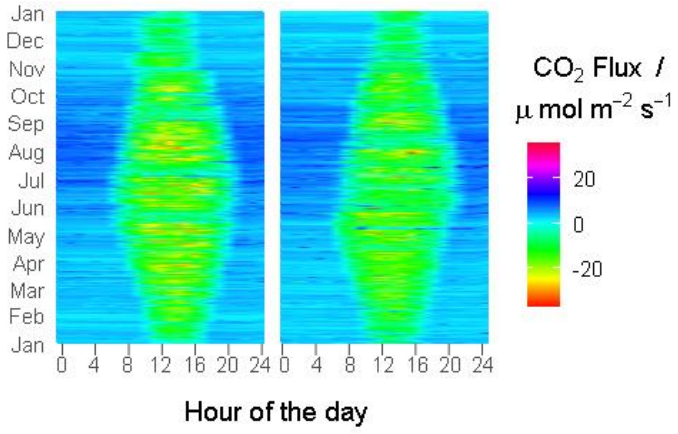

Figure 6. 3: Flux fingerprint depicting the diurnal course of half-hourly fluxes of NEE under a cut (2019) (left) and grazed management (2020) (right). Negative values represent the uptake of CO_2 and positive values represent the release of CO_2 from the system.

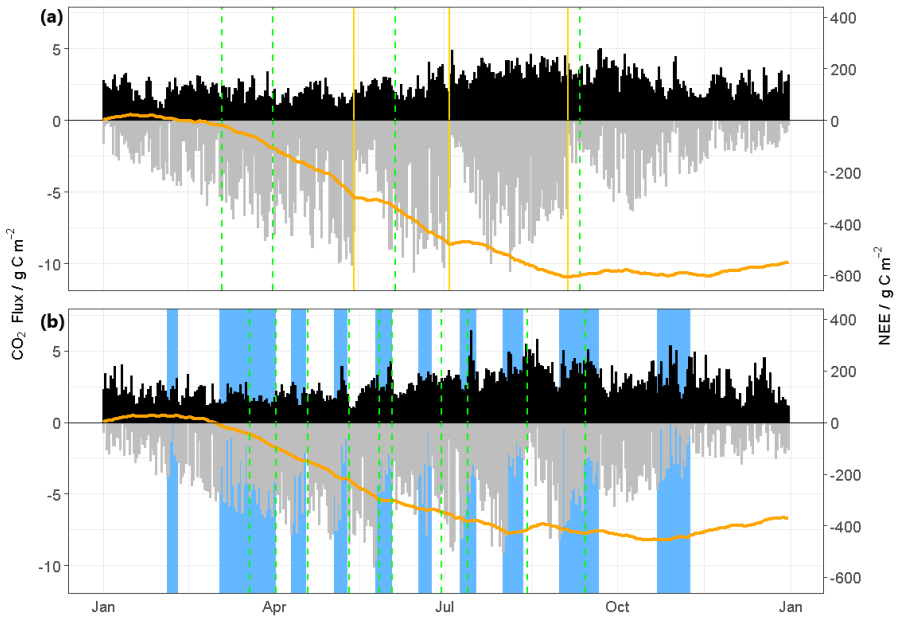

Figure 6. 4: (a) 2019 and (b) 2020 daily total ecosystem respiration (R_{eco}) (grey area), daily gross primary productivity (GPP) (black area) and cumulative net ecosystem exchange (NEE) (solid orange line). The dashed green line represents fertilizer application, the solid yellow line represents silage cuts and blue background blocks represent grazing periods.

6.3.4 Carbon budget

The NBP for the grassland site under a cut (2019) and grazing (2020) regime can be seen in Table 6.3. Annual C assimilation through GPP was 10 % lower (140 g C m^{-2} yr^{-1}) under the grazing management relative to the cut management at -1358.2 and -1498.3 g C m^{-2} yr^{-1}, respectively, while annual C losses through R_{eco} were similar under both management regimes at 950.4 and 988.9 g C m^{-2} yr^{-1} for cut and grazing, respectively. The grassland was a greater sink of C under the cut management compared to the grazing management with NEE values of -547.9 and -369.3 g C m^{-2} yr^{-1}, respectively. The largest C exports from management were from harvests in 2019 at 482.3 g C m^{-2} yr^{-1} and enteric fermentation in 2020 at 23.8 g C m^{-2} yr^{-1}. Exports of DOC were approximately five times lower from the cut management compared to the grazed management at 4.0 and 20.2 g C m^{-2} yr^{-1}, respectively. In 2020 exports of C from

dung were negligible at 0.2 g C $m^{-2} yr^{-1}$, while C exports from milk were considerably larger at 13.6 g C $m^{-2} yr^{-1}$. When incorporating the NEE with the above C exports (M_{ex}) to give the NBP, C was sequestered at a rate of -61.6 ± 24.6 g C $m^{-2} yr^{-1}$ and -311.5 ± 81.8 g C $m^{-2} yr^{-1}$ under the cut and grazing management, respectively. The total soil C content was higher in 2019 compared to 2021 at 5619.4 ± 125.2 and 4940.0 ± 1115.4 g C m^{-2} (Table 6.4).

Table 6. 3: Carbon budget for the grassland site under a cut (2019) and grazed (2020) management (g C $m^{-2} yr^{-1}$) where values in brackets represent the uncertainty calculated using the 95 % C.I. for individual C exports and imports and the least squares method for GPP, R_{eco}, NEE, M_{ex} and the NBP. Negative values represent carbon uptake, while positive values represent carbon loss.

Component	2019		2020	
	g C $m^{-2} yr^{-1}$			
GPP	-1498.3	[20.0]	-1358.2	[80.8]
Reco	950.4	[8.9]	988.9	[49.1]
NEE	-547.9	[21.9]	-369.3	[64.1]
CH_4-C - dung in field	-	-	0.2	[0.004]
CH_4-C - enteric fermentation	-	-	23.8	[00.6]
Harvest	482.3	[2.7]	-	-
DOC	4	[0.3]	20.2	[0.8]
Milk	-	-	13.6	[0.2]
M_{ex}*	486.3	[2.7]	57.8	[1.0]
NBP	-61.6	[24.6]	-311.5	[65.1]

*M_{ex} is the sum of C exports from management at the field scale.

Table 6. 4: Carbon (C) and nitrogen (N) soil stocks measured in 2019 and 2021 at 0 to 10 cm depth.

Year	Total C		Total N	
	g C/m^{-2}	95 % C.I.	g N/m^{-2}	95 % C.I.
2019	5619.4	125.2	-	-
2021	4940.0	1115.4	507.0	0

6.3.5 The net greenhouse gas balance

Values of NEE (CO_2), N_2O, CH_4, NGHGE and NGHGB in 2019 and 2020 are presented in Fig. 6.5 (detailed numbers for each year are listed in Table C.1). The NEE showed the largest contribution to the NGHGB in both years, with higher contributions under the cut management in 2019 at -2010.8 ± 80.5 g CO_2 m^{-2} yr^{-1} relative to the grazing management in 2020 at -1355.3 ± 296.4 g CO_2 m^{-2} yr^{-1}. The grassland was a greater source of N_2O under a grazing management relative to a cut management at 275.6 ± 1.0 g CO_2eq m^{-2} yr^{-1} and 140.1 ± 1.5 g CO_2eq m^{-2} yr^{-1}, respectively, while emissions of CH_4 were greater than N_2O emissions in 2020 at 783.2 ± 18.3 g CO_2eq m^{-2} yr^{-1}. The grassland was a net GHG sink (CO_2+N_2O+CH_4) under both management regimes, but showed a six-fold greater CO_2 sequestration rate under the cut management relative to the grazing management at -1870.7 ± 82.0 g CO_2eq m^{-2} yr^{-1} and -296.1 ± 315.7 g CO_2eq m^{-2} yr^{-1}, respectively. Overall, N_2O emissions reduced the sink strength of the NEE by 7 % and 20 % in 2019 and 2020 respectively, while CH_4 emissions reduced the NEE sink strength by nearly a three-fold more compared to N_2O in 2020 at 58 %. When accounting for CO_2 exported from management (M_{ex}), CO_2 losses from the cut management were an eight-fold greater than CO_2 losses from the grazing management at 1784.7 ± 9.9 g CO_2eq m^{-2} yr^{-1} and 212.1 ± 3.7 g CO_2eq m^{-2} yr^{-1}, respectively. Overall, the NGHGB showed that the grassland system was a net sink of CO_2, with similar CO_2 sequestration rates of –86.0 ± 91.8 and -84.4 ± 258.3 g CO_2eq m^{-2} yr^{-1}, for the cut and grazed management respectively.

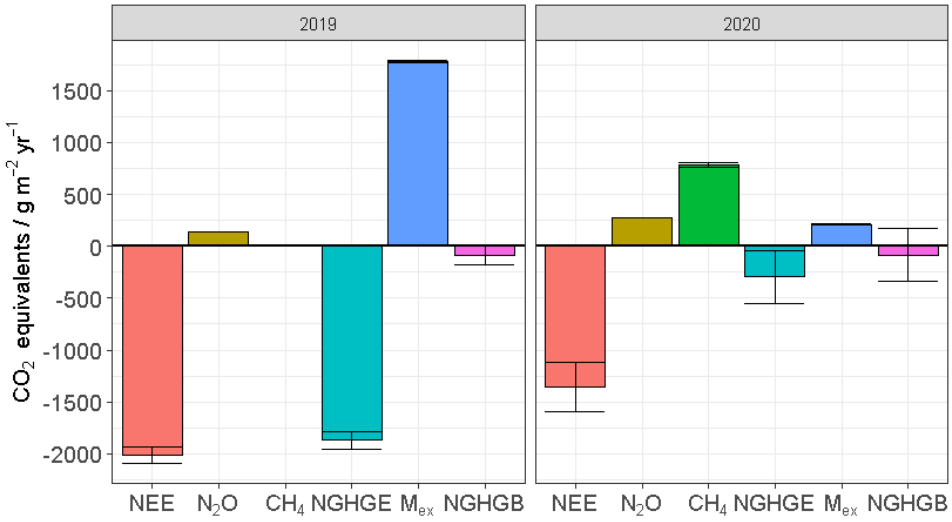

Figure 6. 5: The greenhouse gas (GHG) fluxes of the net ecosystem exchange (NEE), nitrous oxide (N_2O), methane (CH_4), the net GHG exchange (NGHGE) and net GHG balance (NGHGB) which incorporates CO_2 exports from management (M_{ex}). The error bars were calculated according to the least squares method. Negative values represent the uptake of CO_2 into the system and positive values represent the release of CO_2 from the system.

6.4 Discussion

6.4.1 Nitrogen balance

Few studies have attempted to quantify net N balances from managed grasslands (Ammann et al., 2009, Chen et al., 2004, Jones et al., 2017, Syakila and Kroeze, 2011), largely due to the complexity of management related imports and exports which includes various forms of direct and indirect emissions of reactive N. Our results indicate that under a cut management the field site had a net neutral N balance (-0.1 ± 6.0 g N m^{-2} yr^{-1}), while under a grazing management the field site acted as a sink of N (-17.9 ± 5.5 g N m^{-2} yr^{-1}). Large differences in the net N balance between both managements highlights the importance of field scale activities in determining whether grassland systems act as a net source or net sink of N. Indeed, Watson et al. (2007) showed that N fertilizer had a significant effect on the rate of N accumulation

in soils, and due to greater N inputs from CAN and animal excreta from the grazing management, this likely explains in part the higher N storage in 2020 relative to 2019. Our findings are within the range previously reported by Jones et al. (2017) who showed that the N balance of an intensively managed grassland in Scotland varied between 13.2 and -18.2 g N m^{-2} yr^{-1} over a nine year period. In this study total soil N stocks of 507 g N m^{-2} at 10 cm depth were measured in 2021, and are similar to those reported for managed grasslands, ranging from 22 to 870 g N m^{-2} between 0-5 and 0-60cm depth (Denef et al., 2013, Jones et al., 2017).

The largest N imports were from CAN in both years, and the amount applied was determined by national recommendations according to the timing and rates of N fertilizer applications in grazed and non-grazed pastures (Teagasc, 2021a). High N losses from harvests (21.7 g N m^{-2} yr^{-1}) and biomass consumed by livestock (22.2 g N m^{-2} yr^{-1}) were reported in this study. Lower N losses from biomass offtake from intensively managed grasslands have been documented in Scotland at 11.8 and 10.4 g N m^{-2} yr^{-1} over a two year period (Jones et al., 2017) and Switzerland at 6.8 g N m^{-2} (Ammann et al., 2009). Such disparities with this study could be due to a number of reasons which influence plant productivity and thus the amount of N that is assimilated and later removed, for example the amount of organic and inorganic N applied to the system, the timing and frequency of cutting and grazing events which influence the rate at which N is assimilated by plants, as well as differences in climatic conditions which favour plant growth during the time of data collection. While estimated atmospheric N deposition rates calculated in this study were comparable with previously reported values in the literature from other grassland sites (Jones et al., 2017, Kugler et al., 2008), it is important to note that the value used in this study (0.66 g N m^{-2} yr^{-1}) is at

the regional scale and is likely to be an underestimation of N deposition at the field scale. Presumably the majority of NH_3 that volatizes from the field from fertilizer or animal excreta will return back to the pasture in combination with NH_3 sources from adjacent paddocks resulting in higher N deposition rates at the field scale compared to the regional scale. This in turn would mean a higher estimated N storage under both managements.

N losses through milk production were moderate at 1.6 g N m^{-2} yr^{-1}, but similar to modelled values reported by Ryan et al. (2011) at 3.5 – 4.2 g N m^{-2} yr^{-1} for dairy production systems in Ireland. Estimates of NO_3^- leaching were double under the grazing management compared to the cut management at 3.0 and 1.3 g N m^{-2} yr^{-1}, respectively. Grazed pastures often have greater N leaching rates compared to cut pastures as biomass which is consumed by grazing animals is returned to the system in the form of dung and urine patches with high N loading rates (approximately 550 kg N ha^{-1}, Vogeler et al. (2016)), often exceeding plant N demands and thus is liable to leaching. Moreover, Vogeler et al. (2016) used a process based model to show that the risk of direct NO_3^- leaching from fertilizer alone was low, but the risk of indirect NO_3^- leaching increased where fertilizer was applied to urine patches in late winter/early spring. In this study, the second largest estimated N export from the grazing management was from NH_3 volatilization at 5.3 g N m^{-2} yr^{-1} from excretion. The rate of NH_3 volatilization is mediated by a range of meteorological factors such as soil temperature which enhances urease activity in soil (Schwenke et al., 2014) and small rainfall events (<5 mm) with low intensity which help stimulate the hydrolysis of urea (Lockyer and Whitehead, 1990). In this study, weather conditions during grazing were favourable for NH_3 volatilization with mean monthly soil temperate ranging from 6.2

°C (February) to 16.8 °C (June) and VWC ranging from 28.2 % (June) to 45.6 % (October). The volatilization of NH_3 promotes the microbial production of N_2O through nitrification of NH_4^+ and subsequent denitrification of NO_3^-. A detailed discussion on measured N_2O emissions reported in this study are available in Murphy et al. (2022a) and Murphy et al. (2022b). N_2O losses were higher under the grazed management (0.7 g N m^{-2} yr^{-1}) compared to the cut management (0.3 g N m^{-2} yr^{-1}), and subsequently, so were estimated N_2 losses at 0.5 and 0.2 g N m^{-2} yr^{-1}, respectively. Previous studies have also reported higher gaseous losses of N from grazed pastures relative to cut pastures (Flechard et al., 2007, Rafique et al., 2012). There are two likely reasons for this; firstly, the presence of dung and urine patches creates hotspots of N_2O which can enhance C and N cycling through additional C and N inputs from animal excreta (Abdalla et al., 2009a) and secondly, soil compaction by grazing animal reduces soil porosity, increases soil density and reduces hydraulic conductivity which in turn can create anaerobic soil conditions, favouring N_2O production by denitrification (Hyde, 2004).

6.4.2 Impact of management on CO_2 exchange

The range of GPP (1358.16 – 1498.28 g C m^{-2} yr^{-1}) and R_{eco} (950.36 – 988.87 g C m^{-2} yr^{-1}) measured at our field site are within range of previously reported values from other managed temperate grasslands (Jones et al., 2017). Our results showed the extended impact silage cuts have on CO_2 exchange, such as reductions in GPP and NEE following cuts, which have previously been reported and linked to a reduction in leaf area and total biomass (Gitelson et al., 2014, Schmitt et al., 2010, Zheng et al., 2010). Recovery periods following silage cuts to reach pre -harvest C fluxes (in this study ranged from -6.1 to -10.1 g C m^{-2}) varied between 19 and 34 days, which is similar to previously reported periods of 14 to 21 days from the same experimental site (Peichl et al., 2012).

The length of the recovery period depends on the time taken to reach pre-cut fluxes, which will vary according to the presence of favourable conditions for plant growth. For example, shorter recovery periods were observed post the summer silage cut in July where soil temperatures were high (18 ^{o}C), rainfall events occurred (31 mm) and light levels were at their highest (1072 - 1979 µmol m^{-2} s^{-1}, data not shown) to promote plant productivity.

Conversely, the grazing management showed less pronounced effects on NEE, as re-growth of vegetation from earlier grazed strips occurs by the time the last strip is grazed within the paddock during a single rotational grazing period (Peichl et al., 2012). As a result, sharp declines in GPP were not observed following grazing of an individual paddock. Conversely, higher rates of R_{eco} were observed from the grazing management compared to the cut management. This is likely due to presence of grazed strips and grazing animals within the EC footprint (Fig. C.1), releasing carbon either through respiration or excretion. It is also possible that grazing increased labile carbon through an increase of carbon allocation to roots in response to herbivory (Hafner et al., 2012), which in the presence of high soil and air temperatures, would promote higher rates of soil respiration and subsequently $R_{eco.}$ Indeed, Sharkhuu et al. (2016) reported higher rates of soil respiration in lightly grazed plots which had a greater total SOC content relative to ungrazed plots which showed lower rates of soil respiration. Maximum R_{eco} rates during the grazing periods were observed in July, August and October where the mean monthly air temperature values were high at 14, 15 and 11 ^{o}C, respectively. High air temperatures in combination with fertilization effects from urine and dung patches on plant growth and microbial activity have also been shown to increase R_{eco} (Augustine et al., 2003, Bardgett and Wardle, 2003, Li et al., 2013b, Wei

et al., 2012). It is important to note that previous studies have shown that grazing pressure and grazing density can affect the rate of CO_2 fluxes (Cao et al., 2004, Chen et al., 2015, Sjögersten et al., 2012), and therefore it is possible that under a longer grazing management regime and a higher grazing pressure, substrate availability for soil respiration would reduce and consequently R_{eco} (Sharkhuu et al., 2016).

6.4.3 Carbon balance

When all C imports and exports were accounted for and combined with the NEE to give the NBP, we found that under the grazing management the system had a higher net C sink at -311.5 ± 81.8 g C m^{-2} yr^{-1} compared to the cut management at -61.6 ± 24.6 g C m^{-2} yr^{-1}. Lower C sequestration rates under the cut management relative to the grazing management were due to high C exports from biomass removal during silage cuts (482 g C m^{-2} yr^{-1}), whereas a proportion of the biomass consumed by grazing livestock was recycled back into the system in the form of excreta. Similar observations have been reported for European grasslands, for example Soussana et al. (2007) reported the mean NBP from nine managed European grassland sites as -104 ± 73 g C m^{-2} yr^{-1}. Furthermore, the study by Soussana et al. included a grazed grassland in Italy with a similar NBP to that reported in this study, ranging from -253 to -462 g C m^{-2} yr^{-1}. Wall et al. (2019) reported a mean NBP of -71 ± 77 g C m^{-2} yr^{-1} (-45 to -113 g C m^{-2} yr^{-1}) over a three year period from an intensively managed grassland in New Zealand. In the United Kingdom, Myrgiotis et al. (2021) used modelling and earth observations to determine the C balance of Great Britain over a two year period and reported NBP values ranging from -120 ± 103 94 g C m^{-2} yr^{-1} to -232 ± 94 g C m^{-2} yr^{-1}. Mean annual C stocks (5280 g C m^{-2}) measured from this managed grassland system are comparable with values from similar sites found in the literature. For example, Denef et al. (2013)

reported C stocks ranging from 1410 to 4980 g C m^{-2} yr^{-1} between 0-30 cm depth from three grassland sites in Europe. While soil samples were only taken from 0-10cm depth, it is well recognized that the majority of soil C stocks are distributed within this top soil horizon (Carter et al., 1997) and thus are comparable with the cited literature. However, the potential to sequester SOC is more prominent at deeper soil horizons (1 m) where the turnover time and recalcitrance of SOM increases with depth due to an increase in soil anaerobic conditions (Lorenz and Lal, 2005). Consequently, to improve our understanding of C storage dynamics from managed grasslands, it is also necessary to sample soil C beyond the 0 -30cm soil horizon. While this study clearly demonstrates the impact that management activities have on the net C balance of grassland systems, longer term datasets are necessary for more informative quantifications of the long-term C changes from managed pastures. Indeed, Smith (2014) proposed that the legacy effects of management activities are important for assessing the C sequestration potential of managed grasslands and therefore, analysing datasets over longer time periods would provide more meaningful insights into the role of these systems in storing C.

In this study, C offtake through milk exports were on the lower end (13.6 g C m^{-2}) of previously reported values, ranging from 21 to 78 g C m^{-2} yr^{-1}(Byrne et al., 2007, Rutledge et al., 2015). Similar C losses from enteric fermentation (23.8 g C m^{-2} yr^{-1}) estimated in this study were also reported from an intensively managed grassland in Switzerland at 17 ± 1 g C m^{-2} yr^{-1} (Felber et al., 2016). Jones et al. (2017) reported lower C losses from enteric fermentation ranging from 1.5 to 5.2 g C m^{-2} yr^{-1}, although the stocking density was substantially lower (0.27 – 0.99 LSU ha^{-1} yr^{-1}). Exports of C from DOC were approximately five times greater under the grazing management relative to

the cut management. This could be due to greater DM productivity from higher N inputs under the grazing management relative to the cut management. For example, McTiernan et al. (2001) found a signification positive correlation between DOC export from a grazed grassland in south-west England and rates of N fertilizer application, and suggested that enhanced DM production from increased N fertilizer inputs was central to this relationship. Furthermore, increases in DM production would lead to higher returns of organic matter to the soil through leaf litter and decaying roots.

6.4.4 The net GHG balance

In terms of CO_2eq, the grassland remained a net sink of CO_2 with a NGHGB at -86.0 ± 91.8 and -84.4 ± 319.4 g CO_2eq m^{-2} yr^{-1}, under a cut and grazed management respectively. Similarities in the final NGHGB value from both managements was due to the varying influence of C exports and emissions of non-CO_2 gases in offsetting the NEE sink strength. Under the cut management regime, C exports greatly reduced the NEE sink strength by 89 % (primarily through biomass removal from silage cuts), while emissions of N_2O only slightly reduced the NEE sink strength by 7 %. Conversely, C exports from the grazing management had less of an impact in offsetting the NEE sink strength at 16 % relative to the cut management, but emissions of N_2O and CH_4 greatly reduced the NEE sink strength by a total of 78 %. Of this 78 %, CH_4 emissions from enteric fermentation accounted for 58 % (783.2 g CO_2eq m^{-2} yr^{-1}) as a result of a large stocking density (3.2 LSU ha^{-1}). Felber et al. (2016) also reported high CH_4 emission from enteric fermentation of 573 g CO_2eq m^{-2} yr^{-1} from an intensively managed grassland in Switzerland. Likewise, Allard et al. (2007) found a high reduction in the NEE sink strength due to CH_4 emissions from enteric fermentation by 56 and 82 % from an extensive and intensive grazing management, respectively, from a semi-

natural grassland in France. Reductions in the NEE sink, from both management regimes illustrates the impact management practices have on the capacity of managed grasslands to store CO_2. Our results further highlight the urgent need for sustainable agricultural practices in order to mitigate and reduce GHG emissions from intensively managed pastures. Such practices could include the reduction of synthetic N fertilizers in favour for multi-species mixtures (Cummins et al., 2021), lower N inputs through improved livestock diets (Carulla et al., 2005), precision agriculture (Rees et al., 2020), commencing grazing and cutting later in the growing season, inhibiting or reducing the microbial production of N_2O (Villegas et al., 2020) as well as reducing stocking rates (Adler et al., 2015). Additionally, frontier technologies which can enhance soil C sequestration and increase soil C stocks may provide avenues for producing negative emissions in agriculture upon future research and development (Paustian et al., 2019). For example, biochar amendments can increase the soil C stock as it is highly resistant to microbial degradation, with an average residence time of 100 years (Santos et al., 2012, Wang et al., 2016), and thus when introduced to grassland soils can persist for a long time. Furthermore, previous meta-studies have implied that biochar additions may reduce soil derived N_2O emissions, ranging between 9 to 50 % (Cayuela et al., 2014, Verhoeven et al., 2017), although the mechanism driving these observations are uncertain due to the range of abiotic and biotic factors that influence the production of N_2O, for example, soil oxygen concentrations, soil water content and mineral N concentrations (Butterbach-Bahl et al., 2013). Moreover, soil C stocks may also be enhanced through improved cropping systems, for example, utilizing crop species that have deep and extensive root systems, where more dry matter is distributed to the belowground biomass relative to the aboveground. Similarly to the addition of biochar to grassland soils, deep rooting systems would lower nitrate leaching and in turn

possibly N_2O emissions along the soil-plant-atmosphere continuum (Abalos et al., 2016). Relative to annual grain species, perennial grains typically produce lower yields and subsequently lower economic returns (Culman et al., 2016), thus requiring further developments in order to be consider as a viable mitigation tool against climate change.

6.5 Conclusion

Our study shows that over a two year period, management activities at the field scale influenced N and C balances from the grassland system. Additionally, emissions of N_2O and CH_4 greatly reduced (85 %) the CO_2 sink strength from the grassland over the two years, highlighting the impact of the GWP of these GHGs in offsetting CO_2 sinks. Ultimately, there is a strong need for the implementation of sustainable agricultural practices in order to both mitigate and reduce GHG emissions from managed pastures. To further assess and predict the long term changes in the CO_2 storage in managed grasslands, higher temporal resolution datasets (≥ 10 years) which encompass a gradient of management intensities across various agricultural practices and from different soil types as well as measurements of soil organic carbon at different soil horizons, are required for more robust estimates of NGHGBs from managed grasslands.

Chapter 7: General Discussion and Conclusion

7.1 Overview

The agricultural sector accounts for approximately 18 % of global and 37 % of Irelands GHG emissions (CO_2, N_2O and CH_4) (Teagasc, 2020). A large body of work has been undertaken to better understand the mechanisms which control CO_2 emissions at both the cellular and ecosystem level (Fatichi et al., 2016, Iida et al., 2009), as well as the influence of abiotic and biotic factors, and the role of management on autotrophic and heterotrophic CO_2 emissions in grasslands (Wohlfahrt et al., 2008). Additionally, there have been advancements in the development of high frequency gas analysers to quantify CO_2 and CH_4 uptake and emission at different spatial and temporal scales (Zellweger et al., 2016). It is only in more recent years, that ecosystem scale measurements of N_2O have become feasible through the development and deployment of high frequency and precision absorption spectrometers (Liang et al., 2018, Wecking et al., 2020b). Previous studies have highlighted the importance of managed temperate grasslands as a sink of CO_2 but a source of N_2O (Giraud et al., 2021, Li et al., 2013a, Soussana et al., 2007), however there is still a large degree of uncertainty in both national (Duffy et al., 2021) and international inventories (Buendia et al., 2019) of N_2O emissions from agricultural landscapes.

The main aim of this thesis was to add to the understanding of how N_2O emissions vary both in space and time from an intensively managed temperate grassland that is subject to a heterogeneous mix of N sources and loading rates. Static chamber and eddy covariance (EC) flux measurements were central to this work and were used to investigate the differences and uncertainties in N_2O emissions quantified at varying

spatial and temporal scales under a fertilized and cut management (Chapter 4). In Chapter 5 the contrasting limitations of the static chamber and EC techniques in measuring N_2O emissions were overcome by using both methods in parallel to quantify N_2O emissions from a more complex management system, whereby field scale measurements of N_2O emissions were made and the contribution of emissions from a grazing regime (background, fertilizer, urine and dung) were assessed. The effect of a cut (Chapter 4) and grazing (Chapter 5) management, as well as the global warming potential of N_2O and CH_4 emissions, on the carbon (C) sink strength of a temperate grassland was explored further in Chapter 6. This chapter provides synthesis of the research questions from the individual research chapters and discusses the context of the respective results within the scientific community (Section 7.2). To summarize, the conclusions (Section 7.3) and broader implications (Section 7.4) of the work are highlighted along with the limitations of the research (Section 7.5) and suggestions for future research (Section 7.6) are outlined.

7.2 Evaluation of research questions

Research question 1: How do we quantify N_2O emissions at different spatial and temporal scales, and how can we reduce the uncertainty in upscaling localized N_2O flux measurements to the field scale*?*

In Chapter 4, annual N_2O flux measurements were made as single point measurements in space and time using the static chamber technique and as continuous, high frequency (10 Hz), field scale measurements using the EC method. As chamber N_2O flux measurements display a log-normal distribution over time, daily mean flux values were calculated using commonly practiced normal (arithmetic), and log-normal (Bayesian) statistics. Results from this study showed that N_2O flux measurements

using static chambers were most comparable ($R^2 \approx 0.80$) with EC measurements when (1) chamber replication was high (i.e. when all available chamber flux measurements were considered [n = 30]) and (2) when the log-normal distribution of chamber N_2O flux measurements was accounted for using the Bayesian approach. Where the sample size was small (n < 5), the Bayesian approach produced uncertainties that were many orders of magnitude greater than the flux measurement itself. This was due to the inability of the Bayesian model to constrain an arithmetic mean from a log-normal dataset where the sample size was low and the variance was high. The nature of these findings suggests that if field scale measurements of N_2O are made using the static chamber technique, there needs to be high replication (n ≥ 15) and frequent sampling (where possible, at least once a week, with increased frequency following N inputs and/or during/following rainfall events) in order to reduce the uncertainty in flux measurements. Furthermore, normal statistical approaches are not advised when analysing chamber derived N_2O flux data from single management events, as such methods have a tendency to over or underestimate the sample mean of a log-normally distributed data set.

Research question 2: What is the best practice for estimating N_2O emissions at the field scale under a complex N management (i.e. rotation grazing, where there is more than one treatment)?

In Chapter 5 static chamber and EC techniques were used in a complimentary fashion to overcome the contrasting limitations of these methods (as discussed in Chapter 4), to quantify field scale emissions from a rotation-grazed management and to disaggregate between the different emission sources. Results from this study showed higher cumulative emissions but lower uncertainty from EC (6.62 ± 0.34 kg N ha^{-1})

relative to upscaled static chamber flux measurements ($F_{CH\ FIELD}$) (5.09 ±2.01 kg N ha^{-1}), where $F_{CH\ FIELD}$ estimates were derived from local partial EFs of CAN (2.78 ± 0.90 %), SU+CAN (0.59 ± 0.12 %) and dung+CAN (0.64 ± 0.15 %). While cumulative N_2O emissions by EC and $F_{CH\ FIELD}$ were with within the same order of magnitude, disparities between total N_2O-N losses from both techniques were likely due to reasons discussed in Chapter 4 such as (1) the static chamber technique has limited spatial and temporal resolution and therefore subject to high uncertainties and (2) normal statistics on log-normal data is prone to over-or (in this case) under-estimating the sample mean. Of the total N_2O-N emissions estimated by $F_{CH\ FIELD}$, animal excreta accounted for 50 % of emissions, while CAN and background accounted for 36 and 14 %, respectively. This study showed that the EC technique was suitable for measuring field scale emissions of N_2O with low uncertainty, while the $F_{CH\ FIELD}$ used in tandem could help constrain the different source contributions to total field N_2O emissions from rotationally-grazed grassland.

Research question 3: At the field scale, how do management practices affect the net C and N balance of a temperate grassland, and what is the impact of the management related emissions (CO_2, N_2O and CH_4) on the net greenhouse gas balance of grassland systems?

In Chapter 6 the management activities described in chapters 4 and 5 were assessed to understand their impact on N and C sinks, but also on the overall net GHG balance (NGHGB). Results from this study showed that under a cut management the grassland had a net neutral N balance at a rate of 0.1 ± 6.0 g N m^{-2} yr^{-1}, but under a grazing regime where N imports were greater, the net N sink of the grassland increased to -17.9 ± 5.5 g N m^{-2} yr^{-1}. The C balance was dominated by C imports from the gross primary

productivity (GPP) and C exports from ecosystem respiration (R_{eco}), the difference of which yield the net ecosystem exchange (NEE) and showed a higher C sequestration rate under the cut management compared to the grazing management at -547.9 and -369.3 g C $m^{-2} yr^{-1}$. Exports of C greatly reduced the NEE sink strength to -61.6 ± 24.6 g C $m^{-2} yr^{-1}$ and -311.5 ± 81.8 g C $m^{-2} yr^{-1}$ under the cut and grazing management with a notable reduction of 482.3 g C $m^{-2} yr^{-1}$ from silage cuts alone. Findings from this study strongly highlight the influence of field management activities on the net N and C sink of temperate grasslands. In order to assess the impact of non-CO_2 gases on the C sink of the NEE (net greenhouse gas exchange [NGHGE]), budget values were converted to CO_2 equivalents (CO_2eq). Under the cut management, emissions of N_2O only slightly reduced the NEE sink strength by 7 % (-1870.7 g CO_2eq m^{-2} yr^{-1}), while in stark contrast, emissions of N_2O and CH_4 from enteric fermentation reduced the NEE sink strength from the grazing management by 20 and 58 % (-296.5 g CO_2eq m^{-2} yr^{-1}), respectively. This study clearly demonstrated the potency of non-CO_2 gases in offsetting C sinks from managed grasslands. When management exports at the field scale were further deducted from the NGHGE, the grassland remained a sink of CO_2 with a NGHGB of -86.0 ± 91.8 and -84.4 ± 319.4 g CO_2eq $m^{-2} yr^{-1}$, under a cut and grazed management respectively.. In summary, the findings from this study showed that management practices and their associated GHG emissions strongly dictate whether managed grasslands serve as a net sink or source of C and/or GHG emissions, thus advocating for the implementation of more sustainable agricultural practices.

7.3 Conclusions

In conclusion, the work presented in this thesis has contributed to the following findings in the field of methodologies used to quantifying and assess the impact of C

dynamics and N_2O emissions from intensively managed grasslands: (1) This research has demonstrated how best to utilize the static chamber technique, both practically in the field and when post-processing flux data, to make field scale measurements of N_2O comparable with ecosystem scale flux measurements from recently developed high precision absorption spectrometers (EC). (2) It has shown that using the EC and static chamber techniques in tandem to measure field scale emissions of N_2O from grazed pastures, provides data which can support the implementation of source specific GHG mitigation strategies. (3) It has contributed to our understanding of the impacts field scale management practices have on the NGHGE and NGHGB in temperate grasslands.

7.4 Implications of research

7.4.1 Appropriation of methodologies used to measure N_2O

Current methodology guidelines for static chamber flux measurements of N_2O suggest a minimum of three replicates per treatment (Charteris et al., 2020a), with earlier studies showing a 10-fold reduction in N_2O flux measurement error when increasing chamber replication from two to five (Chadwick et al., 2014), however the findings from Chapter 4 and Chapter 5 advocate for far greater chamber replication where logistically feasible ($n > 5$). High chamber replication per treatment is not always viable as observed in Chapter 4, however if implemented as a standardised approach when using static chambers to investigate soil derived N_2O fluxes this would lead to (1) improved experimental design, (2) data sets which are more statically robust and (3) estimates of N_2O emissions with lower uncertainties. In addition to low replication, chamber N_2O flux data is frequently analysed using Gaussian statistics. As discussed in Chapter 4, this is problematic as chamber N_2O flux datasets are typically log-normally distributed. Both Tier 1 emission factors (EFs) (IPCC default) and Tier 2 (Ireland's

national approach) are based on chamber flux data which has historically been analysed using the arithmetic or naïve mean. It is likely that such estimates are either over or under estimating actual N_2O-N losses. Indeed, this has been commented on by many authors (Chadwick et al., 2018, Maire et al., 2020, Wecking et al., 2020b), but it is important to note that such over or under estimations relative to the IPCC default EFs can also be partially attributed to differing climatic conditions and management. The application of log-normal statistics (e.g. Bayesian) for national and international inventories of N_2O emissions would provide the research community with more reliable estimates of uncertainties to base their respective research findings on. However at present, the application of Bayesian statistics for chamber N_2O flux datasets is limited to single management treatments, and thus requires further development in order to broaden its application. As shown in Chapter 5, using both static chambers and EC in a complimentary fashion can provide more insightful and informative conclusions on the effect of management on cumulative N_2O-N losses relative to using both techniques in isolation. Not only is this applicable to intensively managed grasslands, but could also be insightful for other land management approaches where there are multiple sources of emissions, for example peatland sites where there are mixed ecotypes or grasslands consisting of multi-species swards.

7.4.2 N_2O emission factors from grazed pasture systems in Ireland

EFs for N_2O for CAN, SU+CAN and dung+CAN were produced in this research which provide valuable information on the interactive effects of treatments that are characteristic of a rotation grazing management (Chapter 5). Ireland's Tier 2 EF values for CAN, dung and urine are 1.4, 0.3 and 1.2 % respectively. To date, both Ireland and the IPCC do not have interactive EFs for grazing treatments despite previous studies

showing both additive and multiplicative effects from dung+CAN and urine+CAN, respectively (Hyde et al., 2016). Few studies have investigated the implications of mixed treatment effects on N_2O emissions (Hyde et al., 2016, Krol et al., 2016, Krol et al., 2017, Maire et al., 2020) even though such treatments create hotspots of N_2O within agricultural landscapes. By recalculating the N_2O emissions according to Irelands Tier 2 EFs, where interactive EFs are the sum of the EFs from their individual treatments, the emissions from Chapter 5 would change as follows (Table 7.1); N_2O emissions from CAN would decrease by 50 % and urine+CAN and dung+CAN would increase by approximately 430 and 460 %, respectively. By using specific interactive EFs, soil system dynamics at the time of treatment application such as changes in substrate availability, microbial communities, C:N ratios, soil oxygen concentrations etc, which all influence the production of soil derived N_2O, are accounted for and N_2O emissions are less likely to be overestimated as is the case when independent EFs are added together. These research findings highlight the need for Tier 2 aggregated EFs from grazing systems alongside the disaggregated Tier 2 EFs.

Table 7. 1: Comparison of aggregated emission factors (EFs) measured from this study and combined EFs of calcium ammonium nitrate (CAN) and urine, and CAN and dung from Tier 2 EFs.

	Measured				Tier 2			Emission Difference	
	EF	95% C.I.	Cumulative	95% C.I.	EF*	Cumulative	95% C.I.		
Treatment	%		kg N ha^{-1}		%	kg N ha^{-1}		kg N ha^{-1}	
CAN	2.78	0.90	1.24	0.44	1.4	0.62	0.24	0.62	↓
Urine+CAN	0.59	0.12	3.42	0.69	2.6	14.66	0.34	11.24	↑
Dung+CAN	0.64	0.15	3.35	0.83	1.7	8.68	1.95	5.33	↑

*Tier 2 EFs for urine+CAN is $EF_{3cattle\ -urine}$ (1.2 %) + $EF_{1\ CAN}$ (1.4 %) + and dung+CAN is $EF_{3cattle\ -dung}$ (0.31 %) + $EF_{1\ CAN}$.

7.4.3 Management implications on the climate change mitigation potential of grasslands

The results from Chapter 6 contribute to our existing understanding of the impact that agricultural management has on the potential for grassland systems to act as a reservoir of C. Ultimately, farm management can alter the sink strength of grasslands by decoupling soil C and N cycles where C is lost to the atmosphere as CO_2 by either respiring animals during grazing or enhanced soil respiration via N fertilization, and N is imported into the soil primarily through either animal excreta or fertilizer application. Where grasslands are managed for silage production or grazing, the recovery period following biomass removal or plant defoliation will determine the response of the plant-soil system to uptake C and shift towards a C sink following extensive C exports. Therefore, farm management decisions regarding the frequency of grazing and cut events will strongly dictate the capacity of the system to store more C than is lost through farming practices (Wecking, 2021). Policy measures will be required to incentivise farmers to adjust their management practices accordingly to prevent excessive C losses through grazing and harvest cuts, and to increase C inputs through enhanced organic fertilization. This in turn would complement national emission reduction targets of 51 % between 2018 and 2030, and emission neutrality by 2050 as outlined in the Climate Action and Low Carbon Development (Amendment) Bill 2021. Furthermore, as part of Ireland's contribution to the Paris Agreement, the Effort Sharing Regulation framework published by the European Commission in 2016, set a national emission reduction target of 30 % by 2030 relative to 2005 emissions. Of this target, 5.6 % can be achieved through offsetting emissions by C sequestration. However, research findings from Chapter 6 showed that the GWP of N_2O and CH_4 can considerably offset the C sequestered from managed grasslands over time. The

radiative forcing of N_2O and CH_4 is 265 and 28 times that of CO_2 over a 100 year lifespan, respectively. Therefore it is highly recommended that policy measures are implemented to incentive farmers to modify current management practices in order to reduce non-CO_2 emission from managed pastures. This could include switching from CAN to urea based formulas of synthetic N fertilizer (Harty et al., 2016) or encouraging the development of legume-containing pastures for grazing which have previously shown high nitrogen-use efficiency (NUE) from N inputs from animal excreta and low N_2O emissions (Nyameasem et al., 2021).

7.5 Limitations of research

Some of the limitations of this research included:

- Urine and dung patch characteristics (frequency and area), were taken as constant literature values, when in reality these characteristics would vary and ultimately alter the N loading rate.
- Interactive effects of overlapping urine on urine patches and/or dung on dung patches on N_2O emissions were not investigated, which could have possibly bridged the gap between disparities in field scale cumulative N_2O estimates by EC and chambers in Chapter 4.
- N_2 losses from urine depositions through the process of co-denitrification were not accounted for in this research but have been shown to be significantly greater than N_2 losses through denitrification (Selbie et al., 2015), and therefore could have significant implications for the N budget of the site.
- The interaction between the availability of soil organic C (SOC) and nitrogen processes was not measured which could have explained some of the variability observed in N_2O emissions.

- The chamber replication in Chapter 5 was 5 replicates per treatment per grazing i.e. 5 replicates each for four treatments (control, CAN, SU+CAN and dung+CAN) for each of the four grazing events monitored in 2020. Due to the variety of treatments and number of grazing events, as well as time and logistical constraints, it was not feasible to increase the chamber replication however, under optimum circumstances the chamber replication should be greater ($n \geq 15$) to account for variability in N_2O emissions.
- Static chambers and EC both have their strengths and limitations. While the static chamber technique is cheaper, easy to deploy and useful in investigating treatment effects on N_2O emissions (as shown in Chapter 5), its restricted spatial and temporal resolution means flux measurements are often attributed with high uncertainties (as shown in Chapter 4). On the other hand, the EC technique provides high frequency, real time measurements of the GHG exchange across the soil and atmosphere continuum, however as flux measurements are integrated over a given area, the emission sources within that area are not defined.

7.6 Suggestions for future research

- Where high resolution, low uncertainty ecosystem scale GHG measurements are necessary, the EC technique has shown to be successful in capturing the spatial and temporal dynamics in emissions from grassland systems (Chapter 4, 5 and6). To date, there are very few Irish studies investigating the application of the EC technique to quantify terrestrial GHG exchange between the atmosphere and the soil (Kiely et al., 2018). Therefore a significant knowledge gap exists in understanding the variability of N_2O emissions from different land

uses for example, peatlands, arable pastures and forests, as well as different soil types such as mineral and organic/peat soils

- In Ireland, the recently developed National Agricultural Soil Carbon Observatory (NASCO) aims to address some of these knowledge gaps with the overarching aim of constructing long-term GHG datasets for quantifying and modelling future emissions under different managements and climate scenarios and in doing so, would provide a foundation upon which climate change policy decision making can occur.
- In addition to this, such large datasets would allow for the development of process based gap filling models for N_2O, an area of research that is still undeveloped both at the national and international level.
- In order to better understand the relationships between GHGs and C and N cycling, measurements of soil nutrient stocks should be taken alongside flux measurements.
- To date there is extremely limited knowledge on the effect of interactive grazing treatments on the magnitude of N_2O emissions. Future studies may consider investigating this under the following treatments,
    - Urine + Urine
    - Dung + Dung
    - Urine +Dung
    - Urine +Fertilizer
    - Dung + Fertilizer

  and ideally over a period of 12 months to also encompass legacy effects as well as seasonally variability in emissions.
- The development of methodologies that can quantify animal excreta in the field would provide more certainty in the spatial and temporal upscaling of N_2O emissions. This can be achieved in two ways (1) using multi-spectral aerial or

ground-based imagery to assess the grass growth response following animal defaecation and where such imagery datasets are large enough, (2) develop machine learning algorithms to identify animal excreta under a various grazing systems (mobbed or rotation) and different climatic conditions (Maire et al., 2018.)

Appendices

APPENDIX A – Supplementary material for Chapter 4

Table A. 1: Chamber (CH) flux measurements (N_2O-N μg m^{-2} hr^{-1}) derived from the arithmetic and Bayesian method where FP refers to CH measurements inside the footprint of the eddy covariance footprint.

	Arithmetic Method						Bayesian Method					
		95% C.I.			95% C.I.			95% C.I.			95% C.I.	
Date	mean	lwr CH_{All}	upr	mean	lwr CH_{FP}	upr	mean	lwr CH_{Bayes}	upr	mean	lwr $CH_{Bayes-FP}$	upr
8/1/2019	2.67	1.69	3.66	2.82	1.87	3.77	2.69	1.63	3.81	2.84	1.72	3.98
17/1/2019	1.82	1.1	2.53	1.24	0.31	2.17	1.83	1.05	2.64	1.26	0.16	2.42
25/1/2019	3.04	2.09	3.99	3.07	1.68	4.46	3.05	2.02	4.15	3.14	1.25	5.26
1/2/2019	1.52	0.64	2.4	1.16	-0.39	2.72	1.54	0.55	2.55	1.3	-1.02	4.12
7/2/2019	1.97	1.06	2.88	2.38	1.42	3.35	1.98	1	3.01	2.42	1.12	3.89
4/3/2019	1.89	0.64	3.14	4.14	0.59	7.68	1.91	0.66	3.23	4.71	-0.25	11.47
5/3/2019	1.9	0.11	3.69	0.31	-1.19	1.81	1.95	0.24	3.79	0.37	-1.39	2.24
6/3/2019	538.89	359.79	717.99	626.7	490.93	762.47	677.88	400.25	1223.65	670.86	491.66	985.96
7/3/2019	356.28	178.38	534.17	234.11	30.5	437.72	391.46	232.66	701.46	949.89	113.9	25944.48
8/3/2019	165.66	99.28	232.05	147.1	44.64	249.57	202.68	111.35	380.34	318.16	74.1	1211.42
11/3/2019	74.75	44.07	105.43	28.68	-5.46	62.83	80.56	49.22	130.54	33.95	9.53	86.26
12/3/2019	36.27	18.05	54.49	10.77	1.81	19.72	36.8	22.14	57	11.54	3.73	22.31
14/3/2019	7.37	1.86	12.88	1.48	-7.84	10.79	8.06	2.33	15.41	14.76	-7.93	61.6
19/3/2019	7.43	3.99	10.87	2.71	1.75	3.67	7.46	4.59	10.72	2.73	1.6	3.9
26/3/2019	5.62	2.65	8.58	1.93	0.78	3.08	5.65	3.15	8.44	1.98	0.25	3.83
1/4/2019	5.67	1.45	9.89	1.9	-2.45	6.25	5.65	2.45	9.17	3.34	-4.12	15.66
2/4/2019	33.99	15.39	52.6	3.2	2.04	4.36	33.89	20.27	52.36	3.43	0.54	7.24
3/4/2019	18.05	2.97	33.13	-0.2	-1.95	1.54	17.19	8.49	28.67	0.1	-3.8	5.28
4/4/2019	26.19	-0.54	52.92	5.29	-4.55	15.13	22.37	11.82	36.93	9.75	-3.59	36.72
5/4/2019	117.92	53.07	182.77	63.54	0.22	126.87	134.64	70.71	258.17	171.12	24.86	634.1
8/4/2019	79.57	38.65	120.5	26.73	14.52	38.93	81	48.97	132.2	30.3	14.73	58.3
10/4/2019	89.67	46.23	133.12	67.51	1.81	133.22	93.08	56.52	153.62	424.98	24.85	6218.68
11/4/2019	77.84	46.81	108.87	39.48	25.05	53.91	82.2	52.83	127.82	46.14	23.14	89.87
16/4/2019	36.46	19.27	53.65	8.44	4.62	12.27	36.77	23.67	55.03	19.06	2.06	25.26
17/4/2019	16.64	5.06	28.23	8	-9.42	25.41	17.25	8.02	29.85	211.1	-7.43	2405.36
23/4/2019	44.68	13.62	75.74	13.02	5.11	20.94	41.93	23.26	70.38	21.11	2.51	54.37
24/4/2019	20.5	-10.03	51.04	7.01	3.24	10.77	14.67	5.68	26.74	50.58	0.43	34.83
4/6/2019	24.06	14.05	34.07	24.13	14.8	33.46	24.25	16.35	34.25	25.22	15.69	37.79
5/6/2019	18.98	9.56	28.39	10.78	5.53	16.04	18.91	11.87	27.58	12.08	3.52	25.71
6/6/2019	39.63	25.55	53.7	52.76	32.52	73	39.86	28.98	53.88	56.81	35.46	92.08
7/6/2019	15.51	12.07	18.95	18.35	10.46	26.23	15.64	12.28	19.38	19.52	10.51	32.31
8/6/2019	16.49	11.32	21.65	16.92	9.07	24.77	16.64	12.11	21.82	20.53	7.97	39.2
10/6/2019	11.5	9.16	13.85	12.84	9.11	16.56	11.57	9.27	14.09	13.11	8.67	18.27
11/6/2019	8.28	5.82	10.74				8.32	6.1	10.73			
12/6/2019	23.02	15.62	30.43	25.66	12.62	38.71	23.29	16.76	31.02	28.95	13.46	55.17
13/6/2019	22.69	14.67	30.71	21.59	13.49	29.68	22.83	16.52	30.36	22.86	13.44	36.8
17/6/2019	101.03	60.55	141.51	126.67	33.92	219.42	106.14	69.37	164.17	203.53	64.29	620.08
19/6/2019	27.83	18.74	36.92	26.4	5.4	47.4	28.09	20.56	37.16	80.44	8.31	198.83
26/6/2019	12.95	9.79	16.12	21.14	12.41	29.87	13.06	10.02	16.37	23.2	11.75	40.66
27/6/2019	8.56	6.47	10.66	13.95	9.42	18.48	8.62	6.53	10.85	14.57	8.3	22.28
7/8/2019	6.81	3.17	10.44	8.29	-1.22	17.79	7.07	3.24	11.5	13.56	-0.93	37.75
9/8/2019	38.64	14.63	62.64	17.86	6.92	28.79	37.52	23	58.43	20.49	7.73	42.6
13/8/2019	10.96	8.15	13.76	13.56	8.34	18.78	11.01	8.43	13.78	14.01	8.6	20.84
21/8/2019	3.86	2.18	5.54	6.68	0.7	12.66	3.88	2.27	5.56	7.96	0.15	19.91
28/8/2019	1.52	-0.24	3.28	1.28	-3.01	5.58	1.6	-0.23	3.58	1.8	-3.12	8.28
2/9/2019	4.12	2.15	6.09	5.37	1.51	9.23	4.16	2.25	6.27	5.83	0.79	12.43
10/9/2019	14.73	11.09	18.37	14.46	9.19	19.73	14.82	11.34	18.65	14.76	9.78	20.69
12/9/2019	11.44	8.11	14.76	12.13	4.34	19.93	11.6	8.3	15.3	13.26	4.65	25.31
13/9/2019	18.55	14.06	23.03	18.01	7.13	28.9	18.78	14.39	23.73	19.79	8.52	36.58
14/9/2019	1.23	-2.73	5.19	5.22	-4.24	14.67	1.4	-2.15	5.51	6.95	-2.77	22.43
16/9/2019	7.69	4.47	10.91	7.91	3.37	12.45	7.79	4.79	11.19	8.41	3.28	14.95
17/9/2019	17.86	13.71	22	18.61	10.2	27.01	18.03	14.16	22.44	19.49	11.36	30.5
19/9/2019	2.12	-0.9	5.13	-0.42	-6.24	5.41	2.47	-1.07	6.59	1.15	-6.59	13.64
20/9/2019	3.28	0.4	6.17	7.51	-0.91	15.93	3.43	0.54	6.63	9.98	-1.26	30.24
24/9/2019	417.14	221.24	613.04	255.44	147.27	363.61	438.86	279.03	727.07	349.62	167.12	843.77
25/9/2019	127.98	82.16	173.8	84.9	48.31	121.5	131.64	93.19	189.39	92.51	56.63	155.62
1/10/2019	66.95	38.75	95.15	95.42	24.7	166.13	67.24	46.49	96.73	282.22	46.41	1265.31
2/10/2019	67.99	34.56	101.43	94.83	8.46	181.2	71.35	41.91	118.69	510.06	37.71	6100.45
10/10/2019	26.55	10.76	42.34	24.03	7.06	41.01	26.37	15.16	41.41	26.62	11.79	51.1
16/10/2019	15.14	10.43	19.84	19.95	7.42	32.49	15.27	11.07	20.1	22.53	9.23	45.23
22/10/2019	14.07	4.6	23.54				13.75	7.59	21.25			
31/10/2019	5.72	2.31	9.12	10.14	1.88	18.4	5.94	2.44	9.94	11.77	2.14	26.52
4/11/2019	7.65	3.41	11.89	12.54	-8.55	33.64	7.71	4.28	11.71	53.89	-2.67	161.41
14/11/2019	2.5	1.09	3.91	4.04	1.35	6.72	2.53	1.15	4	4.38	0.4	9.38
20/11/2019	9.95	6.46	13.45	14.3	6.36	22.25	10.07	6.9	13.75	15.23	7.2	26.51

27/11/2019	-0.4	-4.19	3.38	-2.62	-13.34	8.09	-0.01	-3.96	4.81	2.68	-11.32	35.51
3/12/2019	5.83	1.86	9.8	15.67	0.99	30.35	5.79	2.77	9.11	19.79	4.02	50.31
11/12/2019	18.85	8.28	29.41	26.16	-1.32	53.64	18.89	10.83	29.17	52.29	7.29	138

Table A. 2: Eddy covariance (EC) flux measurements (N_2O-N μg m^{-2} hr^{-1}) where EC_{CH} are EC flux measurements made during the time of chamber measurements

Date	Mean	lwr	95% C.I. upr	Mean	lwr	95% C.I. upr
			EC_{All}		E_{CH}	
8/1/2019	16.4	10.38	23.67	4.82	3.92	5.46
17/1/2019	39.22	20.32	59.34	9.12	5.51	12.72
25/1/2019	13.44	4.52	20.01			
1/2/2019						
7/2/2019	4.1	-33.88	17.44	2.03	0.53	4.59
4/3/2019	25.1	5.89	53.12	7.2	1.75	9.82
5/3/2019	25	5.31	116.41	4.18	1.67	10.73
6/3/2019	537.74	162.79	1021.16	168.7	160.6	177.36
7/3/2019	218.07	115.45	441.38	71.14	71.14	71.14
8/3/2019	48.03	22.47	76.69	19.56	17.1	22.48
11/3/2019	10.06	-17.68	28.79	4.16	0.55	6.45
12/3/2019	9.92	-7.72	30.55			
14/3/2019	9.72	-5.9	27.45			
19/3/2019	9.99	-14.34	28.85	3.49	0.9	6.33
26/3/2019	9.68	1.39	26.98	2.52	2.52	2.52
1/4/2019	21.05	2.53	86.79			
2/4/2019	61.17	26.91	93.3	14.56	12.91	17.57
3/4/2019	25.41	11.96	55.64			
4/4/2019	98.95	88.17	110.28			
5/4/2019	180.98	70.84	278.95	60.62	45.7	82.95
8/4/2019	307.41	234.05	344.38			
10/4/2019	133.34	98.68	168.46			
11/4/2019	101.08	56.79	136.32	27.66	24.47	31.96
16/4/2019	57.3	32.11	79.06	13.93	12.23	16.39
17/4/2019	39.83	28.1	57.91	10.47	8.61	12.54
23/4/2019	41.08	-19.44	126.04	26.37	20.4	34.53
24/4/2019	46.91	25.19	86.82	13.74	7.15	24.45
4/6/2019	40.54	-1.02	103.26	15.06	13	17.12
5/6/2019	40.36	12.9	71.04	8.77	4.48	17.45
6/6/2019	65.89	12.66	178.47	14.98	4.3	22.05
7/6/2019	138.33	57.21	269.42	24.13	21.82	30.59
8/6/2019	219.31	83.01	325.55	53.5	46.33	60.43
10/6/2019	63.42	63.42	63.42	17.62	17.62	17.62
11/6/2019	81.14	20.24	148.9	27.91	19.83	35.99
12/6/2019	21.41	-42	90.34	1.42	-9.83	6.78
13/6/2019						
17/6/2019	51.12	-0.36	94.35	13.16	11.17	17.72
19/6/2019	237.28	142.7	412.34	71.93	49.83	90.86
26/6/2019	63.74	29.74	96.32	16.8	8.61	22.32
27/6/2019	14.58	-64	65.86	6.57	-7.36	16.95
7/8/2019	17.14	-60.08	80.02	-9.84	-15.78	-5.93
9/8/2019	19.06	7.73	31.66	8.78	8.18	9.83
13/8/2019						
21/8/2019						
28/8/2019	16.71	6.61	28.21	6.04	4.73	7.73
2/9/2019	19.2	-8.12	50.88	11.11	6.09	14.77
10/9/2019	16.17	-0.91	37.41	7.28	3.82	10.25
12/9/2019	29.92	12.09	49.92	5.14	3.7	9.85
13/9/2019	17.57	6.11	37.25	5.82	1.17	10.44
14/9/2019	19.71	8.43	35.66	4.46	2.96	6.17
16/9/2019	19.99	7.16	35.56	4.96	2.92	8.9
17/9/2019	17.04	9.22	28.97	5.09	3.05	7.98
19/9/2019	13.94	6.11	25.15	2.68	1.49	4.38
20/9/2019	17.92	-13.88	80.08	15.32	5.14	36.02
24/9/2019	315.1	127.22	510.38	90.86	66.6	110.8
25/9/2019	270.17	159.41	354.39	70.02	58.71	80.96
1/10/2019	90.16	53.72	135.19			
2/10/2019	82.88	52.05	111.01	21.31	18.01	24.6
10/10/2019	32.1	12.74	59.02	9.61	6.78	11.37
16/10/2019	17.08	5.21	28.5	4.55	3.77	4.95
22/10/2019						
31/10/2019	11.26	-21.39	27.59			
4/11/2019	13.59	-2.36	40.82			
14/11/2019	-1.21	-1.21	-1.21			

20/11/2019	10.39	-7.97	21.21	5.11	4.3	5.92
27/11/2019	15.39	5.76	30.62			
3/12/2019	-3.14	-42.78	20.88	-3.26	-12.75	5.5
11/12/2019	26.27	9.83	45.88	7.17	6.76	8.01

Table A. 3: The full output from a regression subset model explaining the variance in log(N_2O-N) fluxes by water-filled pore space (WFPS %), rainfall (mm) air temperature (Tair °C) and soil temperature (Tsoil °C) over rolling averages of 6 hrs^{-1}, 12 hrs^{-1}, 24 hrs^{-1}, 48hrs^{-1} and 100 hrs^{-1} periods in the 30 days following fertilizer application (Fertilizer) and in the 30 days outside of fertilizer applications (Background).

Variable	Treatment	R^2
WFPS 48 hr^{-1}	Fertilizer	0.50
WFPS 100 hr^{-1}	Fertilizer	0.50
WFPS 6 hr^{-1}	Fertilizer	0.50
Rainfall 100 hr^{-1}	Fertilizer	0.50
Rainfall 48 hr^{-1}	Fertilizer	0.50
Rainfall 24 hr^{-1}	Fertilizer	0.49
Rainfall 12 hr^{-1}	Fertilizer	0.49
Rainfall 6 hr^{-1}	Fertilizer	0.49
Tsoil 100 hr^{-1}	Fertilizer	0.48
Tair 100 hr^{-1}	Fertilizer	0.43
Tair 48 hr^{-1}	Fertilizer	0.40
WFPS 100 hr^{-1}	Background	0.31
Rainfall 48 hr^{-1}	Background	0.31
Rainfall 24 hr^{-1}	Background	0.31
Tsoil 48 hr^{-1}	Background	0.30
Tsoil 12 hr^{-1}	Background	0.29
Tair 100 hr^{-1}	Background	0.27

Table A. 4: Output from a linear multivariate model for log(N_2O-N) emissions measured by eddy covariance 30 days post fertilizer application (Fertilizer) and 30 days outside of the fertilizer application (Background) using rolling averages of air (Tair) and soil temperature (Tsoil), water filled pore space (WFPS%) and rolling sums of rainfall over 6 hrs^{-1}, 12 hrs^{-1}, 24 hrs^{-1}, 48 hrs^{-1} and 100 hrs^{-1} periods

Treatment	Parameter	Estimate	Standard Error	t Value
Fertilizer	Intercept	-1.99	0.51	-3.91
	Tair 48 hr^{-1}	0.24	0.02	10.96
	(Tair 48 hr^{-1}) ^2	-0.01	0.00	-7.22
	Tair 100 hr^{-1}	-0.85	0.04	-23.21
	(Tair 100 hr^{-1}) ^2	0.03	0.00	19.96
	Tsoil 100 hr^{-1}	0.68	0.03	25.86
	(Tsoil 100 hr^{-1}) ^2	-0.02	0.00	-23.81
	(Rainfall 6 hr^{-1}) ^2	0.00	0.00	-8.04
	Rainfall 12 hr^{-1}	-0.03	0.00	-5.27
	(Rainfall 12 hr^{-1}) ^2	0.00	0.00	7.80
	Rainfall 24 hr^{-1}	0.02	0.00	5.35
	(Rainfall 24 hr^{-1}) ^2	0.00	0.00	2.12
	(Rainfall 48 hr^{-1}) ^2	0.00	0.00	-12.95
	Rainfall 100 hr^{-1}	0.00	0.00	22.62
	WFPS 6 hr^{-1}	0.11	0.02	6.91
	(WFPS 6 hr^{-1}) ^ 2	0.00	0.00	-6.08
	WFPS 48 hr^{-1}	0.29	0.03	9.48
	(WFPS 48 hr^{-1}) ^2	0.00	0.00	-8.68
	WFPS 100 hr^{-1}	-0.18	0.03	-5.60
	(WFPS 100 hr^{-1}) ^2	0.00	0.00	3.61
	Days Since Fertilizer App. 24 hr^{-1}	-0.01	0.00	-6.70
	(Days Since Fertilizer App. 24 hr^{-1}) ^2	0.00	0.00	4.07
Background	Intercept	4.04	0.27	14.71
	Tair 100 hr^{-1}	-0.05	0.02	-2.99
	(Tair 100 hr^{-1}) ^2	0.01	0.00	7.25
	(Tsoil 12 hr^{-1}) ^2	0.00	0.00	11.50
	Tsoil 48 hr^{-1}	0.05	0.01	4.12
	(Tsoil 48hr^{-1}) ^2	-0.01	0.00	-11.64
	Rainfall 24 hr^{-1}	0.02	0.00	6.42
	(Rainfall 24 hr^{-1}) ^2	0.00	0.00	-4.54
	Rainfall 48 hr^{-1}	-0.01	0.00	-8.91
	WFPS 6 hr^{-1}	0.15	0.01	10.71
	(WFPS 6 hr^{-1}) ^ 2	0.00	0.00	-9.33
	WFPS 48 hr^{-1}	-0.13	0.02	-8.30
	(WFPS 48 hr^{-1}) ^ 2	0.00	0.00	11.68
	(WFPS 100 hr^{-1}) ^ 2	0.00	0.00	-20.99
	Days Since Fertilizer App. 100hr^{-1}	0.00	0.00	-5.01
	(Days Since Fertilizer App. 100 hr^{-1}) ^ 2	0.00	0.00	3.37

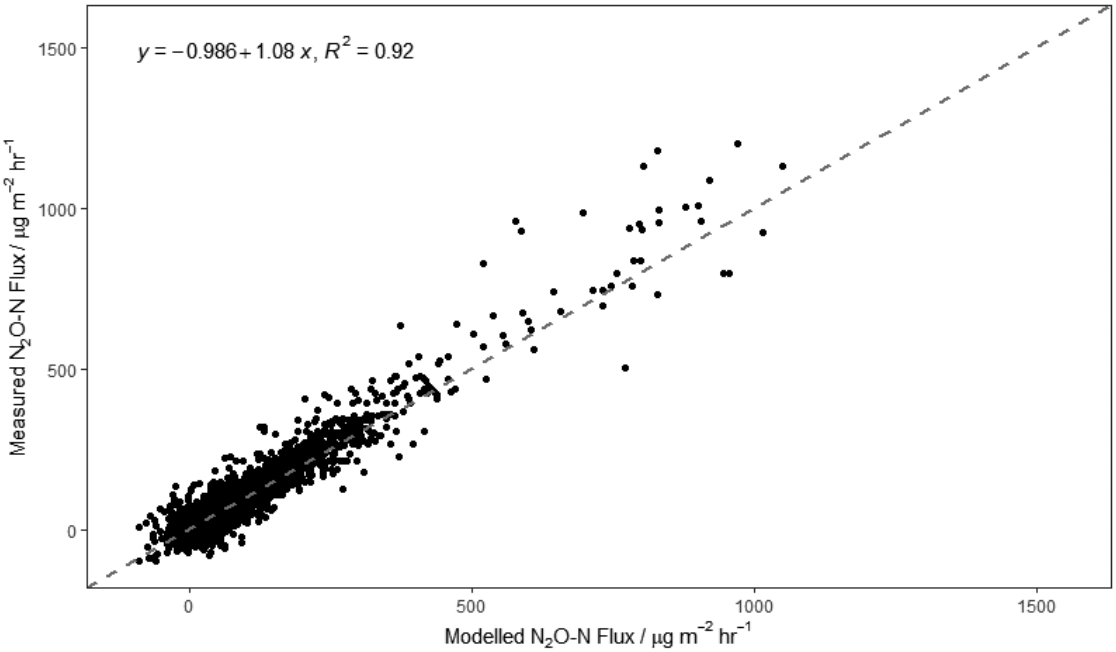

Figure A. 1: The correlation between measured and linearly modelled N_2O-N flux values where the broken line represents the 1:1 ratio.

Table A. 5: Cumulative N_2O fluxes from mean daily chamber and half-hourly eddy covariance (EC) flux measurements from seven comparison periods (see Table 4.1 for dates) where EC_{All} is all measured EC measurements over the comparison period, EC_{CH} is measured EC measurements during the time of chamber measurements, CH_{All} and CH_{Bayes} are all chamber flux measurements daily averaged using the arithmetic and the Bayesian mean, respectively and CH_{FP} and $CH_{Bayes\text{-}FP}$ are daily averaged chamber flux measurements within the footprint of the EC tower using the arithmetic mean and the Bayesian mean, respectively.

Comparison #	EC_{All}				EC_{CH}				CH_{All}				CH_{FP}				$CH_{Bayes\text{-}All}$				$CH_{Bayes\text{-}FP}$			
	N		95% C.I.		*N*		95% C.I.		*N*		95% C.I.		*N*		95% C.I.		*N*		95% C.I.		*N*		95% C.I.	
		mean	upr	lwr		mean	upr	lwr		mean	upr	lwr		mean	upr	lwr		mean	upr	lwr		mean	upr	lwr
	N_2O-N kg^{-1} ha^{-1} $comparison^{-1}$																							
1	94	0.127	0.090	-0.085	12	0.026	0.019	-0.018	105	0.016	0.009	-0.009	43	0.015	0.009	-0.008	105	0.017	0.009	-0.009	43	0.016	0.009	-0.009
2	367	0.257	0.178	-0.168	31	0.079	0.055	-0.054	295	0.366	0.247	-0.221	87	0.303	0.218	-0.200	295	0.430	0.296	-0.261	87	0.582	0.423	-0.351
3	341	0.483	0.265	-0.224	39	0.107	0.048	-0.046	353	0.295	0.141	-0.127	59	0.127	0.059	-0.056	353	0.305	0.148	-0.132	59	0.511	0.217	-0.174
4	321	0.444	0.215	-0.192	43	0.119	0.053	-0.051	390	0.172	0.067	-0.063	94	0.199	0.075	-0.069	390	0.176	0.068	-0.064	94	0.319	0.110	-0.095
5	99	0.064	0.022	-0.021	14	0.025	0.009	-0.008	150	0.054	0.032	-0.031	39	0.049	0.026	-0.025	150	0.054	0.032	-0.031	39	0.056	0.030	-0.029
6	339	0.579	0.180	-0.134	58	0.150	0.050	-0.047	388	0.473	0.157	-0.122	123	0.375	0.119	-0.101	388	0.491	0.163	-0.126	123	0.699	0.192	-0.134
7	283	0.153	0.084	-0.082	34	0.029	0.019	-0.019	299	0.141	0.083	-0.081	69	0.166	0.084	-0.081	299	0.142	0.083	-0.082	69	0.290	0.138	-0.129

APPENDIX B – Supplementary material for Chapter 5

Table B. 1: Mean values of air and soil temperature at 10 cm depth, and total rainfall for each month over a 10 year period (2009 – 2019). Data was retrieved from the Johnstown Castle Weather station which is within 100 m of the experimental field site.

Month	Air temperature (^{0}C)	Soil temperature (^{0}C)	Rainfall (mm)
January	5.76	5.41	1064.50
February	5.87	5.70	824.00
March	6.62	7.11	823.30
April	8.56	10.10	715.50
May	11.09	13.57	695.30
June	13.78	17.19	849.20
July	15.51	18.55	903.50
August	14.99	17.03	920.50
September	13.49	14.85	817.10
October	11.36	11.88	1299.50
November	8.05	8.11	1356.20
December	6.58	6.12	1382.10

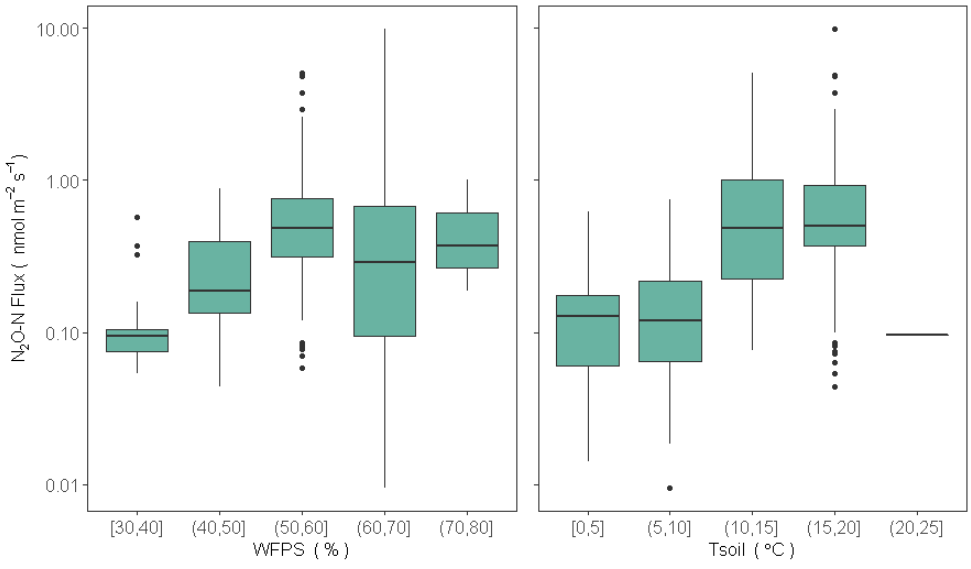

Figure B. 1: Boxplots of N_2O on a log scale against WFPS binned by 10 % groups (left) and soil temperature (Tsoil) binned by 10 % group. The boxplots shows the median with hinges on the 25 % and 75 % quantiles.

Table B. 2: Adjusted R^2 and p values from a linear regression analysis between normalized daily N_2O emissions and water filled pore space (WFPS), rainfall and soil temperature (Tsoil), where the symbol '*' indicates significance.

Date of grazing events	WFPS			rain			Tsoil		
	p value		Adj. R^2	p value		Adj. R^2	p value		Adj. R^2
04/02/2020 - 10/02/2020	0.02	*	0.66	0.00	*	0.85	0.02	*	0.63
03/03/2020 - 02/04/2020	0.02	*	0.20	0.05	*	0.14	0.01	*	0.29
10/04/2020 - 18/04/2020	0.02	*	0.58	0.73		-0.14	0.21		0.12
03/05/2020 - 10/05/2020	0.97		-0.25	0.55		-0.13	0.90		-0.24
25/05/2020 - 03/06/2020	0.08		0.25	0.00	*	0.67	0.51		-0.06
17/06/2020 - 24/06/2020	0.00	*	0.76	0.04	*	0.47	0.16		0.19
09/07/2020 - 18/07/2020	0.04	*	0.34	0.15		0.15	0.13		0.17
01/08/2020 -12/08/2020	0.75		-0.09	0.59		-0.07	0.92		-0.10
31/08/2020 - 21/09/2020	0.07		0.11	0.38		-0.01	0.17		0.05

Table B. 3: Model of a stepwise wise regression analysis for N_2O-N EFs measured from synthetic urine (independent of calcium ammonium nitrate) using cumulative rainfall and soil moisture deficit data measured in this study and combined with measurements made by Krol et al. (2016) and Maire et al. (2020)

Parameter	Estimate	Standard error	t Value	adj R^2
Intercept	2.21	0.17	13.03	-
Cumulative rainfall 3 days prior to application	-0.24	0.02	-10.27	0.13
Cumulative rainfall 3 days prior to application ^2	-0.16	0.02	-6.88	0.47
Mean soil moisture deficit 10 days prior to application	0.28	0.03	6.66	0.56
Mean soil moisture deficit 7 days prior to application	-0.06	0.01	-4.38	0.59
Mean soil moisture deficit 0 days prior to application	0.01	0	10.81	0.64

^2 = squared

Table B. 4: Soil ammonium (NH_4^+) and nitrate (NO_3^-) concentrations for four treatments (control, calcium ammonium nitrate [CAN], synthetic urine [SU]+CAN and dung+CAN) from four grazing events . Summary statistics include arithmetic mean and the standard deviation in brackets.

Grazing	Date	Control		CAN		SU+CAN		dung+CAN		Mean			
		NH_4^+	NO_3^-	NH_4^+	NO_3^-	NH_4^+	NO_3^-	NH_4^+	NO_3^-	NH_4^+		NO_3^-	
		mg N kg^{-1} soil								mg N kg^{-1} soil			
1	04/02/2020	5.2	9.3	9.2	9.2	8.2	9.3	13.0	10.2	8.9	[3.2]	9.5	[0.5]
	04/03/2020	4.9	3.3	5.3	4.0	82.9	2.3	6.4	2.8	24.9	[38.7]	3.1	[0.7]
	11/03/2020	3.6	2.3	3.5	3.2	117.5	18.7	9.8	4.3	33.6	[56.0]	7.1	[7.7]
	18/03/2020	2.9	2.6	3.9	3.7	90.9	37.8	12.4	4.9	27.5	[42.5]	12.3	[17.1]
	25/03/2020	2.3	2.4	3.6	4.4	30.2	70.6	18.7	8.1	13.7	[13.3]	21.4	[32.9]
	29/04/2020	4.3	1.4	5.2	3.8	4.4	42.7	7.0	6.0	5.2	[1.2]	13.5	[19.6]
	06/05/2020	4.1	1.7	4.4	3.7	5.6	37.2	4.9	5.0	4.8	[0.7]	11.9	[16.9]
2	29/04/2020	4.3	1.4	2.3	1.1	2.8	1.3	2.6	1.1	3.0	[0.9]	1.2	[0.1]
	06/05/2020	4.1	1.7	2.9	1.2	179.3	8.9	4.3	1.4	47.7	[87.8]	3.3	[3.7]
	13/05/2020	5.1	1.0	6.5	1.8	142.6	24.7	12.8	4.8	41.7	[67.3]	8.1	[11.2]
	19/05/2020	3.5	2.9	9.6	8.5	73.5	138.0	11.1	9.4	24.4	[32.9]	39.7	[65.6]
	27/05/2020	15.0	14.7	10.3	13.4	40.6	147.4	8.8	8.6	18.7	[14.9]	46.0	[67.6]
	03/06/2020	6.6	4.1	12.0	7.1	14.6	164.1	11.4	6.0	11.1	[3.3]	45.3	[79.2]
	10/06/2020	14.3	8.0	33.9	34.9	44.6	156.6	26.5	18.6	29.8	[12.7]	54.6	[68.9]
	17/06/2020	7.6	7.6	9.0	32.6	29.4	111.8	37.6	52.8	20.9	[14.9]	51.2	[44.4]
	25/06/2020	2.0	3.6	3.9	7.5	5.2	53.6	6.0	8.8	4.3	[1.7]	18.4	[23.6]
3	22/05/2020	9.5	10.6	2.5	0.7	3.0	1.2	2.0	0.4	4.3	[3.5]	3.2	[5.0]
	27/05/2020	15.0	14.7	3.8	1.1	113.6	9.1	3.1	0.8	33.9	[53.4]	6.4	[6.7]
	03/06/2020	6.6	4.1	4.3	1.8	85.2	33.9	6.2	2.7	25.6	[39.8]	10.6	[15.5]
	10/06/2020	14.3	8.0	36.2	37.1	37.9	50.7	12.4	9.7	25.2	[13.7]	26.4	[21.0]
	17/06/2020	7.6	7.6	1.8	19.2	4.9	62.7	2.8	12.3	4.3	[2.6]	25.4	[25.3]
	25/06/2020	2.0	3.6	2.3	2.5	3.7	19.7	2.7	2.7	2.7	[0.7]	7.1	[8.4]
	01/07/2020	4.1	6.6	14.3	16.4	15.9	27.4	11.4	9.4	11.4	[5.2]	14.9	[9.3]
	07/07/2020	5.4	6.5	5.5	6.9	10.3	46.1	6.9	5.7	7.0	[2.3]	16.3	[19.9]
	15/07/2020	6.3	6.4	6.3	7.0	7.8	31.1	7.4	5.3	7.0	[0.8]	12.5	[12.4]
4	27/08/2020	3.6	1.0	4.2	1.0	3.9	1.1	4.1	1.0	3.9	[0.3]	1.0	[0.0]
	02/09/2020	2.1	3.8	2.0	4.4	246.0	6.4	28.4	0.7	69.6	[118.2]	3.8	[2.4]
	09/09/2020	2.9	6.9	3.9	8.3	179.7	100.8	22.6	13.3	52.3	[85.4]	32.3	[45.7]
	15/09/2020	3.1	5.8	10.2	20.2	76.6	163.2	6.1	21.5	24.0	[35.2]	52.7	[74.0]
	21/09/2020	3.2	1.5	11.7	18.9	62.2	176.5	7.0	45.5	21.0	[27.7]	60.6	[79.3]
	30/09/2020	3.4	1.1	10.9	34.1	36.4	157.6	3.6	56.7	13.6	[15.6]	62.4	[67.5]
	06/10/2020	5.3	3.2	4.9	13.0	23.2	120.7	6.4	25.3	10.0	[8.8]	40.5	[54.2]
	14/10/2020	2.9	3.8	3.6	9.4	9.9	67.3	2.7	17.2	4.8	[3.5]	24.4	[29.1]
	21/10/2020	1.6	3.8	3.2	9.4	87.8	67.7	10.7	16.9	25.9	[41.5]	24.5	[29.3]

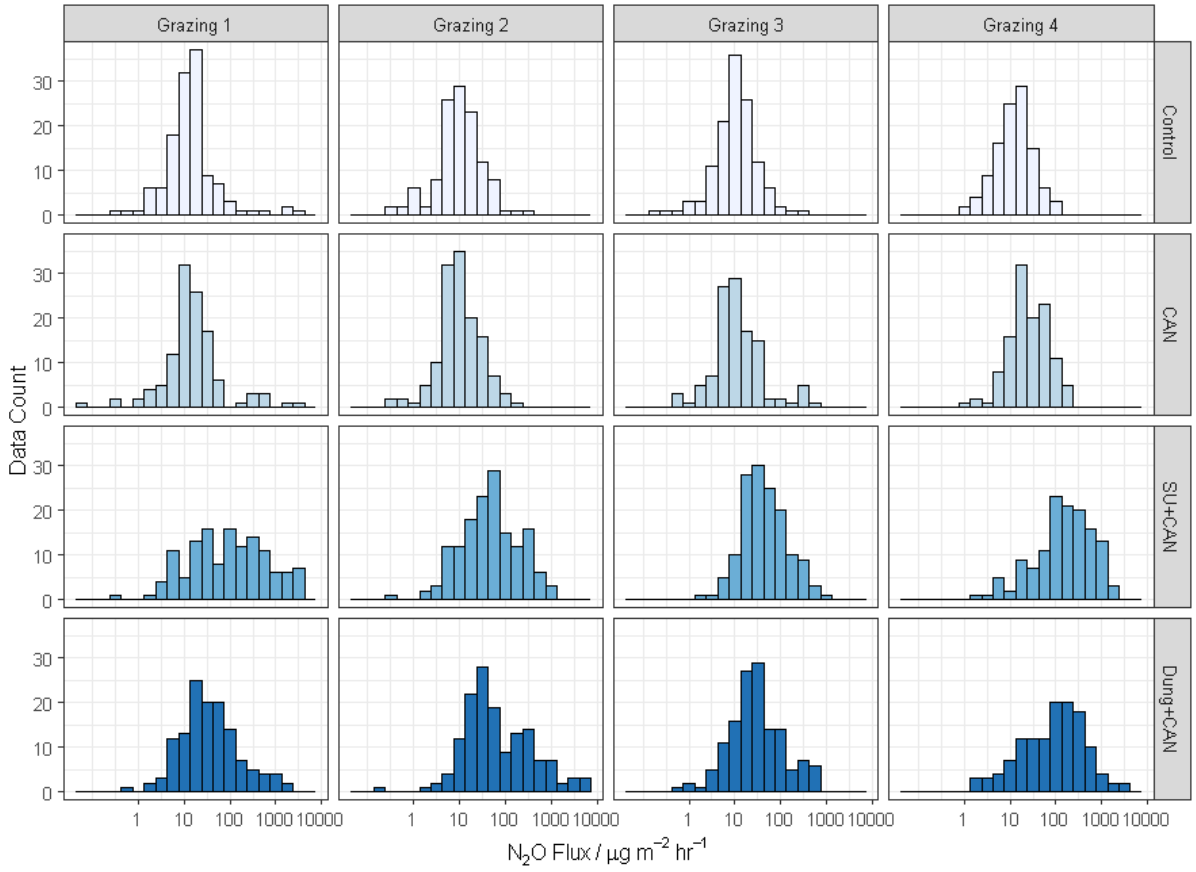

Figure B. 2: Frequency distribution of N_2O fluxes measured using the static chamber technique shown on a log-transformed axis but real values are on the axis. Columns represent fluxes from different grazing events (see Table 5.1 for dates) and rows represent four different treatments – control (i.e. no nitrogen applied), calcium ammonium nitrate (CAN), synthetic urine (SU)+CAN and dung+CAN.

APPENDIX C – Supplementary material for Chapter 6

Table C. 1: Components and uncertainties in brackets expressed using the least squares (LS) method of the net ecosystem exchange (NEE), methane (CH_4), nitrous oxide (N_2O), net greenhouse gas exchange (NGHGE), C exports from management (M_{ex}) and the net greenhouse gas balance (NGHGB) for the experimental site in 2019 and 2020.

Component	2019		2020	
	g CO_2eq m^{-2} yr^{-1}			
CO_2 (NEE)	-2010.8	[80.5]	-1355.3	[296.4]
CH_4	-	-	783.2	[18.3]
N_2O	140.1	[1.5]	275.6	[1.0]
NGHGE	-1870.7	[82.0]	-296.5	[315.7]
M_{ex}	1784.7	[9.9]	212.1	[3.7]
NGHGB	-86.0	[91.8]	-84.4	[319.4]

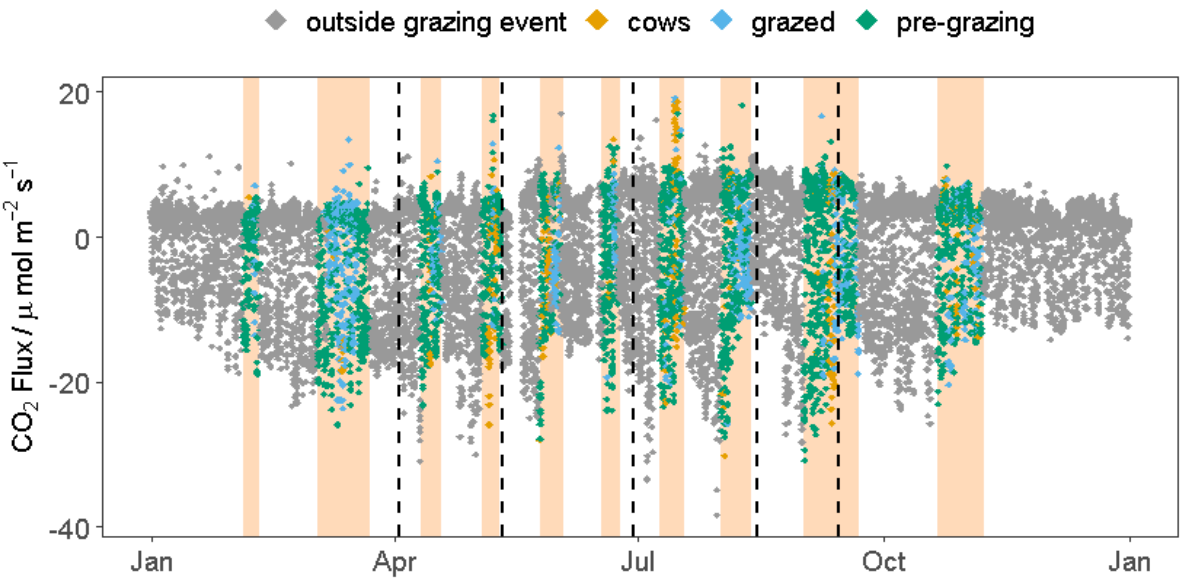

Figure C. 1: Half hourly gap-filled CO_2 fluxes measured in 2020 the peach backdrop represents individual grazing events (see table 6.1 for dates), where grey diamonds represent fluxes measured outside of individual grazing events, orange diamonds represent fluxes measured when cows were in the footprint, blue diamonds represent fluxes that were measured in previously grazed strips within an individual rotation grazing cycle, and green-diamonds represent fluxes that were measured from not grazed strips within an individual grazing event. The black dashed line marks the date of fertilizer application

References

ABALOS, D., BROWN, S. E., VANDERZAAG, A. C., GORDON, R. J., DUNFIELD, K. E. & WAGNER-RIDDLE, C. 2016. Micrometeorological measurements over 3 years reveal differences in N2O emissions between annual and perennial crops. *Global Change Biology,* 22**,** 1244-1255.

ABBASI, M. & ADAMS, W. 2000. Gaseous N emission during simultaneous nitrification–denitrification associated with mineral N fertilization to a grassland soil under field conditions. *Soil Biology and Biochemistry,* 32**,** 1251-1259.

ABDALLA, M., JONES, M., SMITH, P. & WILLIAMS, M. 2009a. Nitrous oxide fluxes and denitrification sensitivity to temperature in Irish pasture soils. *Soil Use and Management,* 25**,** 376-388.

ABDALLA, M., WATTENBACH, M., SMITH, P., AMBUS, P., JONES, M. & WILLIAMS, M. 2009b. Application of the DNDC model to predict emissions of N2O from Irish agriculture. *Geoderma,* 151**,** 327-337.

ADLER, A. A., DOOLE, G. J., ROMERA, A. J. & BEUKES, P. C. 2015. Managing greenhouse gas emissions in two major dairy regions of New Zealand: A system-level evaluation. *Agricultural Systems,* 135**,** 1-9.

ALAND, A., LIDFORS, L. & EKESBO, I. 2002. Diurnal distribution of dairy cow defecation and urination. *Applied Animal Behaviour Science,* 78**,** 43-54.

ALLARD, V., SOUSSANA, J.-F., FALCIMAGNE, R., BERBIGIER, P., BONNEFOND, J.-M., CESCHIA, E., D'HOUR, P., HÉNAULT, C., LAVILLE, P. & MARTIN, C. 2007. The role of grazing management for the net biome productivity and greenhouse gas budget (CO2, N2O and CH4) of semi-natural grassland. *Agriculture, Ecosystems & Environment,* 121**,** 47-58.

AMMANN, C., FLECHARD, C., LEIFELD, J., NEFTEL, A. & FUHRER, J. 2007. The carbon budget of newly established temperate grassland depends on management intensity. *Agriculture Ecosystems & Environment,* 121**,** 5-20.

AMMANN, C., SPIRIG, C., LEIFELD, J. & NEFTEL, A. 2009. Assessment of the nitrogen and carbon budget of two managed temperate grassland fields. *Agriculture, Ecosystems & Environment,* 133**,** 150-162.

AON 2020. Weather, Climate and Catastrophe Insight 2020 Annual Report. Chicago.

ARORA, N. K. 2019. Impact of climate change on agriculture production and its sustainable solutions. Springer.

ASHEKUZZAMAN, S., FORRESTAL, P., RICHARDS, K. & FENTON, O. 2019. Dairy industry derived wastewater treatment sludge: Generation, type and characterization of nutrients and metals for agricultural reuse. *Journal of Cleaner Production,* 230**,** 1266-1275.

ASKEW, E. 2012. Inorganic nonmetallic constituents; Method 4500-NO 3-H. Automated Hydrazine Reduction Method, 4-128. *Standard Methods for the Examination of Waters and Waste Water,* 22.

ATKIN, O. K., BRUHN, D. & TJOELKER, M. G. 2005. Response of plant respiration to changes in temperature: mechanisms and consequences of variations in Q 10 values and acclimation. *Plant respiration*. Springer.

AUERSWALD, K., MAYER, F. & SCHNYDER, H. 2010. Coupling of spatial and temporal pattern of cattle excreta patches on a low intensity pasture. *Nutrient Cycling in Agroecosystems,* 88**,** 275-288.

AUGUSTINE, D. J., MCNAUGHTON, S. J. & FRANK, D. A. 2003. Feedbacks between soil nutrients and large herbivores in a managed savanna ecosystem. *Ecological Applications,* 13**,** 1325-1337.

BAIN, W. G., HUTYRA, L., PATTERSON, D. C., BRIGHT, A. V., DAUBE, B. C., MUNGER, J. W. & WOFSY, S. C. 2005. Wind-induced error in the measurement of soil respiration using closed dynamic chambers. *Agricultural and Forest meteorology,* 131**,** 225-232.

BARDGETT, R. D. & WARDLE, D. A. 2003. Herbivore-mediated linkages between aboveground and belowground communities. *Ecology,* 84**,** 2258-2268.

BARTON, L., WOLF, B., ROWLINGS, D., SCHEER, C., KIESE, R., GRACE, P., STEFANOVA, K. & BUTTERBACH-BAHL, K. 2015. Sampling frequency affects estimates of annual nitrous oxide fluxes. *Scientific reports,* 5**,** 1-9.

BATES, G., QUIN, B. & BISHOP, P. 2015. Low-cost detection and treatment of fresh cow urine patches. *Moving farm systems to improved attenuation, edited by: Currie, LD and Burkitt, LL,* 28**,** 12.

BELL, M., REES, R., CLOY, J., TOPP, C., BAGNALL, A. & CHADWICK, D. 2015. Nitrous oxide emissions from cattle excreta applied to a Scottish grassland: Effects of soil and climatic conditions and a nitrification inhibitor. *Science of the Total Environment,* 508**,** 343-353.

BEREITER, B., EGGLESTON, S., SCHMITT, J., NEHRBASS-AHLES, C., STOCKER, T. F., FISCHER, H., KIPFSTUHL, S. & CHAPPELLAZ, J. 2015. Revision of the EPICA Dome C CO2 record from 800 to 600 kyr before present. *Geophysical Research Letters,* 42**,** 542-549.

BERTORA, C., PEYRON, M., PELISSETTI, S., GRIGNANI, C. & SACCO, D. 2018. Assessment of methane and nitrous oxide fluxes from paddy field by means of static closed chambers maintaining plants within headspace. *Journal of visualized experiments: JoVE*.

BETTERIDGE, K., HOOGENDOORN, C., COSTALL, D., CARTER, M. & GRIFFITHS, W. 2010. Sensors for detecting and logging spatial distribution of urine patches of grazing female sheep and cattle. *Computers and Electronics in Agriculture,* 73**,** 66-73.

BORING, L. R., SWANK, W. T., WAIDE, J. B. & HENDERSON, G. S. 1988. Sources, Fates, and Impacts of Nitrogen Inputs to Terrestrial Ecosystems: Review and Synthesis. *Biogeochemistry,* 6**,** 119-159.

BOX, L. A., EDWARDS, G. R. & BRYANT, R. H. 2017. Milk production and urinary nitrogen excretion of dairy cows grazing plantain in early and late lactation. *New Zealand Journal of Agricultural Research,* 60**,** 470-482.

BRAKER, G., SCHWARZ, J. & CONRAD, R. 2010. Influence of temperature on the composition and activity of denitrifying soil communities. *FEMS Microbiology Ecology,* 73**,** 134-148.

BREMNER, J., BLACKMER, A. & WARING, S. 1980. Formation of nitrous oxide and dinitrogen by chemical decomposition of hydroxylamine in soils. *Soil Biology and Biochemistry,* 12**,** 263-269.

BREMNER, J. M. 1997. Sources of nitrous oxide in soils. *Nutrient cycling in Agroecosystems,* 49**,** 7-16.

BRETSCHER, D. 2013. Agricultural CH4 and N2O emissions Switzerland. *Agroscope Reckenholz Tanikon Research Station (ART) DFE*.

BUCKTHOUGHT, L. E., CLOUGH, T. J., CAMERON, K. C., DI, H. J. & SHEPHERD, M. A. 2015. Fertiliser and seasonal urine effects on N2O emissions from the urine-fertiliser interface of a grazed pasture. *New Zealand Journal of Agricultural Research,* 58**,** 311-324.

BUENDIA, E., TANABE, K., KRANJC, A., BAASANSUREN, J., FUKUDA, M., NGARIZE, S., OSAKO, A., PYROZHENKO, Y., SHERMANAU, P. & FEDERICI, S. 2019. refinement to the 2006 IPCC guidelines for national greenhouse gas inventories. *IPCC: Geneva, Switzerland*.

BUFFAM, I. & MITCHELL, M. E. 2015. Nutrient cycling in green roof ecosystems. *Green roof ecosystems.* Springer.

BURBA, G. & ANDERSON, D. 2010. *A brief practical guide to eddy covariance flux measurements: principles and workflow examples for scientific and industrial applications* , Li-Cor Biosciences.

BUTTERBACH-BAHL, K., BAGGS, E. M., DANNENMANN, M., KIESE, R. & ZECHMEISTER-BOLTENSTERN, S. 2013. Nitrous oxide emissions from soils: how well do we understand the processes and their controls? *Philosophical Transactions of the Royal Society B: Biological Sciences,* 368**,** 20130122.

BUTTERBACH-BAHL, K. & DANNENMANN, M. 2011. Denitrification and associated soil N2O emissions due to agricultural activities in a changing climate. *Current Opinion in Environmental Sustainability,* 3**,** 389-395.

BYRNE, K. A., KIELY, G. & LEAHY, P. 2007. Carbon sequestration determined using farm scale carbon balance and eddy covariance. *Agriculture, Ecosystems & Environment,* 121**,** 357-364.

BYRNES, R. C., NÙÑEZ, J., ARENAS, L., RAO, I., TRUJILLO, C., ALVAREZ, C., ARANGO, J., RASCHE, F. & CHIRINDA, N. 2017. Biological nitrification inhibition by Brachiaria grasses mitigates soil nitrous oxide emissions from bovine urine patches. *Soil Biology and Biochemistry,* 107**,** 156-163.

CAI, T., FLANAGAN, L. B. & SYED, K. H. 2010. Warmer and drier conditions stimulate respiration more than photosynthesis in a boreal peatland ecosystem: analysis of automatic chambers and eddy covariance measurements. *Plant, cell & environment,* 33**,** 394-407.

CAMERON, K. C., DI, H. J. & MOIR, J. L. 2013. Nitrogen losses from the soil/plant system: a review. *Annals of applied biology,* 162**,** 145-173.

CAMPIOLI, M., MALHI, Y., VICCA, S., LUYSSAERT, S., PAPALE, D., PEÑUELAS, J., REICHSTEIN, M., MIGLIAVACCA, M., ARAIN, M. A. & JANSSENS, I. A. 2016. Evaluating the convergence between eddy-covariance and biometric methods for assessing carbon budgets of forests. *Nature Communications,* 7**,** 13717.

CAO, G., TANG, Y., MO, W., WANG, Y., LI, Y. & ZHAO, X. 2004. Grazing intensity alters soil respiration in an alpine meadow on the Tibetan plateau. *Soil Biology and Biochemistry,* 36**,** 237-243.

CARBO, L. 2016. *EMEP/EEA air pollutant emission inventory guidebook 2016*.

CARDENAS, L., BHOGAL, A., CHADWICK, D., MCGEOUGH, K., MISSELBROOK, T., REES, R., THORMAN, R., WATSON, C. J., WILLIAMS, J. & SMITH, K. 2019. Nitrogen use efficiency and nitrous oxide emissions from five UK fertilised grasslands. *Science of the Total Environment,* 661**,** 696-710.

CARLSON, K. M., GERBER, J. S., MUELLER, N. D., HERRERO, M., MACDONALD, G. K., BRAUMAN, K. A., HAVLIK, P., O'CONNELL, C. S., JOHNSON, J. A. & SAATCHI, S. 2017. Greenhouse gas emissions intensity of global croplands. *Nature Climate Change,* 7**,** 63-68.

CARLTON, A., CAMERON, K., DI, H., CLOUGH, T. & EDWARDS, G. 2018. Nitrate leaching losses are lower from diverse forages containing plantain than from standard forages under different irrigation. *New Zealand Journal of Agricultural Research. doi,* 10**,** 1461659.

CARPINELLI, S., DA FONSECA, A. F., WEIRICH NETO, P. H., DIAS, S. H. B. & PONTES, L. D. S. 2020. Spatial and Temporal Distribution of Cattle Dung and Nutrient Cycling in Integrated Crop–Livestock Systems. *Agronomy,* 10**,** 672.

CARTER, M., ANGERS, D., GREGORICH, E. & BOLINDER, M. 1997. Organic carbon and nitrogen stocks and storage profiles in cool, humid soils of eastern Canada. *Canadian Journal of Soil Science,* 77**,** 205-210.

CARULLA, J., KREUZER, M., MACHMÜLLER, A. & HESS, H. 2005. Supplementation of Acacia mearnsii tannins decreases methanogenesis and urinary nitrogen in forage-fed sheep. *Australian journal of agricultural research,* 56**,** 961-970.

CAYUELA, M., VAN ZWIETEN, L., SINGH, B., JEFFERY, S., ROIG, A. & SÁNCHEZ-MONEDERO, M. 2014. Biochar's role in mitigating soil nitrous oxide emissions: A review and meta-analysis. *Agriculture, Ecosystems & Environment,* 191**,** 5-16.

CHADWICK, D., CARDENAS, L., DHANOA, M., DONOVAN, N., MISSELBROOK, T., WILLIAMS, J., THORMAN, R., MCGEOUGH, K., WATSON, C. & BELL, M. 2018. The contribution of cattle urine and dung to nitrous oxide emissions: Quantification of country specific emission factors and implications for national inventories. *Science of the Total Environment,* 635**,** 607-617.

CHADWICK, D., CARDENAS, L., MISSELBROOK, T., SMITH, K., REES, R., WATSON, C., MCGEOUGH, K., WILLIAMS, J., CLOY, J. & THORMAN, R. 2014. Optimizing chamber methods for measuring nitrous oxide emissions from plot-based agricultural experiments. *European Journal of Soil Science,* 65**,** 295-307.

CHANG, J., CIAIS, P., GASSER, T., SMITH, P., HERRERO, M., HAVLÍK, P., OBERSTEINER, M., GUENET, B., GOLL, D. S. & LI, W. 2021. Climate warming from managed grasslands cancels the cooling effect of carbon sinks in sparsely grazed and natural grasslands. *Nature communications,* 12**,** 1-10.

CHANG, J., CIAIS, P., VIOVY, N., VUICHARD, N., SULTAN, B. & SOUSSANA, J. F. 2015. The greenhouse gas balance of European grasslands. *Global change biology,* 21**,** 3748-3761.

CHARTERIS, A. F., CHADWICK, D. R., THORMAN, R. E., VALLEJO, A., DE KLEIN, C. A., ROCHETTE, P. & CÁRDENAS, L. M. 2020a. Global Research Alliance N2O chamber methodology guidelines: Recommendations for deployment and accounting for sources of variability. *Journal of Environmental Quality,* 49**,** 1092-1109.

CHARTERIS, A. F., CHADWICK, D. R., THORMAN, R. E., VALLEJO, A., DE KLEIN, C. A. M., ROCHETTE, P. & CÁRDENAS, L. M. 2020b. Global Research Alliance N2O chamber methodology guidelines: Recommendations for deployment and accounting for sources of variability. *Journal of Environmental Quality,* 49**,** 1092-1109.

CHEN, H., WILLIAMS, D., WALKER, J. T. & SHI, W. 2016. Probing the biological sources of soil N2O emissions by quantum cascade laser-based 15N isotopocule analysis. *Soil Biology and Biochemistry,* 100**,** 175-181.

CHEN, W., HUANG, D., LIU, N., ZHANG, Y., BADGERY, W. B., WANG, X. & SHEN, Y. 2015. Improved grazing management may increase soil carbon sequestration in temperate steppe. *Scientific reports,* 5**,** 1-13.

CHEN, W., MCCAUGHEY, W. P. & GRANT, C. A. 2004. Pasture type and fertilization effects on N2 fixation, N budgets and external energy inputs in western Canada. *Soil Biology and Biochemistry,* 36**,** 1205-1212.

CHENG, L., MCCORMICK, J., HUSSEIN, A. N., LOGAN, C., PACHECO, D., HODGE, M. & EDWARDS, G. 2017. Live weight gain, urinary nitrogen excretion and urination behaviour of dairy heifers grazing pasture, chicory and plantain. *The Journal of Agricultural Science,* 155**,** 669-678.

CHOUDHARY, M., AKRAMKHANOV, A. & SAGGAR, S. 2002. Nitrous oxide emissions from a New Zealand cropped soil: tillage effects, spatial and seasonal variability. *Agriculture, Ecosystems & Environment,* 93**,** 33-43.

CHRISTENSEN, S., AMBUS, P., ARAH, J., CLAYTON, H., GALLE, B., GRIFFITH, D., HARGREAVES, K., KLENZEDTSSON, L., LIND, A.-M. & MAAG, M. 1996. Nitrous oxide emission from an agricultural field: Comparison between measurements by flux chamber and micrometerological techniques. *Atmospheric Environment,* 30**,** 4183-4190.

CIAIS, P., SABINE, C., BALA, G., BOPP, L., BROVKIN, V., CANADELL, J., CHHABRA, A., DEFRIES, R., GALLOWAY, J. & HEIMANN, M. 2014. Carbon and other biogeochemical cycles. *Climate change 2013: the physical science basis. Contribution of Working Group I to the Fifth Assessment Report of the Intergovernmental Panel on Climate Change.* Cambridge University Press.

CICHOTA, R., SNOW, V. O. & VOGELER, I. 2013. Modelling nitrogen leaching from overlapping urine patches. *Environmental Modelling & Software,* 41**,** 15-26.

CLAGNAN, E., THORNTON, S., ROLFE, S., WELLS, N., KNOELLER, K. & FENTON, O. 2018. Investigating "net" provenance, N source, transformation and fate within hydrologically isolated grassland plots. *Agricultural water management,* 203**,** 1-8.

CLOUGH, T. J., ROCHETTE, P., THOMAS, S. M., PIHLATIE, M., CHRISTIANSEN, J. R. & THORMAN, R. E. 2020. Global Research Alliance N2O chamber methodology guidelines: Design considerations. *Journal of Environmental Quality,* 49**,** 1081-1091.

COLLIER, S. M., RUARK, M. D., OATES, L. G., JOKELA, W. E. & DELL, C. J. 2014. Measurement of greenhouse gas flux from agricultural soils using static chambers. *Journal of visualized experiments: JoVE*.

CONGREVES, K. A., PHAN, T. & FARRELL, R. E. 2019. A new look at an old concept: using 15 N 2 O isotopomers to understand the relationship between soil moisture and N 2 O production pathways. *Soil,* 5**,** 265-274.

COURTOIS, E. A., STAHL, C., BURBAN, B., BERGE, J. V. D., BERVEILLER, D., BRÉCHET, L., SOONG, J. L., ARRIGA, N., PEÑUELAS, J. & JANSSENS, I. A. 2019. Automatic high-frequency measurements of full soil greenhouse gas fluxes in a tropical forest. *Biogeosciences,* 16**,** 785-796.

COWAN, N., FAMULARI, D., LEVY, P., ANDERSON, M., BELL, M., REES, R., REAY, D. & SKIBA, U. 2014. An improved method for measuring soil N2O fluxes using a quantum cascade laser with a dynamic chamber. *European journal of soil science,* 65**,** 643-652.

COWAN, N., LEVY, P., DREWER, J., CARSWELL, A., SHAW, R., SIMMONS, I., BACHE, C., MARINHEIRO, J., BRICHET, J. & SANCHEZ-RODRIGUEZ, A. 2019. Application of Bayesian statistics to estimate nitrous oxide emission factors of three nitrogen fertilisers on UK grasslands. *Environment international,* 128**,** 362-370.

COWAN, N., LEVY, P., FAMULARI, D., ANDERSON, M., REAY, D. & SKIBA, U. 2017. Nitrous oxide emission sources from a mixed livestock farm. *Agriculture, Ecosystems & Environment,* 243**,** 92-102.

COWAN, N., LEVY, P., MAIRE, J., COYLE, M., LEESON, S., FAMULARI, D., CAROZZI, M., NEMITZ, E. & SKIBA, U. 2020. An evaluation of four years of nitrous oxide fluxes after application of ammonium nitrate and urea fertilisers measured using the eddy covariance method. *Agricultural and Forest Meteorology,* 280**,** 107812.

COWAN, N., MAIRE, J., KROL, D., CLOY, J. M., HARGREAVES, P., MURPHY, R., CARSWELL, A., JONES, S. K., HINTON, N. & ANDERSON, M. 2021. Agricultural soils: A sink or source of methane across the British Isles? *European Journal of Soil Science,* 72**,** 1842-1862.

COWAN, N., NORMAN, P., FAMULARI, D., LEVY, P., REAY, D. & SKIBA, U. 2015. Spatial variability and hotspots of soil N 2 O fluxes from intensively grazed grassland. *Biogeosciences,* 12**,** 1585-1596.

COWAN, N. J., LEVY, P. E., FAMULARI, D., ANDERSON, M., DREWER, J., CAROZZI, M., REAY, D. S. & SKIBA, U. M. 2016. The influence of tillage on N_2O fluxes from an intensively managed grazed grassland in Scotland. *Biogeosciences,* 13**,** 4811-4821.

CRUTZEN, P. J., ASELMANN, I. & SEILER, W. 1986. Methane production by domestic animals, wild ruminants, other herbivorous fauna, and humans. *Tellus B: Chemical and Physical Meteorology,* 38**,** 271-284.

CSO. 2020. *Environmental Indicators Ireland 2020* [Online]. Available: https://www.cso.ie/en/releasesandpublications/ep/p-eii/environmentalindicatorsireland2020/landuse/ [Accessed 31/05 2021].

CULMAN, S. W., PUGLIESE, J., DEHAAN, L., CREWS, T., SULC, R., RYAN, M., JUNGERS, J., MAUL, J., SCHIPANSKI, M. & SHEAFFER, C. Can the perennial grain crop Kernza yield both forage and grain? American Society of Agronomy meeting, 2016.

CUMMINS, S., FINN, J. A., RICHARDS, K. G., LANIGAN, G. J., GRANGE, G., BROPHY, C., CARDENAS, L. M., MISSELBROOK, T. H., REYNOLDS, C. K. & KROL, D. J. 2021. Beneficial effects of multi-species mixtures on N2O emissions from intensively managed grassland swards. *Science of The Total Environment,* 792**,** 148163.

CURL, R. F., CAPASSO, F., GMACHL, C., KOSTEREV, A. A., MCMANUS, B., LEWICKI, R., PUSHARSKY, M., WYSOCKI, G. & TITTEL, F. K. 2010. Quantum cascade lasers in chemical physics. *Chemical Physics Letters,* 487**,** 1-18.

DA SILVA, F. D., NUNES, P. A. D. A., BREDEMEIER, C., CADENAZZI, M., AMARAL, L. P., PFEIFER, F. M., ANGHINONI, I. & CARVALHO, P. 2020. F. Spatiotemporal distribution of cattle dung

patches in a subtropical soybean-beef system under different grazing intensities in winter. *AGRONOMY-BASEL,* 10.
DAFM 2015. Information on LULUCF actions to limit or reduce emissions and maintain or increase removals from activities defined under Decision 529/2013/EU.
DALLEY, D. E., MALCOLM, B. J., CHAKWIZIRA, E. & DE RUITER, J. M. 2017. Range of quality characteristics of New Zealand forages and implications for reducing the nitrogen leaching risk from grazing dairy cows. *New Zealand Journal of Agricultural Research,* 60**,** 319-332.
DANGAL, S. R., TIAN, H., PAN, S., ZHANG, L. & XU, R. 2020. Greenhouse gas balance in global pasturelands and rangelands. *Environmental Research Letters,* 15**,** 104006.
DAVIDSON, E., SAVAGE, K., VERCHOT, L. & NAVARRO, R. 2002. Minimizing artifacts and biases in chamber-based measurements of soil respiration. *Agricultural and Forest Meteorology,* 113**,** 21-37.
DAVIDSON, E. A. 1991. Fluxes of nitrous oxide and nitric oxide from terrestrial ecosystems. *Microbial production and consumption of greenhouse gases: methane, nitrogen oxides, and halomethanes.***,** 219-235.
DAVIDSON, E. A. 2009. The contribution of manure and fertilizer nitrogen to atmospheric nitrous oxide since 1860. *Nature Geoscience,* 2**,** 659-662.
DAVIDSON, E. A., KELLER, M., ERICKSON, H. E., VERCHOT, L. V. & VELDKAMP, E. 2000. Testing a conceptual model of soil emissions of nitrous and nitric oxides: using two functions based on soil nitrogen availability and soil water content, the hole-in-the-pipe model characterizes a large fraction of the observed variation of nitric oxide and nitrous oxide emissions from soils. *Bioscience,* 50**,** 667-680.
DE KLEIN, C., ECKARD, R. & VAN DER WEERDEN, T. 2010. Nitrous oxide emissions from the nitrogen cycle in livestock agriculture: estimation and mitigation. *Nitrous oxide and climate change***,** 107-144.
DE KLEIN, C. & HARVEY, M. 2015. Nitrous oxide chamber methodology and guidelines. Ministry for Primary Industry, Wellington, New Zealand.
DE KLEIN, C. A., BARTON, L., SHERLOCK, R. R., LI, Z. & LITTLEJOHN, R. P. 2003. Estimating a nitrous oxide emission factor for animal urine from some New Zealand pastoral soils. *Soil Research,* 41**,** 381-399.
DE KLEIN, C. A., HARVEY, M. J., CLOUGH, T. J., PETERSEN, S. O., CHADWICK, D. R. & VENTEREA, R. T. 2020a. Global Research Alliance N2O chamber methodology guidelines: Introduction, with health and safety considerations. *Journal of Environmental Quality,* 49**,** 1073-1080.
DE KLEIN, C. A., VAN DER WEERDEN, T. J., LUO, J., CAMERON, K. C. & DI, H. J. 2020b. A review of plant options for mitigating nitrous oxide emissions from pasture-based systems. *New Zealand Journal of Agricultural Research,* 63**,** 29-43.
DENEF, K., DEL GALDO, I., VENTURI, A. & COTRUFO, M. F. 2013. Assessment of soil C and N stocks and fractions across 11 European soils under varying land uses. *Open Journal of Soil Science,* 3**,** 297-313.
DENNIS, S., MOIR, J. L., CAMERON, K., DI, H., HENNESSY, D. & RICHARDS, K. G. 2011. Urine patch distribution under dairy grazing at three stocking rates in Ireland. *Irish Journal of Agricultural and Food Research***,** 149-160.
DEPARTMENT OF HOUSING LOCAL GOVERNMENT AND HERITAGE. 2021. *Nitrates Directive* [Online]. Available: https://www.gov.ie/en/publication/b87ad-nitrates-directive/#the-slurry-spreading-calendar [Accessed 07/09/2021].
DILLON, E., HENESSY, T., MORAN, B. & LENNON, T. 2019. Teagasc National Farm Survey 2018 Results; Teagasc. *Agricultural Economics and Farm Surveys Department: Dublin, Ireland*.
DOBBIE, K. E. & SMITH, K. A. 2003. Impact of different forms of N fertilizer on N 2 O emissions from intensive grassland. *Nutrient cycling in Agroecosystems,* 67**,** 37-46.

DORICH, C. D., DE ROSA, D., BARTON, L., GRACE, P., ROWLINGS, D., MIGLIORATI, M. D. A., WAGNER-RIDDLE, C., KEY, C., WANG, D. & FEHR, B. 2020. Global Research Alliance N2O chamber methodology guidelines: Guidelines for gap-filling missing measurements. *Journal of Environmental Quality,* 49**,** 1186-1202.

DUFFY, P., BLACK, K., FAHEY, D., HYDE, B., KEHOE, A., MURPHY, J., QUIRKE, B., RYAN, A. M. & PONZI, J. 2021. IRELAND NATIONAL INVENTORY REPORT 2021 GREENHOUSE GAS EMISSIONS 1990 - 2019 REPORTED TO THE UNITED NATIONS FRAMEWORK CONVENTION ON CLIMATE CHANGE.

EGGLESTON, S., BUENDIA, L., MIWA, K., NGARA, T. & TANABE, K. 2006. IPCC guidelines for national greenhouse gas inventories.

EHHALT, D., PRATHER, M., DENTENER, F., DERWENT, R., DLUGOKENCKY, E. J., HOLLAND, E., ISAKSEN, I., KATIMA, J., KIRCHHOFF, V. & MATSON, P. 2001. Atmospheric chemistry and greenhouse gases. Pacific Northwest National Lab.(PNNL), Richland, WA (United States).

EPA. 2019a. *Latest emissions data* [Online]. Available: https://www.epa.ie/our-services/monitoring--assessment/climate-change/ghg/latest-emissions-data/# [Accessed 05/07/2021].

EPA. 2019b. *Summary by gas* [Online]. Available: https://www.epa.ie/our-services/monitoring--assessment/climate-change/ghg/summary-by-gas/#d.en.84384 [Accessed 05/07/2021].

EPA. 2020. *Understanding Global Warming Potentials* [Online]. Available: https://www.epa.gov/ghgemissions/understanding-global-warming-potentials [Accessed 19/08/2021].

FAGERIA, N. K. & BALIGAR, V. 2005. Enhancing nitrogen use efficiency in crop plants. *Advances in agronomy,* 88**,** 97-185.

FALGE, E., BALDOCCHI, D., OLSON, R., ANTHONI, P., AUBINET, M., BERNHOFER, C., BURBA, G., CEULEMANS, R., CLEMENT, R. & DOLMAN, H. 2001. Gap filling strategies for defensible annual sums of net ecosystem exchange. *Agricultural and forest meteorology,* 107**,** 43-69.

FAOSTAT. 2021. *Data* [Online]. Available: http://www.fao.org/faostat/en/#home [Accessed 18/08/2021].

FATICHI, S., LEUZINGER, S., PASCHALIS, A., LANGLEY, J. A., DONNELLAN BARRACLOUGH, A. & HOVENDEN, M. J. 2016. Partitioning direct and indirect effects reveals the response of water-limited ecosystems to elevated CO₂. *Proceedings of the National Academy of Sciences,* 113**,** 12757-12762.

FELBER, R., BRETSCHER, D., MÜNGER, A., NEFTEL, A. & AMMANN, C. 2016. Determination of the carbon budget of a pasture: effect of system boundaries and flux uncertainties. *Biogeosciences,* 13**,** 2959-2969.

FELBER, R., MÜNGER, A., NEFTEL, A. & AMMANN, C. 2015. Eddy covariance methane flux measurements over a grazed pasture: effect of cows as moving point sources. *Biogeosciences,* 12**,** 3925-3940.

FINKELSTEIN, P. L. & SIMS, P. F. 2001. Sampling error in eddy correlation flux measurements. *Journal of Geophysical Research: Atmospheres,* 106**,** 3503-3509.

FIRESTONE, M. & DAVIDSON, E. 1989. Microbiological basis of NO and N 2 O production and consumption in soil. *Exchange of trace gases between terrestrial ecosystems and the atmosphere,* 47**,** 7-21.

FISCHER, K., BURCHILL, W., LANIGAN, G., KAUPENJOHANN, M., CHAMBERS, B., RICHARDS, K. G. & FORRESTAL, P. J. 2016. Ammonia emissions from cattle dung, urine and urine with dicyandiamide in a temperate grassland. *Soil Use and Management,* 32**,** 83-91.

FLECHARD, C., AMBUS, P., SKIBA, U., REES, R., HENSEN, A., VAN AMSTEL, A., VAN DEN POL-VAN DASSELAAR, A., SOUSSANA, J.-F., JONES, M. & CLIFTON-BROWN, J. 2007. Effects of climate and management intensity on nitrous oxide emissions in grassland systems across Europe. *Agriculture, Ecosystems & Environment,* 121**,** 135-152.

FLESSA, H., DÖRSCH, P., BEESE, F., KÖNIG, H. & BOUWMAN, A. 1996. Influence of cattle wastes on nitrous oxide and methane fluxes in pasture land. Wiley Online Library.
FLESSA, H., RUSER, R., DÖRSCH, P., KAMP, T., JIMENEZ, M., MUNCH, J. & BEESE, F. 2002. Integrated evaluation of greenhouse gas emissions (CO2, CH4, N2O) from two farming systems in southern Germany. *Agriculture, Ecosystems & Environment,* 91**,** 175-189.
FLUXNET. 2021. *About the FLUXNET Network* [Online]. Available: https://fluxnet.org/about/ [Accessed 04/08/2021].
FOKEN, T. 2003. Mikrometeorologische Methoden.
FOLLETT, J. R. & FOLLETT, R. F. 2001. Utilization and metabolism of nitrogen by humans. *Nitrogen in the environment: Sources, problems and management.* Elsevier.
FONTAN, O., BERRY, A., FERRAT, M., PORTALIER, J., TAMOKOUE KAMGA, P.-H. & AMALOU, C. 2019. High Council on Climate. Acting in line with ambitions-Annual Carbon Neutrality report, June 2019, First annual report of the High Council on Climate of France+general public version+The recommendations of the 2019 report.
FORRESTAL, P. J., KROL, D. J., LANIGAN, G., JAHANGIR, M. M. & RICHARDS, K. G. 2017. An evaluation of urine patch simulation methods for nitrous oxide emission measurement. *The Journal of Agricultural Science,* 155**,** 725-732.
FRATINI, G., IBROM, A., ARRIGA, N., BURBA, G. & PAPALE, D. 2012. Relative humidity effects on water vapour fluxes measured with closed-path eddy-covariance systems with short sampling lines. *Agricultural and Forest Meteorology,* 165**,** 53-63.
FUCHS, K., HÖRTNAGL, L., BUCHMANN, N., EUGSTER, W., SNOW, V. & MERBOLD, L. 2018. Management matters: testing a mitigation strategy for nitrous oxide emissions using legumes on intensively managed grassland. *Biogeosciences,* 15**,** 5519-5543.
GALLOWAY, J. & COWLING, E. 2002. Reactive Nitrogen and The World: 200 Years of Change. *Ambio,* 31**,** 64-71.
GALLOWAY, J. N., ABER, J. D., ERISMAN, J. W., SEITZINGER, S. P., HOWARTH, R. W., COWLING, E. B. & COSBY, B. J. 2003. The nitrogen cascade. *Bioscience,* 53**,** 341-356.
GALLOWAY, J. N., TOWNSEND, A. R., ERISMAN, J. W., BEKUNDA, M., CAI, Z., FRENEY, J. R., MARTINELLI, L. A., SEITZINGER, S. P. & SUTTON, M. A. 2008. Transformation of the nitrogen cycle: recent trends, questions, and potential solutions. *Science,* 320**,** 889-892.
GAO, Y., HE, N. & ZHANG, X. 2014. Effects of reactive nitrogen deposition on terrestrial and aquatic ecosystems. *Ecological Engineering,* 70**,** 312-318.
GELFAND, I., ABRAHA, M., PAN, D., TANG, J., CHEN, J., ZONDLO, M. A. & ROBERTSON, G. P. Evaluation of field based quantum cascade lasers for measuring N2O fluxes from static chambers and eddy covariance towers. EGU General Assembly Conference Abstracts, 2018. 2530.
GHALY, A. & RAMAKRISHNAN, V. 2015. Nitrogen sources and cycling in the ecosystem and its role in air, water and soil pollution: A critical review. *Journal of Pollution Effects & Control***,** 1-26.
GILTRAP, D., YELURIPATI, J., SMITH, P., FITTON, N., SMITH, W., GRANT, B., DORICH, C. D., DENG, J., TOPP, C. F. & ABDALLA, M. 2020. Global Research Alliance N2O chamber methodology guidelines: Summary of modeling approaches. *Journal of Environmental Quality,* 49**,** 1168-1185.
GIRAUD, M., GROH, J., GERKE, H. H., BRÜGGEMANN, N., VEREECKEN, H. & PÜTZ, T. 2021. Soil Nitrogen Dynamics in a Managed Temperate Grassland Under Changed Climatic Conditions. *Water,* 13**,** 931.
GITELSON, A. A., PENG, Y., ARKEBAUER, T. J. & SCHEPERS, J. 2014. Relationships between gross primary production, green LAI, and canopy chlorophyll content in maize: Implications for remote sensing of primary production. *Remote Sensing of Environment,* 144**,** 65-72.

GOODRICH, J., WALL, A., CAMPBELL, D., FLETCHER, D., WECKING, A. & SCHIPPER, L. 2021. Improved gap filling approach and uncertainty estimation for eddy covariance N2O fluxes. *Agricultural and Forest Meteorology,* 297**,** 108280.

GROFFMAN, P. M., BRUMME, R., BUTTERBACH-BAHL, K., DOBBIE, K. E., MOSIER, A. R., OJIMA, D., PAPEN, H., PARTON, W. J., SMITH, K. A. & WAGNER-RIDDLE, C. 2000. Evaluating annual nitrous oxide fluxes at the ecosystem scale. *Global Biogeochemical Cycles,* 14**,** 1061-1070.

GROFFMAN, P. M., BUTTERBACH-BAHL, K., FULWEILER, R. W., GOLD, A. J., MORSE, J. L., STANDER, E. K., TAGUE, C., TONITTO, C. & VIDON, P. 2009. Challenges to incorporating spatially and temporally explicit phenomena (hotspots and hot moments) in denitrification models. *Biogeochemistry,* 93**,** 49-77.

GROSSI, G., GOGLIO, P., VITALI, A. & WILLIAMS, A. G. 2018. Livestock and climate change: impact of livestock on climate and mitigation strategies. *Animal Frontiers,* 9**,** 69-76.

HAFNER, S., UNTEREGELSBACHER, S., SEEBER, E., LENA, B., XU, X., LI, X., GUGGENBERGER, G., MIEHE, G. & KUZYAKOV, Y. 2012. Effect of grazing on carbon stocks and assimilate partitioning in a T ibetan montane pasture revealed by 13 CO2 pulse labeling. *Global Change Biology,* 18**,** 528-538.

HARGREAVES, P. R., REES, R. M., HORGAN, G. W. & BALL, B. C. 2015. Size and persistence of nitrous oxide hot-spots in grazed and ungrazed grassland. *Environment and Natural Resources Research,* 5**,** 1-15.

HARRIS, E., DIAZ-PINES, E., STOLL, E., SCHLOTER, M., SCHULZ, S., DUFFNER, C., LI, K., MOORE, K., INGRISCH, J. & REINTHALER, D. 2021. Denitrifying pathways dominate nitrous oxide emissions from managed grassland during drought and rewetting. *Science advances,* 7**,** eabb7118.

HARTY, M. A., FORRESTAL, P. J., WATSON, C., MCGEOUGH, K., CAROLAN, R., ELLIOT, C., KROL, D., LAUGHLIN, R. J., RICHARDS, K. G. & LANIGAN, G. 2016. Reducing nitrous oxide emissions by changing N fertiliser use from calcium ammonium nitrate (CAN) to urea based formulations. *Science of the Total Environment,* 563**,** 576-586.

HASZPRA, L., HIDY, D., TALIGÁS, T. & BARCZA, Z. 2018. First results of tall tower based nitrous oxide flux monitoring over an agricultural region in Central Europe. *Atmospheric Environment,* 176**,** 240-251.

HAYATSU, M., TAGO, K. & SAITO, M. 2008. Various players in the nitrogen cycle: diversity and functions of the microorganisms involved in nitrification and denitrification. *Soil Science and Plant Nutrition,* 54**,** 33-45.

HAYNES, R. & WILLIAMS, P. 1993. Nutrient cycling and soil fertility in the grazed pasture ecosystem. *Advances in agronomy,* 49**,** 119-199.

HOFFMANN, M., PEHLE, N., HUTH, V., JURISCH, N., SOMMER, M. & AUGUSTIN, J. 2018. A simple method to assess the impact of sealing, headspace mixing and pressure vent on airtightness of manually closed chambers. *Journal of Plant Nutrition and Soil Science,* 181**,** 36-40.

HÖRTNAGL, L., BARTHEL, M., BUCHMANN, N., EUGSTER, W., BUTTERBACH-BAHL, K., DÍAZ-PINÉS, E., ZEEMAN, M., KLUMPP, K., KIESE, R. & BAHN, M. 2018. Greenhouse gas fluxes over managed grasslands in Central Europe. *Global Change Biology,* 24**,** 1843-1872.

HUHTANEN, P., NOUSIAINEN, J. I., RINNE, M., KYTÖLÄ, K. & KHALILI, H. 2008. Utilization and partition of dietary nitrogen in dairy cows fed grass silage-based diets. *Journal of dairy science,* 91**,** 3589-3599.

HUTCHINSON, G. L. & LIVINGSTON, G. P. 2002. 4.5 Soil–Atmosphere Gas Exchange. *Methods of Soil Analysis: Part 4 Physical Methods,* 5**,** 1159-1182.

HYDE, B. 2004. *Nitrous Oxide Emissions from an Irish Grassland.* University College Dublin.

HYDE, B., FORRESTAL, P. J., JAHANGIR, M. M., RYAN, M., FANNING, A., CARTON, O. T., LANIGAN, G. & RICHARDS, K. G. 2016. The interactive effects of fertiliser nitrogen with dung and

urine on nitrous oxide emissions in grassland. *Irish Journal of Agricultural and Food Research,* 55**,** 1-9.
IIDA, K., YOKOGAWA, D., IKEDA, A., SATO, H. & SAKAKI, S. 2009. Carbon dioxide capture at the molecular level. *Phys Chem Chem Phys,* 11**,** 8556-9.
INATOMI, M., HAJIMA, T. & ITO, A. 2019. Fraction of nitrous oxide production in nitrification and its effect on total soil emission: A meta-analysis and global-scale sensitivity analysis using a process-based model. *Plos one,* 14**,** e0219159.
IPCC 2021a. Climate Change 2021: The Physical Science Basis. Contribution of Working Group I to the Sixth

Assessment Report of the Intergovernmental Panel on Climate Change. *In:* MASSON-DELMOTTE, V., P. ZHAI, A. PIRANI, S., L. CONNORS, C. P., S. BERGER, N. CAUD, Y. CHEN, L. GOLDFARB, M. I. GOMIS, M. HUANG, K. LEITZELL, E. LONNOY, J. B. & R. MATTHEWS, T. K. M., T. WATERFIELD, O. YELEKÇI, R. YU, B. ZHOU (eds.). UK: Cambridge Univeristy Press

IPCC. 2021b. *Land Use, Land-Use Change and Forestry* [Online]. Available: https://archive.ipcc.ch/ipccreports/sres/land_use/index.php?idp=77 [Accessed 04/08/2021].
JAHANGIR, M. M. R., KHALIL, M., RICHARDS, K., JOHNSTON, P., CARDENAS, L. & HATCH, D. 2010. *Denitrification and the N2/(N20+N2) ratios at various soil depths under grazed grassland in Ireland*.
JARVIS, S., LOVELL, R. & PANAYIDES, R. 1995a. Patterns of methane emission from excreta of grazing animals. *Soil Biology and Biochemistry,* 27**,** 1581-1588.
JARVIS, S. C., SCHOLEFIELD, D. & PAIN, B. 1995b. Nitrogen cycling in grazing systems. *Nitrogen fertilization in the environment,* 38.
JKI. 2021. *Managed grassland* [Online]. Available: https://www.julius-kuehn.de/en/pb/fields-of-activity/managed-grassland/ [Accessed 20/10/2021].
JOLLY, B., LUO, J., MEHRA, P., FORRESTAL, P., O'NEILL, M., RICHARDS, K. G., SINGH, B. P., BATES, G. & SAGGAR, S. 2021. Evaluation of proximal sensing technologies for mapping bovine urine patches under grazing pastures. *Computers and Electronics in Agriculture,* 188**,** 106309.
JONES, D. & WILLETT, V. 2006. Experimental evaluation of methods to quantify dissolved organic nitrogen (DON) and dissolved organic carbon (DOC) in soil. *Soil Biology and Biochemistry,* 38**,** 991-999.
JONES, S., FAMULARI, D., DI MARCO, C., NEMITZ, E., SKIBA, U., REES, R. & SUTTON, M. 2011. Nitrous oxide emissions from managed grassland: a comparison of eddy covariance and static chamber measurements. *Atmospheric Measurement Techniques,* 4**,** 2179-2194.
JONES, S. K., HELFTER, C., ANDERSON, M., COYLE, M., CAMPBELL, C., FAMULARI, D., MARCO, C. D., DIJK, N. V., TANG, Y. S. & TOPP, C. F. 2017. The nitrogen, carbon and greenhouse gas budget of a grazed, cut and fertilised temperate grassland. *Biogeosciences,* 14**,** 2069-2088.
JOOS, F., ROTH, R., FUGLESTVEDT, J. S., PETERS, G. P., ENTING, I. G., BLOH, W. V., BROVKIN, V., BURKE, E. J., EBY, M. & EDWARDS, N. R. 2013. Carbon dioxide and climate impulse response functions for the computation of greenhouse gas metrics: a multi-model analysis. *Atmospheric Chemistry and Physics,* 13**,** 2793-2825.
KAIMAL, J. C. & FINNIGAN, J. J. 1994. *Atmospheric boundary layer flows: their structure and measurement*, Oxford university press.
KEANE, B. J., INESON, P., VALLACK, H. W., BLEI, E., BENTLEY, M., HOWARTH, S., MCNAMARA, N. P., ROWE, R. L., WILLIAMS, M. & TOET, S. 2018. Greenhouse gas emissions from the energy crop oilseed rape (Brassica napus); the role of photosynthetically active radiation in diurnal N2O flux variation. *GCB Bioenergy,* 10**,** 306-319.

KEBREAB, E., FRANCE, J., BEEVER, D. & CASTILLO, A. 2001. Nitrogen pollution by dairy cows and its mitigation by dietary manipulation. *Nutrient cycling in agroecosystems,* 60**,** 275-285.
KHDYER, I. & CHO, C. 1983. Nitrification and denitrification of nitrogen fertilizers in a soil column. *Soil Science Society of America Journal,* 47**,** 1134-1139.
KIELY, G., LEAHY, P., LEWIS, C., SOTTOCORNOLA, M., LAINE, A. & KOEHLER, A.-K. 2018. GHG Fluxes from Terrestrial Ecosystems in Ireland. Co. Wexford, Ireland: EPA.
KLJUN, N., CALANCA, P., ROTACH, M. & SCHMID, H. P. 2015. A simple two-dimensional parameterisation for Flux Footprint Prediction (FFP). *Geoscientific Model Development,* 8**,** 3695-3713.
KLUMPP, K., FONTAINE, S., ATTARD, E., LE ROUX, X., GLEIXNER, G. & SOUSSANA, J. F. 2009. Grazing triggers soil carbon loss by altering plant roots and their control on soil microbial community. *Journal of Ecology,* 97**,** 876-885.
KORMANN, R. & MEIXNER, F. X. 2001. An analytical footprint model for non-neutral stratification. *Boundary-Layer Meteorology,* 99**,** 207-224.
KROL, D. J., CAROLAN, R., MINET, E., MCGEOUGH, K., WATSON, C., FORRESTAL, P. J., LANIGAN, G. & RICHARDS, K. G. 2016. Improving and disaggregating N2O emission factors for ruminant excreta on temperate pasture soils. *Science of the Total Environment,* 568**,** 327-338.
KROL, D. J., MINET, E., FORRESTAL, P. J., LANIGAN, G., MATHIEU, O. & RICHARDS, K. G. 2017. The interactive effects of various nitrogen fertiliser formulations applied to urine patches on nitrous oxide emissions in grassland. *Irish journal of agricultural and food research,* 56**,** 54-64.
KROON, P., HENSEN, A., VAN DEN BULK, W., JONGEJAN, P. & VERMEULEN, A. 2008. The importance of reducing the systematic error due to non-linearity in N 2 O flux measurements by static chambers. *Nutrient cycling in Agroecosystems,* 82**,** 175-186.
KUGLER, S., HORVÁTH, L. & MACHON, A. 2008. Estimation of nitrogen balance between the atmosphere and Lake Balaton and a semi natural grassland in Hungary. *Environmental Pollution,* 154**,** 498-503.
KUMAR, A., BHATIA, A., FAGODIYA, R., MALYAN, S. & MEENA, B. 2017. Eddy Covariance Flux Tower: A Promising Technique for Greenhouse Gases Measurement. Eddy Covariance Flux Tower: A Promising Technique for Greenhouse Gases Measurement.
KUMAR, A., MEDHI, K., FAGODIYA, R. K., SUBRAHMANYAM, G., MONDAL, R., RAJA, P., MALYAN, S. K., GUPTA, D. K., GUPTA, C. K. & PATHAK, H. 2020. Molecular and ecological perspectives of nitrous oxide producing microbial communities in agro-ecosystems. *Reviews in Environmental Science and Bio/Technology***,** 1-34.
LAI, T. V. & DENTON, M. D. 2018. N2O and N2 emissions from denitrification respond differently to temperature and nitrogen supply. *Journal of Soils and Sediments,* 18**,** 1548-1557.
LALRAMMAWIA, C. & PALIWAL, K. 2010. Seasonal changes in net ecosystem exchange of CO_2 and respiration of Cenchrus ciliaris L. grassland ecosystem in semi-arid tropics: an eddy covariance measurement. *Current Science***,** 1211-1218.
LAMMIRATO, C., LEBENDER, U., TIERLING, J. & LAMMEL, J. 2018. Analysis of uncertainty for N2O fluxes measured with the closed-chamber method under field conditions: Calculation method, detection limit, and spatial variability. *Journal of Plant Nutrition and Soil Science,* 181**,** 78-89.
LANIGAN, G., DONNELLAN, T., HANRAHAN, K., CARSTEN, P., SHALLOO, L., KROL, D., FORRESTAL, P. J., FARRELLY, N., O'BRIEN, D. & RYAN, M. 2018. An analysis of abatement potential of Greenhouse Gas emissions in Irish agriculture 2021-2030. Teagasc.
LAVILLE, P., HÉNAULT, C., RENAULT, P., CELLIER, P., ORIOL, A., DEVIS, X., FLURA, D. & GERMON, J. 1997. Field comparison of nitrous oxide emission measurements using micrometeorological and chamber methods. *Agronomie,* 17**,** 375-388.
LEAHY, P., KIELY, G. & SCANLON, T. M. 2004. Managed grasslands: A greenhouse gas sink or source? *Geophysical Research Letters,* 31.

LEBENDER, U., SENBAYRAM, M., LAMMEL, J. & KUHLMANN, H. 2014. Impact of mineral N fertilizer application rates on N2O emissions from arable soils under winter wheat. *Nutrient Cycling in Agroecosystems,* 100**,** 111-120.

LEDGARD, S., SCHILS, R., ERIKSEN, J. & LUO, J. 2009. Environmental impacts of grazed clover/grass pastures. *Irish journal of Agricultural and food research***,** 209-226.

LEMAIRE, G., HODGSON, J. & CHABBI, A. 2011a. *Grassland productivity and ecosystem services*, Cabi.

LEMAIRE, G., HODGSON, J. & CHABBI, A. 2011b. Introduction: food security and environmental impacts-challenge for grassland sciences. *Grassland productivity and ecosystem services*.

LEVY, P., COWAN, N., VAN OIJEN, M., FAMULARI, D., DREWER, J. & SKIBA, U. 2017. Estimation of cumulative fluxes of nitrous oxide: uncertainty in temporal upscaling and emission factors. *European Journal of Soil Science,* 68**,** 400-411.

LI, D., WATSON, C. J., YAN, M. J., LALOR, S., RAFIQUE, R., HYDE, B., LANIGAN, G., RICHARDS, K. G., HOLDEN, N. M. & HUMPHREYS, J. 2013a. A review of nitrous oxide mitigation by farm nitrogen management in temperate grassland-based agriculture. *Journal of Environmental Management,* 128**,** 893-903.

LI, M., SHIMIZU, M. & HATANO, R. 2015. Evaluation of N2O and CO2 hot moments in managed grassland and cornfield, southern Hokkaido, Japan. *CATENA,* 133**,** 1-13.

LI, X., ZHANG, C., FU, H., GUO, D., SONG, X., WAN, C. & REN, J. 2013b. Grazing exclusion alters soil microbial respiration, root respiration and the soil carbon balance in grasslands of the Loess Plateau, northern China. *Soil Science and Plant Nutrition,* 59**,** 877-887.

LIANG, L. L., CAMPBELL, D. I., WALL, A. M. & SCHIPPER, L. A. 2018. Nitrous oxide fluxes determined by continuous eddy covariance measurements from intensively grazed pastures: Temporal patterns and environmental controls. *Agriculture, Ecosystems & Environment,* 268**,** 171-180.

LICOR 2017. EddyPro software instruction manual. *LI-COR Inc., Lincoln, Nebraska, USA*.

LINN, D. M. & DORAN, J. W. 1984. Effect of water-filled pore space on carbon dioxide and nitrous oxide production in tilled and nontilled soils. *Soil Science Society of America Journal,* 48**,** 1267-1272.

LLOYD, J. & TAYLOR, J. 1994. On the temperature dependence of soil respiration. *Functional ecology***,** 315-323.

LOCKYER, D. & WHITEHEAD, D. 1990. Volatilization of ammonia from cattle urine applied to grassland. *Soil Biology and Biochemistry,* 22**,** 1137-1142.

LOGNOUL, M., DEBACQ, A., DE LIGNE, A., DUMONT, B., MANISE, T., BODSON, B., HEINESCH, B. & AUBINET, M. 2019. N2O flux short-term response to temperature and topsoil disturbance in a fertilized crop: An eddy covariance campaign. *Agricultural and Forest Meteorology,* 271**,** 193-206.

LÓPEZ-AIZPÚN, M., HORROCKS, C. A., CHARTERIS, A. F., MARSDEN, K. A., CIGANDA, V. S., EVANS, J. R., CHADWICK, D. R. & CÁRDENAS, L. M. 2020. Meta-analysis of global livestock urine-derived nitrous oxide emissions from agricultural soils. *Global change biology,* 26**,** 2002-2013.

LORENZ, K. & LAL, R. 2005. The depth distribution of soil organic carbon in relation to land use and management and the potential of carbon sequestration i n subsoil horizons. *Advances in agronomy,* 88**,** 35-66.

LUO, G., KIESE, R., WOLF, B. & BUTTERBACH-BAHL, K. 2013. Effects of soil temperature and moisture on methane uptake and nitrous oxide emissions across three different ecosystem types. *Biogeosciences,* 10**,** 3205-3219.

LUO, J., BALVERT, S., WISE, B., WELTEN, B., LEDGARD, S., DE KLEIN, C., LINDSEY, S. & JUDGE, A. 2018. Using alternative forage species to reduce emissions of the greenhouse gas nitrous oxide from cattle urine deposited onto soil. *Science of the Total Environment,* 610**,** 1271-1280.

LUO, J., WYATT, J., VAN DER WEERDEN, T. J., THOMAS, S. M., DE KLEIN, C. A., LI, Y., ROLLO, M., LINDSEY, S., LEDGARD, S. F. & LI, J. 2017. Potential hotspot areas of nitrous oxide emissions from grazed pastoral dairy farm systems. *Advances in Agronomy,* 145**,** 205-268.

MAAG, M. & VINTHER, F. P. 1996. Nitrous oxide emission by nitrification and denitrification in different soil types and at different soil moisture contents and temperatures. *Applied Soil Ecology,* 4**,** 5-14.

MAAMARY, R., CUI, X., FERTEIN, E., AUGUSTIN, P., FOURMENTIN, M., DEWAELE, D., CAZIER, F., GUINET, L. & CHEN, W. 2016. A Quantum Cascade Laser-Based Optical Sensor for Continuous Monitoring of Environmental Methane in Dunkirk (France). *Sensors (Basel, Switzerland),* 16**,** 224-224.

MAIRE, J., GIBSON-POOLE, S., COWAN, N., REAY, D. S., RICHARDS, K. G., SKIBA, U., REES, R. M. & LANIGAN, G. J. 2018. Identifying Urine Patches on Intensively Managed Grassland Using Aerial Imagery Captured From Remotely Piloted Aircraft Systems. *Frontiers in Sustainable Food Systems,* 2.

MAIRE, J., KROL, D., PASQUIER, D., COWAN, N., SKIBA, U., REES, R., REAY, D., LANIGAN, G. J. & RICHARDS, K. G. 2020. Nitrogen fertiliser interactions with urine deposit affect nitrous oxide emissions from grazed grasslands. *Agriculture, Ecosystems & Environment,* 290**,** 106784.

MAIRE, J. L. M. 2020. *Nitrous oxide emissions from grazed*

grasslands: novel approaches to assessing

spatial heterogeneity. Phd, Edinburgh.

MC GUIRE, J., ROGAN, F., DALY, H., GLYNN, J., BALYK, O. & GALLACHÓIR, B. Ó. 2020. The role of carbon budgets in translating the Paris Agreement into national climate policy.

MCAULIFFE, G., LÓPEZ-AIZPÚN, M., BLACKWELL, M., CASTELLANO-HINOJOSA, A., DARCH, T., EVANS, J., HORROCKS, C., LE COCQ, K., TAKAHASHI, T. & HARRIS, P. 2020. Elucidating three-way interactions between soil, pasture and animals that regulate nitrous oxide emissions from temperate grazing systems. *Agriculture, ecosystems & environment,* 300**,** 106978.

MCCLAIN, M. E., BOYER, E. W., DENT, C. L., GERGEL, S. E., GRIMM, N. B., GROFFMAN, P. M., HART, S. C., HARVEY, J. W., JOHNSTON, C. A. & MAYORGA, E. 2003. Biogeochemical hot spots and hot moments at the interface of terrestrial and aquatic ecosystems. *Ecosystems***,** 301-312.

MCDANIEL, M. D., SIMPSON, R. R., MALONE, B., MCBRATNEY, A., MINASNY, B. & ADAMS, M. 2017. Quantifying and predicting spatio-temporal variability of soil CH4 and N2O fluxes from a seemingly homogeneous Australian agricultural field. *Agriculture, Ecosystems & Environment,* 240**,** 182-193.

MCGLYNN, E., HARPER, K., LI, S. & BERGER, M. 2019. Reducing climate policy risk: Improving certainty and accuracy in the US land use, land use change, and forestry greenhouse gas inventory. *ClimateWorks Foundation*.

MCTIERNAN, K. B., JARVIS, S., SCHOLEFIELD, D. & HAYES, M. 2001. Dissolved organic carbon losses from grazed grasslands under different management regimes. *Water research,* 35**,** 2565-2569.

MENON, S., DENMAN, K. L., BRASSEUR, G., CHIDTHAISONG, A., CIAIS, P., COX, P. M., DICKINSON, R. E., HAUGLUSTAINE, D., HEINZE, C. & HOLLAND, E. 2007. Couplings between changes in the climate system and biogeochemistry. Lawrence Berkeley National Lab.(LBNL), Berkeley, CA (United States).

MERBOLD, L., DECOCK, C., EUGSTER, W., FUCHS, K., WOLF, B., BUCHMANN, N. & HÖRTNAGL, L. 2021. Are there memory effects on greenhouse gas emissions (CO2, N2O and CH4) following grassland restoration? *Biogeosciences,* 18**,** 1481-1498.

MERBOLD, L., EUGSTER, W., STIEGER, J., ZAHNISER, M., NELSON, D. & BUCHMANN, N. 2014. Greenhouse gas budget (CO 2, CH 4 and N2O) of intensively managed grassland following restoration. *Global change biology,* 20**,** 1913-1928.

MET EIREANN. 2021. *Rosslare 1978-2007 averages* [Online]. Available: https://www.met.ie/climate-ireland/1981-2010/rosslare.html [Accessed 28/07/2021].

MIKHAYLOV, O., ZAGIROVA, S. & MIGLOVETS, M. 2019. Seasonal and inter-annual variability of carbon dioxide exchange at a boreal peatland in north-east European Russia. *MIRES AND PEAT,* 24.

MINISTRY FOR THE ENVIRONMENT. 2018. *New Zealand's greenhouse gas inventory 1990–2016. Fulfillin reporting requirements under the United Nations Framework Convention on Climate Change and the Kyoto Protocol. New Zealand Government.* [Online]. Available: https://apo.org.au/sites/default/files/resource-files/2020-04/apo-nid303278.pdf [Accessed 25/08/2021].

MINISTRY OF ECOLOGY SUSTAINABLE DEVELOPMENT AND ENERGY. 2015. *France national low-carbon strategy* [Online]. Available: https://www.ecologie.gouv.fr/sites/default/files/SNBC_France_low_carbon_strategy_2015.pdf [Accessed 02/09/2021].

MISHUROV, M. & KIELY, G. 2011. Gap-filling techniques for the annual sums of nitrous oxide fluxes. *Agricultural and forest meteorology,* 151**,** 1763-1767.

MISSELBROOK, T., CARDENAS, L., CAMP, V., THORMAN, R., WILLIAMS, J., ROLLETT, A. & CHAMBERS, B. 2014. An assessment of nitrification inhibitors to reduce nitrous oxide emissions from UK agriculture. *Environmental Research Letters,* 9**,** 115006.

MISSELBROOK, T., FLEMING, H., CAMP, V., UMSTATTER, C., DUTHIE, C.-A., NICOLL, L. & WATERHOUSE, T. 2016. Automated monitoring of urination events from grazing cattle. *Agriculture, Ecosystems & Environment,* 230**,** 191-198.

MISSELBROOK, T., POWELL, J., BRODERICK, G. & GRABBER, J. 2005. Dietary manipulation in dairy cattle: Laboratory experiments to assess the influence on ammonia emissions. *Journal of dairy science,* 88**,** 1765-1777.

MOFFAT, A. M., PAPALE, D., REICHSTEIN, M., HOLLINGER, D. Y., RICHARDSON, A. D., BARR, A. G., BECKSTEIN, C., BRASWELL, B. H., CHURKINA, G. & DESAI, A. R. 2007. Comprehensive comparison of gap-filling techniques for eddy covariance net carbon fluxes. *Agricultural and Forest Meteorology,* 147**,** 209-232.

MOIR, J. L., CAMERON, K. C., DI, H. J. & FERTSAK, U. 2011. The spatial coverage of dairy cattle urine patches in an intensively grazed pasture system. *The Journal of Agricultural Science,* 149**,** 473-485.

MONCRIEFF, J., CLEMENT, R., FINNIGAN, J. & MEYERS, T. 2004. Averaging, detrending, and filtering of eddy covariance time series. *Handbook of micrometeorology.* Springer.

MORRISON, R., COOPER, H., CUMMING, A., EVANS, C., THORNTON, J., WINTERBOURN, B., RYLETT, D. & DAVID, J. 2020. Eddy covariance measurements of carbon dioxide, energy and water fluxes at a cropland and a grassland on lowland peat soils, East Anglia, UK, 2016-2019.

MOSIER, A., DELGADO, J., COCHRAN, V., VALENTINE, D. & PARTON, W. 1997. Impact of agriculture on soil consumption of atmospheric CH 4 and a comparison of CH 4 and N 2 O flux in subarctic, temperate and tropical grasslands. *Nutrient Cycling in Agroecosystems,* 49**,** 71-83.

MULLIGAN, F., DILLON, P., CALLAN, J., RATH, M. & O'MARA, F. 2004. Supplementary concentrate type affects nitrogen excretion of grazing dairy cows. *Journal of dairy science,* 87**,** 3451-3460.

MUMFORD, M., ROWLINGS, D., SCHEER, C., DE ROSA, D. & GRACE, P. 2019. Effect of irrigation scheduling on nitrous oxide emissions in intensively managed pastures. *Agriculture, Ecosystems & Environment,* 272**,** 126-134.

MURPHY, R. M., RICHARDS, K. G., KROL, D. J., GEBREMICHAEL, A. W., LOPEZ-SANGIL, L., RAMBAUD, J., COWAN, N., LANIGAN, G. J. & SAUNDERS, M. 2022a. Assessing nitrous oxide emissions in time and space with minimal uncertainty using static chambers and eddy covariance from a temperate grassland. *Agricultural and Forest Meteorology,* 313**,** 108743.

MURPHY, R. M., SAUNDERS, M., RICHARDS, K. G., KROL, D. J., GEBREMICHAEL, A. W., RAMBAUD, J., COWAN, N. & LANIGAN, G. J. 2022b. Nitrous oxide emission factors from an intensively grazed temperate grassland: A comparison of cumulative emissions determined by eddy covariance and static chamber methods. *Agriculture, Ecosystems & Environment,* 324**,** 107725.

MYRGIOTIS, V., SMALLMAN, T. L. & WILLIAMS, M. 2021. The carbon budget of the managed grasslands of Great Britain constrained by earth observations. *Biogeosciences Discussions***,** 1-35.

NAKICENOVIC, N., ALCAMO, J., DAVIS, G., VRIES, B. D., FENHANN, J., GAFFIN, S., GREGORY, K., GRUBLER, A., JUNG, T. Y. & KRAM, T. 2000. Special report on emissions scenarios.

NEUKOM, R., STEIGER, N., GÓMEZ-NAVARRO, J. J., WANG, J. & WERNER, J. P. 2019. No evidence for globally coherent warm and cold periods over the preindustrial Common Era. *Nature,* 571**,** 550-554.

NI CHONCUBHAIR, O. 2014. *Impact of Land-Use Change to Bioenergy Crops on Carbon Cylce Dynamics.* PhD, University College Dublin.

NÍ CHONCUBHAIR, Ó., OSBORNE, B., FINNAN, J. & LANIGAN, G. 2017. Comparative assessment of ecosystem C exchange in Miscanthus and reed canary grass during early establishment. *Gcb Bioenergy,* 9**,** 280-298.

NISHINA, K., TAKENAKA, C. & ISHIZUKA, S. 2009. Spatiotemporal variation in N 2 O flux within a slope in a Japanese cedar (Cryptomeria japonica) forest. *Biogeochemistry,* 96**,** 163-175.

NOAA. 2021. *Carbon cycle greenhouse gases* [Online]. Available: https://gml.noaa.gov/ccgg/trends/ [Accessed 18/10/2021].

NORTON, J. & OUYANG, Y. 2019. Controls and Adaptive Management of Nitrification in Agricultural Soils. *Frontiers in microbiology,* 10**,** 1931-1931.

NYAMEASEM, J. K., MALISCH, C. S., LOGES, R., TAUBE, F., KLUß, C., VOGELER, I. & REINSCH, T. 2021. Nitrous oxide emission from grazing is low across a gradient of plant functional diversity and soil conditions. *Atmosphere,* 12**,** 223.

O'CONNELL, C., JUDSON, H. & BARRELL, G. K. Sustained diuretic effect of plantain when ingested by sheep. 2016. New Zealand Society of Animal Production.

O'CONNELL, K., HUMPHREYS, J. & WATSON, C. J. Quantification of nitrogen sources for grassland. Winter Scientific Meeting, The Fertiliser Association of Ireland, 2004. 15-28.

O'NEILL, M., GALLEGO-LORENZO, L., LANIGAN, G., FORRISTAL, P. & OSBORNE, B. 2020. Assessment of nitrous oxide emission factors for arable and grassland ecosystems. *Journal of Integrative Environmental Sciences***,** 1-21.

O'NEILL, M., SAGGAR, S., RICHARDS, K. G., LUO, J., SINGH, B. P., MEHRA, P. & FORRESTAL, P. J. 2021. Nitrous oxide emission factors in conventionally and naturally simulated cattle urine patches. *Nutrient Cycling in Agroecosystems*.

OUDSHOORN, F. W., KRISTENSEN, T. & NADIMI, E. S. 2008. Dairy cow defecation and urination frequency and spatial distribution in relation to time-limited grazing. *Livestock Science,* 113**,** 62-73.

PACHAURI, R. K., ALLEN, M. R., BARROS, V. R., BROOME, J., CRAMER, W., CHRIST, R., CHURCH, J. A., CLARKE, L., DAHE, Q. & DASGUPTA, P. 2014. *Climate change 2014: synthesis report. Contribution of Working Groups I, II and III to the fifth assessment report of the Intergovernmental Panel on Climate Change*, Ipcc.

PAIELLA, R. 2011. 5.16 - Quantum Cascade Lasers. *In:* BHATTACHARYA, P., FORNARI, R. & KAMIMURA, H. (eds.) *Comprehensive Semiconductor Science and Technology*. Amsterdam: Elsevier.
PAQUAY, R., DE BAERE, R. & LOUSSE, A. 1970. Statistical research on the fate of water in the adult cow. II. The lactating cow. *The Journal of Agricultural Science,* 75**,** 251-255.
PARIS AGREEMENT. Paris agreement. Report of the Conference of the Parties to the United Nations Framework Convention on Climate Change (21st Session, 2015: Paris). Retrived December, 2015. HeinOnline, 2017.
PAUSTIAN, K., LARSON, E., KENT, J., MARX, E. & SWAN, A. 2019. Soil C Sequestration as a Biological Negative Emission Strategy. *Frontiers in Climate,* 1.
PAVELKA, M., ACOSTA, M., KIESE, R., ALTIMIR, N., BRÜMMER, C., CRILL, P., DARENOVA, E., FUß, R., GIELEN, B. & GRAF, A. 2018. Standardisation of chamber technique for CO2, N2O and CH4 fluxes measurements from terrestrial ecosystems.
PEICHL, M., CARTON, O. & KIELY, G. 2012. Management and climate effects on carbon dioxide and energy exchanges in a maritime grassland. *Agriculture, ecosystems & environment,* 158**,** 132-146.
PETERSEN, S. O., SOMMER, S. G., AAES, O. & SØEGAARD, K. 1998. Ammonia losses from urine and dung of grazing cattle: effect of N intake. *Atmospheric Environment,* 32**,** 295-300.
PETERSON, R. A. & CAVANAUGH, J. E. 2019. Ordered quantile normalization: a semiparametric transformation built for the cross-validation era. *Journal of Applied Statistics*.
PHILIBERT, A., LOYCE, C. & MAKOWSKI, D. 2013. Prediction of N2O emission from local information with Random Forest. *Environmental pollution,* 177**,** 156-163.
PICKETT, S. T. A. & WHITE, P. S. 1985. Preface. *In:* PICKETT, S. T. A. & WHITE, P. S. (eds.) *The Ecology of Natural Disturbance and Patch Dynamics.* San Diego: Academic Press.
PIHLATIE, M., AMBUS, P., RINNE, J., PILEGAARD, K. & VESALA, T. 2005a. Plant-mediated nitrous oxide emissions from beech (Fagus sylvatica) leaves. *New Phytol,* 168**,** 93-8.
PIHLATIE, M., RINNE, J., AMBUS, P., PILEGAARD, K., DORSEY, J., RANNIK, Ü., MARKKANEN, T., LAUNIAINEN, S. & VESALA, T. 2005b. Nitrous oxide emissions from a beech forest floor measured by eddy covariance and soil enclosure techniques. *Biogeosciences,* 2**,** 377-387.
PITCAIRN, C., SKIBA, U., SUTTON, M., FOWLER, D., MUNRO, R. & KENNEDY, V. 2002. Defining the spatial impacts of poultry farm ammonia emissions on species composition of adjacent woodland groundflora using Ellenberg Nitrogen Index, nitrous oxide and nitric oxide emissions and foliar nitrogen as marker variables. *Environmental Pollution,* 119**,** 9-21.
PLUMMER. 2015. *JAGS: A Program for Analysis of Bayesian Graphical Models Using*

Gibbs Sampling. [Online]. Available: http://citeseer.ist.psu.edu/plummer03jags.html [Accessed 04/04/2019].
POSTGATE, J. R. 1982. *The fundamentals of nitrogen fixation*, CUP Archive.
POULSEN, H. D. & KRISTENSEN, V. F. 1998. *Standard values for farm manure: a revaluation of the Danish standard values concerning the nitrogen, phosphorus and potassium content of manure*, Ministeriet for Fødevarer, Landbrug og Fiskeri, Danmarks JordbrugsForskning.
PRATHER, M. J., HOLMES, C. D. & HSU, J. 2012. Reactive greenhouse gas scenarios: Systematic exploration of uncertainties and the role of atmospheric chemistry. *Geophysical Research Letters,* 39.
RABINOWITCH, E. I. 1951. *Photosynthesis and related processes*, LWW.
RAFIQUE, R., ANEX, R., HENNESSY, D. & KIELY, G. 2012. What are the impacts of grazing and cutting events on the N2O dynamics in humid temperate grassland? *Geoderma,* 181**,** 36-44.
RAFIQUE, R., HENNESSY, D. & KIELY, G. 2011. Nitrous oxide emission from grazed grassland under different management systems. *Ecosystems,* 14**,** 563-582.
RAPSON, T. D. & DACRES, H. 2014. Analytical techniques for measuring nitrous oxide. *TrAC Trends in Analytical Chemistry,* 54**,** 65-74.

REAY, D. S., DAVIDSON, E. A., SMITH, K. A., SMITH, P., MELILLO, J. M., DENTENER, F. & CRUTZEN, P. J. 2012. Global agriculture and nitrous oxide emissions. *Nature climate change,* 2**,** 410-416.

REES, R. M., MAIRE, J., FLORENCE, A., COWAN, N., SKIBA, U., VAN DER WEERDEN, T. & JU, X. 2020. Mitigating nitrous oxide emissions from agricultural soils by precision management. *Frontiers of Agricultural Science and Engineering,* 7**,** 75-80.

REICHSTEIN, M., FALGE, E., BALDOCCHI, D., PAPALE, D., AUBINET, M., BERBIGIER, P., BERNHOFER, C., BUCHMANN, N., GILMANOV, T. & GRANIER, A. 2005. On the separation of net ecosystem exchange into assimilation and ecosystem respiration: review and improved algorithm. *Global change biology,* 11**,** 1424-1439.

REX, D., CLOUGH, T. J., RICHARDS, K. G., CONDRON, L. M., DE KLEIN, C. A., MORALES, S. E. & LANIGAN, G. J. 2019. Impact of nitrogen compounds on fungal and bacte rial contributions to codenitrification in a pasture soil. *Scientific reports,* 9**,** 1-10.

REX, D., CLOUGH, T. J., RICHARDS, K. G., DE KLEIN, C., MORALES, S. E., SAMAD, M. S., GRANT, J. & LANIGAN, G. J. 2018. Fungal and bacterial contributions to codenitrification emissions of N 2 O and N 2 following urea deposition to soil. *Nutrient cycling in agroecosystems,* 110**,** 135-149.

ROCHE, L., FORRESTAL, P., LANIGAN, G., RICHARDS, K., SHAW, L. & WALL, D. 2016. Impact of fertiliser nitrogen formulation, and N stabilisers on nitrous oxide emissions in spring barley. *Agriculture, ecosystems & environment,* 233**,** 229-237.

ROCHETTE, P. 2011. Towards a standard non-steady-state chamber methodology for measuring soil N2O emissions. *Animal Feed Science and Technology,* 166**,** 141-146.

ROCHETTE, P., BERTRAND, N., CARTER, M. & GREGORICH, E. 2008. Soil-surface gas emissions. *Soil sampling and methods of analysis. CRC Press, Boca Raton, FL***,** 851-861.

ROCHETTE, P. & ERIKSEN-HAMEL, N. S. 2008. Chamber measurements of soil nitrous oxide flux: are absolute values reliable? *Soil Science Society of America Journal,* 72**,** 331-342.

ROCHETTE, P. & HUTCHINSON, G. L. 2005. Measurement of soil respiration in situ: chamber techniques.

RSTUDIO TEAM 2020. RStudio: Integrated Development for R. *In:* RSTUDIO, P. (ed.). Boston, MA.

RUMPEL, C., CRÈME, A., NGO, P., VELÁSQUEZ, G., MORA, M. & CHABBI, A. 2015. The impact of grassland management on biogeochemical cycles involving carbon, nitrogen and phosphorus. *Journal of soil science and plant nutrition,* 15**,** 353-371.

RUTLEDGE, S., MUDGE, P. L., CAMPBELL, D. I., WOODWARD, S. L., GOODRICH, J. P., WALL, A. M., KIRSCHBAUM, M. U. F. & SCHIPPER, L. A. 2015. Carbon balance of an intensively grazed temperate dairy pasture over four years. *Agriculture, Ecosystems & Environment,* 206**,** 10-20.

RYAN, W., HENNESSY, D., MURPHY, J., BOLAND, T. & SHALLOO, L. 2011. A model of nitrogen efficiency in contrasting grass-based dairy systems. *Journal of Dairy Science,* 94**,** 1032-1044.

SANTOS, F., TORN, M. S. & BIRD, J. A. 2012. Biological degradation of pyrogenic organic matter in temperate forest soils. *Soil Biology and Biochemistry,* 51**,** 115-124.

SAUNDERS, M., TOBIN, B., SWEENEY, C., GIORIA, M., BENANTI, G., CACCIOTTI, E. & OSBORNE, B. 2014. Impacts of exceptional and extreme inter-annual climatic events on the net ecosystem carbon dioxide exchange of a Sitka spruce forest. *Agricultural and forest meteorology,* 184**,** 147-157.

SCANLON, T. M. & KIELY, G. 2003. Ecosystem-scale measurements of nitrous oxide fluxes for an intensely grazed, fertilized grassland. *Geophysical Research Letters,* 30.

SCHMITT, M., BAHN, M., WOHLFAHRT, G., TAPPEINER, U. & CERNUSCA, A. 2010. Land use affects the net ecosystem CO 2 exchange and its components in mountain grasslands. *Biogeosciences,* 7**,** 2297-2309.

SCHRIER-UIJL, A., KROON, P., HENSEN, A., LEFFELAAR, P., BERENDSE, F. & VEENENDAAL, E. 2010. Comparison of chamber and eddy covariance-based CO2 and CH4 emission estimates in a heterogeneous grass ecosystem on peat. *Agricultural and Forest Meteorology,* 150**,** 825-831.

SCHWENKE, G. D., MANNING, W. & HAIGH, B. M. 2014. Ammonia volatilisation from nitrogen fertilisers surface-applied to bare fallows, wheat crops and perennial-grass-based pastures on Vertosols. *Soil Research,* 52**,** 805-821.

SELBIE, D., CAMERON, K. C., DI, H. J., MOIR, J. L., LANIGAN, G. & RICHARDS, K. 2014. The effect of urinary nitrogen loading rate and a nitrification inhibitor on nitrous oxide emissions from a temperate grassland soil. *The Journal of Agricultural Science,* 152**,** 159-171.

SELBIE, D. R., LANIGAN, G. J., LAUGHLIN, R. J., DI, H. J., MOIR, J. L., CAMERON, K. C., CLOUGH, T. J., WATSON, C. J., GRANT, J. & SOMERS, C. 2015. Confirmation of co-denitrification in grazed grassland. *Scientific Reports,* 5**,** 1-9.

SHARKHUU, A., PLANTE, A. F., ENKHMANDAL, O., GONNEAU, C., CASPER, B. B., BOLDGIV, B. & PETRAITIS, P. S. 2016. Soil and ecosystem respiration responses to grazing, watering and experimental warming chamber treatments across topographical gradients in northern Mongolia. *Geoderma,* 269**,** 91-98.

SHCHERBAK, I. & ROBERTSON, G. P. 2019. Nitrous Oxide (N 2 O) Emissions from Subsurface Soils of Agricultural Ecosystems. *Ecosystems,* 22**,** 1650-1663.

SHUKLA, P., SKEA, J., CALVO BUENDIA, E., MASSON-DELMOTTE, V., PÖRTNER, H., ROBERTS, D., ZHAI, P., SLADE, R., CONNORS, S. & VAN DIEMEN, R. 2019. IPCC, 2019: Climate Change and Land: an IPCC special report on climate change, desertification, land degradation, sustainable land management, food security, and greenhouse gas fluxes in terrestrial ecosystems.

SHURPALI, N. J., RANNIK, Ü., JOKINEN, S., LIND, S., BIASI, C., MAMMARELLA, I., PELTOLA, O., PIHLATIE, M., HYVÖNEN, N. & RÄTY, M. 2016. Neglecting diurnal variations leads to uncertainties in terrestrial nitrous oxide emissions. *Scientific reports,* 6**,** 1-9.

SIGNOR, D. & CERRI, C. E. P. 2013. Nitrous oxide emissions in agricultural soils: a review. *Pesquisa Agropecuária Tropical,* 43**,** 322-338.

SIMON, P. L., DIECKOW, J., DE KLEIN, C. A., ZANATTA, J. A., VAN DER WEERDEN, T. J., RAMALHO, B. & BAYER, C. 2018. Nitrous oxide emission factors from cattle urine and dung, and dicyandiamide (DCD) as a mitigation strategy in subtropical pastures. *Agriculture, Ecosystems & Environment,* 267**,** 74-82.

SJÖGERSTEN, S., VAN DER WAL, R. & WOODIN, S. J. 2012. Impacts of grazing and climate warming on C pools and decomposition rates in Arctic environments. *Ecosystems,* 15**,** 349-362.

SKIBA, U., JONES, S., DRAGOSITS, U., DREWER, J., FOWLER, D., REES, R., PAPPA, V., CARDENAS, L., CHADWICK, D. & YAMULKI, S. 2012. UK emissions of the greenhouse gas nitrous oxide. *Philosophical Transactions of the Royal Society B: Biological Sciences,* 367**,** 1175-1185.

SKIBA, U., PITCAIRN, C., SHEPPARD, L., KENNEDY, V. & FOWLER, D. 2005. The influence of atmospheric N deposition on nitrous oxide and nitric oxide fluxes and soil ammonium and nitrate concentrations. *Water, Air, & Soil Pollution: Focus,* 4**,** 37-43.

SMITH, K. A. 2010. *Nitrous oxide and climate change*, Earthscan.

SMITH, K. A., DOBBIE, K. E., THORMAN, R., WATSON, C. J., CHADWICK, D. R., YAMULKI, S. & BALL, B. C. 2012. The effect of N fertilizer forms on nitrous oxide emissions from UK arable land and grassland. *Nutrient cycling in Agroecosystems,* 93**,** 127-149.

SMITH, P. 2014. Do grasslands act as a perpetual sink for carbon? *Global change biology,* 20**,** 2708-2711.

SNOW, V. O., CICHOTA, R., MCAULIFFE, R., HUTCHINGS, N. J. & VEJLIN, J. 2017. Increasing the spatial scale of process-based agricultural systems models by representing heterogeneity: The case of urine patches in grazed pastures. *Environmental Modelling & Software,* 90**,** 89-106.

SOBANSKI, N., TUZSON, B., SCHEIDEGGER, P., LOOSER, H., KUPFERSCHMID, A., ITURRATE, M., PASCALE, C., HÜGLIN, C. & EMMENEGGER, L. 2021. Advances in High-Precision NO2 Measurement by Quantum Cascade Laser Absorption Spectroscopy. *Applied Sciences,* 11**,** 1222.

SONG, X., WEI, H., REES, B. & JU, X. 2021. Soil oxygen depletion and corresponding nitrous oxide production at hot moments in an agricultural soil. *Environmental pollution (Barking, Essex : 1987),* 292**,** 118345.

SOTTOCORNOLA, M. & KIELY, G. 2010. Hydro-meteorological controls on the CO2 exchange variation in an Irish blanket bog. *Agricultural and forest meteorology,* 150**,** 287-297.

SOUSSANA, J.-F., ALLARD, V., PILEGAARD, K., AMBUS, P., AMMAN, C., CAMPBELL, C., CESCHIA, E., CLIFTON-BROWN, J., CZÓBEL, S. & DOMINGUES, R. 2007. Full accounting of the greenhouse gas (CO2, N2O, CH4) budget of nine European grassland sites. *Agriculture, Ecosystems & Environment,* 121**,** 121-134.

SOUSSANA, J.-F. & LEMAIRE, G. 2014. Coupling carbon and nitrogen cycles for environmentally sustainable intensification of grasslands and crop-livestock systems. *Agriculture, Ecosystems & Environment,* 190**,** 9-17.

SOUSSANA, J.-F., TALLEC, T. & BLANFORT, V. 2010. Mitigating the greenhouse gas balance of ruminant production systems through carbon sequestration in grasslands. *animal,* 4**,** 334-350.

STAMS, A. J. 1994. Metabolic interactions between anaerobic bacteria in methanogenic environments. *Antonie van Leeuwenhoek,* 66**,** 271-294.

STANDING COMMITEE OF ANALYSTS 1981. *Ammonia in Waters 1981(Methods For the Examination of Water and Associated Materials).* UK, HMSO.

STEVENS, R. & LAUGHLIN, R. 1998. Measurement of nitrous oxide and di-nitrogen emissions from agricultural soils. *Nutrient Cycling in Agroecosystems,* 52**,** 131-139.

STOCKER, T. 2013. Close Climate Change 2013: The Physical Science Basis. Contribution of Working Group I to the Fifth Assessment Report of the Intergovernmental Panel on Climate Change.

SUBBARAO, G., NAKAHARA, K., ISHIKAWA, T., ONO, H., YOSHIDA, M., YOSHIHASHI, T., ZHU, Y., ZAKIR, H., DESHPANDE, S. & HASH, C. 2013. Biological nitrification inhibition (BNI) activity in sorghum and its characterization. *Plant and soil,* 366**,** 243-259.

SUTTIE, J. M., REYNOLDS, S. G. & BATELLO, C. 2005. *Grasslands of the world*, Food & Agriculture Org.

SYAKILA, A. & KROEZE, C. 2011. The global nitrous oxide budget revisited. *Greenhouse gas measurement and management,* 1**,** 17-26.

TAN, I. Y., VAN ES, H. M., DUXBURY, J. M., MELKONIAN, J. J., SCHINDELBECK, R. R., GEOHRING, L. D., HIVELY, W. D. & MOEBIUS, B. N. 2009. Single-event nitrous oxide losses under maize production as affected by soil type, tillage, rotation, and fertilization. *Soil and Tillage Research,* 102**,** 19-26.

TATENO, M. & CHAPIN III, F. 1997. The logic of carbon and nitrogen interactions in terrestrial ecosystems. *The American Naturalist,* 149**,** 723-744.

TEAGASC. 2017. *Soil sampling* [Online]. Available: https://www.teagasc.ie/crops/soil--soil-fertility/soil-analysis/soil-sampling/ [Accessed 8/11/2021].

TEAGASC. 2020. *Agricultural Emissions - greenhouse gases and ammonia* [Online]. Available: https://www.teagasc.ie/publications/2020/agricultural-emissions---greenhouse-gases-and-ammonia.php [Accessed 28/06/2021].

TEAGASC. 2021a. *Grassland* [Online]. Available: https://www.teagasc.ie/crops/soil--soil-fertility/grassland/ [Accessed 16/6/2021].

TEAGASC. 2021b. *Nitrous Oxide* [Online]. Available: https://www.teagasc.ie/environment/climate-change--air-quality/nitrous-oxide/ [Accessed 02/09/2021].

THOMPSON, K., BENT, E., ABALOS, D., WAGNER-RIDDLE, C. & DUNFIELD, K. 2016. Soil microbial communities as potential regulators of in situ N2O fluxes in annual and perennial cropping systems. *Soil Biology and Biochemistry,* 103**,** 262-273.

THORMAN, R. E., NICHOLSON, F. A., TOPP, C. F. E., BELL, M. J., CARDENAS, L. M., CHADWICK, D. R., CLOY, J. M., MISSELBROOK, T. H., REES, R. M., WATSON, C. J. & WILLIAMS, J. R. 2020. Towards Country-Specific Nitrous Oxide Emission Factors for Manures Applied to Arable and Grassland Soils in the UK. *Frontiers in Sustainable Food Systems,* 4.

TIAN, H., LU, C., CIAIS, P., MICHALAK, A. M., CANADELL, J. G., SAIKAWA, E., HUNTZINGER, D. N., GURNEY, K. R., SITCH, S., ZHANG, B., YANG, J., BOUSQUET, P., BRUHWILER, L., CHEN, G., DLUGOKENCKY, E., FRIEDLINGSTEIN, P., MELILLO, J., PAN, S., POULTER, B., PRINN, R., SAUNOIS, M., SCHWALM, C. R. & WOFSY, S. C. 2016. The terrestrial biosphere as a net source of greenhouse gases to the atmosphere. *Nature,* 531**,** 225-228.

TIPPING, E., SOMERVILLE, C. J. & LUSTER, J. 2016. The C:N:P:S stoichiometry of soil organic matter. *Biogeochemistry,* 130**,** 117-131.

TOTTY, V., GREENWOOD, S., BRYANT, R. H. & EDWARDS, G. 2013. Nitrogen partitioning and milk production of dairy cows grazing simple and diverse pastures. *Journal of Dairy Science,* 96**,** 141-149.

TURNER, D. A., CHEN, D., GALBALLY, I., LEUNING, R., EDIS, R., LI, Y., KELLY, K. & PHILLIPS, F. 2008. Spatial variability of nitrous oxide emissions from an Australian irrigated dairy pasture. *Plant and Soil,* 309**,** 77-88.

UNITED NATIONS. 2019. *World Population Prospects 2019* [Online]. Available: https://population.un.org/wpp/Download/Standard/Population/ [Accessed 18/08/2021].

VAN DEN POL-VAN DASSELAAR, A., BASTIAANSEN-AANTJES, L., BOGUE, F., O'DONOVAN, M. & HUYGHE, C. 2019. Grassland use in Europe, a syllabus for young farmers. ISBN: 978-2-7592-3145-4. Quae Éditions, 263 pp.

VAN DER WEERDEN, T. J., NOBLE, A., DE KLEIN, C. A., HUTCHINGS, N., THORMAN, R. E., ALFARO, M. A., AMON, B., BELTRAN, I., GRACE, P. & HASSOUNA, M. 2021. Ammonia and nitrous oxide emission factors for excreta deposited by livestock and land-applied manure. *Journal of Environmental Quality,* 50**,** 1005-1023.

VAN GROENIGEN, J. W., VELTHOF, G. L., VAN DER BOLT, F. J., VOS, A. & KUIKMAN, P. J. 2005. Seasonal variation in N_2O emissions from urine patches: effects of urine concentration, soil compaction and dung. *Plant and Soil,* 273**,** 15-27.

VAN VUUREN, A., VAN DER KOELEN, C., VALK, H. & DE VISSER, H. 1993. Effects of partial replacement of ryegrass by low protein feeds on rumen fermentation and nitrogen loss by dairy cows. *Journal of dairy science,* 76**,** 2982-2993.

VELTHOF, G. L., LESSCHEN, J., WEBB, J., PIETRZAK, S., MIATKOWSKI, Z., PINTO, M., KROS, J. & OENEMA, O. 2014. The impact of the Nitrates Directive on nitrogen emissions from agriculture in the EU-27 during 2000–2008. *Science of the Total Environment,* 468**,** 1225-1233.

VELTHOF, G. L. & LOSADA, J. M. 2011. Calculation of nitrous oxide emission from agriculture in the Netherlands: update of emission factors and leaching fraction. Alterra.

VERHOEVEN, E., PEREIRA, E., DECOCK, C., SUDDICK, E., ANGST, T. & SIX, J. 2017. Toward a Better Assessment of Biochar–Nitrous Oxide Mitigation Potential at the Field Scale. *Journal of Environmental Quality,* 46**,** 237-246.

VICKERS, D. & MAHRT, L. 1997. Quality control and flux sampling problems for tower and aircraft data. *Journal of atmospheric and oceanic technology,* 14**,** 512-526.

VILLEGAS, D., AREVALO, A., NUÑEZ, J., MAZABEL, J., SUBBARAO, G., RAO, I., DE VEGA, J. & ARANGO, J. 2020. Biological Nitrification Inhibition (BNI): Phenotyping of a Core Germplasm Collection of the Tropical Forage Grass Megathyrsus maximus Under Greenhouse Conditions. *Frontiers in Plant Science,* 11.

VOGELER, I., LUCCI, G. & SHEPHERD, M. 2016. An assessment of the effects of fertilizer nitrogen management on nitrate leaching risk from grazed dairy pasture. *The Journal of Agricultural Science,* 154**,** 407.
VOGLMEIER, K., SIX, J., JOCHER, M. & AMMANN, C. 2019. Grazing-related nitrous oxide emissions: from patch scale to field scale. *Biogeosciences,* 16**,** 1685-1703.
WALDO, S., RUSSELL, E. S., KOSTYANOVSKY, K., PRESSLEY, S. N., O'KEEFFE, P. T., HUGGINS, D. R., STÖCKLE, C. O., PAN, W. L. & LAMB, B. K. 2019. N2O emissions from two agroecosystems: High spatial variability and long pulses observed using static chambers and the flux-gradient technique. *Journal of Geophysical Research: Biogeosciences,* 124**,** 1887-1904.
WALL, A. M., CAMPBELL, D. I., MUDGE, P. L., RUTLEDGE, S. & SCHIPPER, L. A. 2019. Carbon budget of an intensively grazed temperate grassland with large quantities of imported supplemental feed. *Agriculture, Ecosystems & Environment,* 281**,** 1-15.
WALL, D. & LANIGAN, G. 2020. *Protecting soil carbon stocks and enhancing Carbon Sequestration* [Online]. Available: https://www.teagasc.ie/publications/2020/protecting-soil-carbon-stocks-and-enhancing-carbon-sequestration.php#:~:text=Optimise%20grazing%20management%3A%20Moderate%20grazing,carbon%20storage%20in%20the%20soil. [Accessed 28/07/2021].
WANG, C., AMON, B., SCHULZ, K. & MEHDI, B. 2021. Factors That Influence Nitrous Oxide Emissions from Agricultural Soils as Well as Their Representation in Simulation Models: A Review. *Agronomy,* 11**,** 770.
WANG, D., WANG, K., ZHENG, X., BUTTERBACH-BAHL, K., DÍAZ-PINÉS, E. & CHEN, H. 2020. Applicability of a gas analyzer with dual quantum cascade lasers for simultaneous measurements of N2O, CH4 and CO2 fluxes from cropland using the eddy covariance technique. *Science of The Total Environment,* 729**,** 138784.
WANG, J., XIONG, Z. & KUZYAKOV, Y. 2016. Biochar stability in soil: meta-analysis of decomposition and priming effects. GCB Bioenergy 8: 512–523.
WANG, K., LIU, C., ZHENG, X., PIHLATIE, M., LI, B., HAAPANALA, S., VESALA, T., LIU, H., WANG, Y. & LIU, G. 2013. Comparison between eddy covariance and automatic chamber techniques for measuring net ecosystem exchange of carbon dioxide in cotton and wheat fields. *Biogeosciences,* 10**,** 6865-6877.
WATSON, C., JORDAN, C., KILPATRICK, D., MCCARNEY, B. & STEWART, R. 2007. Impact of grazed grassland management on total N accumulation in soil receiving different levels of N inputs. *Soil use and management,* 23**,** 121-128.
WEBB, E. K., PEARMAN, G. I. & LEUNING, R. 1980. Correction of flux measurements for density effects due to heat and water vapour transfer. *Quarterly Journal of the Royal Meteorological Society,* 106**,** 85-100.
WECKING, A. R. 2021. *Paddock scale nitrous oxide emissions from intensively grazed pasture: Quantification and mitigation.* Doctor of Philosophy (PhD) Doctoral, The University of Waikato.
WECKING, A. R., CAVE, V. M., LIÁNG, L. L., WALL, A. M., LUO, J., CAMPBELL, D. I. & SCHIPPER, L. A. 2020a. A novel injection technique: using a field-based quantum cascade laser for the analysis of gas samples derived from static chambers. *Atmos. Meas. Tech.,* 13**,** 5763-5777.
WECKING, A. R., WALL, A. M., LIÁNG, L. L., LINDSEY, S. B., LUO, J., CAMPBELL, D. I. & SCHIPPER, L. A. 2020b. Reconciling annual nitrous oxide emissions of an intensively grazed dairy pasture determined by eddy covariance and emission factors. *Agriculture, Ecosystems & Environment,* 287**,** 106646.
WEEDA, W. 1967. The effect of cattle dung patches on pasture growth, botanical composition, and pasture utilisation. *New Zealand Journal of Agricultural Research,* 10**,** 150-159.
WEI, D., WANG, Y., WANG, Y., LIU, Y. & YAO, T. 2012. Responses of CO 2, CH 4 and N 2 O fluxes to livestock exclosure in an alpine steppe on the Tibetan Plateau, China. *Plant and Soil,* 359**,** 45-55.

WELLS, C. 2001. Total Energy Indicators of Agricultural Sustainability: Dairy Farming Case Study. Wellington, New Zealand: Technical paper, Ministry of Agriculture and Forestry.
WHITE, S., SHEFFIELD, R., WASHBURN, S., KING, L. & GREEN JR, J. 2001. Spatial and time distribution of dairy cattle excreta in an intensive pasture system. *Journal of environmental quality,* 30**,** 2180-2187.
WILD, P., HORDAN, R., LEPLAY, A. & VINCENT, R. 1996. Confidence intervals for probabilities of exceeding threshold limits with censored log-normal data. *Environmetrics,* 7**,** 247-259.
WILKINSON, S. & LOWREY, R. 1973. Cycling of mineral nutrients in pasture ecosystems. *Chemistry and biochemistry of herbage*.
WMO. 2019. *WMO GREENHOUSE GAS BULLETIN The State of Greenhouse Gases in the Atmosphere Based on Global Observations through 2018.* [Online]. Available: https://library.wmo.int/doc_num.php?explnum_id=10100 [Accessed 29/01/2020].
WOHLFAHRT, G., ANDERSON-DUNN, M., BAHN, M., BALZAROLO, M., BERNINGER, F., CAMPBELL, C., CARRARA, A., CESCATTI, A., CHRISTENSEN, T., DORE, S., EUGSTER, W., FRIBORG, T., FURGER, M., GIANELLE, D., GIMENO, C., HARGREAVES, K., HARI, P., HASLWANTER, A., JOHANSSON, T., MARCOLLA, B., MILFORD, C., NAGY, Z., NEMITZ, E., ROGIERS, N., SANZ, M. J., SIEGWOLF, R. T. W., SUSILUOTO, S., SUTTON, M., TUBA, Z., UGOLINI, F., VALENTINI, R., ZORER, R. & CERNUSCA, A. 2008. Biotic, Abiotic, and Management Controls on the Net Ecosystem CO_2 Exchange of European Mountain Grassland Ecosystems. *Ecosystems,* 11**,** 1338-1351.
WOJTAS, J., BIELECKI, Z., STACEWICZ, T., MIKOLAJCZYK, J., MEDRZYCKI, R. & RUTECKA, B. 2011. Application of Quantum Cascade Lasers in Nitric Oxide and Nitrous Oxide Detection. *Acta Physica Polonica, A.,* 120.
WOLFE, A. H. & PATZ, J. A. 2002. Reactive nitrogen and human health: acute and long-term implications. *Ambio: A journal of the human environment,* 31**,** 120-125.
WRAGE, N., VELTHOF, G. L., VAN BEUSICHEM, M. L. & OENEMA, O. 2001. Role of nitrifier denitrification in the production of nitrous oxide. *Soil Biology and Biochemistry,* 33**,** 1723-1732.
WU, Y. F., WHITAKER, J., TOET, S., BRADLEY, A., DAVIES, C. A. & MCNAMARA, N. P. 2021. Diurnal variability in soil nitrous oxide emissions is a widespread phenomenon. *Global Change Biology*.
YAN, T., FROST, J., KEADY, T., AGNEW, R. & MAYNE, C. 2007. Prediction of nitrogen excretion in feces and urine of beef cattle offered diets containing grass silage. *Journal of animal science,* 85**,** 1982-1989.
ZANATTA, J. A., BAYER, C., VIEIRA, F. C., GOMES, J. & TOMAZI, M. 2010. Nitrous oxide and methane fluxes in South Brazilian Gleysol as affected by nitrogen fertilizers. *Revista Brasileira de Ciência do Solo,* 34**,** 1653-1665.
ZELLWEGER, C., EMMENEGGER, L., FIRDAUS, M., HATAKKA, J., HEIMANN, M., KOZLOVA, E., SPAIN, T. G., STEINBACHER, M., SCHOOT, M. V. & BUCHMANN, B. 2016. Assessment of recent advances in measurement techniques for atmospheric carbon dioxide and methane observations. *Atmospheric Measurement Techniques,* 9**,** 4737-4757.
ZHENG, S., REN, H., LAN, Z., LI, W., WANG, K. & BAI, Y. 2010. Effects of grazing on leaf traits and ecosystem functioning in Inner Mongolia grasslands: scaling from species to community. *Biogeosciences,* 7**,** 1117-1132.
ZHOU, M., ZHU, B., WANG, S., ZHU, X., VEREECKEN, H. & BRÜGGEMANN, N. 2017. Stimulation of N2O emission by manure application to agricultural soils may largely offset carbon benefits: A global meta-analysis. *Global Change Biology,* 23**,** 4068-4083.
ZHU, Y., MERBOLD, L., LEITNER, S., XIA, L., PELSTER, D. E., DIAZ-PINES, E., ABWANDA, S., MUTUO, P. M. & BUTTERBACH-BAHL, K. 2020. Influence of soil properties on N2O and CO2 emissions from excreta deposited on tropical pastures in Kenya. *Soil Biology and Biochemistry,* 140**,** 107636.

ZISTL-SCHLINGMANN, M., FENG, J., KIESE, R., STEPHAN, R., ZUAZO, P., WILLIBALD, G., WANG, C., BUTTERBACH-BAHL, K. & DANNENMANN, M. 2019. Dinitrogen emissions: an overlooked key component of the N balance of montane grasslands. *Biogeochemistry,* 143**,** 15-30.